

**SELF-ASSEMBLY OF ORGANIC MOLECULES ON A SMECTIC
CLAY SURFACE**

THESIS

Presented to the Graduate Council
of Texas State University-San Marcos
in Partial Fulfillment
of the Requirements

for the Degree
Master of SCIENCE

by

Marcus Goss, B.S.

San Marcos, Texas
December 2005

ACKNOWLEDGEMENTS

I would like to first thank Dr. Gary Beall, Associate Professor of Chemistry at Texas State University – San Marcos, for recognizing in me the ability to succeed and giving me many opportunities and rewards. His understanding and patience with me has made this research possible. I would also like to thank Dr. Chad Booth, Assistant Professor of Chemistry, for coaching me along with some of the organic aspects of this research, and Dr. Patrick Cassidy, Professor of Chemistry, for inspiration and advice on the many uncertainties that arise with a project such as this. I want to thank Dr. Clois Powell for guiding me when I could not see the way and helping with those mechanisms that might otherwise have not been found. I appreciate the editing and reviewing that these gentlemen have done so that this writing could come to fruition.

Appreciation goes to all of the faculty and staff of the Department of Chemistry and Biochemistry at Texas State University – San Marcos. I would like to express my gratitude to all of the graduate and undergraduate students who assisted me in this research. In particular, I thank Jesse Hancock, Steward Harris, and Elizabeth Peterson for their contributions and training on instruments and techniques. Daniel Adame, Jeremy Bartels, Sergio Crosby, Sebastian Grajales, and Todd Hudnall all gain my admiration for being colleagues and friends and helping in numerous ways. I also extend my gratitude to Southern Clay Products for their donations of materials and time. A special thanks goes to my girlfriend, Mahdi Martin, for her support and patience.

Lastly, I would like to thank my parents, Robert and Carolyn Goss, for imparting, in me a determination not to give up on my endeavors but to persevere and to realize my dreams. They have given me more than I could have ever wanted by teaching me how to learn.

This thesis was submitted on October 3, 2005.

TABLE OF CONTENTS

	Page
ACKNOWLEDGEMENTS	iii
LIST OF TABLES	vii
LIST OF FIGURES	viii
ABSTRACT	x
1.0 INTRODUCTION.....	1
1.1 Background	1
1.2 Smectic Clay	4
1.3 Modification of MMT	7
1.4 Self-assembling Molecules	9
1.5 Wide Angle X-ray Diffraction	10
1.6 Synthesis of Mesogenic Molecules.....	12
2.0 EXPERIMENTAL.....	18
2.1 Materials	18
2.1.1 Chemicals and Materials for Organoclay Intercalates	18
2.1.2 Chemicals and Materials for Mesogenic Synthesis	19
2.2 Organoclay Preparation.....	19
2.2.1 Dry Process Method.....	20
2.2.2 Wet Process Method	21
2.3 Testing Methods.....	22
2.3.1 Wide Angle X-ray Diffraction (WAXD).....	23
2.3.2 Thermal Gravimetric Analysis (TGA).....	24
2.4 Synthesis of Mesogenic Molecules.....	24
2.4.1 Synthesis Scheme 1.....	25
2.4.2 Synthesis Scheme 2.....	26
2.5 Molecular Modeling.....	29

3.0	RESULTS AND DISCUSSION	30
3.1	X-Ray Diffraction	30
3.1.1	Alcohol Organoclays	31
3.1.2	Aldehyde Organoclays.....	33
3.1.3	Pyrrolidone Organoclays	33
3.2	Thermal Gravimetric Analysis.....	41
3.3	Organoclay Stability	45
3.4	Molecular Modeling.....	50
3.5	Organic Synthesis	57
4.0	CONCLUSIONS	61
	APPENDICES	64
	Appendix A: Wide Angle X-ray Diffractions of Organoclays	65
	Appendix B: Wide Angle X-ray Diffraction of Aged Organoclays	87
	Appendix C: Thermal Gravimetric Analysis Data.....	133
	Appendix D: Wide Angle X-ray Diffractions of Pure Alcohols.....	170
	REFERENCES	173

LIST OF TABLES

	Page
Table 1. Thermal gravimetric analysis data of alcohol intercalated organoclays	42
Table 2. Thermal gravimetric analysis data of aldehyde intercalated organoclays	43
Table 3. Thermal gravimetric analysis of pyrrolidone intercalated organoclays	44
Table 4. WAXD data of selected fresh and aged organoclay samples	49
Table 5. Comparison of molecular modeling and experimental WAXD data for selected samples	56

LIST OF FIGURES

		Page
Figure 1.	Electro-active organic molecule containing a thiol-based moiety	2
Figure 2.	SEM image of the nanocell contacts, and gold nanowires	3
Figure 3.	The structure of layered silicate as found in montmorillonite clay.....	5
Figure 4.	Solvated Na ⁺ MMT	8
Figure 5.	Bragg's law diagram of WAXD	10
Figure 6.	Schematic diagram of organoclay systems.....	12
Figure 7.	Substitution reaction to yield the brominated biphenyl ether compound.....	14
Figure 8.	Synthetic route of 1-[4-(Biphenyl-4-yloxy)-alkyl]-pyrrolidin-2-one	15
Figure 9.	Formation of hydroxy-alkyl pyrrolidone	16
Figure 10.	Synthesis of 1-[4-(Biphenyl-4-yloxy)-alkyl]-pyrrolidin-2-one molecule	17
Figure 11.	Sieve pan -200 mesh	21
Figure 12.	Typical reactor set-up for synthesis of organic molecules.....	28
Figure 13.	Alkyl chain length versus basal d-spacing in primary alcohol intercalated organoclays with 3 to1 milliequivalent ratios	32
Figure 14.	Comparison of N-octyl pyrrolidone intercalated organoclay series with 3 to1, 2 to1, and 1 to1 milliequivalent ratios	35

Figure 15.	d-spaces of N-pyrrolidone intercalated organoclays at 3 to1 milliequivalent ratios	37
Figure 16.	WAXD pattern for HEP intercalated organoclays; 3 to1, 2 to1, and 1 to1 milliequivalent ratios	38
Figure 17.	Diffraction patterns of the CHP intercalated organoclays; 3 to1, 2 to1, and 1 to1 milliequivalent ratios	39
Figure 18.	WAXD pattern for N-phenyl pyrrolidone intercalated organoclays; 2 to1, and 1 to1 milliequivalent ratios	40
Figure 19.	Comparison of WAXD for the octadecanol intercalated organoclay and pure octadecanol	47
Figure 20.	Comparison of the WAXD of fresh and aged tetradecanol at a 3to1 milliequivalent ratio	48
Figure 21.	Ion-dipole interaction between the organic modifiers and the resident sodium ion	50
Figure 22.	Model of dodecyl aldehyde on MMT	52
Figure 23.	π -Electron interaction between biphenyl moieties	53
Figure 24.	Partial interdigitation of biphenyl functional groups	54
Figure 25.	Space filling model of 3to1 ratio of 1-[12-(biphenyl-4-yloxy)-dodecyl]-pyrrolidin-2-one organoclay	55
Figure 26	IR spectra of a series of hydroxypyrrolidones	58
Figure 27	¹ H NMR of hydroxydodecylpyrrolidone	59
Figure 28	¹ H NMR of 1-[4-(Biphenyl-4-yloxy)-butyl]-pyrrolidin-2-one product	60

ABSTRACT

Self-assembly of molecules to form complex systems have enormous potential in a variety of areas. A point where computer processors cannot be further miniaturized due to physical and economic constraints is rapidly approaching. Solid-state silicon circuitry and silicon-based semiconductor technology will have to seek new methods to keep up with demands. Silicon-based semiconductor manufacture utilizing lithography is currently unable to obtain feature sizes below 0.1 micrometers. Utilizing current methods, the lower limit is forecast to be 30 nanometers. The solution to this problem may be in the investigation of single molecule switches and nanoscale memory systems. Construction of these nanoscale systems of circuits and memory devices requires self-assembly. Some methods currently used to fabricate such systems are chemical self-assembly, physical self-assembly, and colloidal self-assembly; however, these methods have not, as yet, achieved a system of ordered arrangement.

The research proposed here explores a novel approach to creating a self-assembled nanoscale system of molecules *via* ion-dipole interaction with cationic counterions on smectic clay surfaces. Molecular modeling of the candidates was conducted to assess the viability of self-assembly prior to experimental determinations. A study of ion-dipole bonding to the exchangeable cation on the smectic clay surface was conducted.

Candidates were intercalated in montmorillonite clay and basal d-spacing was determined with X-ray diffraction. This suggests the extent of self-assembly in the system. Thermal analysis was conducted to assess the retention of organic molecules on the clay surface.

Additional reinforcement of the self-assembled structure is believed to be possible with the addition of π - electron interaction in the tail. An attempt to synthesize and characterize mesogenic species, to examine π - electron interaction, was conducted. Inadequate time and investment resulted in the inability to synthesize sufficient quantities of these compounds to form and investigate organoclay systems.

It was found that the ion-dipole interaction is controlled by a polar head group, and Van der Waals interaction in the alkyl chain. The identity of the head group and the length of the alkyl tail group both contributed to self assembly of the system. Furthermore, it was discovered that the organoclay systems will reorder themselves over time.

These studies are a prelude to the synthesis of liquid crystalline mesogenic candidates, the self-assembly of these molecules in the smectic system, and experimentation of self-assembly on a vermiculite surface. Additionally, the synthesis of electro-active molecules such as those in the oligo(phenylene ethynylene) class combined with a head group favorable to self-assembling structures can be accomplished followed by the eventual testing of organoclays made with these compounds or the dispersal of these organoclays in a polymer matrix.

1.0 INTRODUCTION

1.1 Background

Self-assembly is the automatic arrangement of parts to make up a complex system.¹ It has proven impracticable to construct a nanosized system piece by piece due to cost and time constraints. The physical manipulation of molecules into a prearranged pattern is very expensive.² If a system is capable of self-assembling its parts into a desired configuration without direction by manual forces the system might well prove to be commercially viable. The physical limitation on the size of silicon based semiconductor manufacturing using optical lithography is rapidly approaching an end.³ The use of electro-active organic oligomers as nano-switches has come to the forefront as a means to decrease the size of electronic circuits beyond the capabilities of photolithographic techniques.⁴ Miniaturization of the feature size of computer components and microchips has been reduced to 0.13 micrometers with an expectation of 30 nanometers as an absolute limit.⁴ In a system based on organic molecules, or molecular scale devices, the scale of miniaturization can be greater than one hundred times smaller or two orders of magnitude.⁵ Studies have shown that by using a variety of oligo(phenylene ethynylene) (OPEs) molecules, electronic devices can be built. These molecules contain a nitro group exhibiting a reversible switching behavior allowing a voltage to result in a single electron reduction, turning the molecule on or off. This effect

has great potential as nanoscale electronic switches and memory devices.⁵ An OPE molecule, shown in Figure 1, is fully conjugated and contains electron withdrawing groups

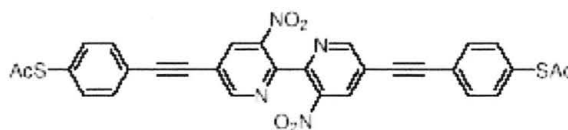


Figure 1: Electro-active organic molecule containing a thiol-based moiety typical of Tour's work in molecular electronics⁵

Tour's work centers around self-assembled monolayers (SAMs) connected to gold surface substrates used as contactors *via* a thiol based moiety. The molecules are self-assembling, but molecules within the bundles do not interact with one another to stabilize the assembly. Islands of bundles are formed between substrate layers.⁶ The nanocell is comprised of a silicon dioxide wafer with gold islands on its surface linked by gold nanowires coated with the SAMs and is capable of rudimentary memory storage for time periods of several days.⁷ Figure 2 demonstrates the scale of a single nanowire and the nanocell contacts.

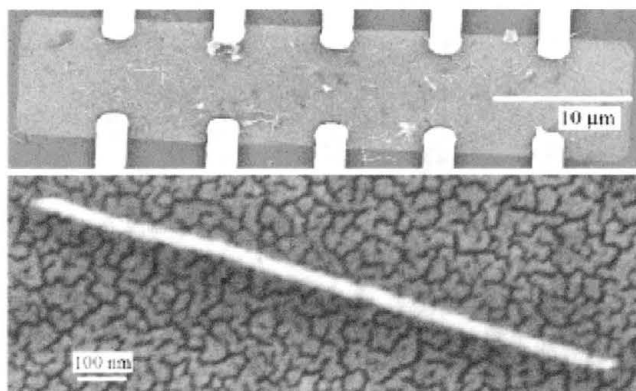


Figure 2: SEM image of the nanocell contacts (top), and gold nanowires (bottom). The OPEs are not observable⁵

One problem faced by Tour is the disordered arrangement of the molecules on the surface. This requires more space and nanowires to connect the islands.⁸ This problem may be overcome by organizing these electro-active species on a surface that enables an ordered array to be constructed by means of self-assembly to form a template then transferred to a conductive surface. This research focuses on identifying potential candidates for favorable ion-dipole interaction with smectic clay surface counter-ions, synthesis of self-assembling molecular moieties similar to electro active organic oligomer species or liquid crystalline functionalities, and discovering a method for constructing an ordered array of such molecules. Series of intercalates with various head and tail groups will be investigated.

1.2 Smectic Clay

The self-assembly of molecules *via* ion-dipole interaction has been shown to occur on the surfaces of some clay minerals.⁹ Smectic clays of this type have a layered structure consisting of octahedrally coordinated aluminum layers between tetrahedrally coordinated silicon atoms. Figure 3 shows the general structure of the tri-layered system. The layers are stacked in platelets with cations, typically sodium, calcium, or other alkaline earth metal ions, suspended near the surface of the platelets in between the clay plates, often referred to as the gallery. These exchangeable cations are located above charge deficient areas resulting from isomorphous substitutions of Mg or Fe²⁺ for aluminum in the octahedral layer of the clay. Coulombic attraction holds these cations over the charge deficient areas.¹⁰ The cation exchange capacity (CEC) for smectic clays is the amount of cations that can be exchanged on the clay surface.¹¹ The CEC is normally presented in units of milliequivalents per 100 grams of clay since a well defined molecular weight for clays is difficult to ascertain. For the purpose of this research this value represents the moles of surface ions per gram of clay. Analysis of smectic clays indicates that there are a number of levels of organization in the clay. The smallest particles are on the order of 10 nm arranged in stacks of parallel lamella averaging 10 sheets per particle. These layers are about 1 nm thick and have an enormous surface to thickness ratio.¹⁵ This feature lends itself not only to dispersal of clays into organic materials, but also allows for the intercalation of organics between the clay layers. This intercalation will allow the self-assembly of certain organic molecules between the layers.¹²

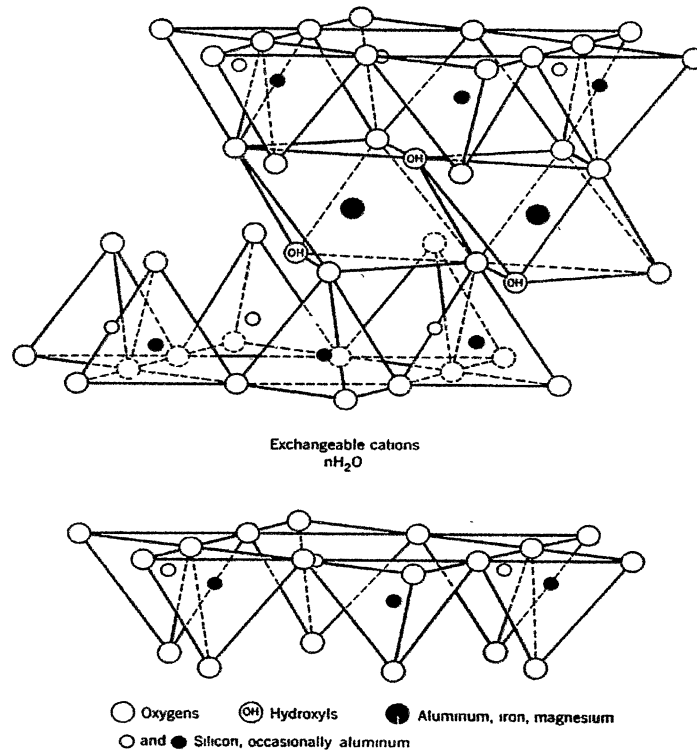


Figure 3: Structure of layered silicate as found in montmorillonite clay¹⁰

A commonly used mineral form of this type of clay is montmorillonite (MMT). A product of bentonite, MMT is a naturally occurring clay resulting from volcanic sediment found near the earth's surface. MMT has a random arrangement of isomorphous substitutions of Al^{3+} for Mg^{2+} in the octahedral layer. These result in a charge deficiency on the surface of the clay. The number of these substitutions is constant in a given clay so it is consistent in its CEC across its surface.¹⁰ The MMT is able to intercalate organic material easily and with a great deal of consistency without exfoliation. This occurs when the clay layers completely separate from one another and

form a random arrangement, a condition known as delamination.¹³ MMT also possess a large surface area relative to its plate thickness. This is known as the aspect ratio and it provides MMT a pseudo two-dimensional character. The typical surface area per gram is 750 square meters when dispersed as individual plates.¹⁷ Another feature of MMT clay is that it exhibits a turbostratic structure. A turbostratic structure is one in which there is no crystallographic relationship between the individual sheets. This enables the clay to swell as water or organic material is adsorbed. The nature of this feature is that the clay platelets can slip sideways when adsorbing compounds. This leads to an increase in the basal d-space and allows adsorption to increase.¹⁴

The terminal edges of MMT contain hydroxyl groups that can interact with intercalating materials.¹⁶ In this research, edge treatments of the clay plates will not be employed since the presence of polar hydroxyl groups should not carry a significant influence on the organic modifiers being intercalated.

1.3 Modification of MMT

Numerous investigations into the modification of smectic clays have been conducted. Its origins in the nanocomposite field are rich in history beginning in the 1940's. Jordan discovered that smectic clay could be dispersed into various solvents resulting in significant changes in the character of the clay including a conversion to an organophilic nature. The formation of organoclays through cation exchange reactions allowed the determination of the thixotropy and the liquid-binding capacity of these clay systems.¹⁸ In the 1980's Toyota Central Research developed the first commercial application of clay-nanocomposites using organically modified MMT in polycaprolactam.¹⁹ The enhancement of polymer properties by formation of nanocomposites resulted in a marked increase in the polymer heat deformation temperature. This has allowed the use of plastics in under-the-hood parts and other high temperature applications. Another exciting aspect of polymer nanocomposites utilizing MMT is the relatively low filler concentrations required compared to that of conventional fillers. Today the commercial applications of MMT include cosmetics, paint, grease, nanocomposite polymers, and fire retardant systems, to name a few.²⁰

The principle modification of MMT used in polymer nanocomposite applications is ion-exchange reactions where the resident surface ions on the clay surface are exchanged for organic molecules bearing a net positive charge. Some common examples of organo-modifiers are quaternary ammonium ions.²¹ The modification is performed to change the inter-gallery or Van der Waals gaps from a hydrophilic nature to a hydrophobic one. Most polymer systems are hydrophobic and will only intercalate into the gallery space if it is also hydrophobic. Naturally occurring MMT exists in a hydrated

state with water occupying the gallery space. Inter-gallery water molecules can be seen in Figure 4, a model of the MMT unit cell.

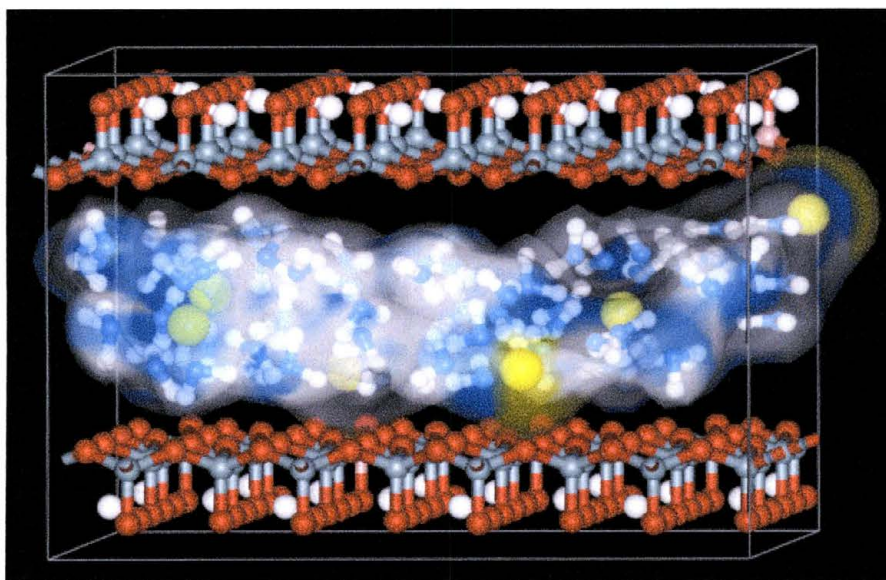


Figure 4: Solvated Na⁺ MMT (Only the tetrahedral layers of the clay matrix are shown)²²

Because only a limited number of organic ion exchange molecules are commercially available and most attempts at fully exfoliated polymer nano-composite systems have not been successful, a novel method of ion-dipole modification has been studied.^{9,23} These types of interactions were first documented by Bradley in 1945.²⁴ It was shown by Brindley that the partial negative dipole of alcohols and glycols would form ion dipole interactions with the surface ions on smectic clays.²⁵ Many of the earlier experiments involved saturated systems where the CEC of the clay was not considered and formations of molecular monolayers were formed.²⁶

1.4 Self-assembling Molecules

Molecular candidates for self-assembly of this type on the surface require a partially negative charge on the oxygen atom. Unlike studies involving the free exchange of surface cations with other cationic species, the organic molecules in this study do not exchange for the cation, but are held close to the existing ion by ion-dipole forces.²³ This research investigates the effectiveness of a variety of functional groups for interaction with the surface ions *via* these forces. Additionally, the tail group, aliphatic or aromatic in nature, was investigated as to its participation in the assembly of these post-like secondary structures. The accompanying stability of Van der Waals interactions in the molecule's tail group requires some flexibility in the molecule. Some candidates contained no carbons or short, saturated alkyl chains between the head and tail functional groups. These molecules might contain only one of these types of interaction but not both. Self-assembly of the dual interaction type is suspected to be more viable with long carbon chain spacers since chain interaction is likely to assist in the rigidity of the self-assembled posts.²³ Additionally, an aromatic tail group might allow for more support through π electron interactions. In order to obtain higher probabilities of this type of interaction it is proposed that an ether linkage be incorporated into the structure to increase flexibility. An ether linkage also allows for a more favorable reaction selection in the various synthetic routes.

In the first stage, a suitable head group of the molecule must be identified. It was found that pyrrolidones can be bonded to sodium ions located on the surface.⁹ Alcohols and aldehydes were examined to determine the effect of the primary hydroxyl and carbonyl group attractions. Concurrently, the study of chain length variation on the self-

assembly was investigated as well as variation in loading of the organic molecules with respect to the sodium cations. Previous studies by Brindley have examined the effects of saturated systems on the extent of exfoliation in smectic clay systems. It was determined that in saturated systems the organic modifiers have little or no freedom of movement.²⁵ These systems would not work well in the formation of self-assembled arrays for electronic memory.

1.5 Wide Angle X-ray Diffraction

Another reason for the use of MMT in this research is that the stacking of clay layers or platelets form interlayers or galleries. The intercalation of organic molecules into these galleries can result in increased distance between the layers.²⁷ This distance, known as the basal d-spacing or $d(001)$ can be determined by X-ray diffraction. Figure 5 is a typical diagram of Bragg's law showing the angle θ .

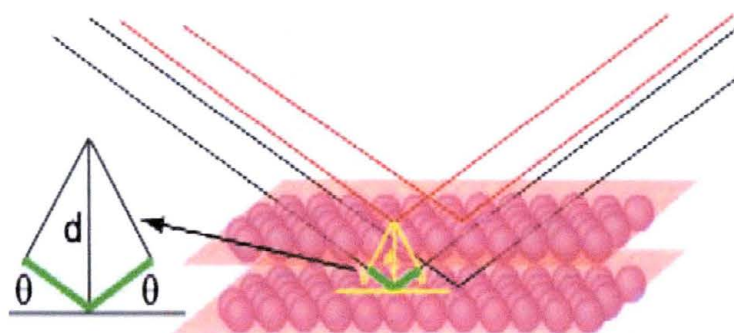


Figure 5: Bragg's law diagram of WAXD²⁹

Bragg's law equation: $n\lambda = 2d \sin \theta$, allows for the determination of the basal d-space. Absence of a basal X-ray diffraction peak indicates full delamination of the layers, otherwise known as exfoliation.²⁸ By comparing the 2θ values of X-ray peaks to determine differences in gallery height, assembly can be implied in systems with large distances. The large distances can be accounted for by taking the expected distance occupied by the intercalated molecule and doubling it to account for molecules inverted from the opposing surface of the platelet above. If the basal-d distance is less than twice the length of the intercalated molecule it is inferred that some of the molecules have formed an interdigitated arrangement. If the gallery height corresponds to the length of the molecule, or less, we consider the system to have little or no self-assembled structure. For example, a d-space greater than 30 angstroms, is considered to be the result of a self-assembled structure since the volume of the organic modifier itself is not large enough to fill all of the free-volume in the gallery in any other arrangement. Additional information gained in the diffraction pattern is from the order of the diffraction angle. The value of n in the equation denotes the order of the X-ray peak, as in $n = 1, 2, 3, \dots$. The presence of orders greater than 1 occurs when the plates are in very good register and can be used to back-calculate the value of d when the first order peak is less than ideal or at very low angles or when the main peak may be read incorrectly, since intense main beam scatter tends to move the peak to lower angles.³⁰

When the intercalated molecules do not self-assemble they lie parallel to the surface of the clay or interdigitate thus allowing the platelets to come closer together. This positioning occupies a greater amount of the clay surface area but allows the clay sheets to get nearer or closer to one another. When the alkyl chains of the molecules

interact they form rigid posts nearly perpendicular to the surfaces, which prevent the layers from reducing the gallery to a smaller state at lower loadings. Figure 6 demonstrates some possible configurations of the organoclay systems.

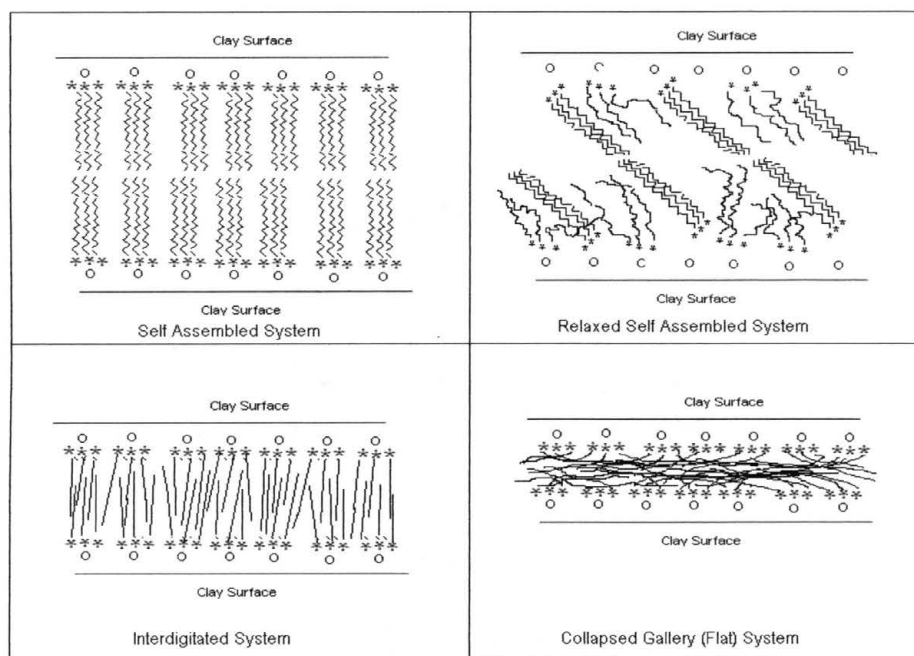


Figure 6: Schematic diagram of organoclay systems

1.6 Synthesis of Mesogenic Molecules

Once an optimal head group is identified it will need to be attached to a structure that will drive self-assembly. A mesogenic compound, containing both a rigid part for liquid crystalline behavior and a flexible moiety, might function well. Also, biphenyl mesogenic structures are common to many liquid crystalline systems.³¹ These molecules demonstrate the ability to interact with one another through π -electron interactions in the aromatic rings. The synthesis of the molecular candidates was attempted using two

distinct routes. The first route, a Williamson ether synthesis, is the reaction of a dibromo compound and 4-phenyl phenol resulting in brominated biphenyl ether. This is followed by a substitution of 2-pyrrolidone onto the brominated biphenyl ether.³² The second method begins with an hydroxyamine and a γ -butyrolactone forming an hydroxypyrrolidone, then a benzyne reaction onto a brominated bi-phenyl.³³ Both routes provide identical products but at different yields. Numerous purification steps must be performed between steps to insure maximum yields at completion.

Figure 7 details the synthetic route used for the formation of the brominated biphenyl ether starting from dibromo compounds and 4-phenyl phenol. Excess dibromo molecules help to ensure against double substitutions, which, when they occur, are easily separated by extraction.

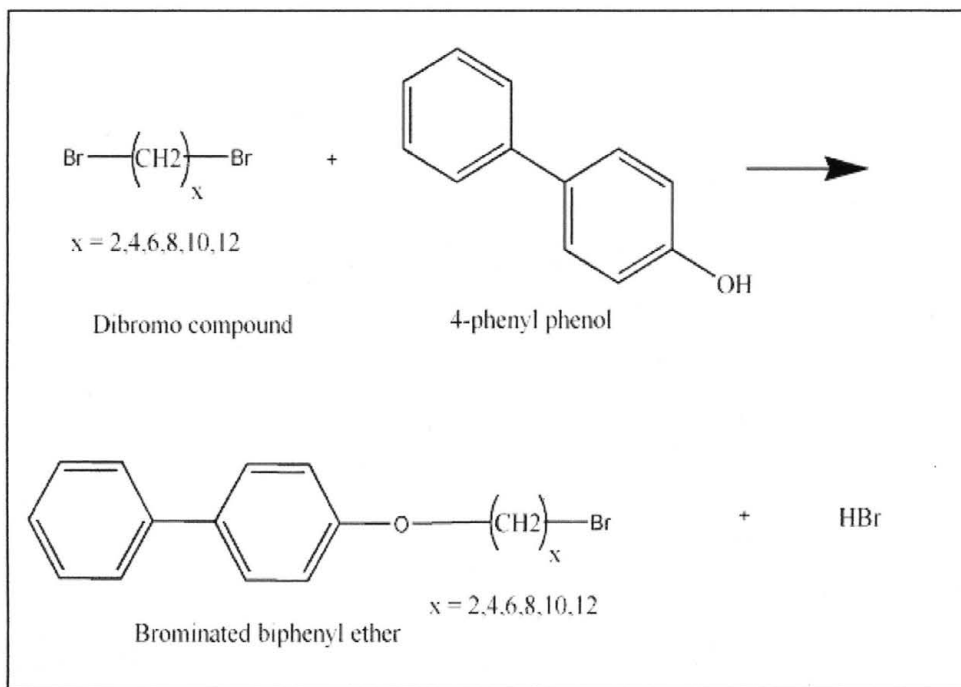


Figure 7: Substitution reaction to yield the brominated biphenyl ether compound

After isolation, purification, and characterization of the product from the first step, the brominated biphenyl ether compound is reacted with 2-pyrrolidone to form the target molecule. Figure 8 shows the substitution reaction connecting the reactants at the nitrogen atom of the pyrrolidone. The product is isolated from any side products and unreacted components of the mixture.

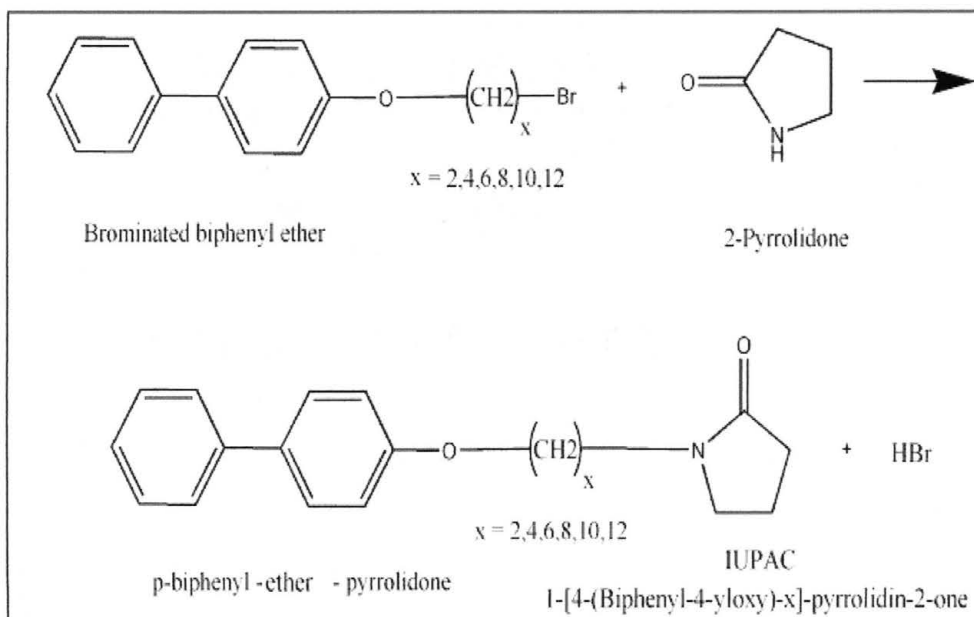


Figure 8: Synthetic route of 1-[4-(Biphenyl-4-yloxy)-alkyl]-pyrrolidin-2-one

One obstacle of this route is the deprotonation of the 2-pyrrolidone molecule. This is carried out by use of an extremely strong base; but this can be a complicated path, since the basic environment can cause other problems. Because of this issue an alternative route was also attempted.

The second synthesis route yields the target molecule in three steps. This synthesis is similar to the commercial synthesis of pyrrolidones. The first step is detailed in Figure 9 and results in the formation of the pyrrolidone functional group from γ -butyrolactone and an amino alcohol.³⁴ This is a condensation reaction, producing water which is collected and is used to monitor the progress of the synthesis.

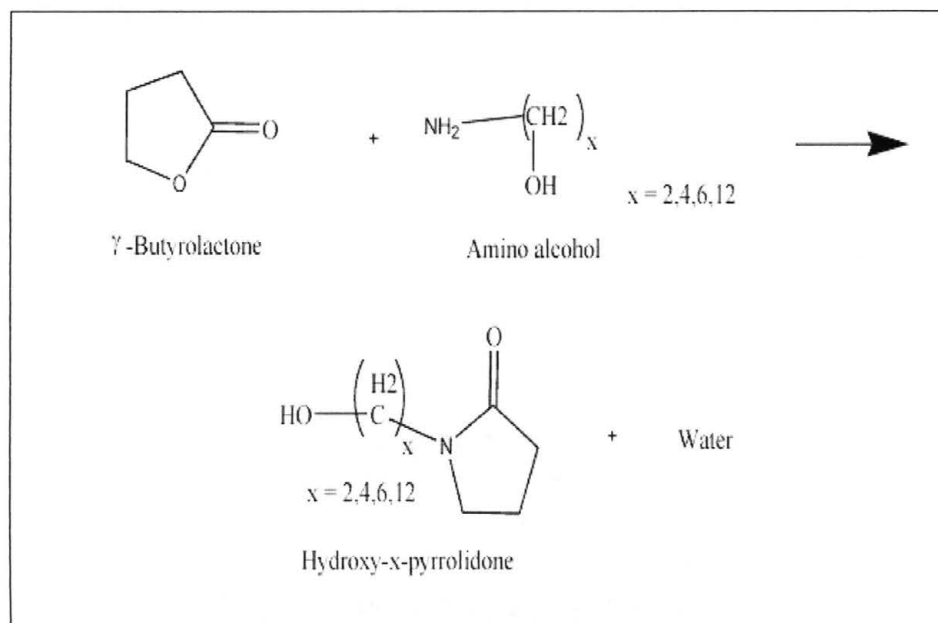


Figure 9: Formation of hydroxy-alkyl pyrrolidone

This reaction is followed by the formation of an alkoxide intermediate then a benzyne reaction connecting the 4-bromobiphenyl to the pyrrolidone *via* an ether linkage. The benzyne reaction will result in the *para* form of the product because the phenyl substituent is *para*-directing. Figure 10 shows the second step resulting in the target molecule. Primarily aqueous HBr is produced, but some liquid bromine as well as hydrogen gas is formed. Isolation of the target molecule from side products is performed to yield the pure hydroxyl form and prevent carrying over any unreacted amino alcohol to the following step.

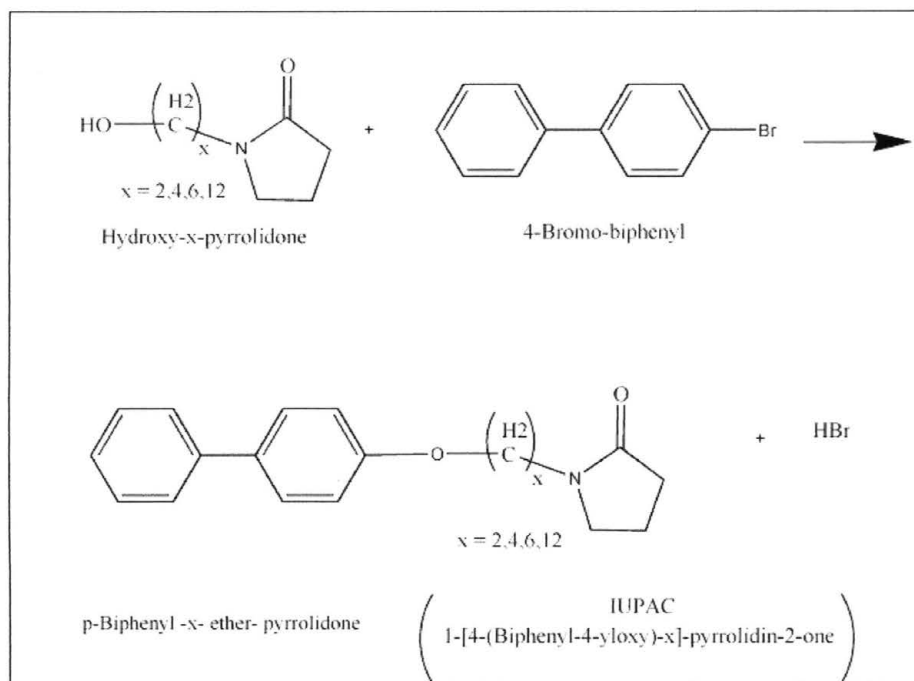


Figure 10: Synthesis of 1-[4-(Biphenyl-4-yloxy)-alkyl]-pyrrolidin-2-one molecule

The length of the spacer units between the head group and the phenyls was varied to determine chain length effects on the self-assembly. The products of the synthesis will be characterized and purified to insure against competing species. Determination of the structure of these products is accomplished using NMR and IR spectroscopy. As with the preliminary alkyl candidates, the aromatic structures will be added to the MMT at various loadings. Samples will be analyzed by X-ray diffraction to determine basal spacing and TGA to determine the extent of retention.

2.0 EXPERIMENTAL

2.1 Materials

2.1.1 Chemicals and Materials for Organoclay Intercalates

This study used montmorillonite clay obtained from Southern Clay Products (SCP), Gonzales, Texas. The type of clay was sodium Cloisite with an exchange capacity of 92.6 milliequivalents sodium ions per 100 grams of clay. The Cloisite Na⁺ contained less than 2 percent moisture. The clay was used in powder form or in slurry as 2.08% solids by weight. The powder was used without washing and with no further modification performed on the clay prior to its use. All calculations regarding the equivalence of the clay ions were rounded to 95 milliequivalents per 100 grams of clay for ease of measure.

The alcohols used in this study: n-butanol, n-hexanol, n-octanol, n-decanol, n-dodecanol, n-tetradecanol, and n-octadecanol; were obtained from Sigma-Aldrich Chemical Supply. These alcohols were reagent grade and were used as supplied from the manufacturer. The alcohols were stored in temperature and humidity controlled containers. The aldehydes used in this study: n-butanal, n-hexanal, n-octanal, n-decanal, and n-dodecanal were also obtained from Sigma- Aldrich and were reagent grade and used as received from the manufacturer. These chemicals were also stored under controlled temperature and humidity. The pyrrolidones used in this study: N-pyrrolidone, N-hydroxyethylpyrrolidone, N-cyclohexylpyrrolidone, N-phenyl pyrrolidone, N-methyl

pyrrolidone, N-octylpyrrolidone and N-dodecylpyrrolidone were obtained from ISP Specialty Chemicals. These pyrrolidones were used as received from the manufacturer with no further modifications and were stored in a controlled environment.

2.1.2 Chemicals and Materials for Mesogenic Synthesis

The synthesis of 1-[4-(Biphenyl-4-yloxy)-butyl]-pyrrolidin-2-one, 1-[6-(Biphenyl-4-yloxy)-hexyl]-pyrrolidin-2-one, 1-[8-(Biphenyl-4-yloxy)-octyl]-pyrrolidin-2-one and 1-[12-(Biphenyl-4-yloxy)-dodecyl]-pyrrolidin-2-one was carried out via two synthesis routes. The first route used dibromobutane, dibromohexane, dibromooctane, dibromododecane, 4-phenylphenol, and N-pyrrolidone. The second synthesis route required hydroxyethylpyrrolidone, γ -butyrolactone, 4-bromobiphenyl, 4-amino-1-butanol, 6-amino-1-hexanol, and 12-amino-1-dodecanol.

The solvents used in these processes were methanol and absolute ethanol, chloroform, ethyl ether, anhydrous tetrahydrofuran (THF) and anhydrous dimethylsulfoxide.(DMSO) Deionized water (DI H₂O)was also used. The ionic and mineral content of the deionized water was not known.

2.2 Organoclay Preparation

Clay samples were prepared by intercalation of the silicate clay layers with an organic molecule for the purpose of exploring the ion-dipole interactions between them and the resident surface ions. Two processes: a so called dry process and a wet process were utilized to prepare organoclay samples.

2.2.1 Dry Process Method

The dry method was utilized when batch sizes exceeded 150 grams of dry clay. The method utilized equipment that could not be used with smaller quantities of material. Most of the samples used in this study were prepared using this method. In these samples 250 grams of Na⁺ Cloisite was measured and then wetted with deionized water to 70 percent water content by weight. The amount of deionized water was calculated by weight and assuming a 2.0 % moisture content existed prior to wetting. The clay samples were stirred in a Kitchen Aid bowl mixer for approximately 15 minutes to insure adequate expansion of the clay layers by the water. This was followed by the addition of the organic modifier with continued stirring for a minimum of 20 minutes. In this way, ratios of 1:1, 2:1, and 3:1 were prepared based on milliequivalence with the sodium ions on the clay surface and the formula weight of the organic modifier. The amount of organic modifier was measured by weight. In cases where the organic was solid at room temperature a heated double boiler was employed to convert the modifier to a liquid state. In a few of the samples a small quantity of methanol or ethanol was used to maintain this liquid state for the addition to the clay, typically 5-10 milliliters.

After the mixing was complete, the sample was extruded through a Hobart commercial auger grinder machine, model 4522. The machine is a single screw extruder with an average rotation speed of 200 rpm depending on the viscosity of the sample. No controls for rotational speed, back pressure, or temperature were available. A sample was passed through the extruder 4 to 6 times to insure adequate shear and mixing of the material to achieve intercalation. The visual appearance of steam at the extruder plate

indicates sufficient shear forces to drive the modifier between the clay platelets and suggest that water was being forced out from the clay galleries.

The collected organoclay samples were chopped into pellets and air dried on aluminum pans. In some cases the organoclay samples were dried in a vacuum oven at 60° C with a vacuum of 20 torr for a period no less than 10 hours. When the samples were deemed to be dry they were further chopped to small particles and then ground to a fine powder in a commercial coffee grinder. The samples were then passed through a series of sieves until the particle size did not exceed 75 micrometers in any dimension. Figure 11 shows a typical sieve pan used to achieve fine particles.

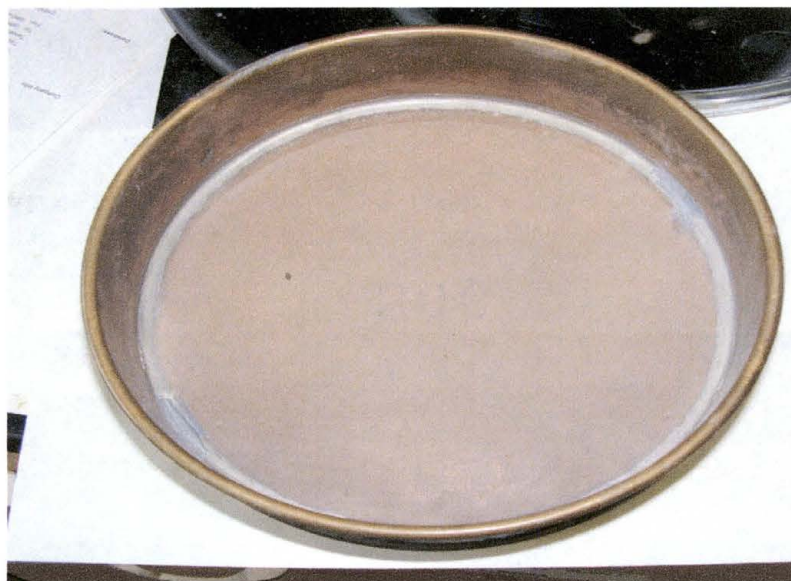


Figure 11: Sieve Pan 200 mesh (75 μ m)

2.2.2 Wet Process Method

The wet process was utilized when the limited quantity of organic modifier dictated that smaller batches be produced. In this process method the modifier was added

to a slurry of Na⁺ Cloisite in deionized water. The slurry was prepared in a Hamilton Beach commercial blender by mixing dry stock clay with deionized water to obtain a 2.5 percent by weight clay slurry. The slurry was blended at the highest setting for a minimum of 20 minutes. In some cases the clay slurry was obtained directly from SCP and was 2.08 percent clay determined by the manufacturer.

In order to obtain similar 1:1, 2:1, and 3:1 ratios of organic modifier to sodium ions the amount of clay slurry needed was determined and weighted out based on the formula weight of the organic modifier and the amount available. The slurry was heated to a temperature of 55° C then the weighed organic modifier was added with stirring for 1 hour. The organoclay slurry samples were placed in a high shear mixer for a period of 1 minute at 1000 rpm. Following the dispersion, the samples were poured onto Pyrex glass baking pans and dried in an oven at 65° C for a period of no less than 24 hours. When the organoclays were dry, the resulting film was peeled from the glass pan and cut into small pieces. The pieces were then ground to a fine powder in a commercial coffee grinder. The samples were then passed through a series of sieves until the particle size was less than 75 micrometers in any dimension.

2.3 Testing Methods

Two methods were utilized to measure the intercalation of organic species. The first, wide angle x-ray diffraction is used to indicate the change in basal d-spacing. Second, the thermal analysis gives data on the percent composition of the organic intercalate and water content of the organoclay.

2.3.1 Wide Angle X-ray Diffraction (WAXD)

The organoclay samples were subjected to wide angle X-ray diffraction (WAXD) to determine the basal d-spacing between the layered sheets of the clay. This allows the determination of the effects of the organic material on the clay surface by considering the resulting distance between the clay sheets.

The initial WAXD of samples were performed on a Bede diffractometer within two weeks of the formation of the organoclay. The instrument was set in the powder reflective mode utilizing $\text{CuK}\alpha$ X-ray radiation with a wavelength of 1.54 angstroms. The powder samples were placed into grooved glass microscope slides and attached to the sample plate by double-sided adhesive tape. A scan rate of 2 degrees per minute was used from 1 to 15 degrees 2θ . WAXD scans and data from this instrument can be found in Appendix A.

Following a period of 2 years, the organoclays were remeasured on a Bruker AXS D8 Focus diffractometer. The powder samples were placed into a holder cup and the upper surface of the sample was smoothed to achieve a uniform surface. At a scan rate of 2 degrees per minute, the sample was typically scanned from 1 to 25 degrees 2θ . These data can be found in Appendix B. Additionally, Southern Clay Products conducted measurements of some of these organoclay samples on a Scintag diffractometer also using $\text{CuK}\alpha$ X-ray radiation and at similar parameters. Selected data from this source were used but the majority of these analyses were replaced with data from the Bede diffractometer.

2.3.2 Thermal Gravimetric Analysis (TGA)

The amount of organic modifier intercalated into the clay was determined by thermal gravimetric analysis. The process involves the controlled heating of a small sample while continuously monitoring the sample's mass. The change in sample mass with respect to the temperature indicates the loss of hydration, the organic modifier's approximate decomposition temperature and the dehydroxylation of the clay structure at high temperature. Additionally, the percentage of water and percentage of organic modifier, by weight, is determined. This verifies the quantity of the organic modifier in the sample.

Analysis was carried out on a TA Instruments Q50 thermal gravimetric analyzer under argon from ambient room temperature to 800°C at a rate of 20°C per minute. The typical sample size was between 15-20 mg. See Appendix B for the complete list of TGA data and graphs.

2.4 Synthesis of Mesogenic Molecules

After determination of the optimal head group the next step was to examine the self-assembly of molecules containing a biphenyl functionality in the tail. As before, a series of varying tail lengths were tested. It was necessary to synthesize these liquid crystalline candidates because they were not commercially available. Two synthesis schemes were explored but neither route successfully produced sufficient quantities to form organoclay systems.

2.4.1 Synthesis Scheme 1

A Williamson ether synthesis reaction was carried out on 4-phenyl phenol with a series of straight chain dibromo compounds of 4, 6, 8, and 10 carbon spacers. The following reactions were performed in a variety of solvents before the most successful were found. Some differences in recovery technique were required to compensate for increasing spacer length in the molecules. A phase transfer catalyst, t-butylammoniumchloride hydrate, was also used in some early reactions but suspected formation of micelles prevented adequate reaction conditions. It was decided to carry out the reactions in single phase systems.

2.4.1.1 Synthesis of 1-[4-(Biphenyl-4-yloxy)-butyl]-bromine

4-phenylphenol (17.0g, 0.1 mol) and 1,4-dibromobutane (129.6g, 0.6mol) were placed in a 500mL round-bottom flask with KBr (12.5g, 0.105 mol) in acetone with magnetic stirring. Argon was used to protect the reaction during reflux at 50°C overnight. The mixture was cooled and extracted with ether:hexane:H₂O then recrystallized from ethanol to yield a flaky iridescent solid (26.8g, 88% yield).

2.4.1.2 Synthesis of 1-[4-(Biphenyl-4-yloxy)-butyl]-pyrrolidin-2-one

A second step involved substituting a pyrrolidone functional group at the molecule on the terminal bromine of the product in the previous step. Dry THF (25 mL) was combined with NaH (2.5g, 0.0035 mol) in a 100mL round-bottom flask under argon purge and with mechanical stirring. 2-pyrrolidone (2.73mL, 0.00356 mol) was added slowly to the flask by syringe. Considerable effervescence was noted along with a sharp

temperature increase. Brominated biphenyl butyl ether (9.4g, 0.030 mol) from the previous step, dissolved in dry THF (15mL), was added after the reaction cooled and no more bubbling was evidenced. The mixture was heated to 65°C and allowed to progress for 5 days. Solids were waxy and faded pink in color and were filtered from the THF, washed 3 times with slightly acidic H₂O then recrystallized from chloroform. The resulting solid was waxy and beige. Additional drying was performed in a convection oven at 60°C but the solid remained waxy and an accurate weight was not measured. Thin layer chromatography (TLC) indicated a multi-component mixture and column chromatography was attempted to separate the components. The target molecule, 1-[4-(Biphenyl-4-yloxy)-butyl]-pyrrolidin-2-one, was not able to be recovered in sufficient quantity for formation of an organoclay intercalate.

2.4.2 Synthesis Scheme 2

Due to the limited quantity of product formed in Scheme 1 an alternative approach was employed. The second scheme for the synthesis of the biphenylpyrrolidone ether molecules was a three step approach starting with the formation of a series of N-hydroxypyrrolidones then conversion to the corresponding alkoxides, and finally a benzyne reaction to form the target biphenylpyrrolidone ether molecule.

2.4.2.1 Synthesis of N-hydroxybutyl pyrrolidone

4-amino-1-butanol (2.0g, 0.0224 mol) was combined with γ -butyrolactone (2.0 mL, 0.026 mol) in a 100 mL round-bottom flask. Mechanical stirring without heat was used for 24 hours. The mixture hardened into a waxy white solid. Recrystallization of the product from ethanol yielded a white powder (3.2g, 0.0206 mol, 92%). This reaction was also carried out for 6, 8, and 12 carbon species with comparable yields.

2.4.2.2 Synthesis of 1-[4-(Biphenyl-4-yloxy)-butyl]-pyrrolidin-2-one

NaH (0.6g) was placed in a dry 100 mL round-bottom flask under argon protection. Dry DMSO (20 mL) was added slowly to the NaH. Next, the N-hydroxybutyl pyrrolidone formed previously (2.13g, 0.0135 mol) was dissolved in DMSO (4 mL) and added drop wise to the reactor. Formation of bubbles indicated the conversion to the alkoxide. After 10 minutes the temperature was raised to 120°C, and *para*-Bromobiphenyl (3.0g, 0.0129 mol) was slowly added to the reactor. After about 10 minutes the temperature raised sharply and the mixture turned dark brown or black. The mixture was poured over 300 mL of water saturated with NaCl while still hot. Three extractions were performed using hexane, then a DI H₂O wash was performed on the extracted hexane. The solvent was evaporated and the yellowish white crystals were collected (0.82g, 0.0027mol, 21%) Figure 12 shows a typical reactor set-up for these reactions. An oil bath was used for heating. In some reactions condensation products were collected using a Dean-Stark trap attached to a distillation head above the condenser.



Figure 12: Typical reactor set-up for synthesis of organic molecules

2.5 Molecular Modeling

Extensive molecular modeling of these systems was performed to determine the viability of a particular molecule for self-assembly. The modeling was performed on the software package Cerius 2 from Accelrys. The goal of the model was to determine a minimum energy state and assess a distance of the z axis in the unit cell equivalent to the basal d-spacing of a smectic clay sample. These types of molecular dynamics simulations allow the molecules to position themselves according to the Newton-Euler laws of motion.³⁵ The calculations were force field-based and charge assignments of each atom were calculated. The universal force field supplied in the software was used as it was capable of crystalline system calculations. The clay layer was constrained to simplify the model. The dynamics were performed under constant moles, volume, pressure and temperature of 298 K.

Models were constructed in stages to reduce false minima. The organic molecule was constructed and charges were assigned. The molecule was then moved onto a model of the MMT unit cell. The organic function was positioned near a sodium ion and the model was run through numerous iterations to find a minimum energy. A second organic molecule was positioned near another ion and minimized. This process was repeated until all ions were occupied. The c-axis of the self-assembled model was then slowly reduced with energy minimizations and dynamics until a minimum energy value was recorded. The value of the c-axis at this minimum is regarded to be the natural state and the resulting expected basal d-spacing.

3.0 RESULTS AND DISCUSSION

This research examines the effects of various organic modifiers intercalated into the gallery of sodium Cloisite clay. The principle tool for identifying the effective self-assembly of organic molecules around the resident sodium surface ions is wide angle X-ray powder diffraction. The samples were also analyzed in thermal gravimetric analysis to determine the percent organic composition and clay water content. Lastly, these surface interaction systems were investigated utilizing molecular modeling software to predict the potential for self assembling systems. The synthesis of modifier molecules containing a biphenyl moiety is discussed and the results of the reactions are reported.

3.1 X-Ray Diffraction

Appendix A of this work contains the original patterns utilized for the determination of the gallery's basal d-spacing and the extent of self-assembly. Appendix B contains the aged organoclay diffraction patterns. This section will provide figures of comparison taken from those contained in the appendices. Some plots of interest are also presented to define the results of the organoclay modification.

3.1.1 Alcohol Organoclays

Primary alcohols were chosen due to their terminal hydroxyl groups which possess a moderate partial negative charge on the oxygen atom. Alcohols range from butyl alcohol with 4 carbons to octadecanol with 18 carbons. The length typically progresses by 2's since these are commercially available and generally made from natural products. Prior studies show that methanol, ethanol and propanol are not retained on the clay surface in an amount leading to an expansion of the clay gallery.²⁴ It is thus assumed that these molecules form no assembly and are the basis for the hypothesis that forces beyond mere ion-dipole interactions between partial negative charges and surface cations are required to allow a significant increase in the basal d-spacing beyond that of hydrated clay.

Butanol, hexanol, and octanol all are retained in the gallery to some degree but show no appreciable influence on the d-spacing above that of normally hydrated montmorillonite at about 13 angstroms.¹⁰ Since the clay tri-layer occupies about 9 angstroms, the gallery space is, at this value, 4 angstroms.

Decyl alcohol, at a 3 to 1 milliequivalent ratio, shows an increase in the gallery of 2 angstroms (15 Å d-space). This indicates that some assembly may be occurring and this is allowing more of the alcohol to remain on the surface. It is probable that this organization follows the interdigitated model and the formation of rigid posts is not prevalent. Figure 13 shows that the influence of alkyl chain interaction begins at decyl alcohol and becomes more pronounced as carbons are added.

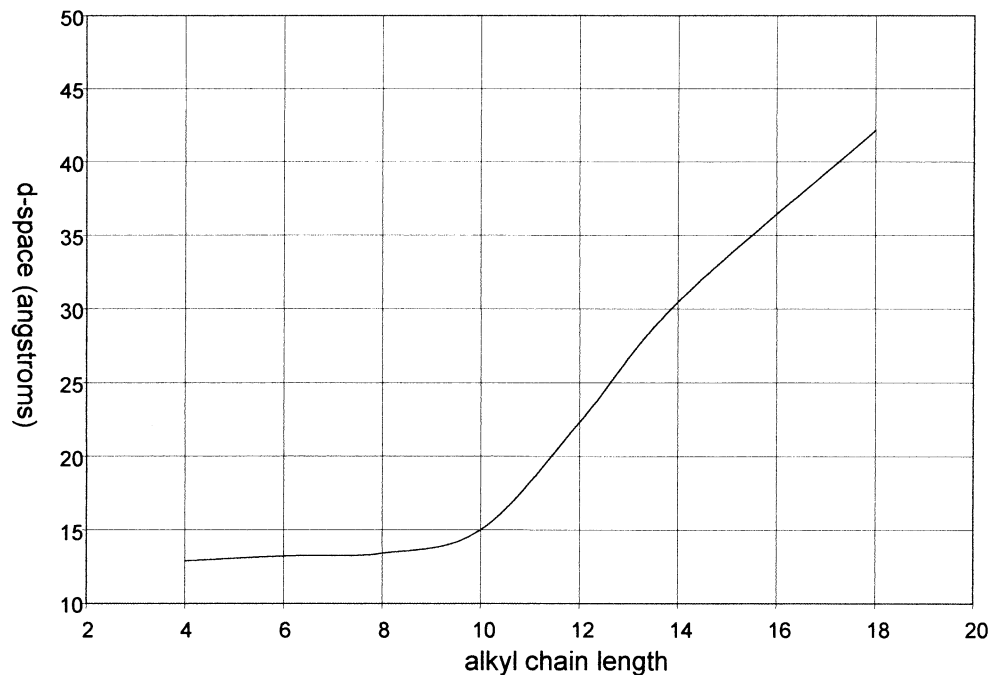


Figure 13: Alkyl chain length versus basal d-spacing in primary alcohol intercalated organoclays with 3 to 1 milliequivalent ratios

The dodecyl alcohol complex shows a significant effect on the d-spacing at all 3 loadings with an increase to 22 angstroms. This distance however still indicates that interdigitation is the most widely seen configuration since the dodecyl alcohol molecule is about 15 angstroms in length. There may be a great deal of molecules leaning or positioned parallel to the surface.

In the tetradecanol and octadecanol systems the basal d-space increased drastically at loading beyond 1 to 1. The octadecanol 3 to 1 organoclay displayed a d-spacing of 42 angstroms. This value is only slightly lower than the spacing expected if two molecules are stacked end to end. This result can only be achieved by the formation

of rigid post since the inter gallery free-volume space in the clay would allow for rearrangement and interdigitation without some enhancement to the molecular rigidity.

It is also interesting that the increase in the gallery spacing in the alcohol series seems to increase logarithmically between 8 and 10 carbons and linearly at 12 and above. It is assumed that additional length beyond 18 carbons may increase the d-spacing more but at some point measurement of this system becomes difficult at such a low 2θ angle. It is also probable that platelet exfoliation will occur at some d-space maximum but that is not known.

3.1.2 Aldehyde Organoclays

The aldehydes, as with the alcohol series, were chosen based on commercial availability. Butanal was selected as the smallest aldehyde and dodecanal was the longest. It was suspected that the carbonyl carbon of the aldehydes would function well in ion-dipole interaction due to its accessible lone pair electrons. The WAXD data show a minimal effect to the basal d-spacing over all lengths. The patterns indicate some low angle peaks in the decyl and dodecyl aldehydes. These peaks may indicate some interdigitation expanding the peaks but the increase does not follow a logical progression nor does it agree with predictions based on molecular dimensions.

3.1.3 Pyrrolidone Organoclays

The pyrrolidone series includes both straight N-alkyl pyrrolidones and other functional tail groups such as; hydroxyl, cyclohexyl, and phenyl pyrrolidone. The smallest pyrrolidone chosen was N-methyl pyrrolidone. N-methyl pyrrolidone (NMP)

was complexed to see if it was retained on the clay with ion-dipole interaction alone. The methyl functional group was believed to be too short to contribute to the stability with hydrogen interaction. The diffraction data suggest that the NMP associates well with the sodium ion and forms an assembled system. The peaks are very well pronounced (sharp) and in all three loadings indicate a d-spacing of 13 angstroms. This gallery size is the same as in hydrated clay but it also is in agreement with the molecular dimensions of NMP molecules positioned so that the ring is parallel to the surface.

In the N-octylpyrrolidone (OP) series the peaks were sharper and at smaller 2θ angles thus indicating an increase in the d-spacing. Figure 14 shows a comparison of the diffraction patterns for the 1 to 1, 2 to 1, and 3 to 1 milliequivalent ratios for OP. Note that the gallery spacing increases as the ratio increases. This supports the idea that the structural strength of the self-assembled rigid posts is improved from the 2 to 1 to the 3 to 1 system allowing the organic molecules to hold the clay platelets apart more effectively.

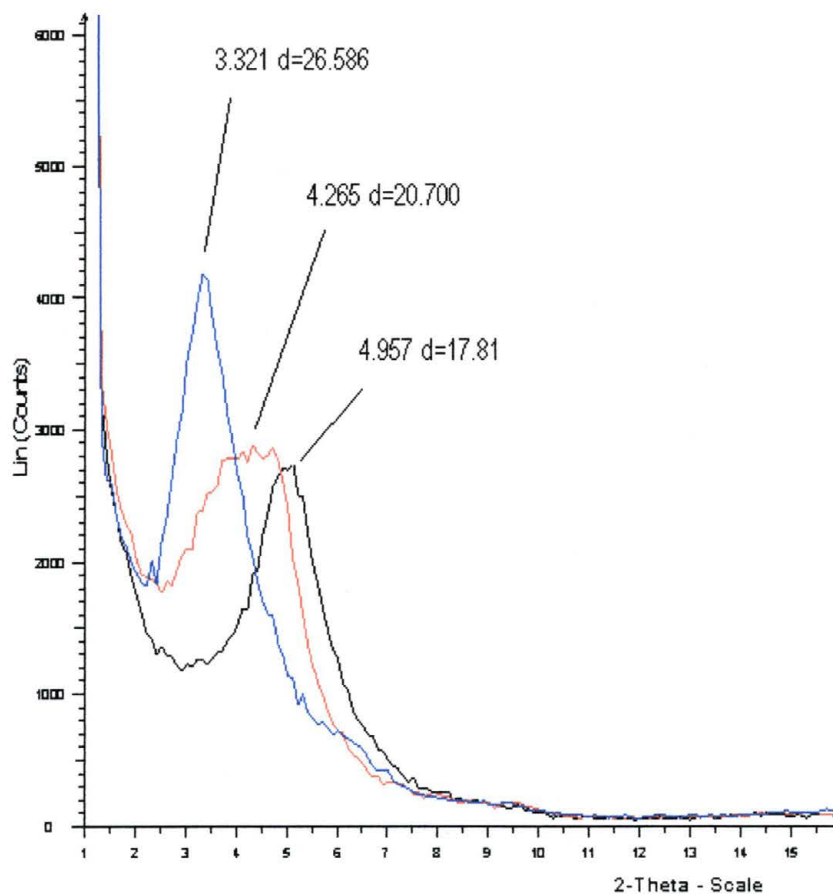


Figure 14: Comparison of N-octyl pyrrolidone intercalated organoclay series with 3 to 1 (blue), 2 to 1 (red), and 1 to 1 (black) milliequivalent ratios

The 3 to 1 peak is sharp indicating a good registry between plates in the sample. In the 2 to 1 sample the peak broadens, this is a result of greater variation in the sample's ordering. The gallery d-spacings are in agreement with the dimensions of the OP molecules. In the 3 to 1 sample a d-space of 2.66 nm corresponds to the distance occupied by two OP molecules end to end with their rings at a 90° angle to the chain (clay layer thickness = 0.91 nm). In the 2 to 1 sample the diffraction indicates a d-spacing of 2.07 nm. It is proposed that this is the effect of the posts leaning slightly since the free-

volume of this system is greater than that of the 3 to1 sample. The OP system shows good self-assembly around the sodium surface ions.

In the N-dodecyl pyrrolidone (DDP) system more pronounced self-assembly occurred. The peak intensities were considerably stronger and a greater amount of additional order peaks are visible. The DDP diffraction patterns for the 2 to1 and 3 to1 systems indicate a gallery spacing of 32 angstroms. This is in accord with the model dimension for the DDP system. A DDP molecule with its ring structure perpendicular to the chain has a length of about 12 angstroms. A second order peak can be seen in the diffraction pattern of the 3 to1 and 2 to1 milliequivalent ratio in the DDP system. The presence of additional orders of peaks in the pattern indicates a greater registry of platelets at that spacing and typically can be seen when the first order peak is at lower angles.

It is hypothesized that the addition chain length allows for greater stability resulting in less leaning. Figure 15 shows a comparison of the d-spacing in the 3 to1 loadings for the N-alkyl pyrrolidone series. Notice that there is good agreement with a linear progression as the chain length is increased.

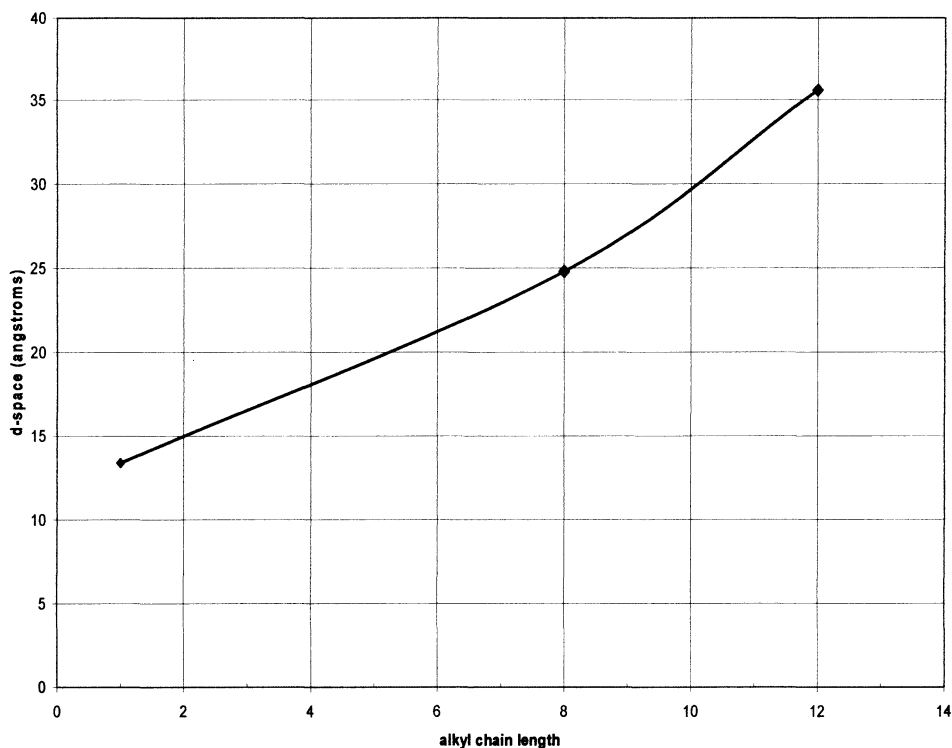


Figure 15: d-spaces of N-pyrrolidone intercalated organoclays at 3 to 1 milliequivalent ratios

Since the pyrrolidone head group shows the best potential for self-assembly, tail groups with other functionality were examined. The intercalation of sodium Cloisite with N-hydroxyethylpyrrolidone (HEP) was performed to measure the potential for ion-dipole competition between the pyrrolidone and hydroxyl functional groups and the sodium surface ions. Figure 16 shows the diffraction of the HEP series.

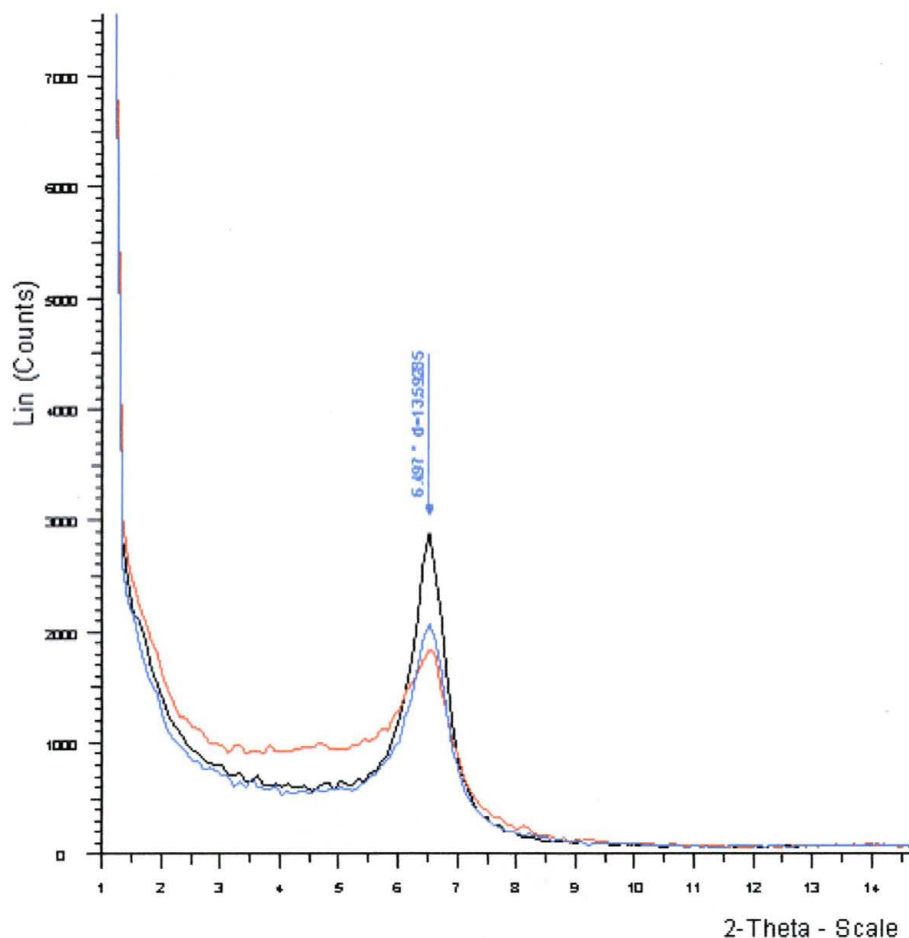


Figure 16: WAXD pattern for HEP intercalated organoclays; 3 to1 (black), 2 to1 (blue), and 1 to1 (red) milliequivalent ratios

It appears that varying the amount of modifier in this system has no effect on the gallery spacing. This supports the idea that both hydroxyl oxygen and the carbonyl oxygen of the pyrrolidone can form ion-dipole bonding with the surface ions and that when competing, no preference is noted. More study on this premise is required to fully understand the strengths of competing functionalities.

Systems of N-cyclohexyl pyrrolidone (CHP) and N-phenyl pyrrolidone (PP) were constructed to determine if interaction in the tail group of the modifier would effect the

ordering of the organoclay. In the CHP organoclay diffractions for 1 to1, 2 to1, and 3 to1 ratios, a shift in the peak was noted at loadings above 1 to1. Figure 17 indicates that some ordering is possible in the CHP system since the 1 to1 peak is broad.

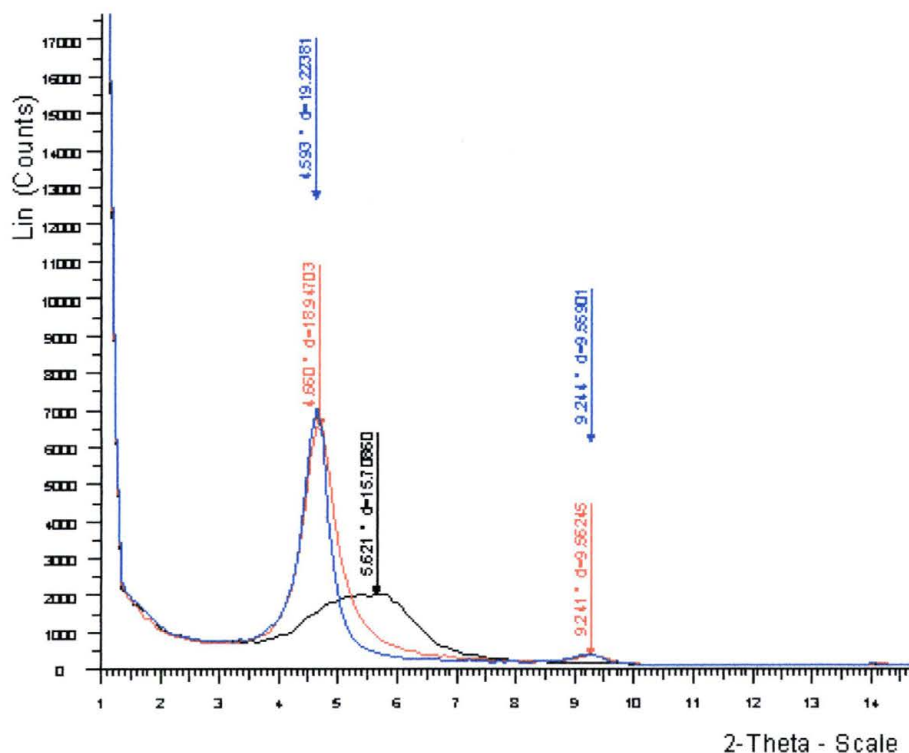


Figure 17: Diffraction patterns of the CHP intercalated organoclay; 3 to1 (blue), 2 to1 (red) and 1 to1 (black) milliequivalent ratios

The N-phenyl pyrrolidone intercalated system could demonstrate if π - electron interaction could result in a more ordered system. It was found that the PP molecules were too short to allow both ion-dipole interaction between the carbonyl oxygen and the resident ion and an effective π - electron interaction at the phenyl ring. The result in the model study was interesting in that the pairs of PP molecules arranged themselves in such

a way as to allow ion-dipole interaction at the sodium ion and some degree of π - electron interaction with the hydrogen in the ring of the pyrrolidone. Figure 18 is the diffraction pattern for 1 to1 and 2 to1 milliequivalent ratio organoclays. It is in agreement with the model predictions for the system at about 1.8 nm, but this fails to demonstrate if the pi- electron interaction can stabilize the tails of the organic modifiers.

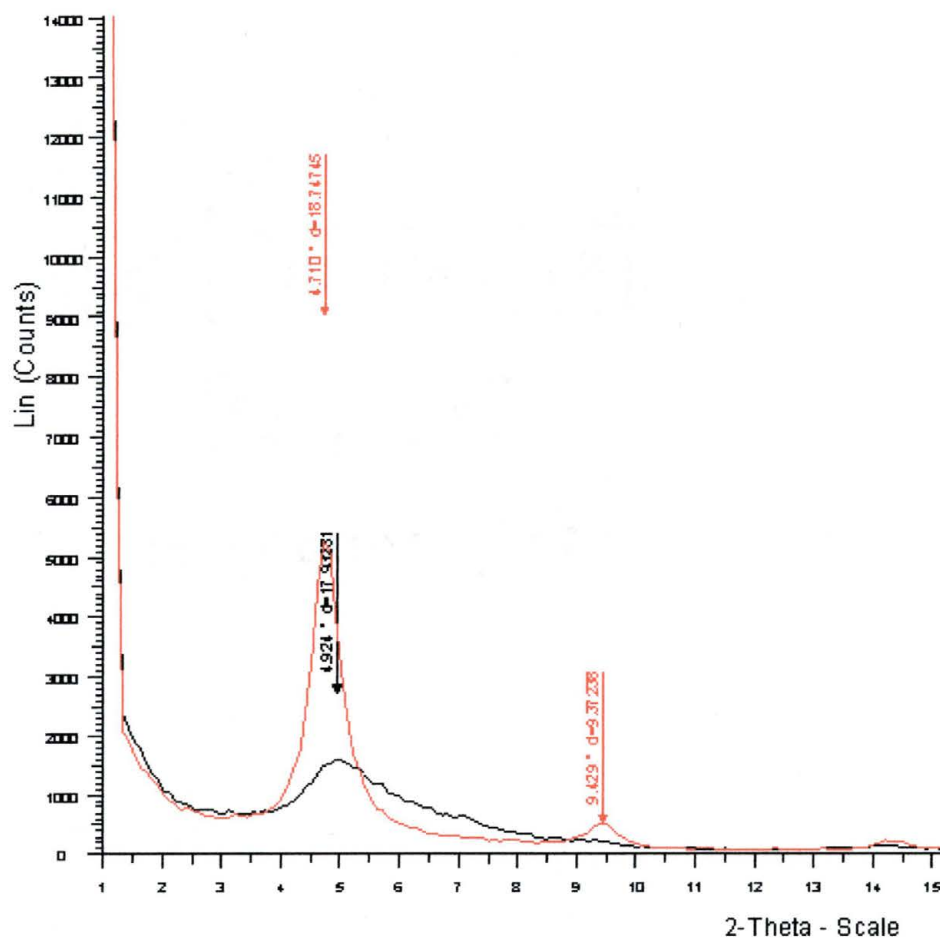


Figure 18: WAXD pattern for N-phenyl pyrrolidone intercalated organoclays; 2 to1 (red) and 1 to1 (black) milliequivalent ratios

Again, we see a second order peak in the 2 to1 system; this indicates a higher level of ordering than that of the 1to1 system. Both 1to1 and 2 to1 samples show greater gallery spacing than that of hydrated Cloisite alone.

3.2 Thermal Gravimetric Analysis (TGA)

Thermal analysis was carried out to determine the quantity of the organic intercalates adsorbed on the clay surface. The analysis also affords the opportunity to establish the amount of water in the sample, or the amount of hydration. The data were tabulated to show the relative amounts of organic components on the clay. In some of the samples it is evident that the amount of organic cannot be differentiated from the water due to the similarity of boiling points.

Organoclay	Ratio	Theoretical % Organic	Actual % Organic	% Variance	Actual % Water	Total Wt % Loss
Butyl Alcohol	1 to 1	6.8	11.3		*	16.4
Butyl Alcohol	2 to 1	12.3	12		*	17.6
Butyl Alcohol	3 to 1	18.2	13.3		*	17.9
Hexyl Alcohol	1 to 1	9.2	11.4	19.2	11.4	17.2
Hexyl Alcohol	2 to 1	16.9	11.4	32.5	5.7	16.8
Hexyl Alcohol	3 to 1	23.4	12.7	45.7	3.5	18.6
Octyl Alcohol	1 to 1	11.5	6.2	46	5.6	16.9
Octyl Alcohol	2 to 1	20.7	12.6	41.3	6.2	24.2
Octyl Alcohol	3 to 1	28.2	23.9	15.2	0.5	29.7
Decyl Alcohol	1 to 1	13.6	8	39.4	3.7	17.3
Decyl Alcohol	2 to 1	24	12.3	48.7	3.3	20.4
Decyl Alcohol	3 to 1	32.2	34.4	6.4	2.6	32.4
Dodecyl Alcohol	1 to 1	18.6	26.4	29.5	2.6	34.5
Dodecyl Alcohol	2 to 1	27.1	31.4	13.6	2.3	37.5
Dodecyl Alcohol	3 to 1	35.8	34.8	2.2	2.1	41.6
Tetradecyl Alcohol	1 to 1	17.6	9.3	47.1	8.4	22.6
Tetradecyl Alcohol	2 to 1	30	18.9	37	2.5	25.9
Tetradecyl Alcohol	3 to 1	39.1	32.9	15.8	5.5	42.6
Octadecyl Alcohol	1 to 1	21.3	22.4	4.9	5.6	31.8
Octadecyl Alcohol	2 to 1	35.1	32.3	7.9	3.4	41.4
Octadecyl Alcohol	3 to 1	44.8	42.3	5.5	3.7	49.1

* Boiling point of organic close to BP of water

Table 1: Thermal gravimetric analysis data of alcohol intercalated organoclays

Additionally, it is observed in Table 1, that when self-assembly is minimal or incomplete the ion-dipole bonding fails to retain the organic in the gallery. Many samples show a large variance between the amount of modifier added to the clay and the amount retained. The highest agreement in theoretical and actual organic percentage occurs in the longer alkyl chains. The evidence supports the hypothesis that if hydrophobic interaction between alkyl chains is favorable and occurring, the substance can be retained by this mechanistic state. If assembly cannot overcome the dynamics of the exfoliation process, the modifier simply leaves the intercalated clay and is subsequently washed out of the system. This interaction is due to Van der Waals attraction between hydrogens and nearby carbon, typically on a neighboring chain.

It is worthwhile to note that the water content of the alcohol intercalated organoclays decreases with increasing alkyl chain length. The water content is reduced even when the amount of the alcohol is not enough to saturate the system. This is due to a reduction in the available volume of the system. The water content is also reduced to a greater extent when more partial negative species compete for the surface ions. If the ion is crowded by stronger partial negative charges, as in hydroxyl end groups, the water molecules fail to associate and are forced out.

Table 2 contains TGA data about the aldehyde organoclays. In many samples the aldehyde modifiers show a greater ability to stay in the gallery of the clay. It is evident that the carbonyl functionality of the aldehyde surpasses the hydroxyl group in ionic interaction strength.

Organoclay	Ratio	Theoretical % Organic	Actual % Organic	% Variance	Actual % Water	Total Wt % Loss
Butyl Aldehyde	1 to 1	7.6	7.7			13.3
Butyl Aldehyde	2 to 1	12.5	8.5			13.5
Butyl Aldehyde	3 to 1	17.8	9.14			15.2
Hexyl Aldehyde	1 to 1	10.4	8.6	17.3	6.1	13.9
Hexyl Aldehyde	2 to 1	16.7	14.4	13.7	5.8	19.6
Hexyl Aldehyde	3 to 1	23.6	19.8	16.1	5.1	24.4
Octyl Aldehyde	1 to 1	11.3	7.5	33.6	6.5	18.1
Octyl Aldehyde	2 to 1	20.3	17.2	15.3	4.1	26.1
Octyl Aldehyde	3 to 1	27.4	22.8	16.7	2.7	29.5
Decyl Aldehyde	1 to 1	13.5	13.6	0.7	3	21.6
Decyl Aldehyde	2 to 1	23.8	24.2	1.6	2.6	31.2
Decyl Aldehyde	3 to 1	31.9	34.4	7.2	1.4	38.9
Dodecyl Aldehyde	1 to 1	15.5	16.1	3.7	3.5	24.1
Dodecyl Aldehyde	2 to 1	27	25.7	4.8	1.9	32.1
Dodecyl Aldehyde	3 to 1	36.1	35.4	1.9	2.3	35.3

* Boiling point of organic close to Bp of water

Table 2: Thermal gravimetric analysis data of aldehyde intercalated organoclays

There appears to be little or no correlation between the number of aldehydes present relative to the milliequivalent sodium and their propensity to remain on the clay. The general trend of increasing alkyl chain length supporting higher percentage of organic present is the same as in the alcohol series. This supports the claim that Van der Waals interaction between the chains is a strong contributing factor in the self-assembly.

Organoclay	Ratio	Theoretical % Organic	Actual % Organic	% Variance	Actual % Water	Total Wt % Loss
Methyl Pyrrolidone	1 to 1	9	9.6	6.2	2.2	17.3
Methyl Pyrrolidone	2 to 1	16.5	10.6	36	3.5	21.3
Methyl Pyrrolidone	3 to 1	22.9	11.5	50	2.4	19.4
Octyl Pyrrolidone	1 to 1	16.3	16.3	0	2.4	23.3
Octyl Pyrrolidone	2 to 1	27.6	24.9	9.7	0.9	30.2
Octyl Pyrrolidone	3 to 1	37.8	30.9	18.2	0.4	35.6
Dodecyl Pyrrolidone	1 to 1	20.2	22	8.1	2.2	27.8
Dodecyl Pyrrolidone	2 to 1	28.3	35.8	20.9	0.9	35.6
Dodecyl Pyrrolidone	3 to 1	43.2	43.1	0.2	0.7	47.3
Cyclohexyl Pyrrolidone	1 to 1	14.5	12.2	5.6	5.6	24.3
Cyclohexyl Pyrrolidone	2 to 1	25	17.2	31	1.8	23
Phenyl Pyrrolidone	1 to 1	13.7	11.8	13.8	5.1	23.5
Phenyl Pyrrolidone	2 to 1	24.2	19.3	20.2	3.3	28.3
Hydroxy-ethyl Pyrrolidone	1 to 1	11.4	10.6	7	4.5	20.1
Hydroxy-ethyl Pyrrolidone	2 to 1	20.5	16.9	17.5	3.9	25.6

Table 3: Thermal gravimetric analysis of pyrrolidone intercalated organoclays

The pyrrolidone samples contain other tail group functionalities because they appear to be the best at ion dipole interaction with the surface cation. Table 3 shows that the length of the alkyl chain tail group again supports a greater degree of retention. At only eight carbons the chain shows significant retention. It is also important to see that the group in general, supports the highest amount of self-assembly. This assembly is most likely improved due to the pyrrolidone function group geometry.

3.3 Organoclay Stability

It was discovered during the course of this research that the self assembled system may be unstable and over time the expanded gallery space may collapse. It was also discovered that in samples where the normal melting point of the organic intercalate was greater than ambient room temperature a delayed recrystallization of the organic component was occurring. When the organoclays were formed there was little or no evidence for the formation of crystalline structures in the samples but after a period of two years WAXD indicates the presence of organic crystalline structures with distinct morphologies. These morphological changes were seen in a study conducted on long chain primary alcohols by Ventolà *et al.*³⁶ WAXD of the pure organic crystal was conducted to compare with the WAXD of these crystal structures in the aged organoclay samples. The change in the kinetics of this type of recrystallization is not fully understood, but there seems to be a collapse of the inter-gallery space to a distance comparable to the normal hydrated state. The WAXD of the aged organoclays indicates strongly that in cases where there were previously self-assembled structures these clays show a collapsed state with smaller gallery spacing. It is not known if the existing self-

assembled posts have fully disassembled or if they have assumed a position parallel to the sheets since there was no quantification of the recrystallized material. The reduction of the basal d-space in the aged samples provides additional evidence that the self-assembly of the organic intercalates is the source of the expanded clay layers.

Figure 19 shows the characteristic crystalline peaks evidenced in the diffractions of both the aged organoclay and in the pure organic intercalate. The small peak that can be seen at 2.30 degrees 2θ in both diffraction patterns is a crystalline peak of the octadecanol. The main basal d-space peak in the organoclay scan conceals two of the crystallized alcohol peaks at 4.2 and 6.2 degrees 2θ . The high angle peaks beyond 20 degrees 2θ in both scans matches very well.

In comparison of the organoclay scans from when the clays were produced and the aged clay we see a definite change in the main peak location. Figure 20 indicates a reduction in the gallery space after 2 years of storage. The gallery in this system has collapsed more than 1.5 angstroms, an 11% reduction. The crystalline peaks of the organic are not as evident.

In the case of the N-substituted pyrrolidone series the collapse is much less evident with a reduction in d-space of less than 10%. This further suggests that the pyrrolidone functional group is optimal for the self-assembly of the alkyl chains. In Table 4 it is seen that the N-substituted pyrrolidone organoclays have retained their self-assembled character over time. It is not clear how rapidly the alcohols, and aldehydes to a lesser extent, have lost their organization.

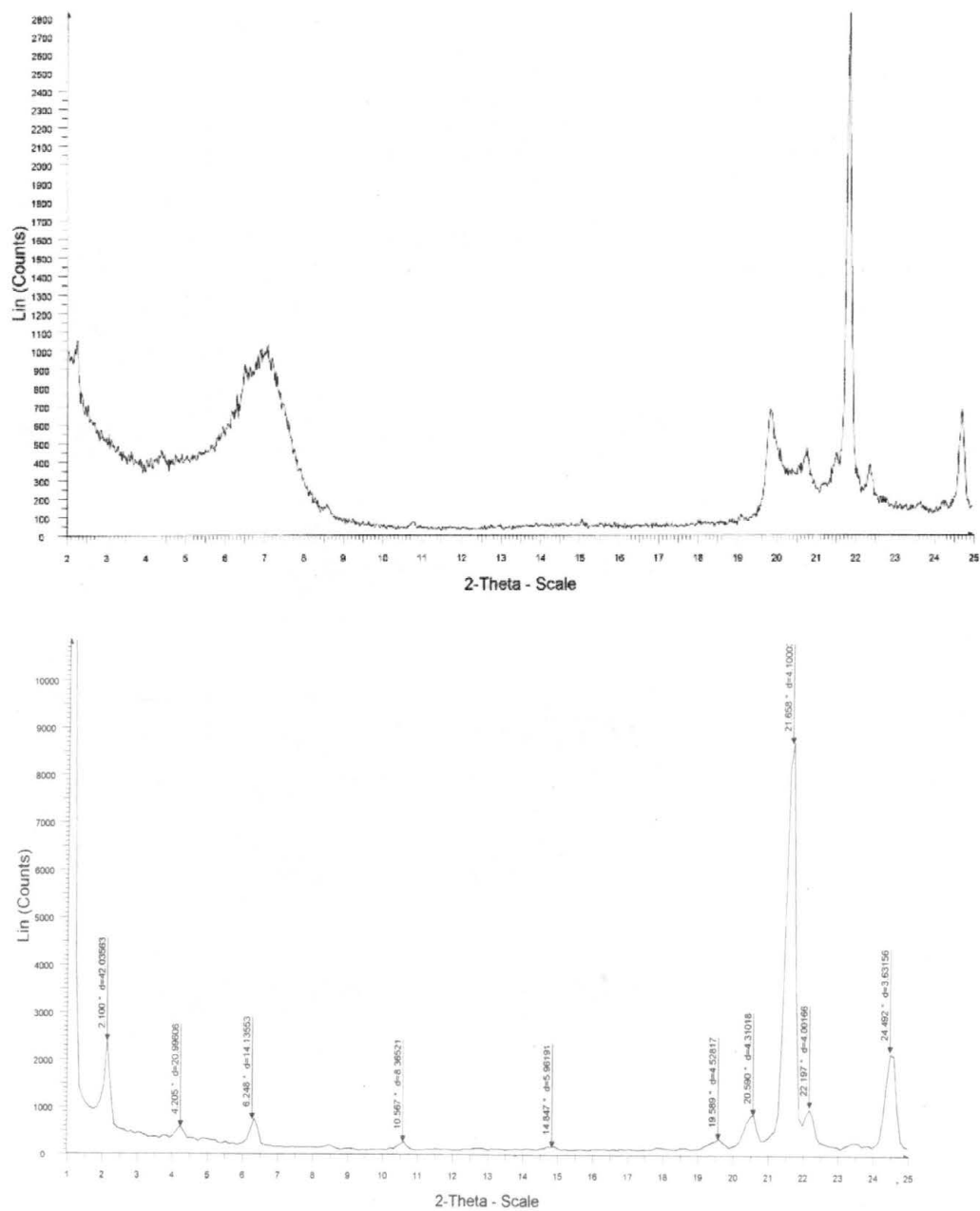


Figure 19: Comparison of WAXD for the octadecanol intercalated organoclay (top) and pure octadecanol (bottom)

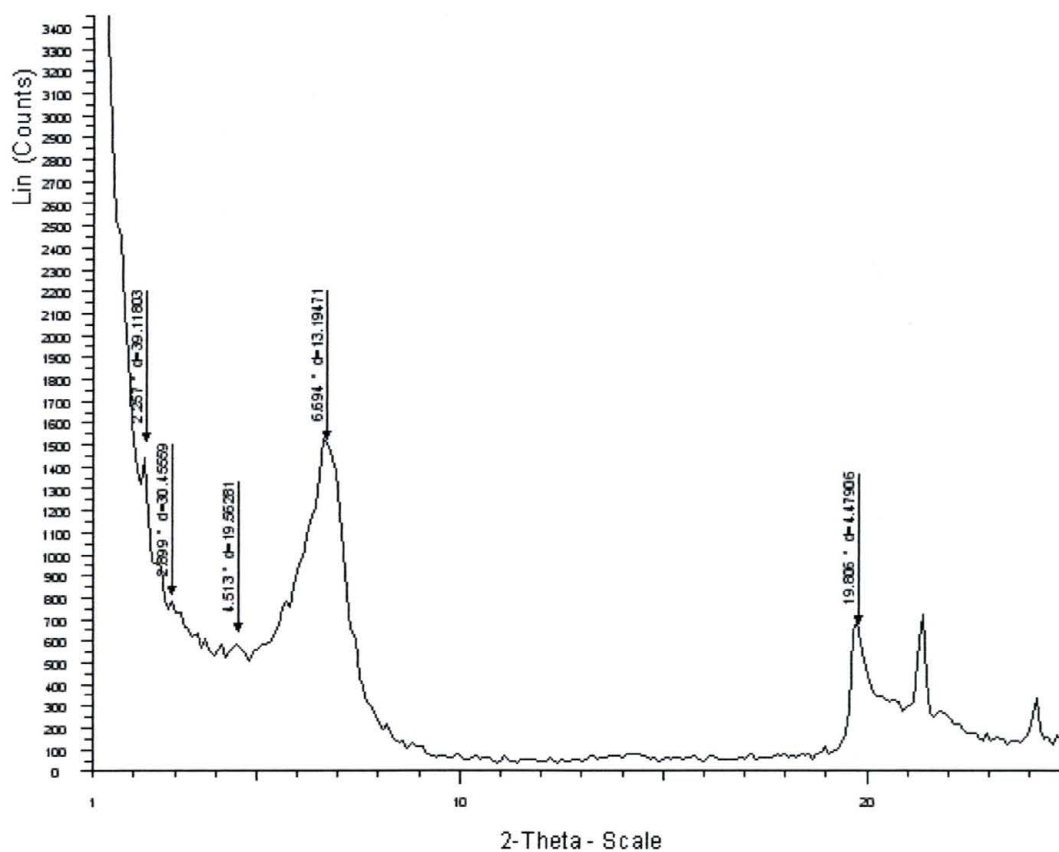
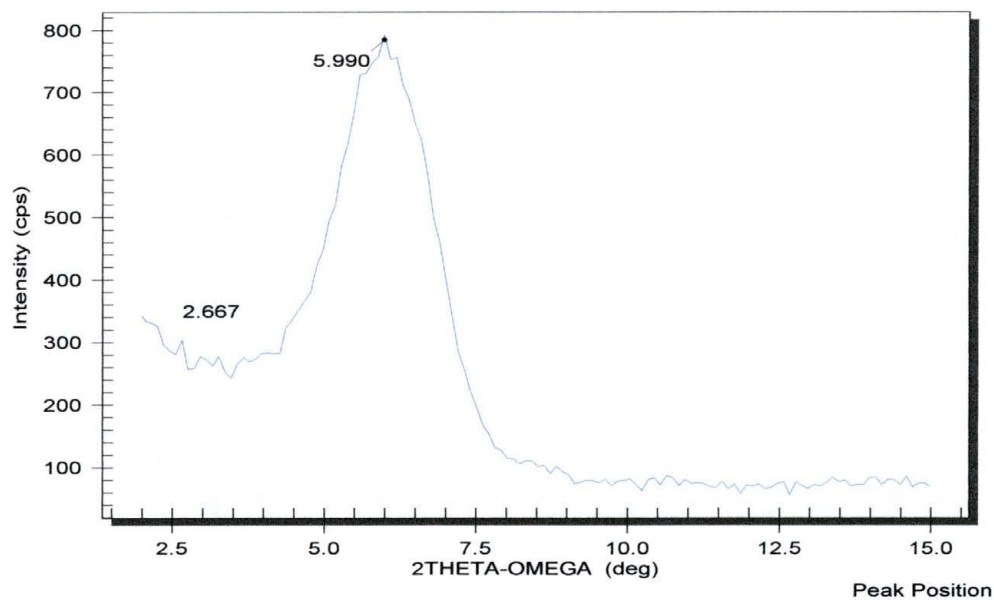


Figure 20: Comparison of the WAXD of fresh (top) and aged (bottom) tetradecanol at a 3 to1 milliequivalent ratio

	Bede Diffraction Data			BrukerAXS Diffraction Data		Crystalline peaks in aged sample
Organoclay	2 θ angle	d-space (main)		2 θ angle	d-space	2 θ angle
Decyl alc. 1 to1	5.9	14.9816324		6.875	12.865104	
Decyl alc. 2 to1	6.05	14.61151759		6.82	12.968359	
Decyl alc. 3 to1	5.09	17.35789143		5.882	15.027317	1.907
Dodecyl alc. 1 to1	5.87	15.05792939		4.062	21.740388	
Dodecyl alc. 2 to1	3.239	27.25610214		6.218	14.218228	1.6
Dodecyl alc. 3 to1	3.04	29.03845837		6.163	14.344618	1.601
Tetradecyl alc. 1 to1	6.583	13.43307469		6.917	12.787364	
Tetradecyl alc. 2 to1	5.99	14.75733505		6.671	13.256659	
Tetradecyl alc. 3 to1	6	14.73282924		6.694	13.211317	2.25
Octadecyl alc. 1 to1	6.837	12.93626583		6.906	12.807633	
Octadecyl alc. 2 to1	3.88	22.75849882		6.932	12.759828	2.21
Octadecyl alc. 3 to1	3.133	28.17730192		6.99	12.654472	2.23
Decyl ald. 1 to1	6.691	13.2172131		6.7	13.199539	
Decyl ald. 2 to1	6.6	13.39862693		3.113	28.358152	3.11
Decyl ald. 3 to1	5.933	14.89859848		3.8	23.2369	3.8
Dodecyl ald. 1 to1	6.617	13.36435657		6.758	13.086775	2.7
Dodecyl ald. 2 to1	6.609	13.38046179		6.724	13.152642	2.7
Dodecyl ald. 3 to1	6.674	13.25072698		6.758	13.086775	2.724
N-methyl pyr. 1 to1	6.663	13.27250376		6.741	13.119625	
N-methyl pyr. 2 to1	6.634	13.33026224		6.74	13.121562	
N-methyl pyr. 3 to1	6.613	13.3724043		6.754	13.094489	
N-octyl pyr. 1 to1	4.696	18.81055487		5.058	17.46742	
N-octyl pyr. 2 to1	4.048	21.81545173		3.929	22.475106	
N-octyl pyr. 3 to1	3.56	24.80120778		3.338	26.448602	
N-dodecyl pyr. 1 to1	2.778	31.77468714		3.135	28.159344	
N-dodecyl pyr. 2 to1	2.721	32.43979273		2.586	34.132044	
N-dodecyl pyr. 3 to1	2.481	35.57560682		2.773	31.831935	
N-Cyclohexyl pyr. 1 to1	-	-		5.739	15.400456	
N-Cyclohexyl pyr. 2 to1	-	-		4.681	18.870697	
N-Cyclohexyl pyr . 3 to1	-	-		4.606	19.177293	
N-phenyl pyr. 1 to1	-	-		4.967	17.786615	
N-phenyl pyr. 2 to1	-	-		4.733	18.663835	
N-HEP 1 to1	-	-		6.483	13.639374	
N-HEP 2 to1	-	-		6.539	13.523067	
N-HEP 3 to1	-	-		6.5	13.603854	

Table 4: WAXD data of selected fresh and aged organoclay samples

3.4 Molecular Modeling

Molecular models were constructed for many of the modified organoclays to form predictions of the behavior of the system. The models provided a basic numerical value of the basal d-space based on the minimum energy obtainable through repetitive iteration of molecular dynamics. The strongest prediction seen in the molecular modeling was the spatial organization of the N-substituted pyrrolidone molecules. The five-member ring of the pyrrolidone is shown to be capable of organizing parallel to the clay surface while its alkyl chain tail orients up, away from the clay. This orientation is noted in Figure 21. The orientation of these tail groups provides a better chance for molecules to find their neighbors for Van der Waals interactions. In the small tail groups, 1 to 6 carbons in length, there is little flexibility to allow both ion-dipole interaction and hydrogen-carbon chain interactions.

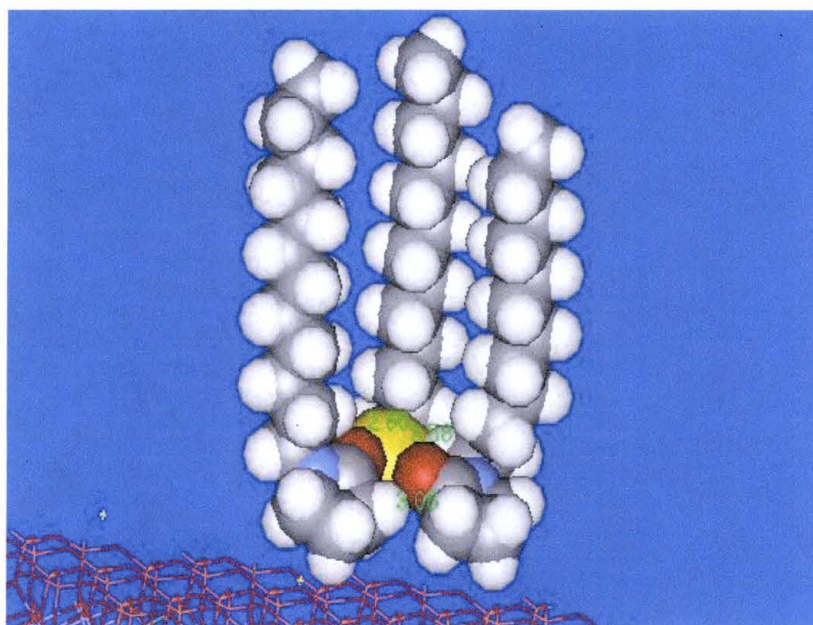


Figure 21: Ion-dipole interaction between the organic modifiers and the resident sodium ion

The partial negative oxygen atom of the pyrrolidone head group is attracted to the positive charged sodium ion. The average distance between the oxygen atom and the sodium ion is 2 to 3.5 angstroms. At this distance the alkyl chains are arranged so that the hydrogen-carbon Van der Waals interaction distance is about 4 angstroms which is in good agreement with the cross sectional methyl carbon group radius, which is 2 angstroms.

In the aldehyde series there appears to be a general interdigitation of the system. This interdigitation is characterized in the model as a random distribution of molecules in the gallery. It was found that these molecules are not lost due to ineffective self-assembly which was originally believed. The presence of the modifier in the interdigitated state greatly reduces the free-volume of the system. At 3 to 1 milliequivalence with the sodium ion the free volume was calculated to be only 7.0 percent. This is much less than that of a self-assembled system. Figure 22 shows a fully interdigitated system.

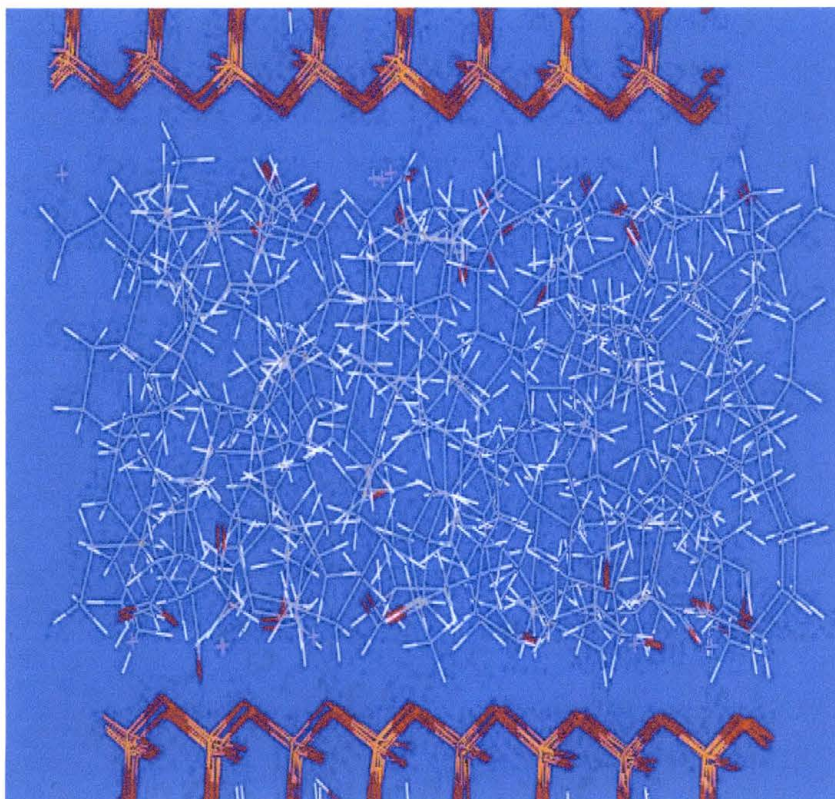


Figure 22: Model of dodecyl aldehyde on MMT

The molecular modeling also indicates that an organic modifier containing a pyrrolidone head group and a biphenyl moiety shows exceptional self-assembly. The biphenyl functionality, being liquid crystalline in nature can be expected to interact through considerable π - electron interaction. This interaction was shown to enable a large amount of self-assembly.

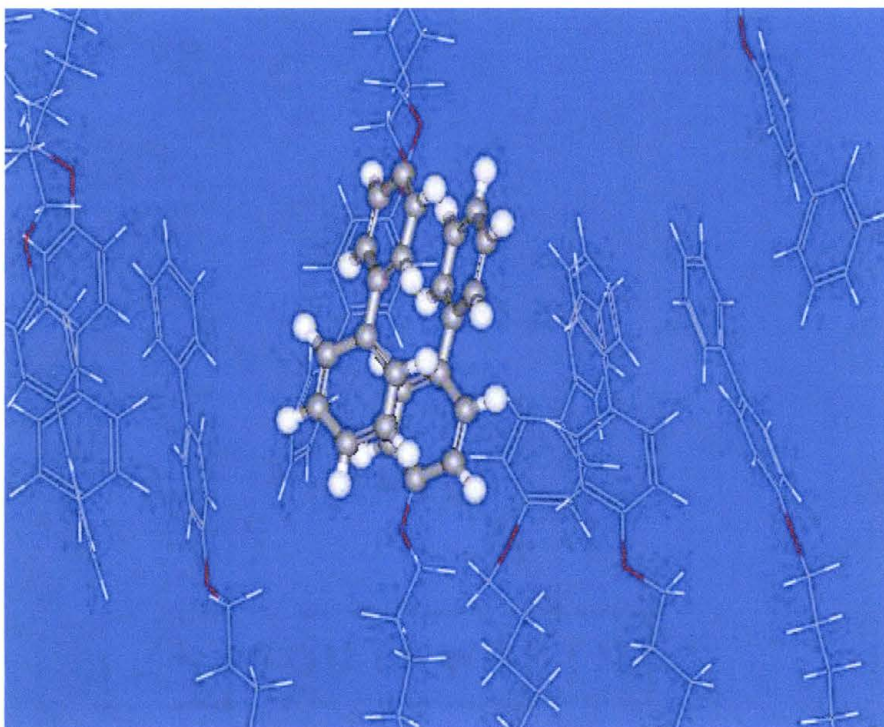


Figure 23: π -Electron interaction between biphenyl moieties

In an organoclay system where organic molecules are sparse, as in the 1 to 1 milliequivalent ratio to the sodium ions, the organic molecules from the top of one sheet and the molecules from the bottom of another sheet could partially interdigitate to form π - electron interaction between them. Figures 23 and 24 are examples of this behavior. This is seen commonly in mesogenic pendant groups in polymeric systems.³⁵

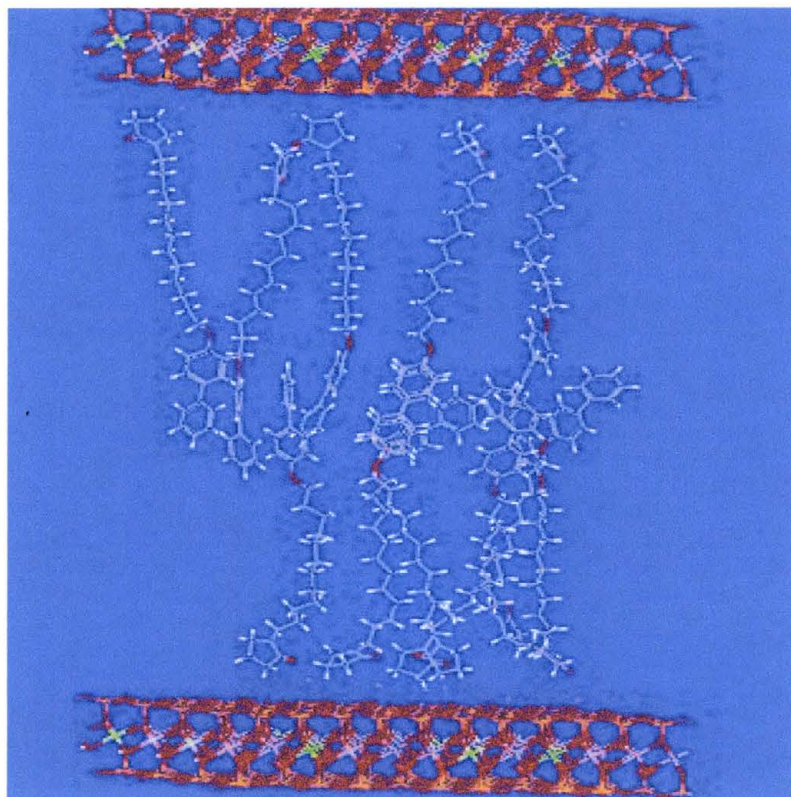


Figure 24: Partial interdigitation of biphenyl functional groups

It can be seen from the model that the alkyl chain spacers tend to stay fairly rigid even without any hydrogen interaction, but some instances of bending result in a reduction of the gallery space from that of purely dimensional calculations.

When the system was loaded to a 3 to 1 ratio the free volume space was significantly reduced. At this loading the layers of organics were unable to interdigitate due to a lack of room for movement. The energy minimum suggests a configuration as in Figure 25. The basal d-space of this model is predicted to be 6.30 nm.

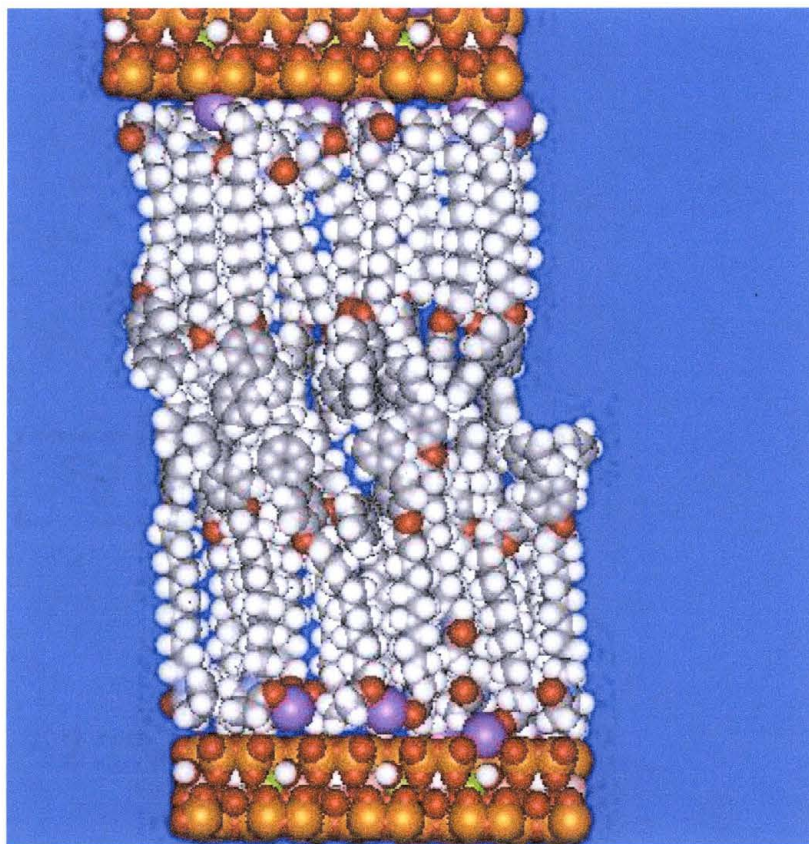


Figure 25: Space filling model of 3to1 ratio of 1-[12-(biphenyl-4-yloxy)-dodecyl]-pyrrolidin-2-one organoclay

A heavily loaded system, as in the 3 to 1 ratio, seems to result in much more rigidity in the alkyl spacer. This again is due to hydrogen interaction between the chains. It is not clear if a gallery space of 63 angstrom is possible. It would be nearly undetectable in a first order XRD since the 2θ angle would be very small. If the diffractometer shows orders beyond 1st order then it would be measurable.

Overall the predictions set by the molecular modeling gives a reasonable picture of the actual system. As with any simplification, errors occur frequently especially when multiple aspects of the model deviate from real conditions. Table 5 is a comparison of

the model predicted d-spaces based on minimum energy, and the WAXD obtained from the experimental sample.

Organoclay System	Predicted d-space	Experimentally determined d-space
Butyl Alcohol 3 to1	12	12.65
Hexyl Alcohol 3 to1	12.5	12.3
Octyl Alcohol 3 to1	13.5	12.54
Decyl Alcohol 3 to1	20	14.88
Dodecyl Alcohol 3 to1	29	29.03
Tetradecyl Alcohol 3 to1	37	40.52
Octadecyl Alcohol 3 to1	40	31.83
Hexyl Aldehyde 1 to1	12.5	12.63
Hexyl Aldehyde 2 to1	12.5	12.37
Hexyl Aldehyde 3 to1	13.5	12.42
Dodecyl Aldehyde 1 to1	12	13.3
Dodecyl Aldehyde 2 to1	13.5	13.38
Dodecyl Aldehyde 3 to1	13	13.25
N-Methyl Pyr. 3 to1	13	13.37
N-Octyl Pyr. 2 to1	18	21.8
N-Octyl Pyr. 3 to1	21.5	24.8
N-Dodecyl Pyr. 1 to1	18	31.7
N-Dodecyl Pyr. 2 to1	29	32.44
N-Dodecyl Pyr. 3 to1	41	35.58
N-Cyclo-hexyl Pyr. 1 to1	12	15.39
N-Cyclo-hexyl Pyr. 2 to1	12.5	18.86
N-Phenyl Pyr. 1 to1	12.5	17.71
N-Phenyl Pyr. 2 to1	17	18.65
N-Biphenyl Ether Butyl Pyr. 3 to1	31	NA
N-Biphenyl Ether Dodecyl Pyr. 3 to1	62.5	NA

Measurements in Angstroms.

Table 5: Comparison of molecular modeling and experimental WAXD data for selected samples

The results of the molecular modeling were very promising for the N-(diphenyl ether alkyl) pyrrolidone intercalated organoclay; however, no WAXD was performed due to the inability to isolate a sufficient amount to make an intercalated organoclay sample.

3.5 Organic Synthesis

Two independent schemes were utilized to synthesize a series of biphenyl-pyrrolidone ethers. The molecules possess a pyrrolidone functional group at one end to facilitate the ion-dipole interaction with the resident cations on a smectic surface. The biphenyl functional group is located on the other end of an alkyl chain that is attached at the nitrogen atom of the pyrrolidone ring. An ether linkage connects the alkyl chain to the biphenyl *para* to the terminal ring. The series of molecules have alkyl chains from 2 to 12 carbons in length. Although numerous attempts using both methods were made the quantity and purity of the target molecule was insufficient to form organoclays. Figure 26 is a series of infrared spectra of the N-hydroxypyrrolidones formed in the second scheme. The reaction between γ -butyrolactone and the amino alcohol to form the pyrrolidone is currently being verified. The series is of N-hydroxyethylpyrrolidone (from stock), N-hydroxybutyl, and N-hydroxyhexylpyrrolidone. All three samples show a characteristic broad O-H stretch at 3400 cm^{-1} and a peak at 1670 cm^{-1} indicating a C=O stretch. It would be difficult to determine if a N-H stretch peak is present due to overlap of the O-H stretch. The presence of the N-H stretch could confirm the presence of unreacted amino alcohol. The O-H stretch, aliphatic C-H stretch at 2920 cm^{-1} , the accompanying C=O stretch, and the similarity between the synthesized samples and the stock solution helps to confirm the success of the reaction.

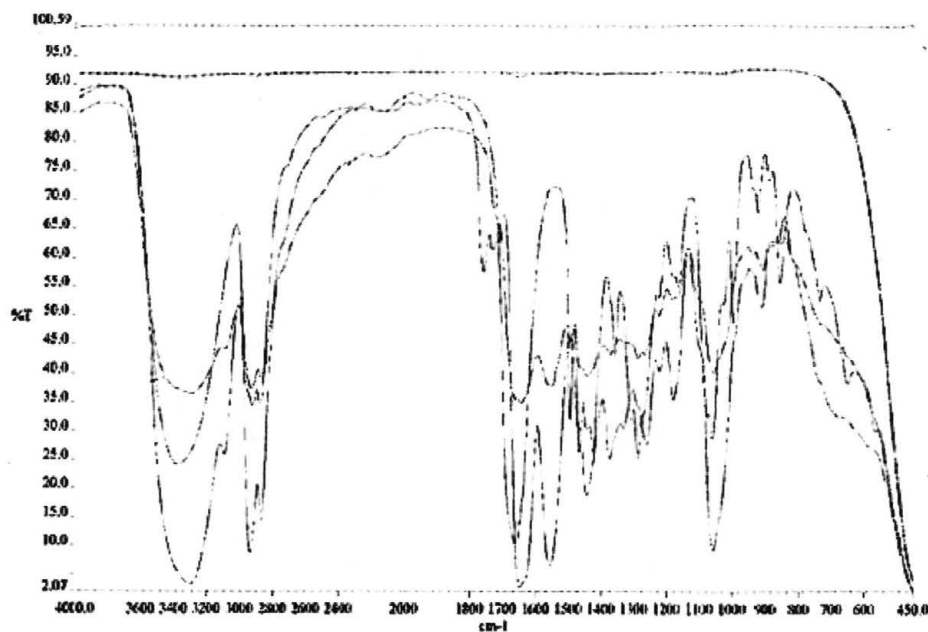


Figure 26: IR spectra of a series of hydroxypyrrolidones

Further evidence was sought by use of proton NMR to verify the N-hydroxy(alkyl) pyrrolidone was made. Figure 27 is a ^1H NMR of N-hydroxydodecyl pyrrolidone synthesized in the lab. The presence of the peak above 7 ppm and the doublet at 4.3 ppm are unexplainable. The peak at 4 is the hydroxyl proton and the 5 other peaks fit for the molecule. This evidence is very poor and indicative of gross impurity.

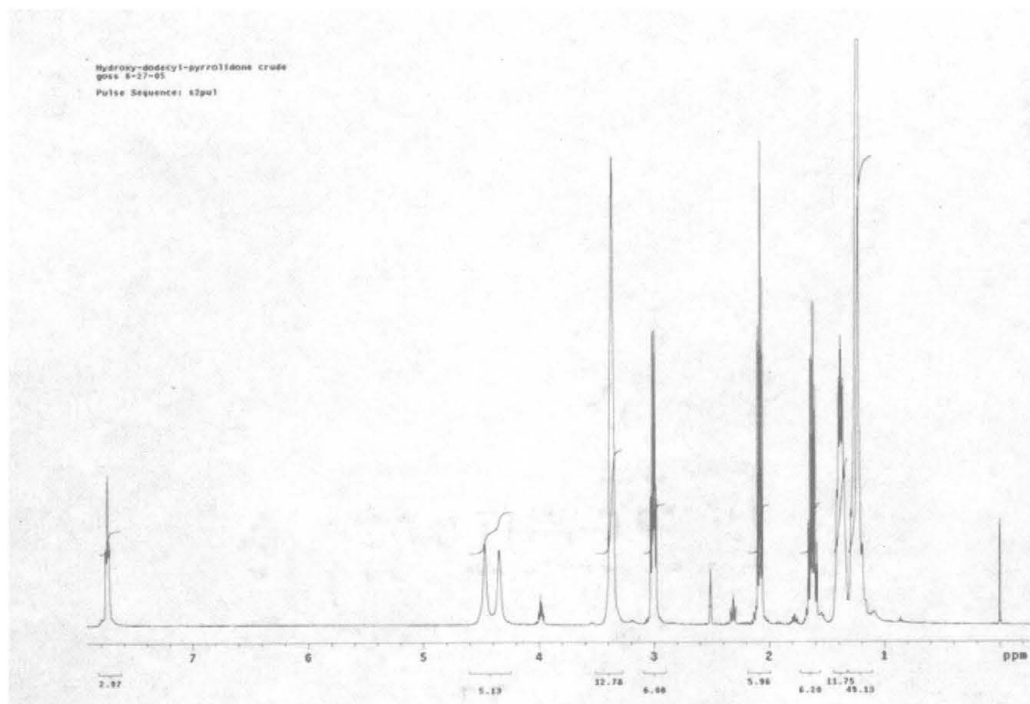


Figure 27: ^1H NMR of hydroxydodecylpyrrolidone

Proton NMR was used to determine the success of the ether synthesis. The aromatic protons of the biphenyl display resonance in the 7-8 ppm range and the hydroxy proton, around 4 ppm, disappears from the spectra. The pyrrolidone hydrogens will go unchanged from the hydroxy form and some downfield shift will be evident in the protons alpha to the ether oxygen. Figure 28 is the ^1H NMR of the 1-[4-(Biphenyl-4-yloxy)-butyl]-pyrrolidin-2-one product.

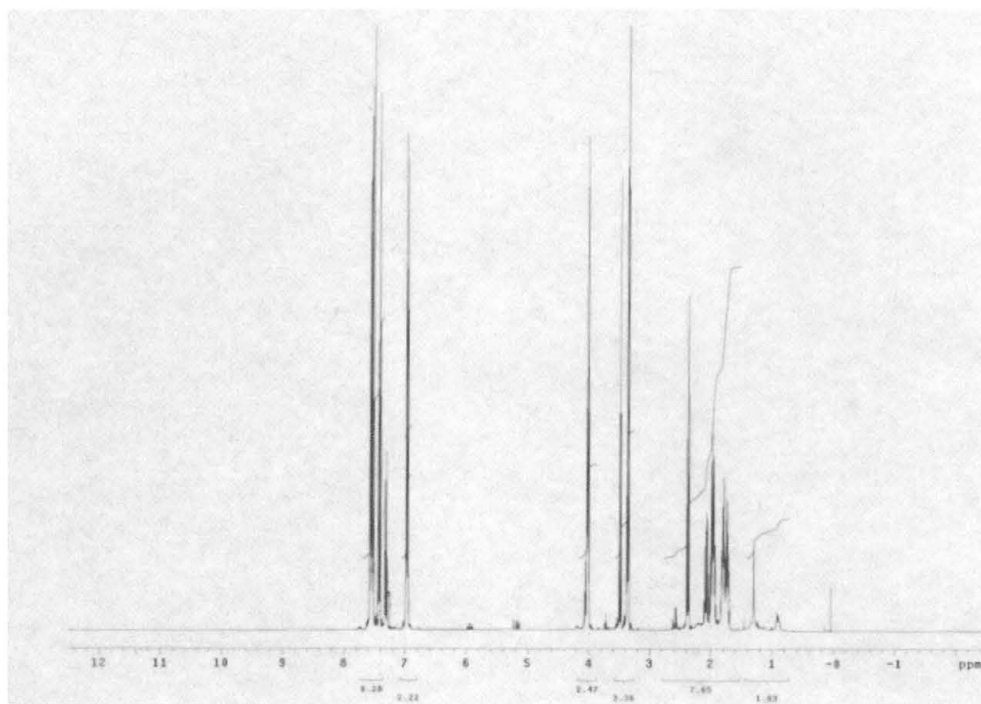


Figure 28: ^1H NMR of 1-[4-(Biphenyl-4-yloxy)-butyl]-pyrrolidin-2-one product

The spectrum indicates the presence of the biphenyl and the pyrrolidone protons but there are still a number of anomalies that suggest that the product is impure. The large peak at 4 ppm does not fit with the expectation for the target molecule as well as the peak at 1.2 ppm. The small peaks around 5 ppm and 6 ppm are also not part of the desired product. Overall the spectra collected in this research supports minimal success of this synthesis.

Considerable improvements in the purification steps will be required before adequate proof of synthesis is realized. More exacting laboratory practices, better moisture control and other reaction parameters will be needed to accomplish this synthesis. Some refinement in the separation of the product is also needed including a greater ability to separate micelles in solution as this is suspected in this synthesis due to the polarity differences at each end of the molecule.

4.0 CONCLUSIONS

One method of organically modifying smectic clay is to utilize an ion-dipole approach to form a macrostructure of rigid posts centered around surface sodium ions on the clay platelet surfaces. This research has identified two aspects that play a key role in these self-assembled structures. The structure of the polar head group directs the position of the molecule with respect to the ions. Evidence suggests that a terminal pyrrolidone functional group aligns the organic intercalate to optimize the other contributing force, hydrogen interaction in an alkyl chain tail. The length of the tail group plays a part in so far as increases in tail length correspond to improved rigidity, and stability. This increase directly affects the basal d-space of the clay. Many of the organoclay samples show X-ray diffraction patterns that indicate gallery spaces corresponding to the distance occupied by end-to-end positioning of the organic molecules. This end-to-end arrangement can be accomplished only by rigid steric hindrance preventing interdigitation. The alcohol and aldehyde organics were not as effective as the pyrrolidone in this respect.

This research also sought to identify the effectiveness of π -electron interaction between aromatic ring structures on the organic modifier tail for adding stability to the macrostructures. In N-phenyl pyrrolidone it was suggested that the presence of π -electron interaction was minimal due to the molecules inability to flex into an accommodating position. The synthesis of a series of molecules containing both the

pyrrolidone head group and a biphenyl tail separated by an alkyl tail containing an ether linkage was attempted. The result of this synthesis was that there were insufficient quantities to intercalate into clay. It was believed that some product was obtained but that isolation was minimal at best. The research concluded that this system had a high potential for agreement with molecular modeling results, but that could not be confirmed.

It was also discovered that the organoclay species can reorder or collapse over time. The organic modifier was shown to have recrystallized in the sample with the gallery spacing collapsing to a smaller distance than when the organoclay was fresh. This further demonstrates that self-assembly of these species was responsible for the large basal d-space. The rate at which this reordering occurs was not determined. It is unclear what percentage of the organic modifier remains in the gallery after recrystallization occurs or how much hydration of the clays results when the organic leaches out.

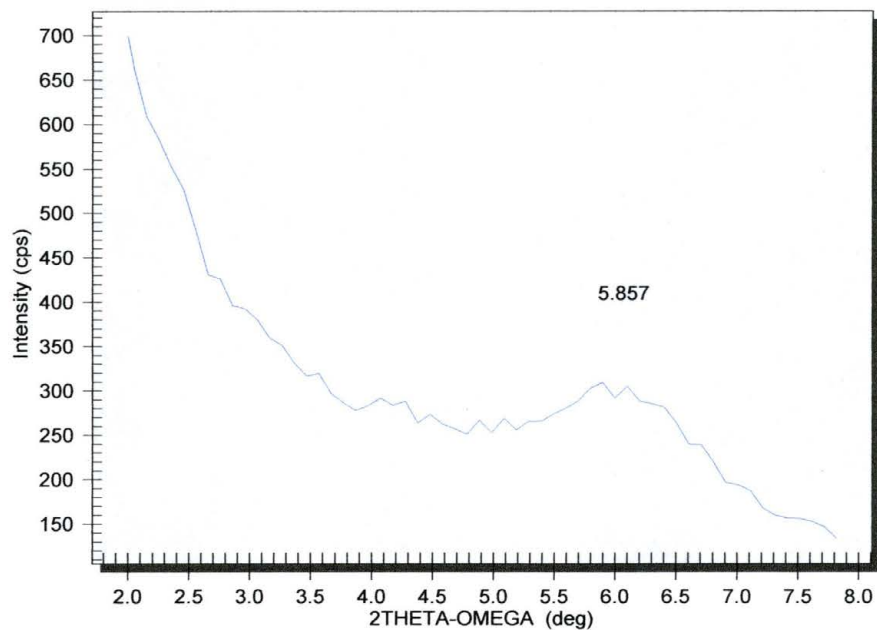
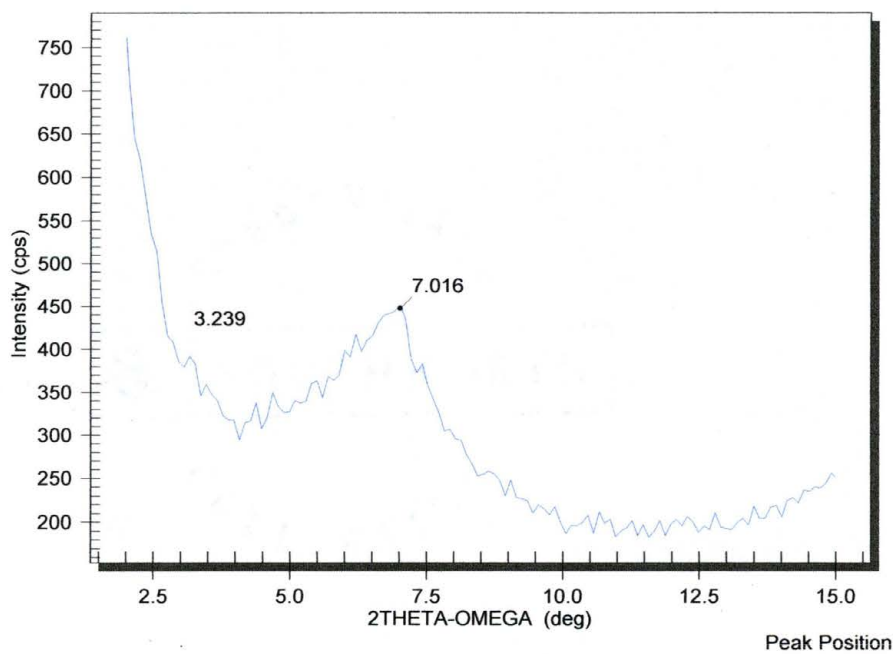
These results further support that the stability of the self-assembly is greatest for a pyrrolidone head group, with alcohols forming metastable self-assembled systems, and the aldehydes not forming self-assembled structures at all.

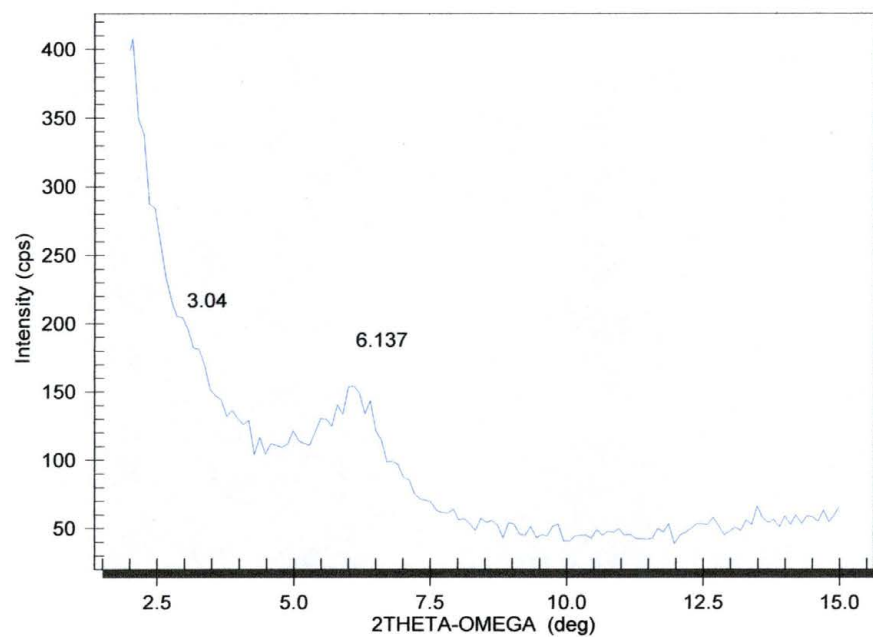
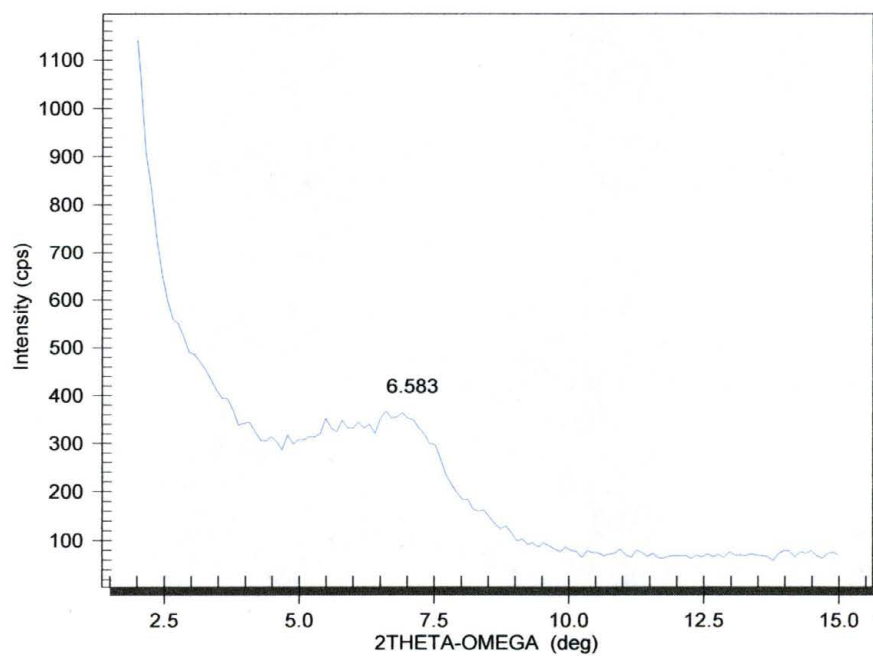
Future work on this project should include the study of these self-assembled posts on vermiculite clay where an ordered array might be achievable. Additionally, some experimentation could be performed to assess the ability of this type of clay modification in providing compatible chemistry to allow clay exfoliation into polymer systems. There is some evidence to suggest that a liquid crystalline array might be able to be intercalated *via* ion-dipole interaction if the oligomers contained pyrrolidone pendant groups *trans* to

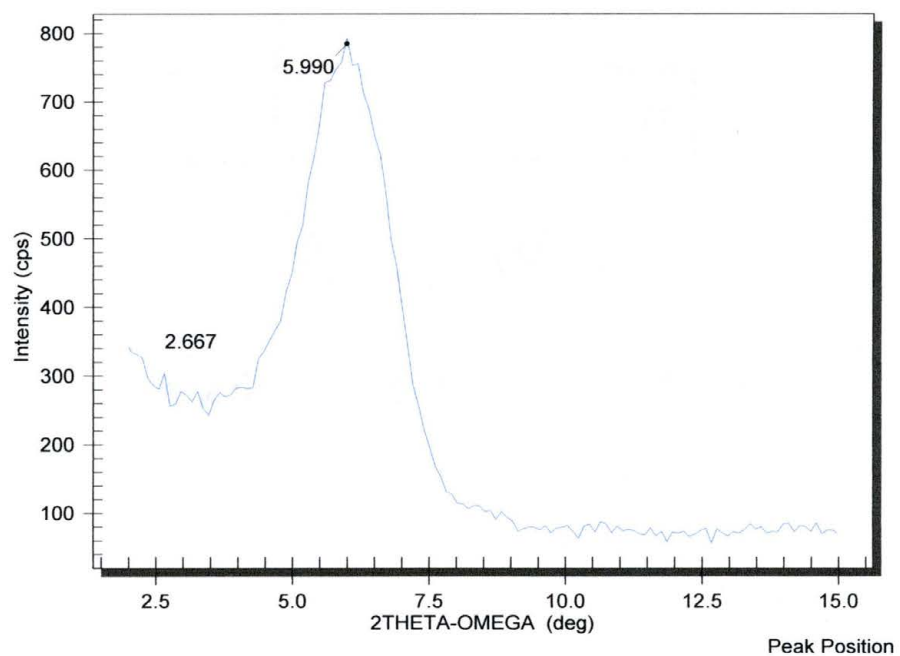
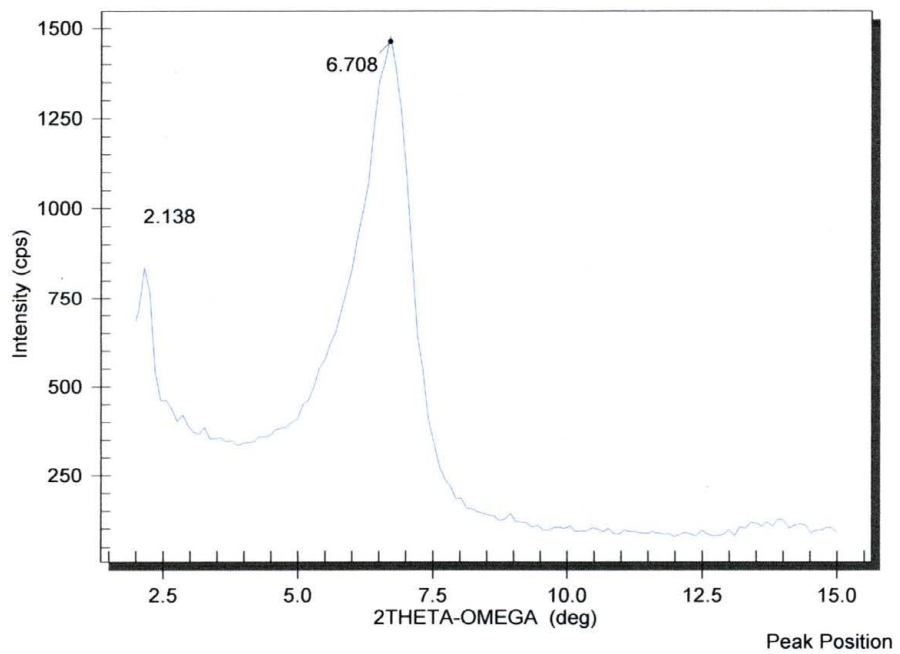
LC moieties. The potential for an interdigitation of the LC component suggests that an electronically tunable system is achievable.

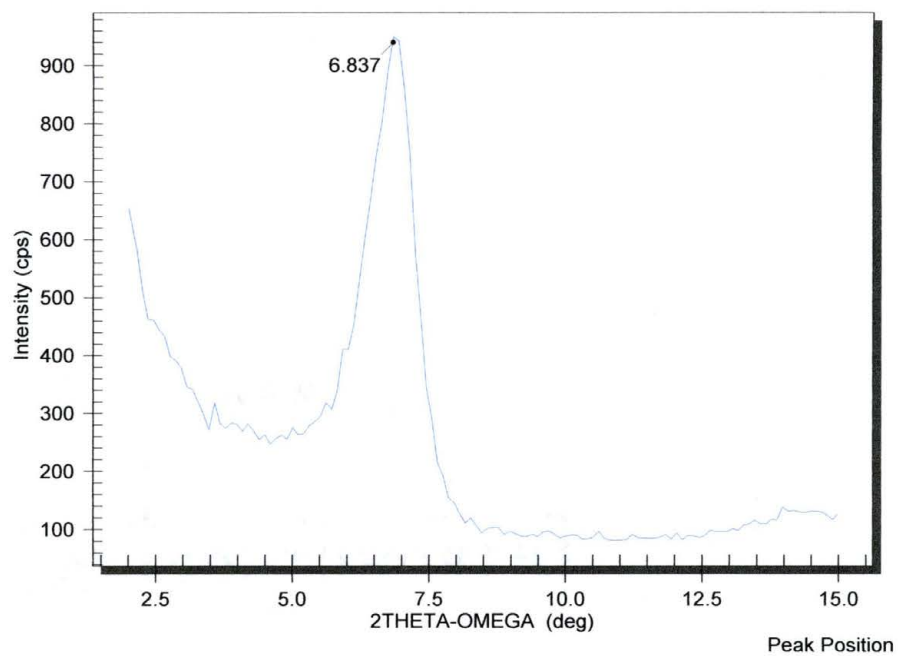
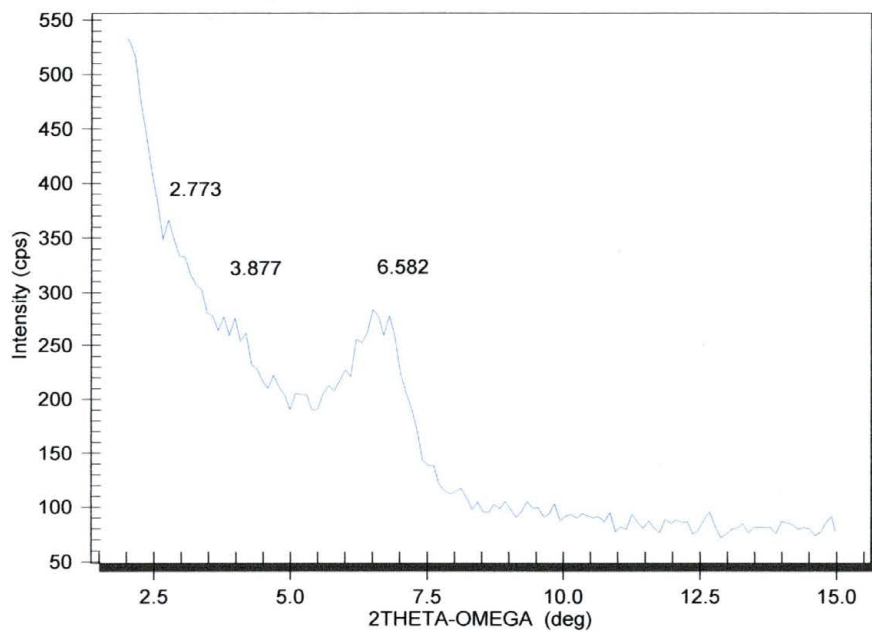
APPENDICES

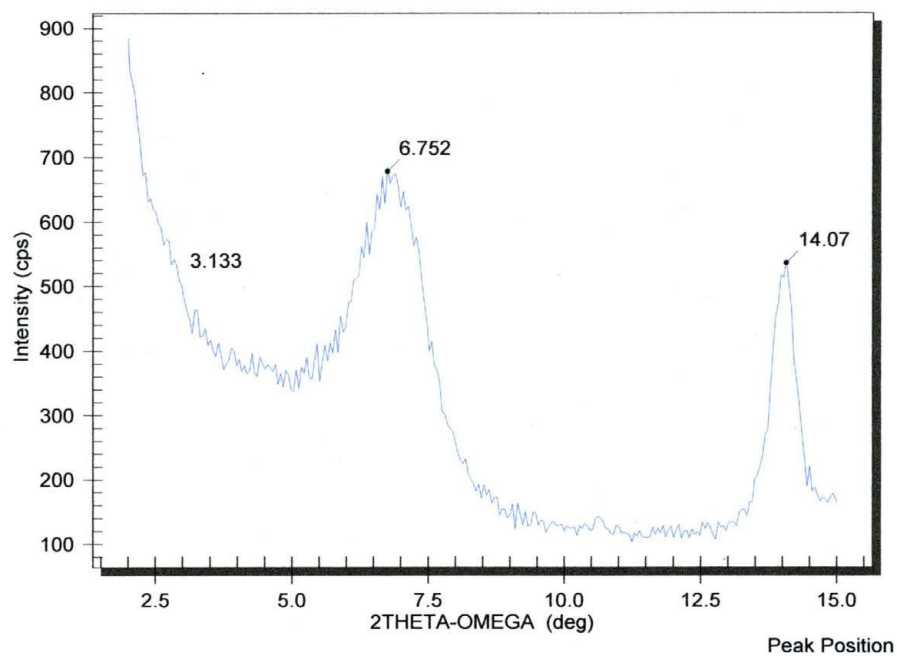
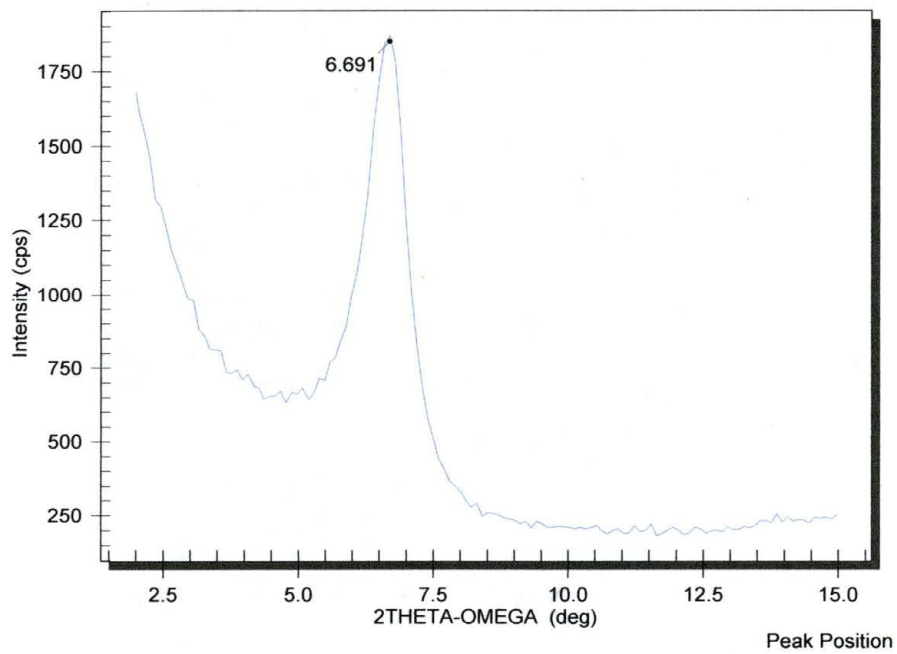
Appendix A: Wide Angle X-ray Diffractions of Organoclays

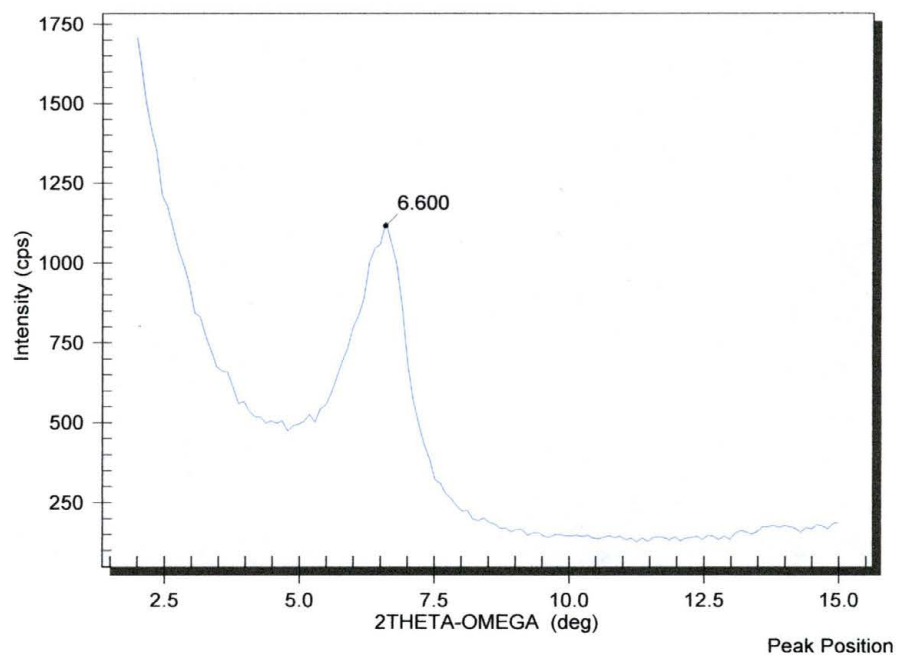
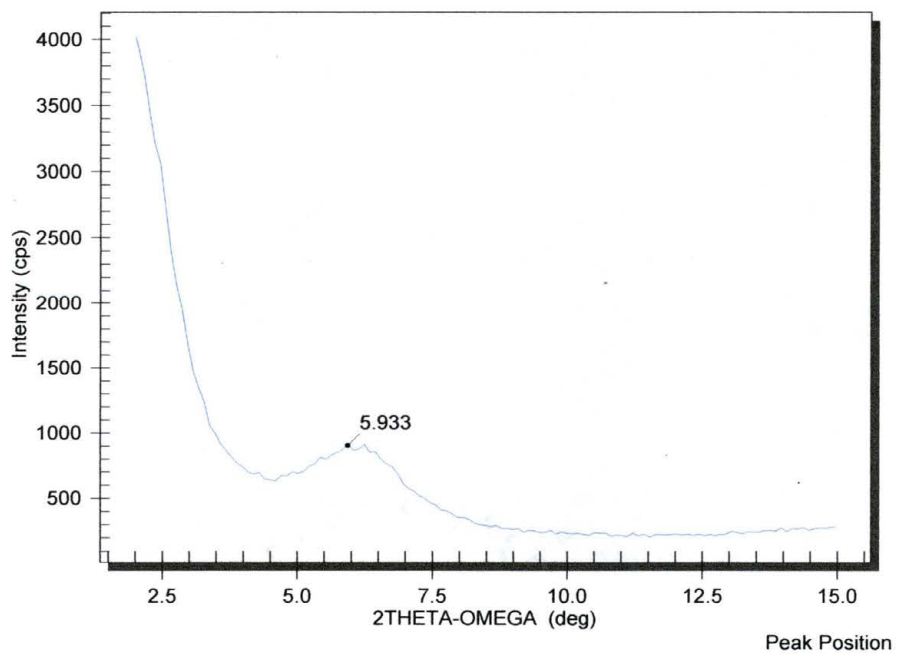
Appendix A1-a: WAXD of Dodecyl Alcohol 1:1 Organoclay**Appendix A1-b: WAXD of Dodecyl Alcohol 2:1 Organoclay**

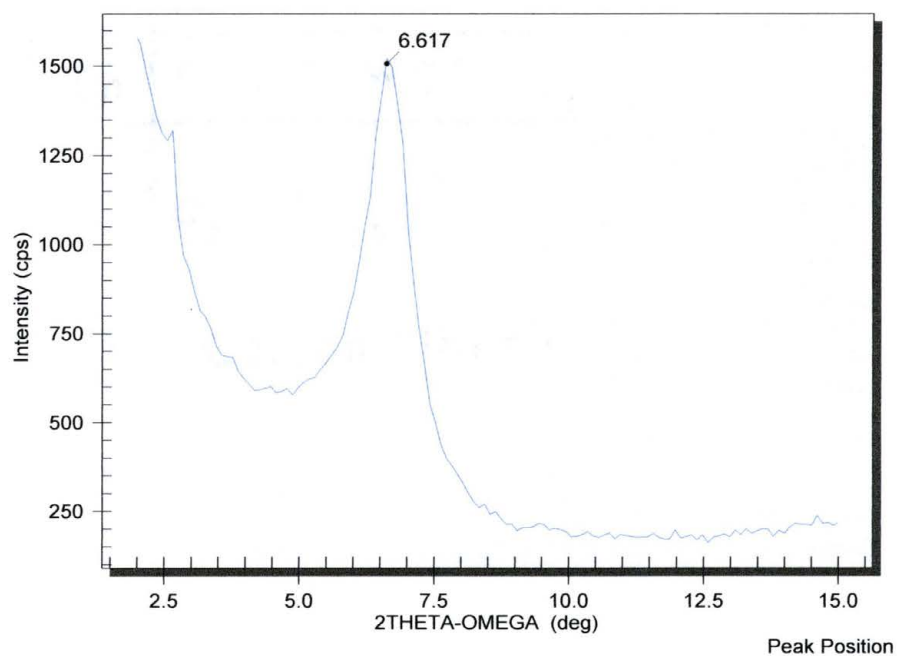
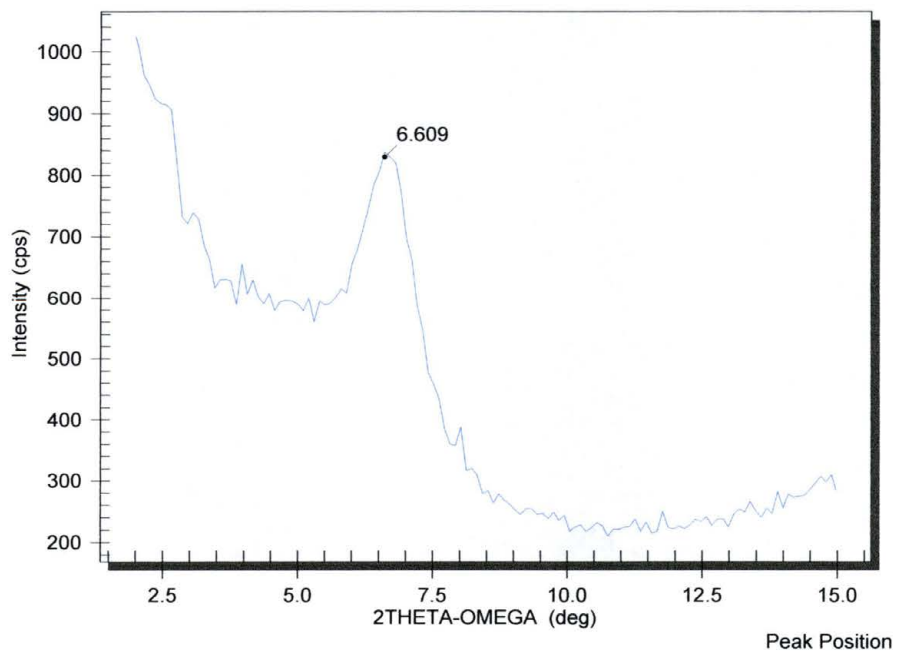
Appendix A1-c: WAXD of Dodecyl Alcohol 3:1 Organoclay**Appendix A2-a: WAXD of Tetradecyl Alcohol 1:1 Organoclay**

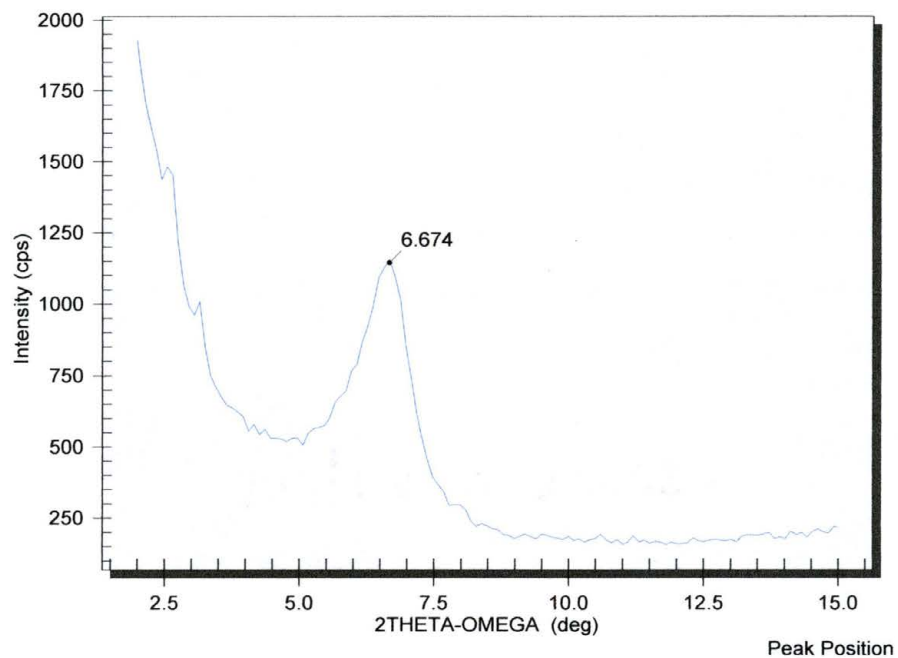
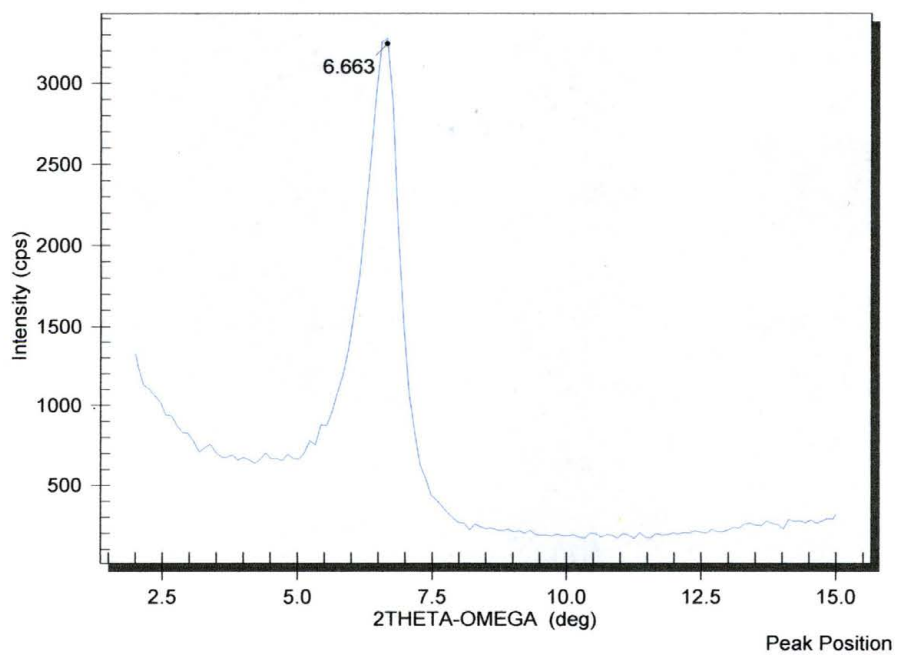
Appendix A2-b: WAXD of Tetradecyl Alcohol 2:1 Organoclay**Appendix A2-c: WAXD of Tetradecyl Alcohol 3:1 Organoclay**

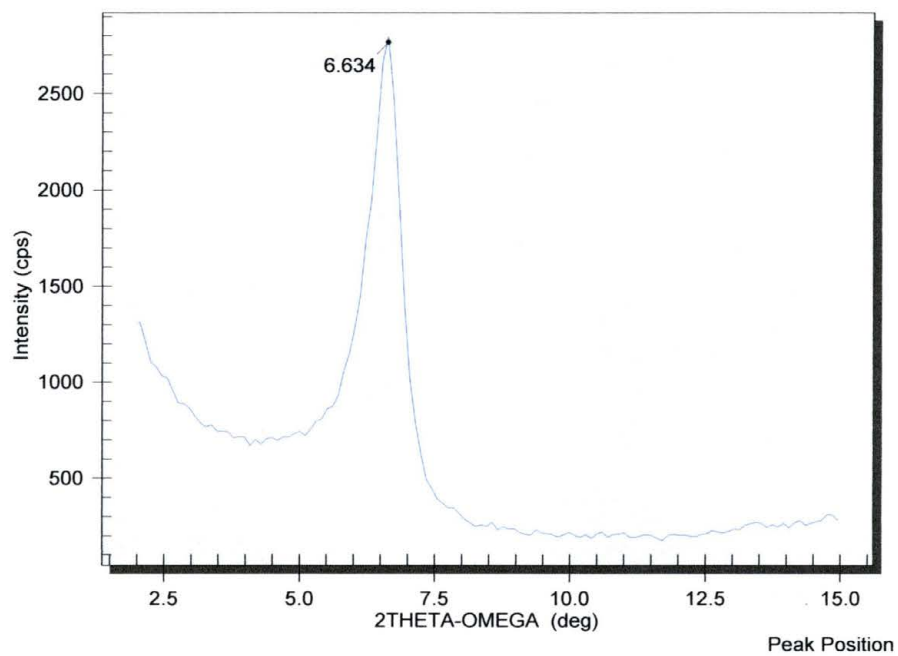
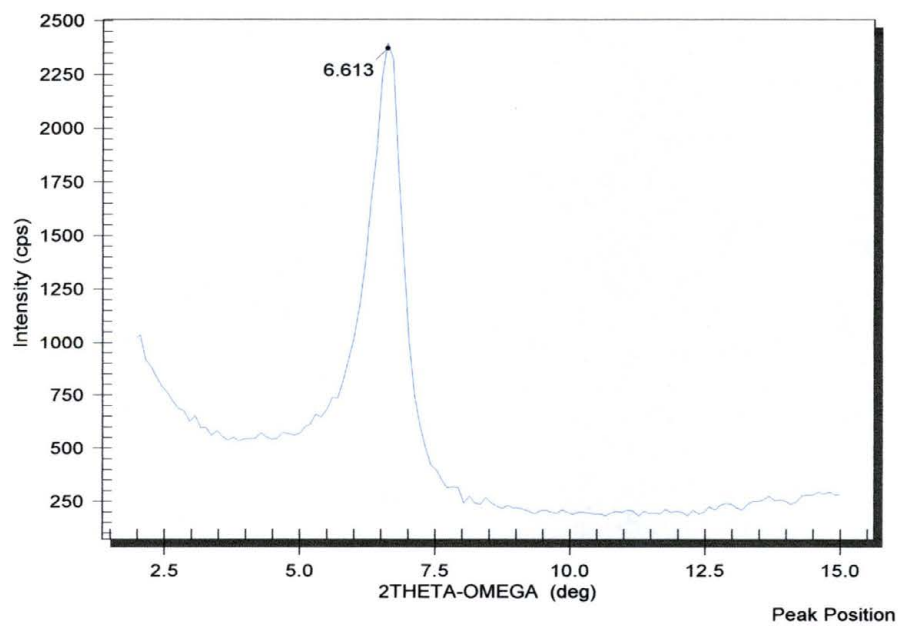
Appendix A3-a: WAXD of Octadecyl Alcohol 1:1 Organoclay**Appendix A3-b: WAXD of Octadecyl Alcohol 2:1 Organoclay**

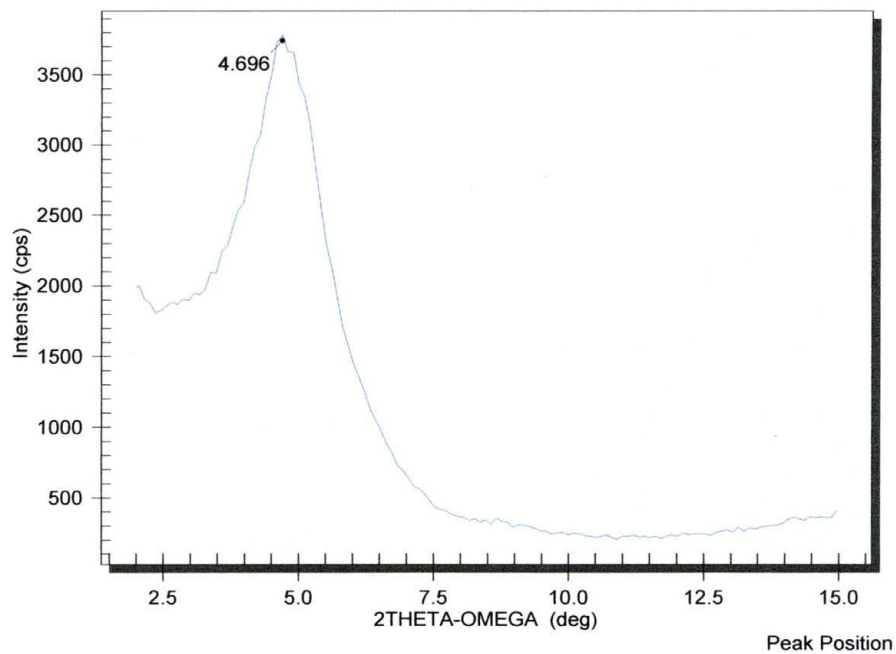
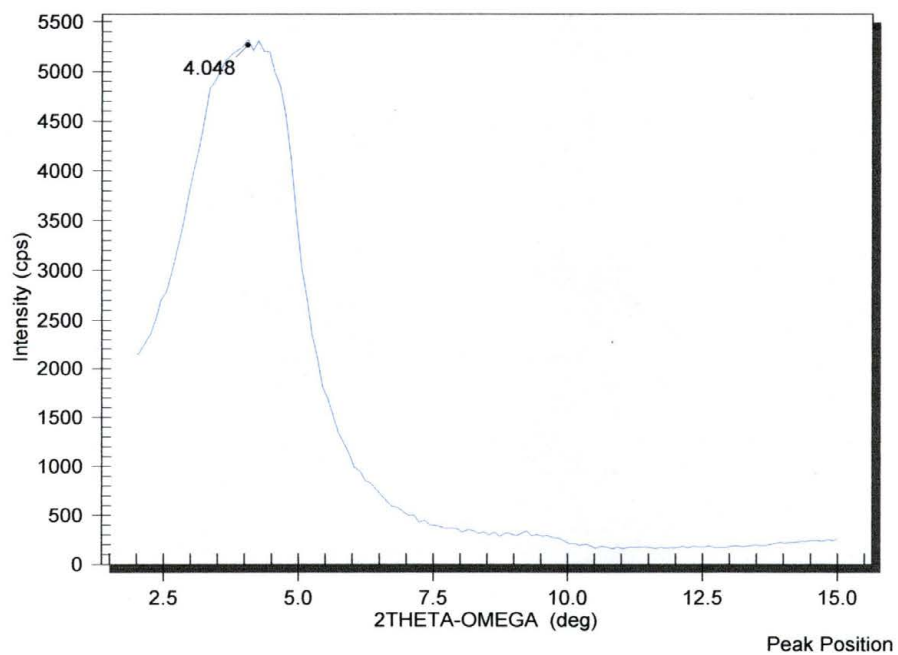
Appendix A3-c: WAXD of Octadecyl Alcohol 3:1 Organoclay**Appendix A4-a: WAXD of Decyl Aldehyde 1:1 Organoclay**

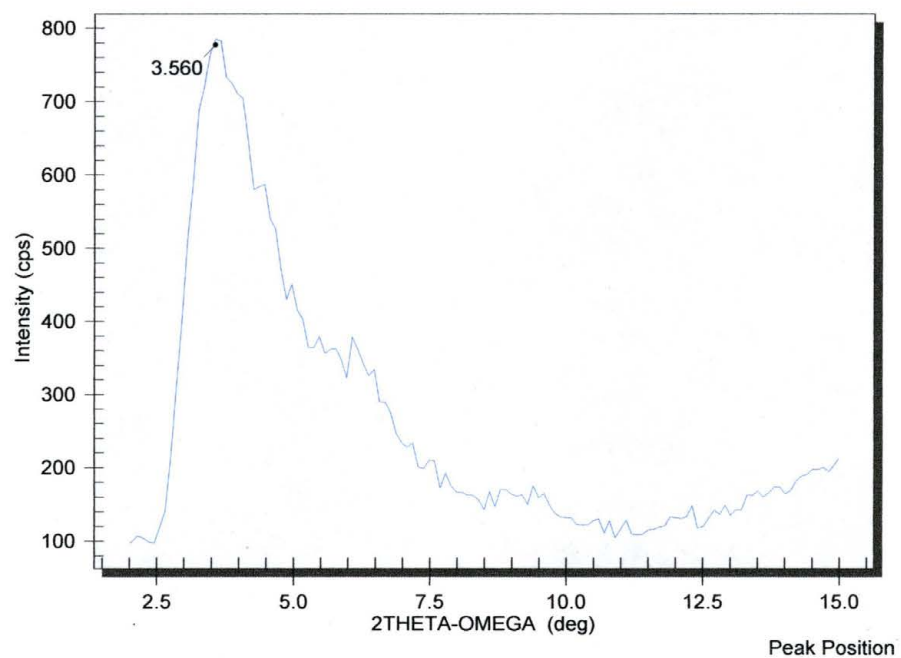
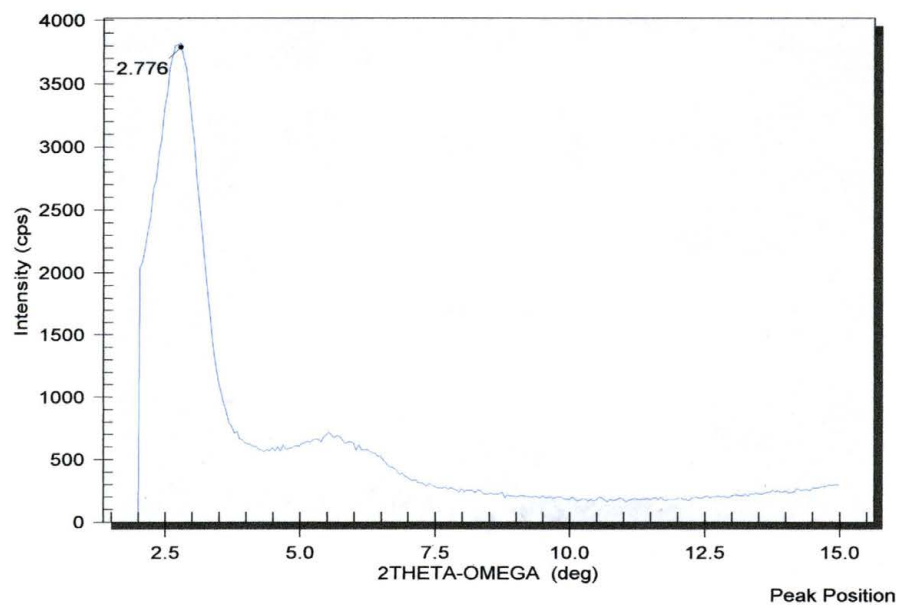
Appendix A4-b: WAXD of Decyl Aldehyde 2:1 Organoclay**Appendix A4-c: WAXD of Decyl Aldehyde 3:1 Organoclay**

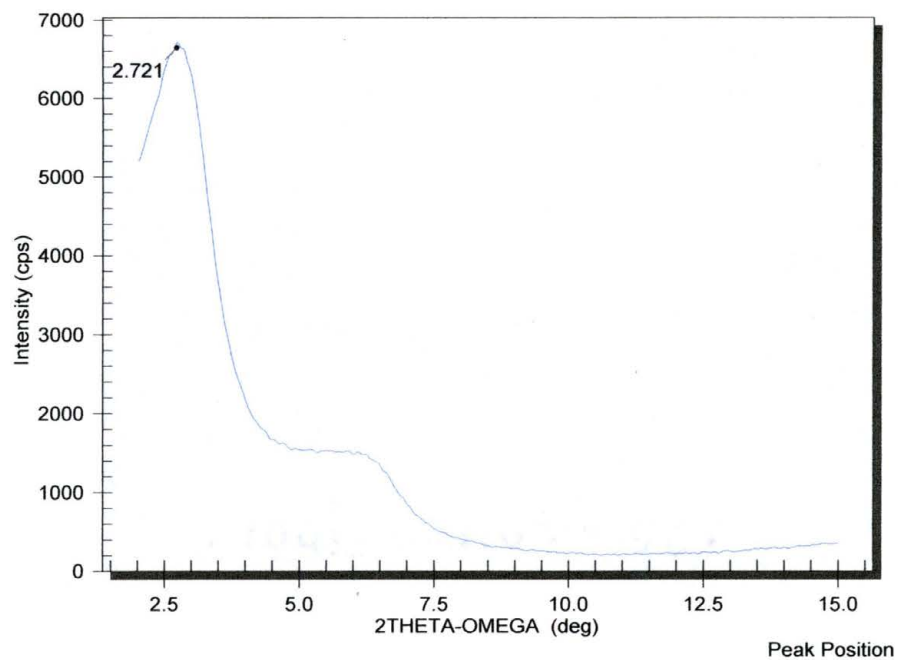
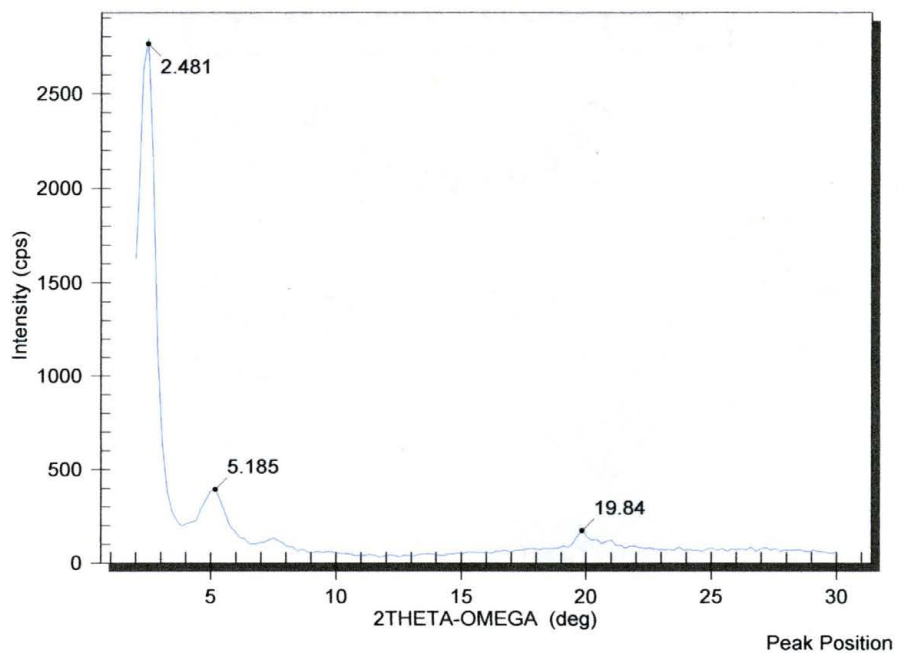
Appendix A5-a: WAXD of Dodecyl Aldehyde 1:1 Organoclay**Appendix A5-b: WAXD of Dodecyl Aldehyde 2:1 Organoclay**

Appendix A5-c: WAXD of Dodecyl Aldehyde 3:1 Organoclay**Appendix A6-a: WAXD of N-Methyl Pyrrolidone 1:1 Organoclay**

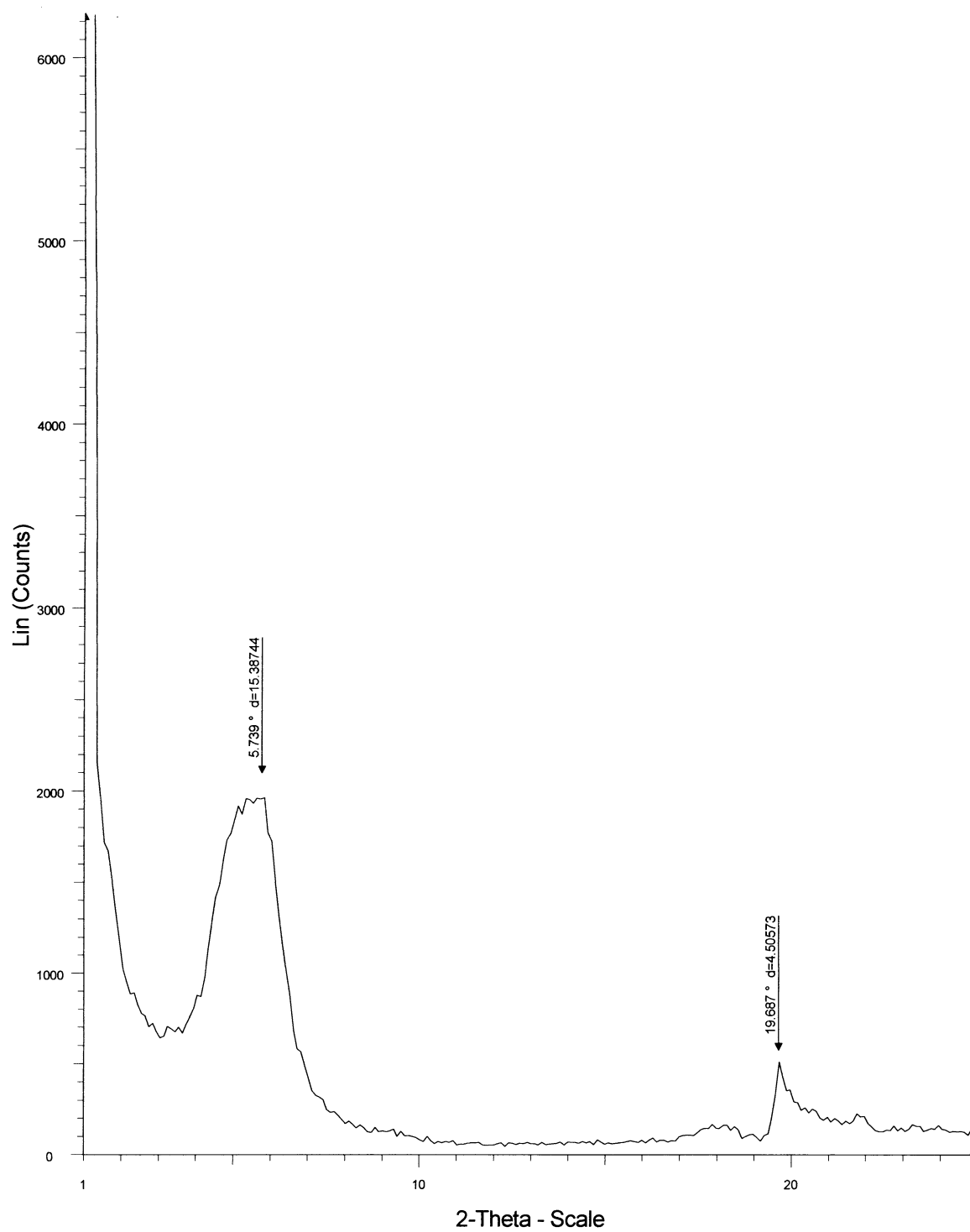
Appendix A6-b: WAXD of N-Methyl Pyrrolidone 2:1 Organoclay**Appendix A6-c: WAXD of N-Methyl Pyrrolidone 3:1 Organoclay**

Appendix A7-a: WAXD of N-Octyl Pyrrolidone 1:1 Organoclay**Appendix A7-b: WAXD of N-Octyl Pyrrolidone 2:1 Organoclay**

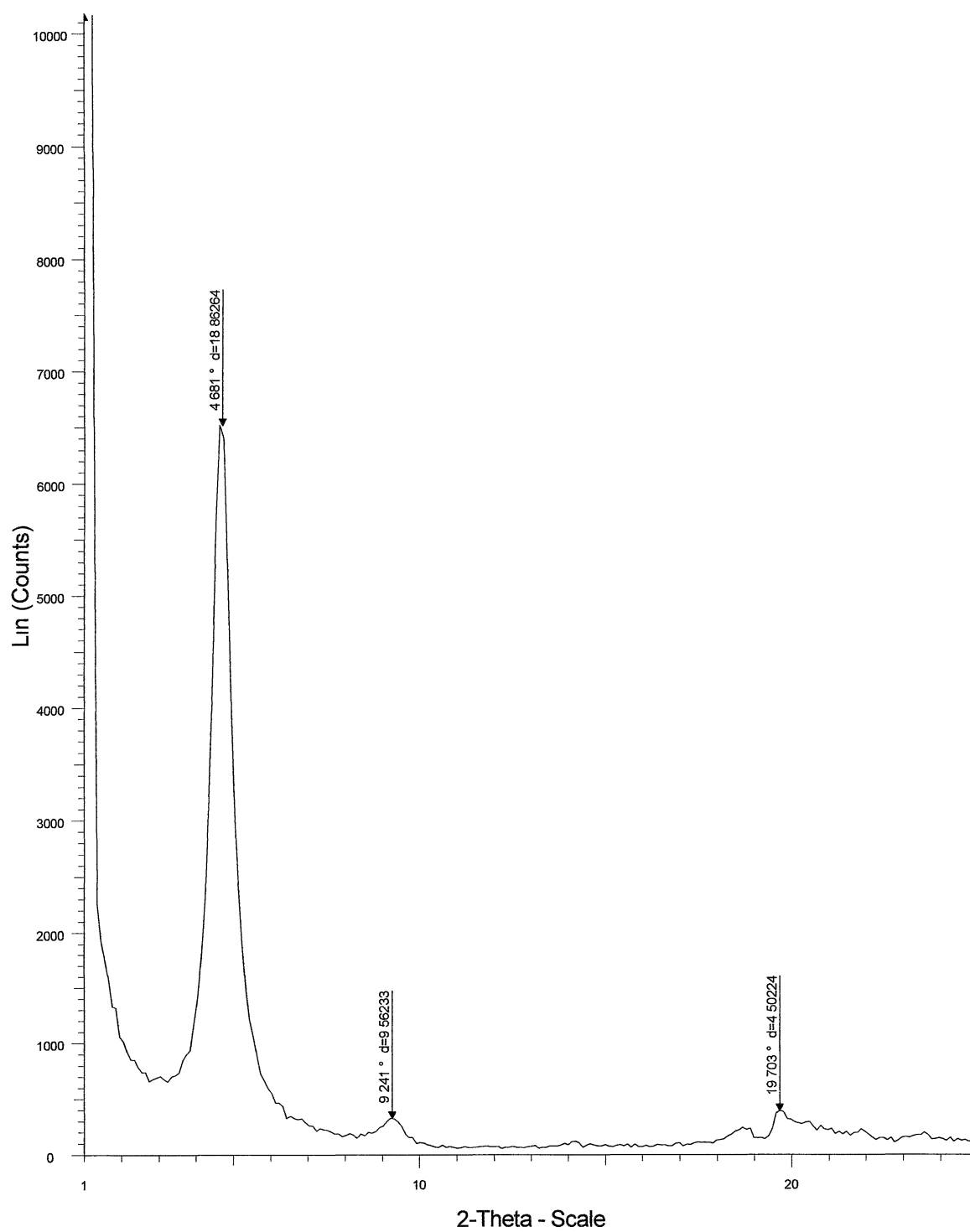
Appendix A7-c: WAXD of N-Octyl Pyrrolidone 3:1 Organoclay**Appendix A8-a: WAXD of N-Dodecyl Pyrrolidone 1:1 Organoclay**

Appendix A8-b: WAXD of N-Dodecyl Pyrrolidone 2:1 Organoclay**Appendix A8-c: WAXD of N-Dodecyl Pyrrolidone 3:1 Organoclay**

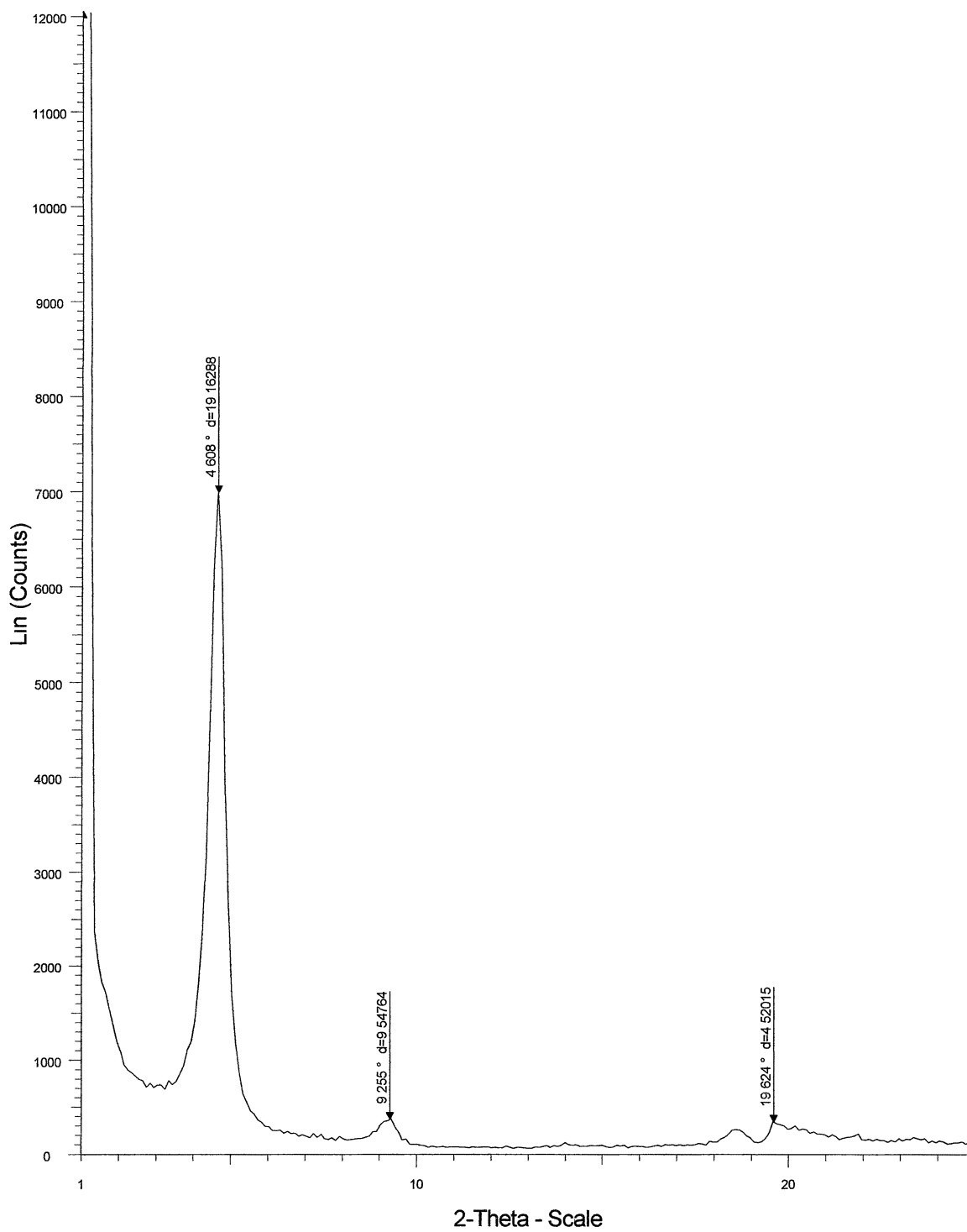
Appendix A9-a: WAXD of N-Cyclohexyl Pyrrolidone 1:1 Organoclay



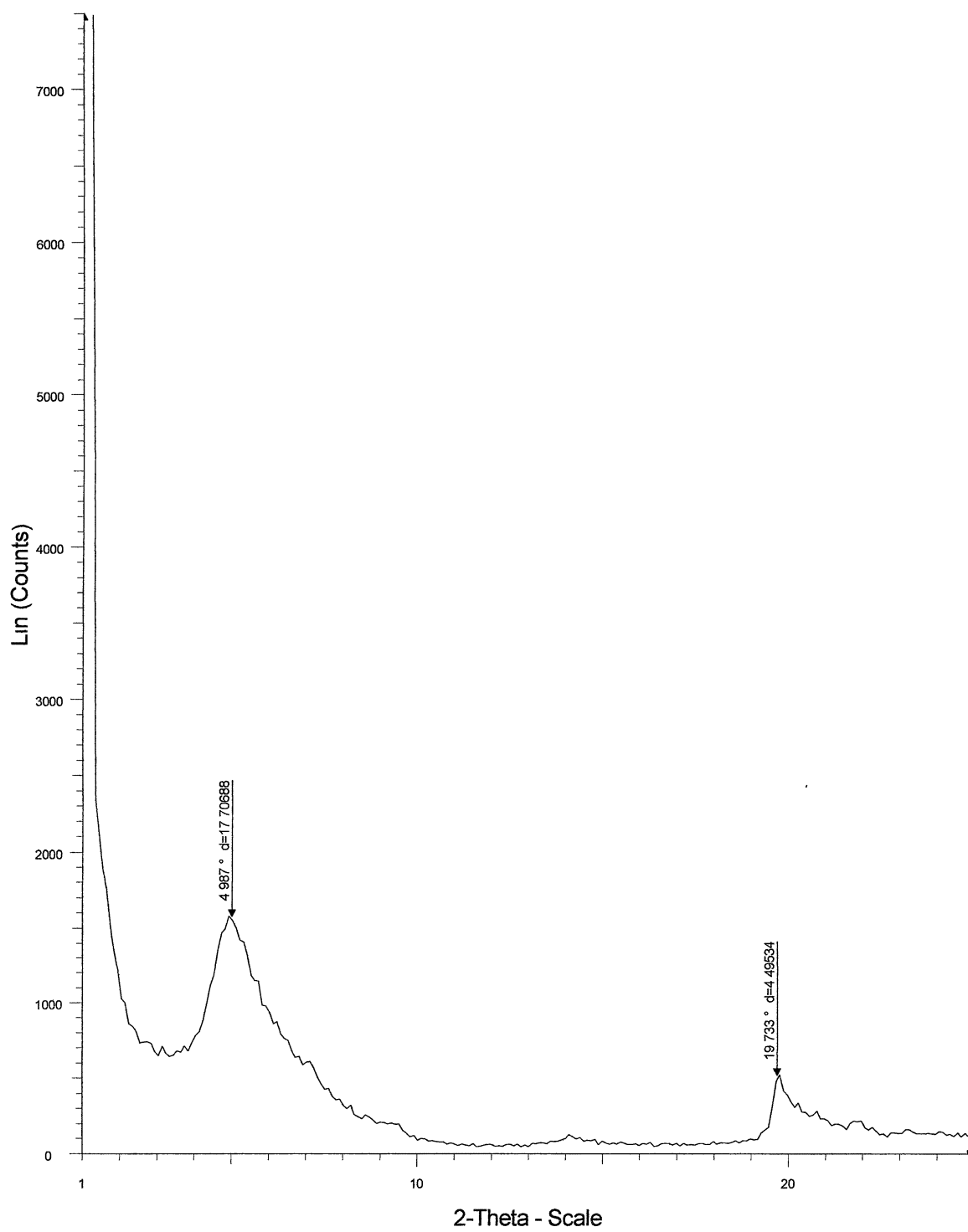
Appendix A9-b: WAXD of N-Cyclohexyl Pyrrolidone 2:1 Organoclay



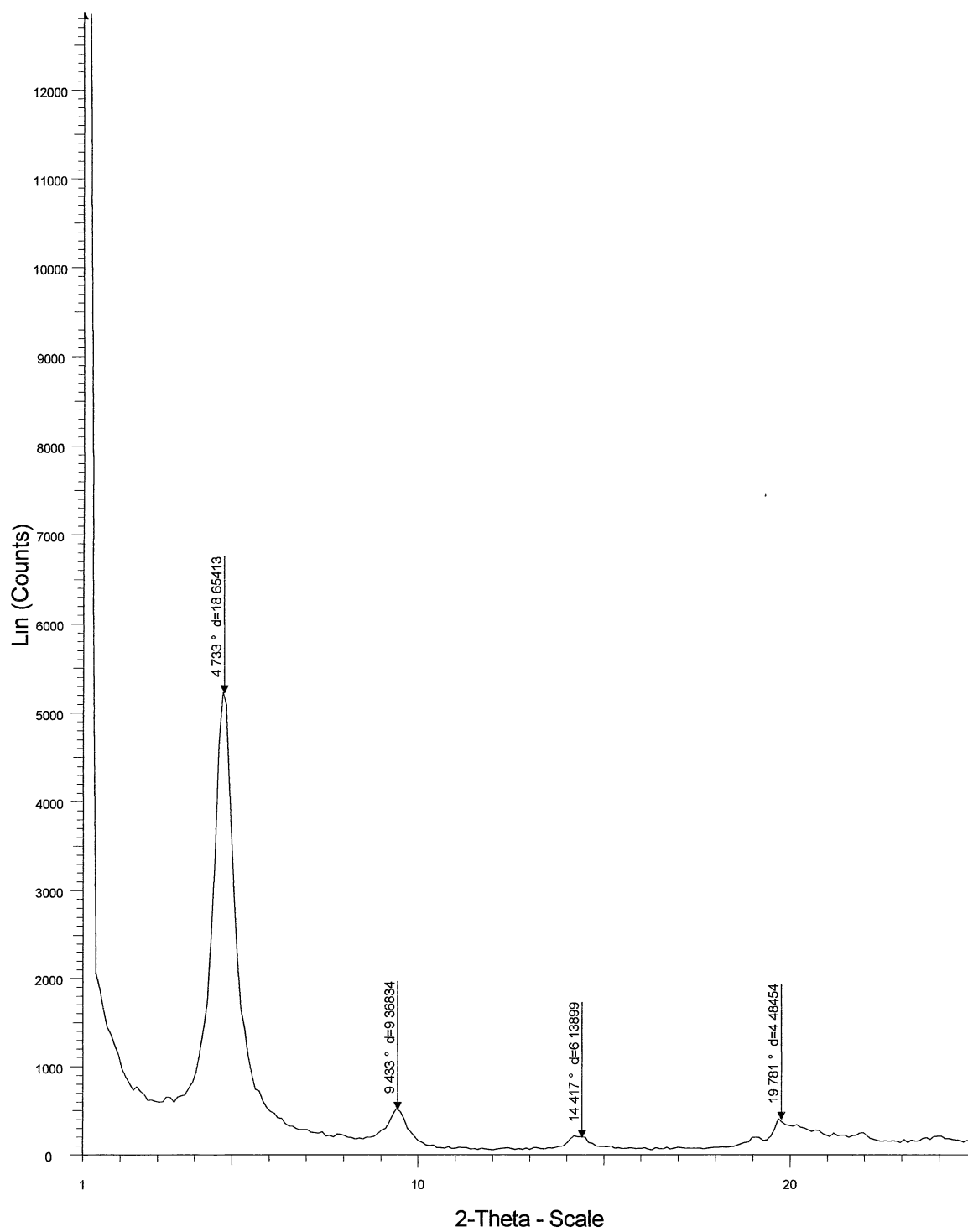
Appendix A9-c: WAXD of N-Cyclohexyl Pyrrolidone 3:1 Organoclay



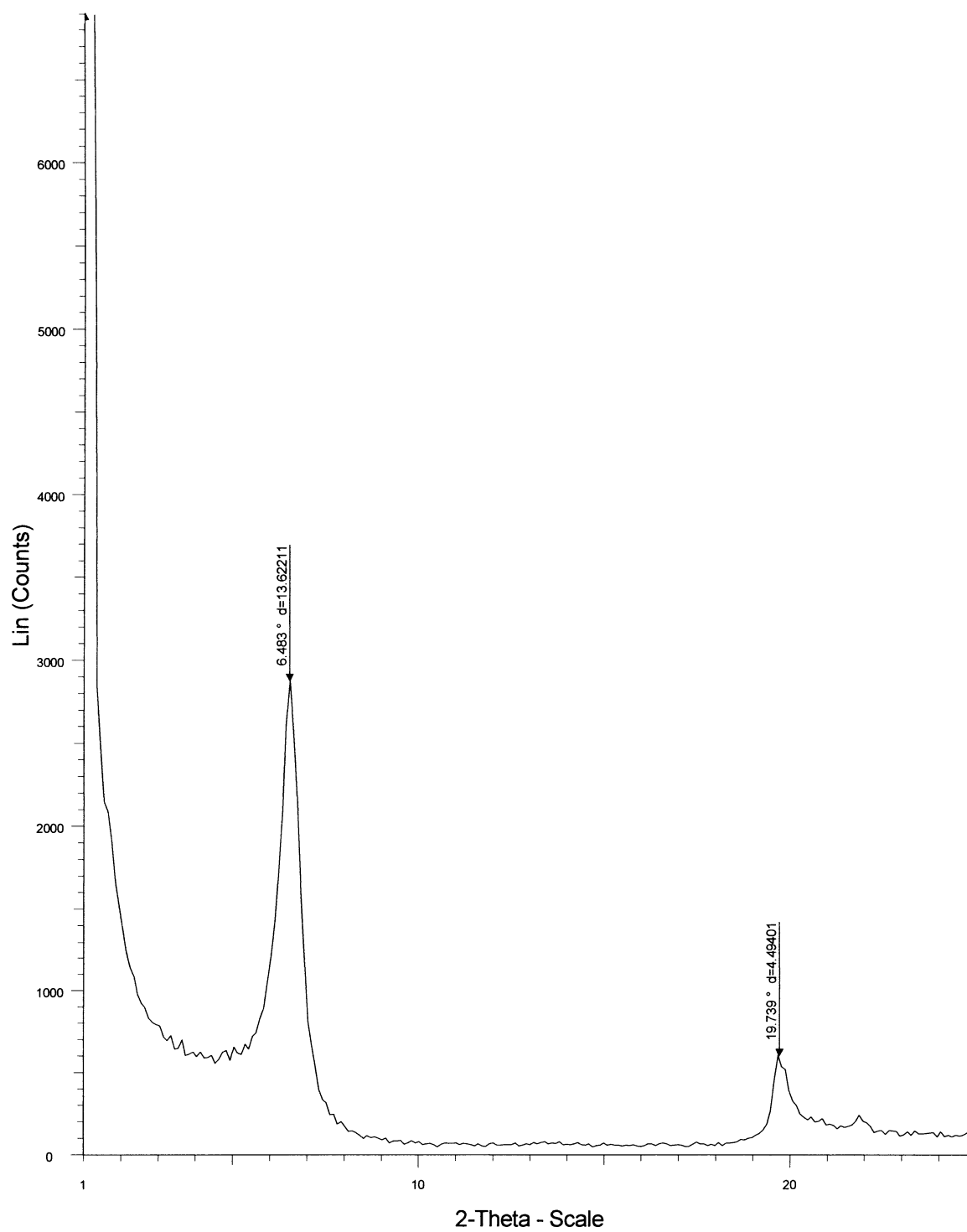
Appendix A10-a: WAXD of N-Phenyl Pyrrolidone 1:1 Organoclay



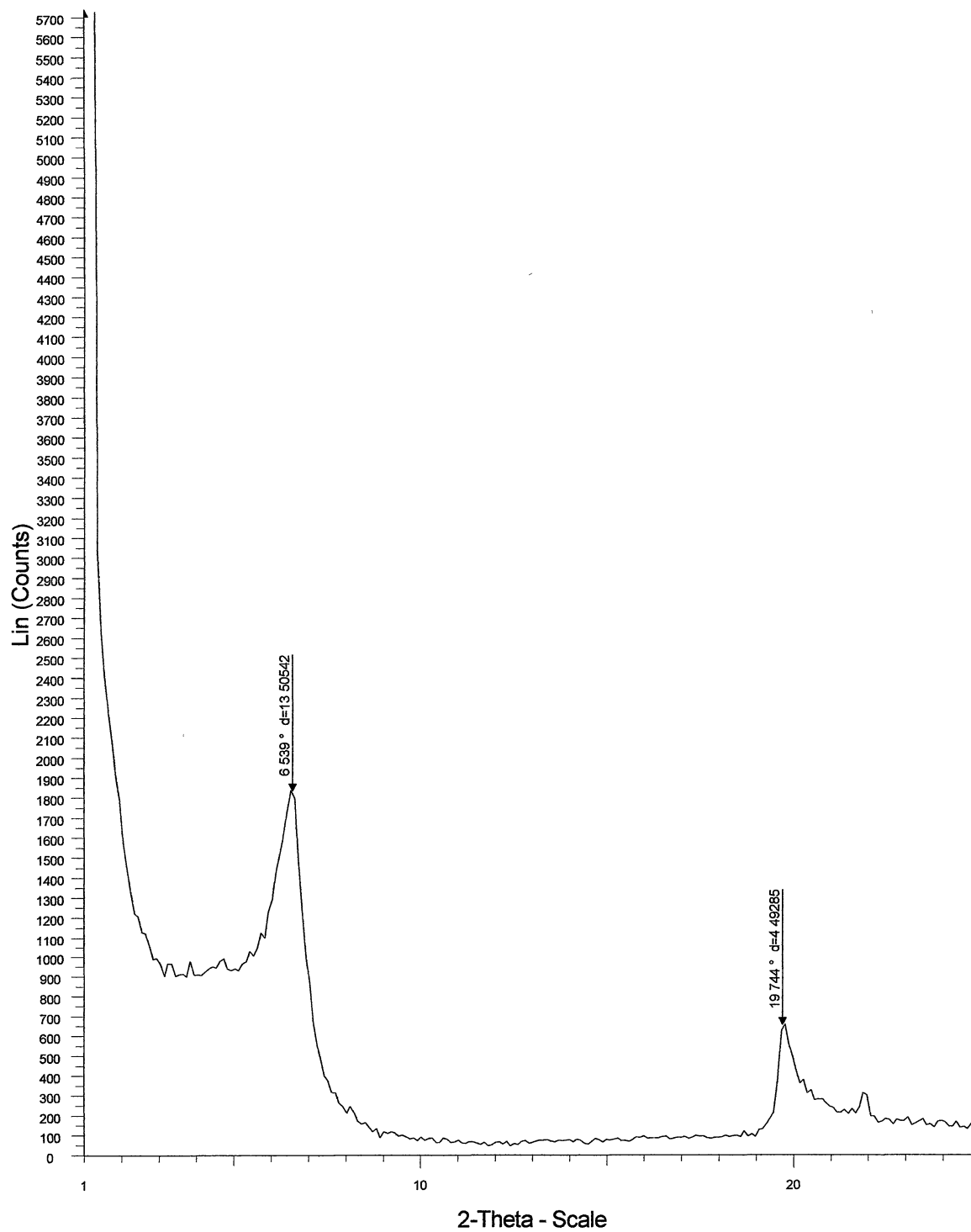
Appendix A10-b: WAXD of N-Phenyl Pyrrolidone 2:1 Organoclay

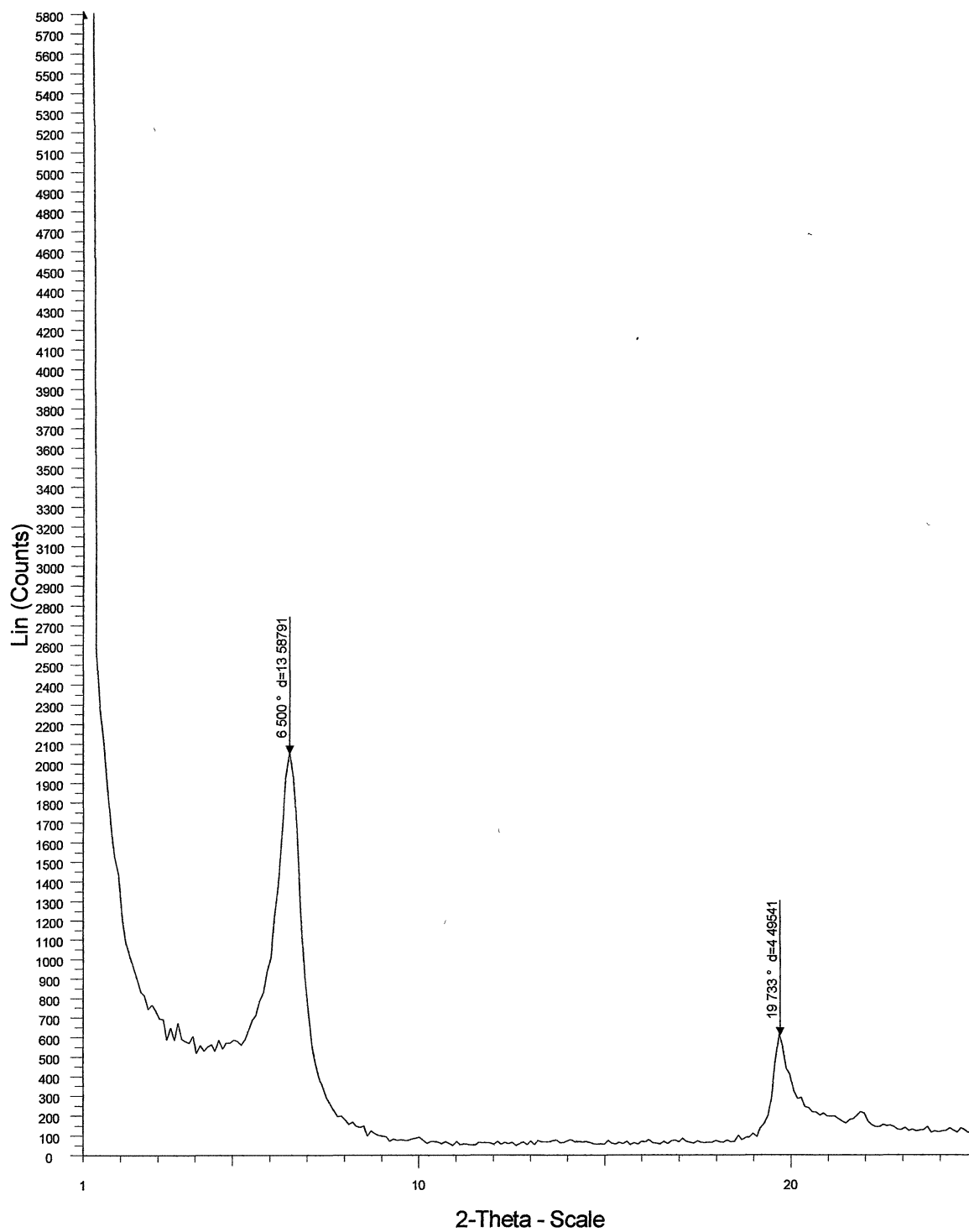


Appendix A11-a: WAXD of Hydroxy Ethyl Pyrrolidone 1to1 Organoclay

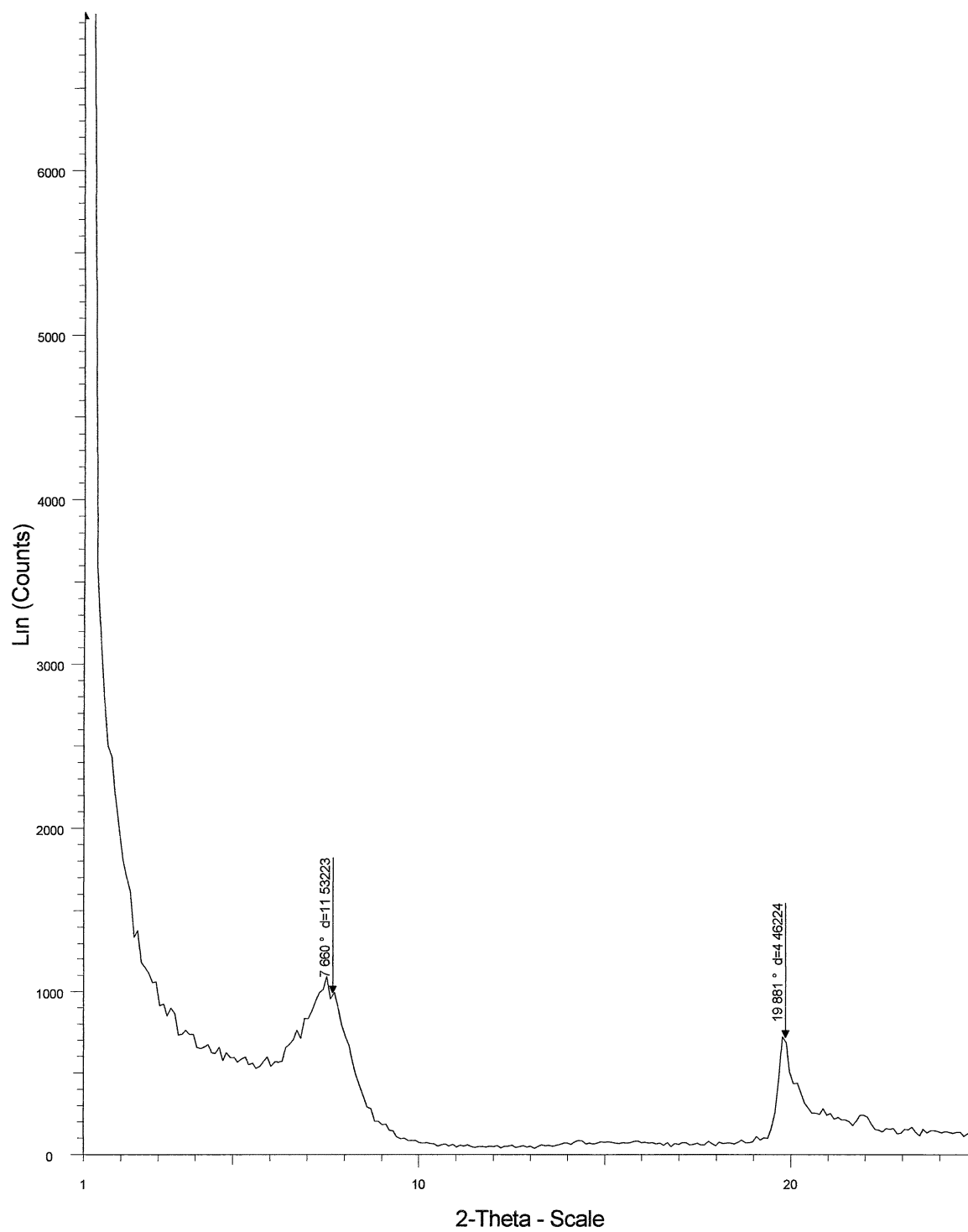


Appendix A11-b: WAXD of Hydroxy Ethyl Pyrrolidone 2to1 Organoclay

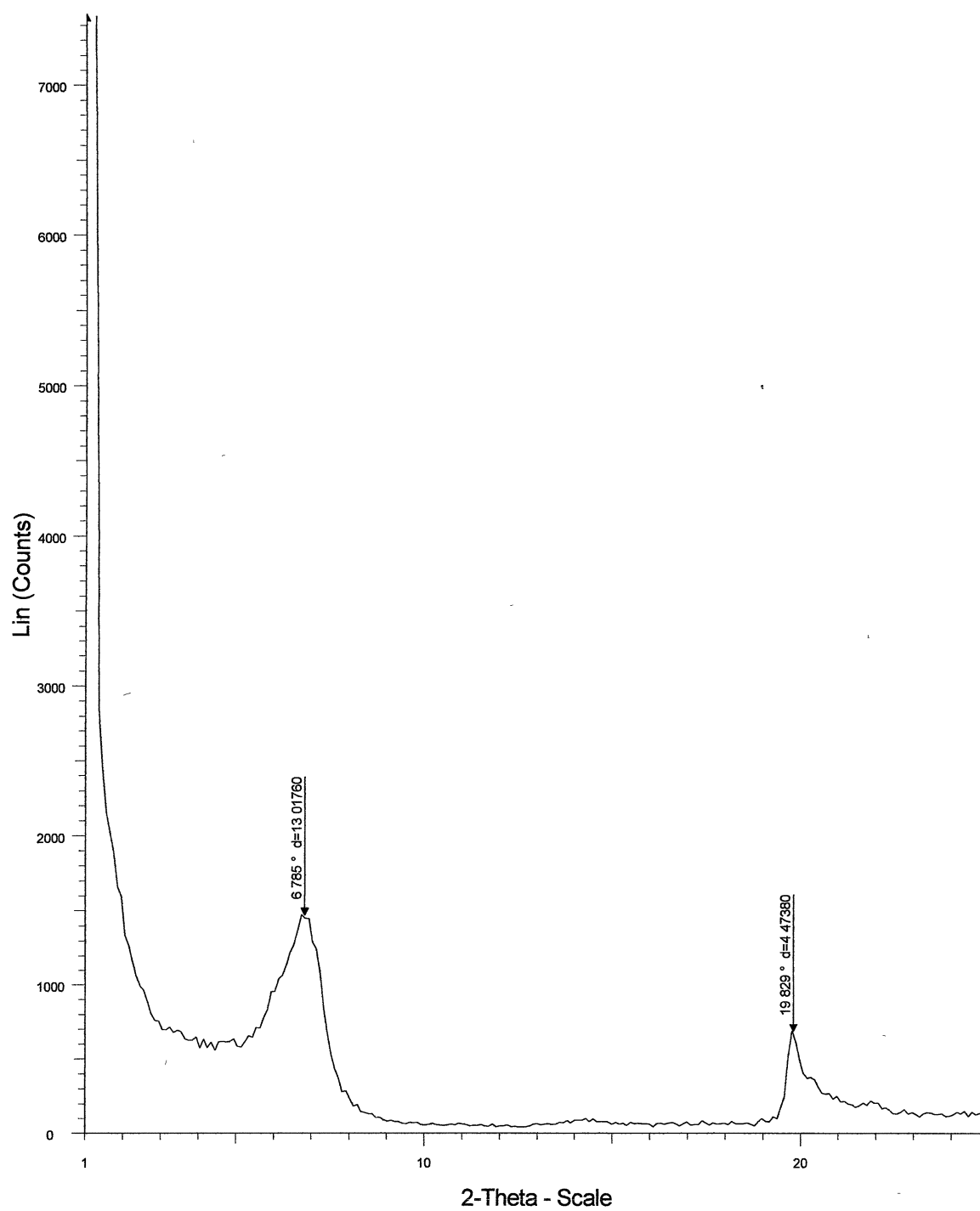


Appendix A11-c: WAXD of Hydroxy Ethyl Pyrrolidone 3to1 Organoclay

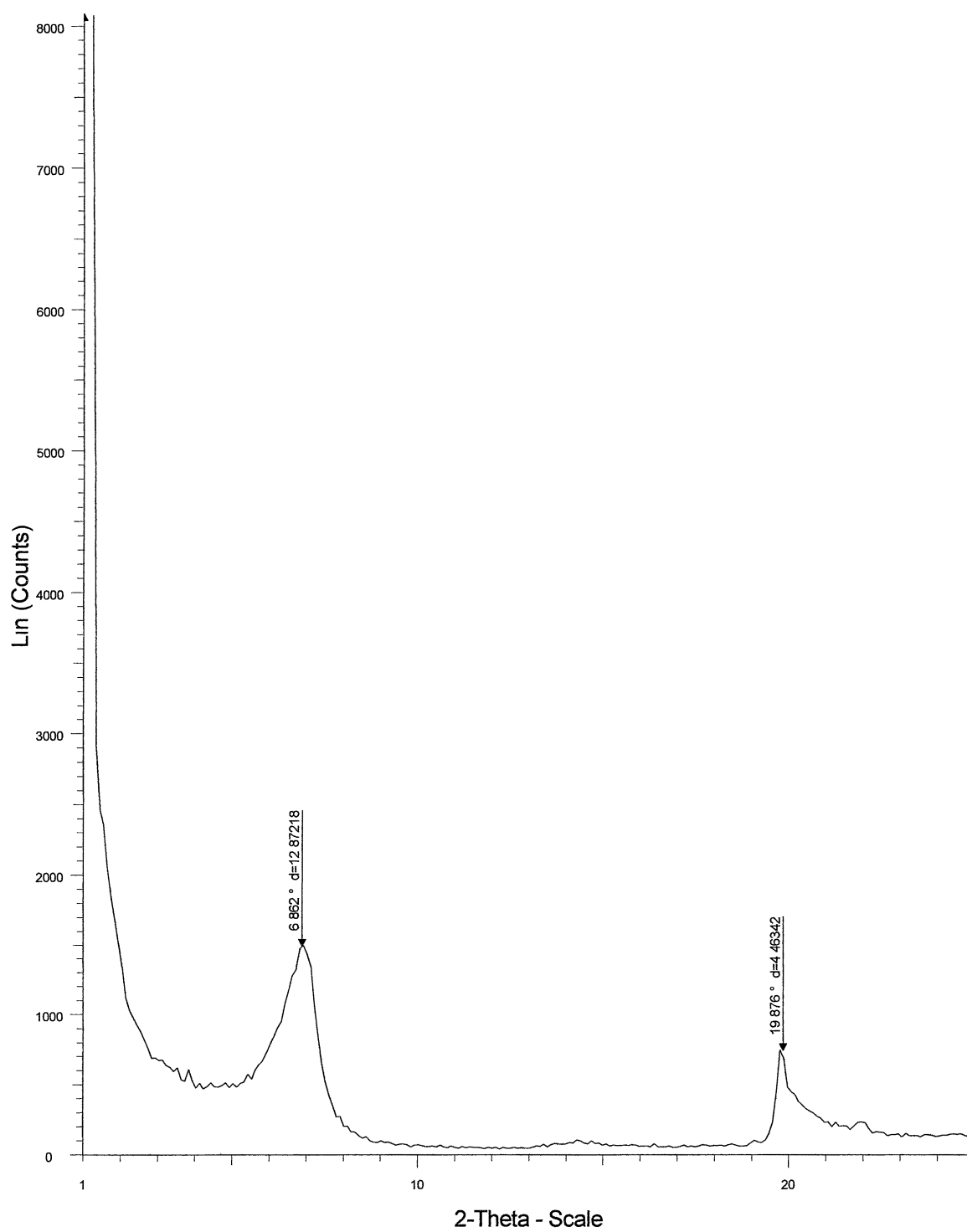
Appendix A12: WAXD of 95meq Sodium Cloisite



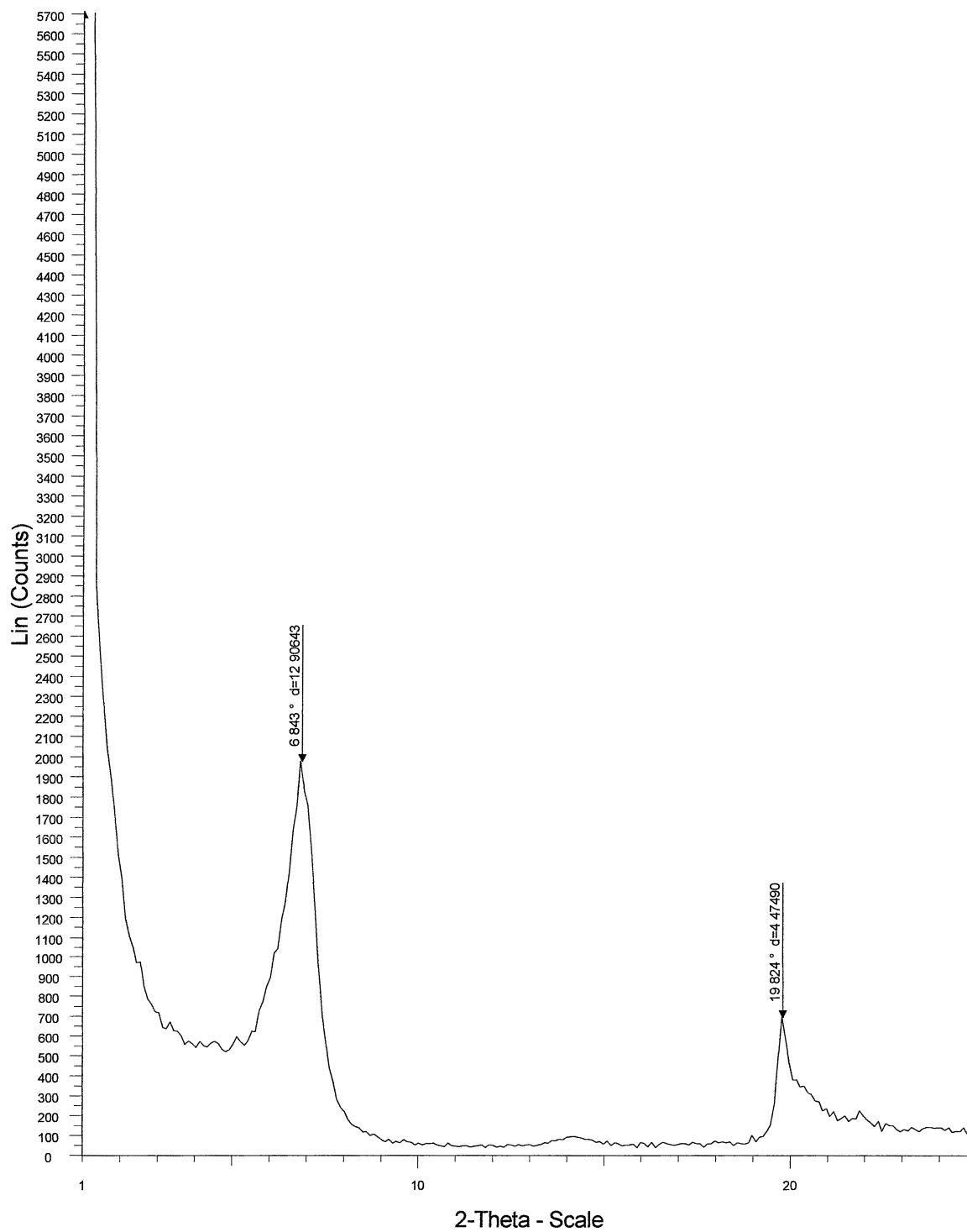
Appendix B: Wide Angle X-ray Diffractions of Aged Organoclays

Appendix B1-a: WAXD of Aged Butyl Alcohol 1:1 Organoclay

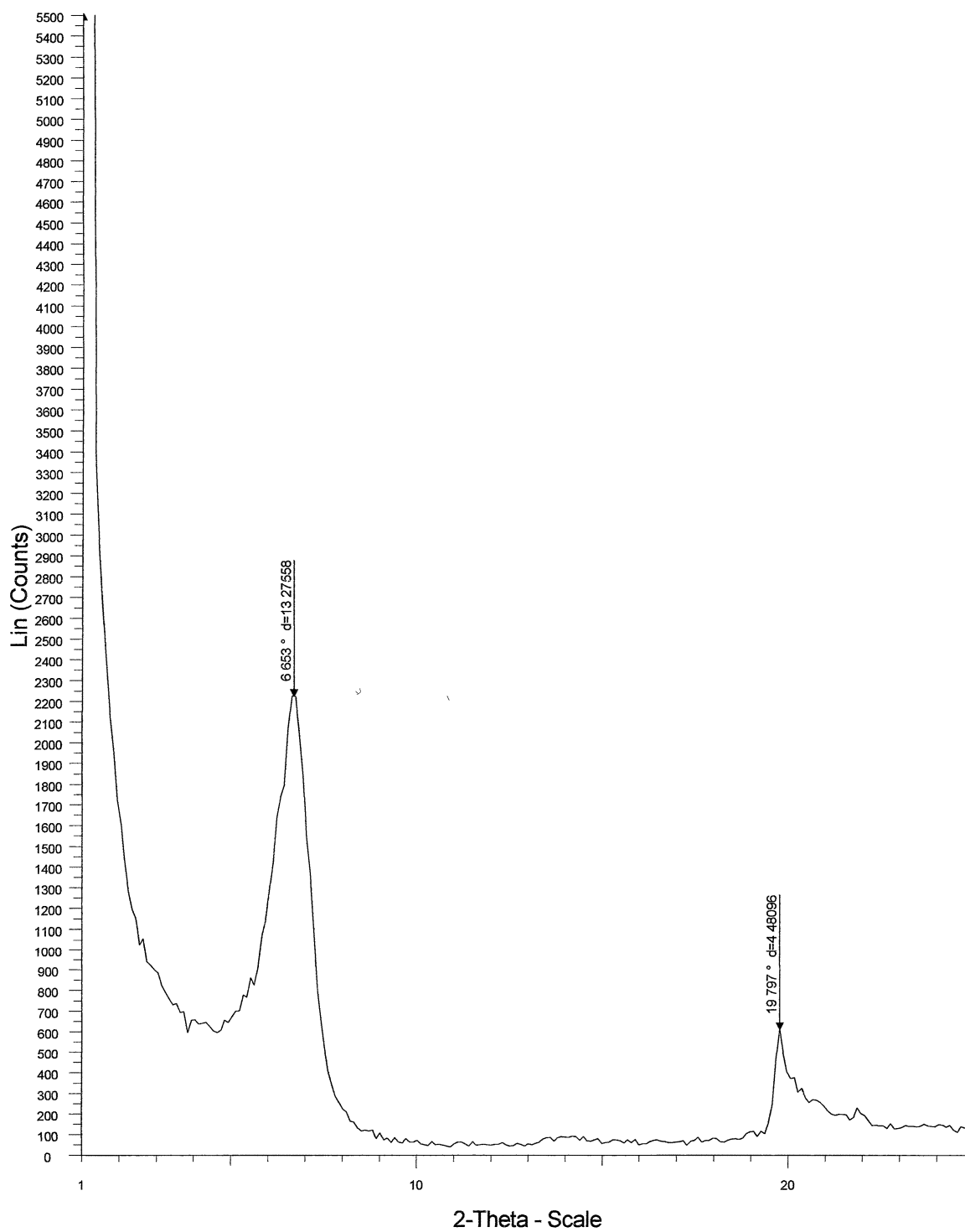
Appendix B1-b: WAXD of Aged Butyl Alcohol 2:1 Organoclay



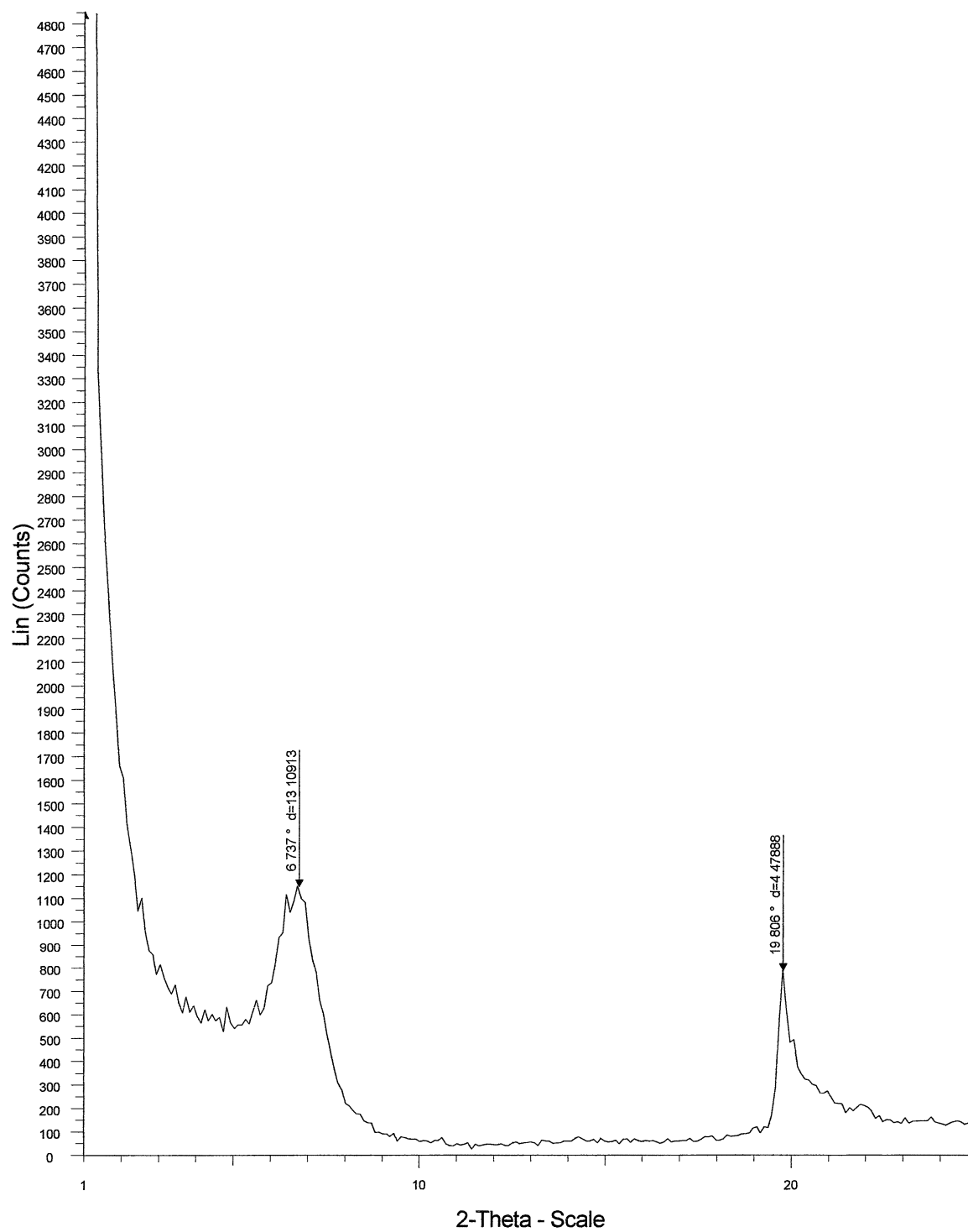
Appendix B1-c: WAXD of Aged Butyl Alcohol 3:1 Organoclay



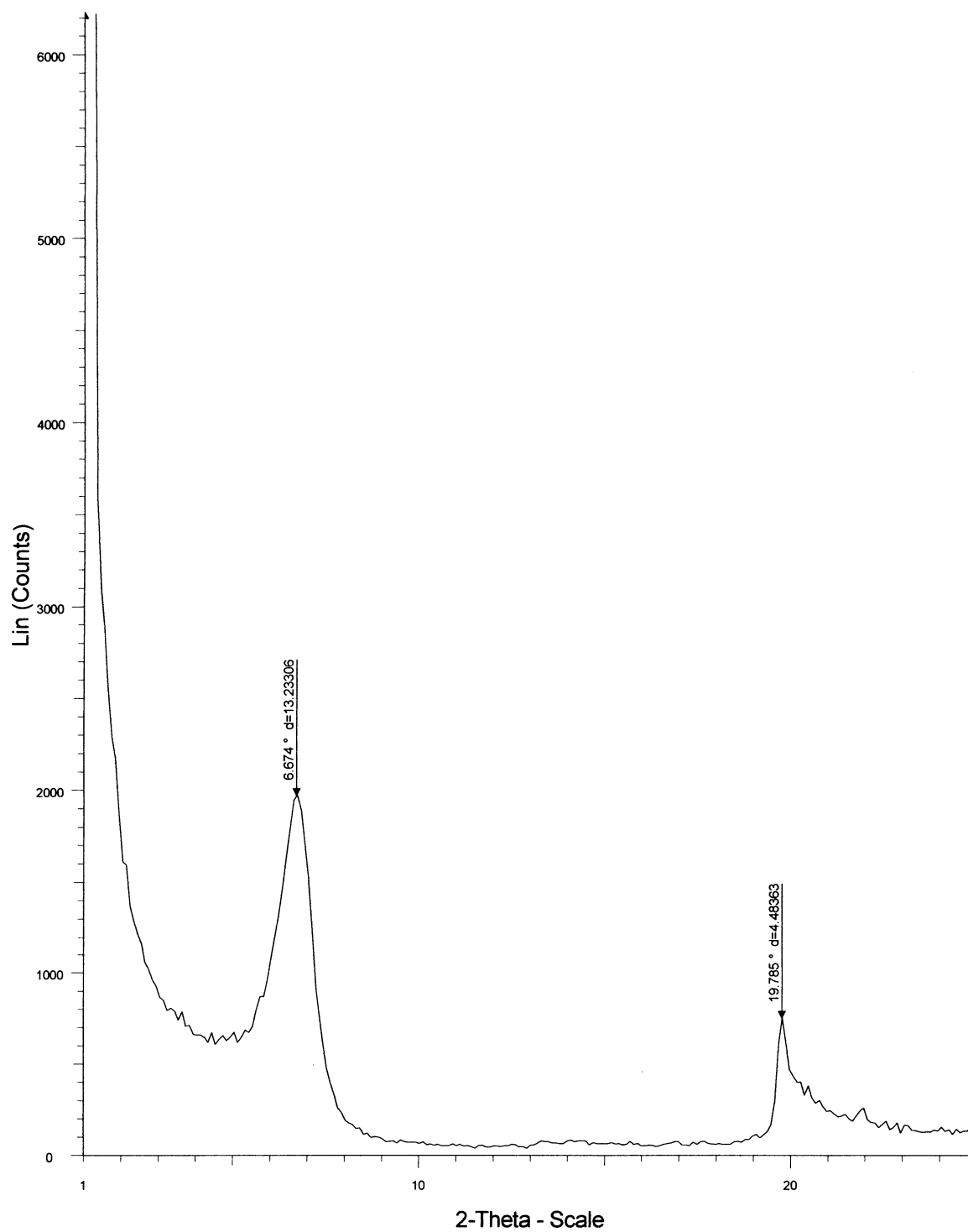
Appendix B2-a: WAXD of Aged Hexyl Alcohol 1:1 Organoclay



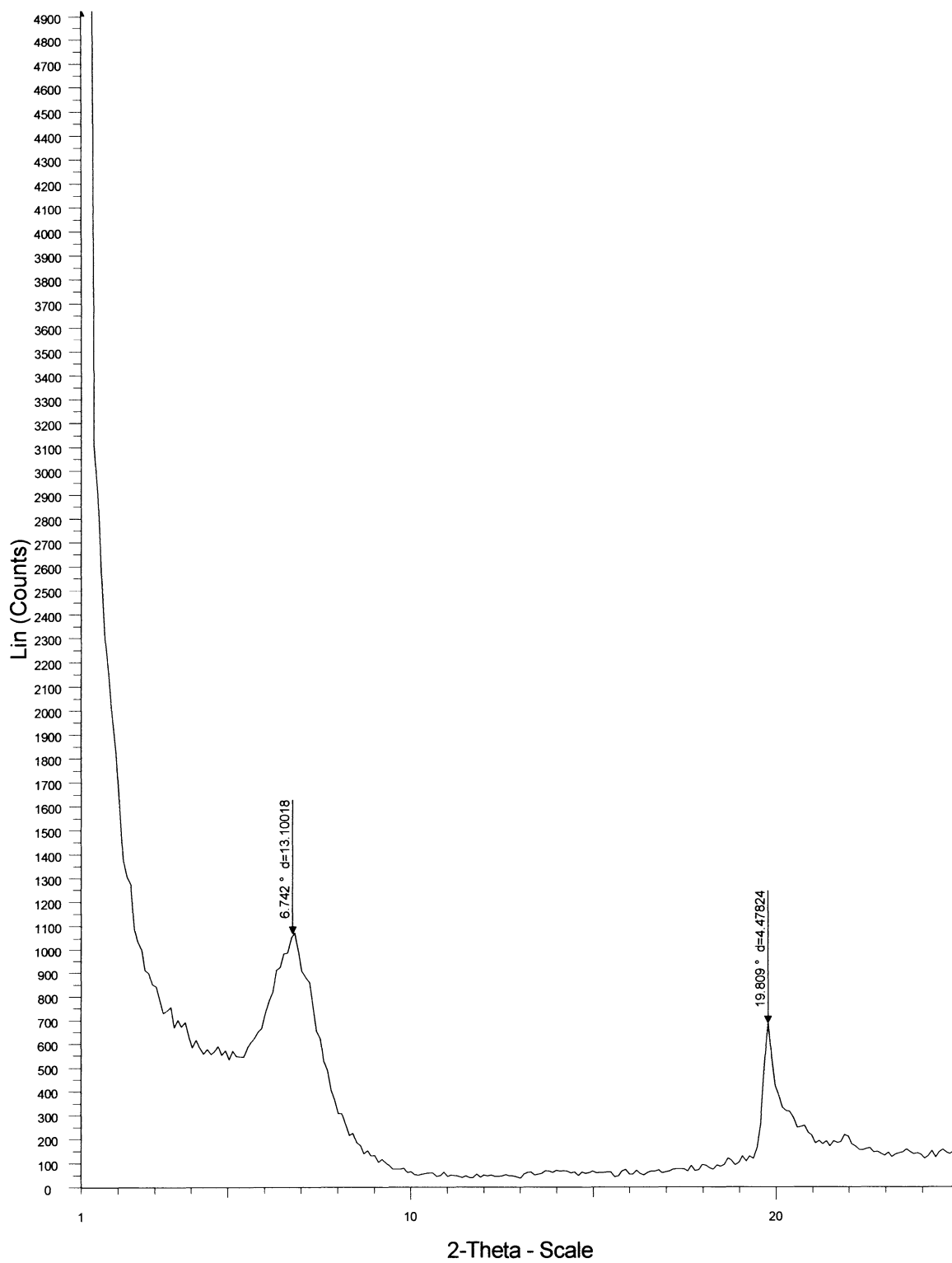
Appendix B2-b: WAXD of Aged Hexyl Alcohol 2:1 Organoclay



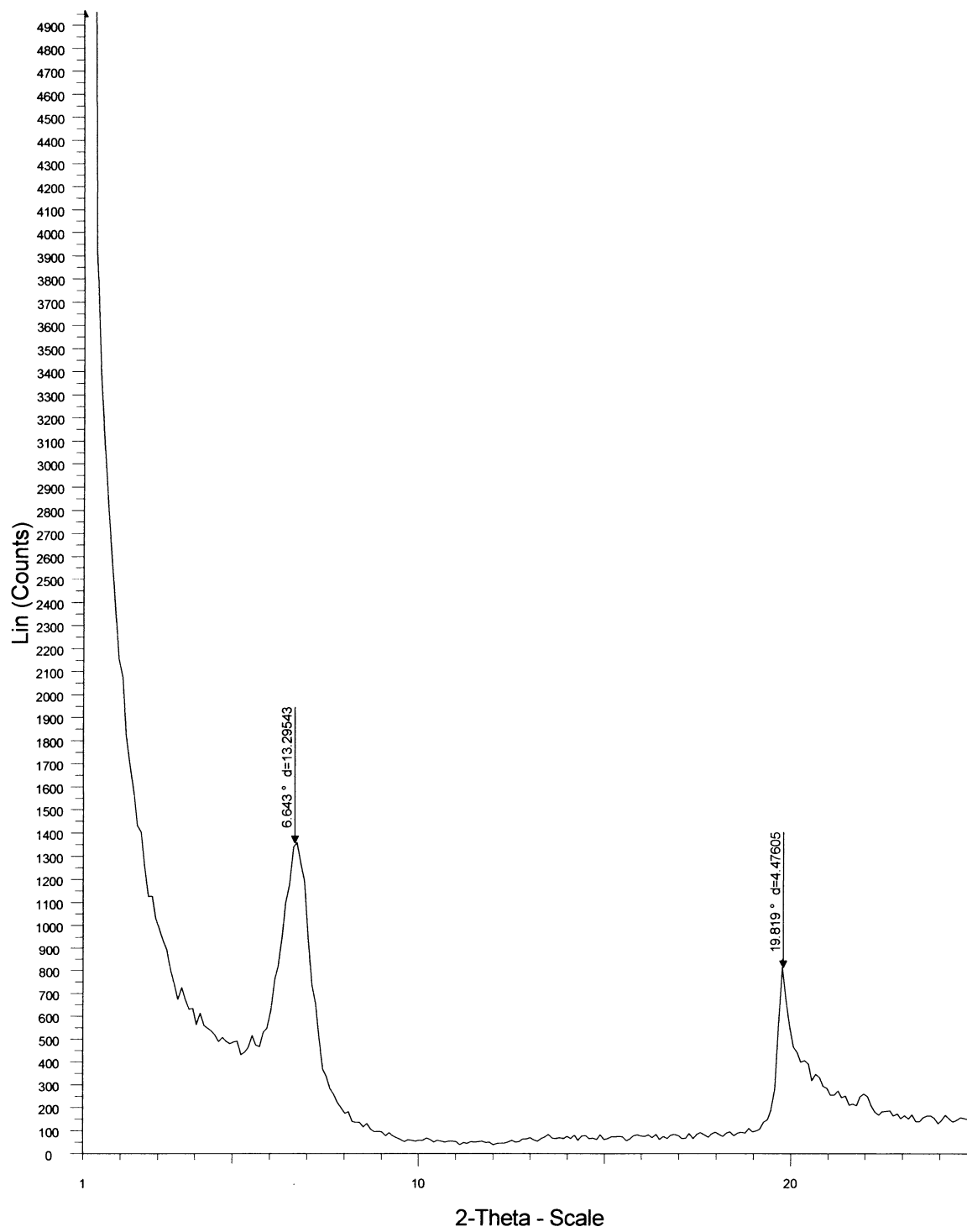
Appendix B2-c: WAXD of Aged Hexyl Alcohol 3:1 Organoclay



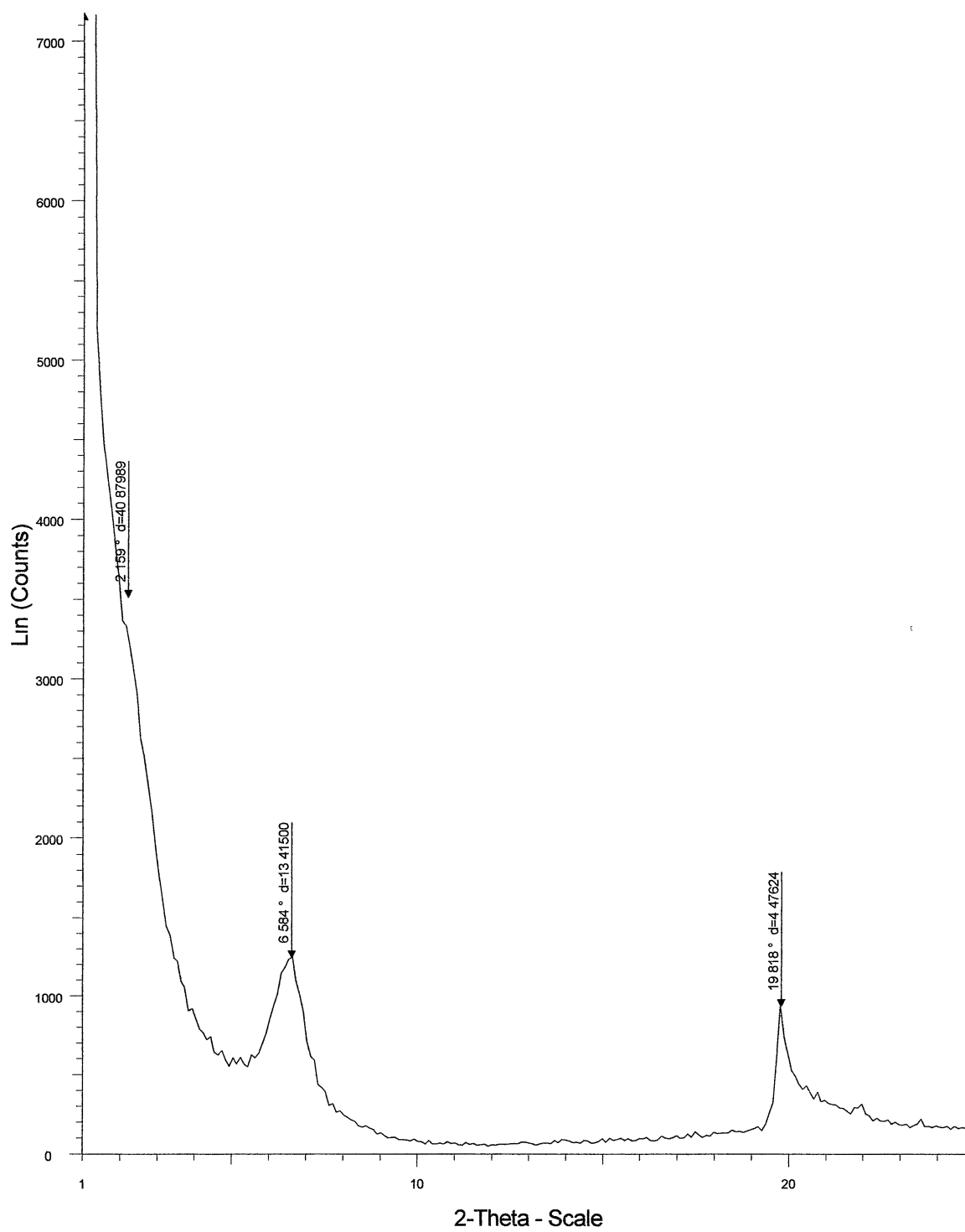
Appendix B3-a: WAXD of Aged Octyl Alcohol 1:1 Organoclay



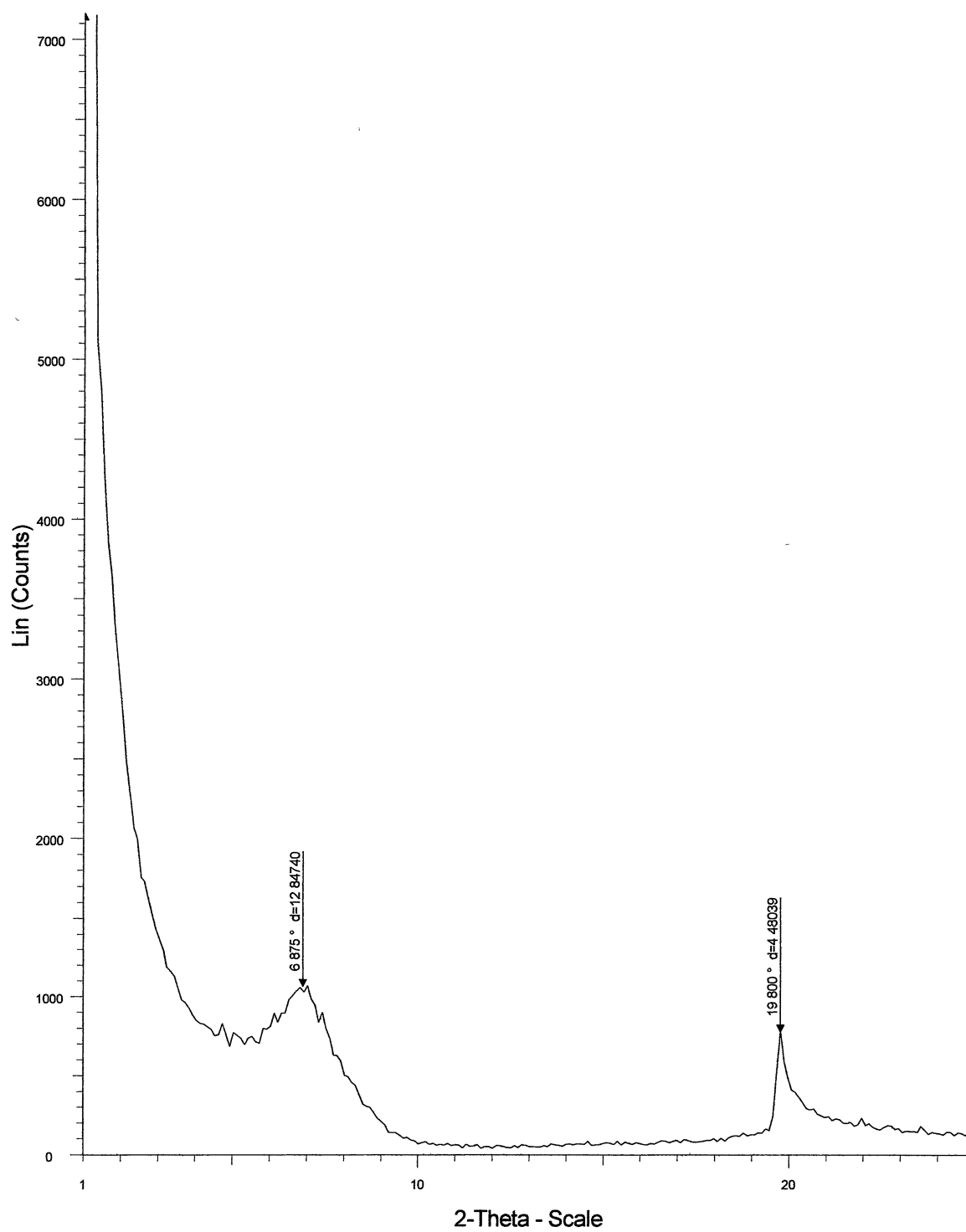
Appendix B3-b: WAXD of Aged Octyl Alcohol 2:1 Organoclay

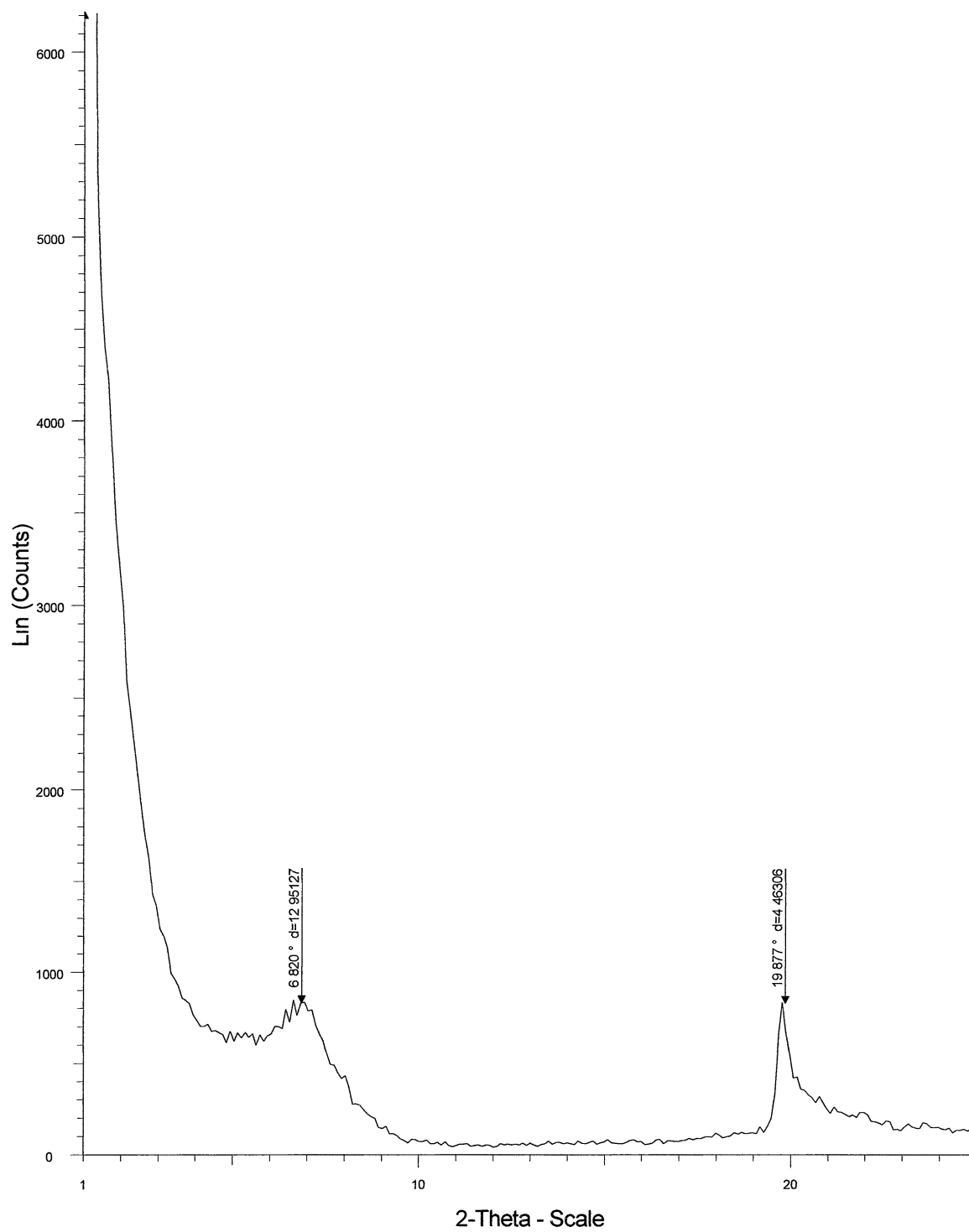


Appendix B3-c: WAXD of Aged Octyl Alcohol 3:1 Organoclay

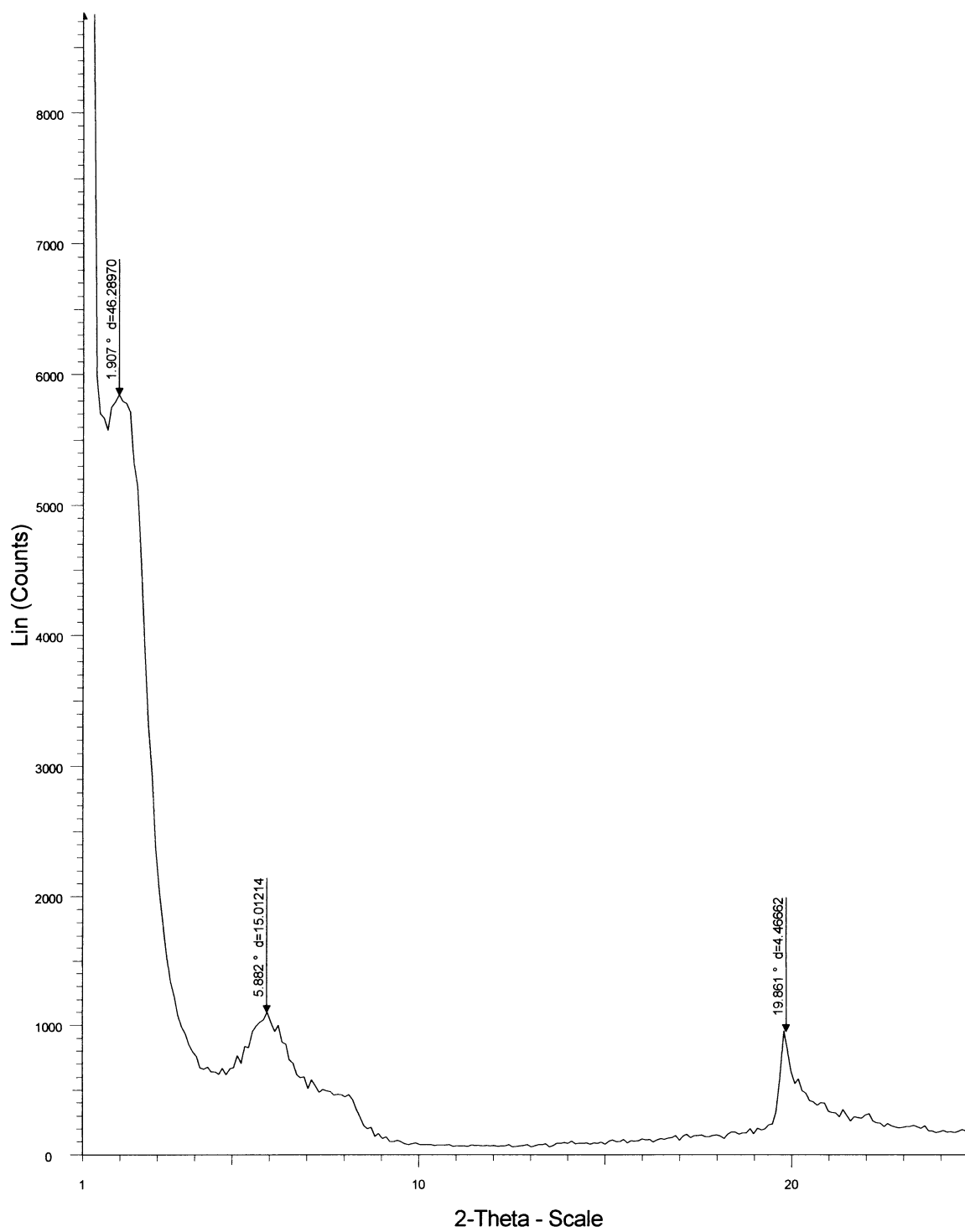


Appendix B4-a: WAXD of Aged Decyl Alcohol 1:1 Organoclay

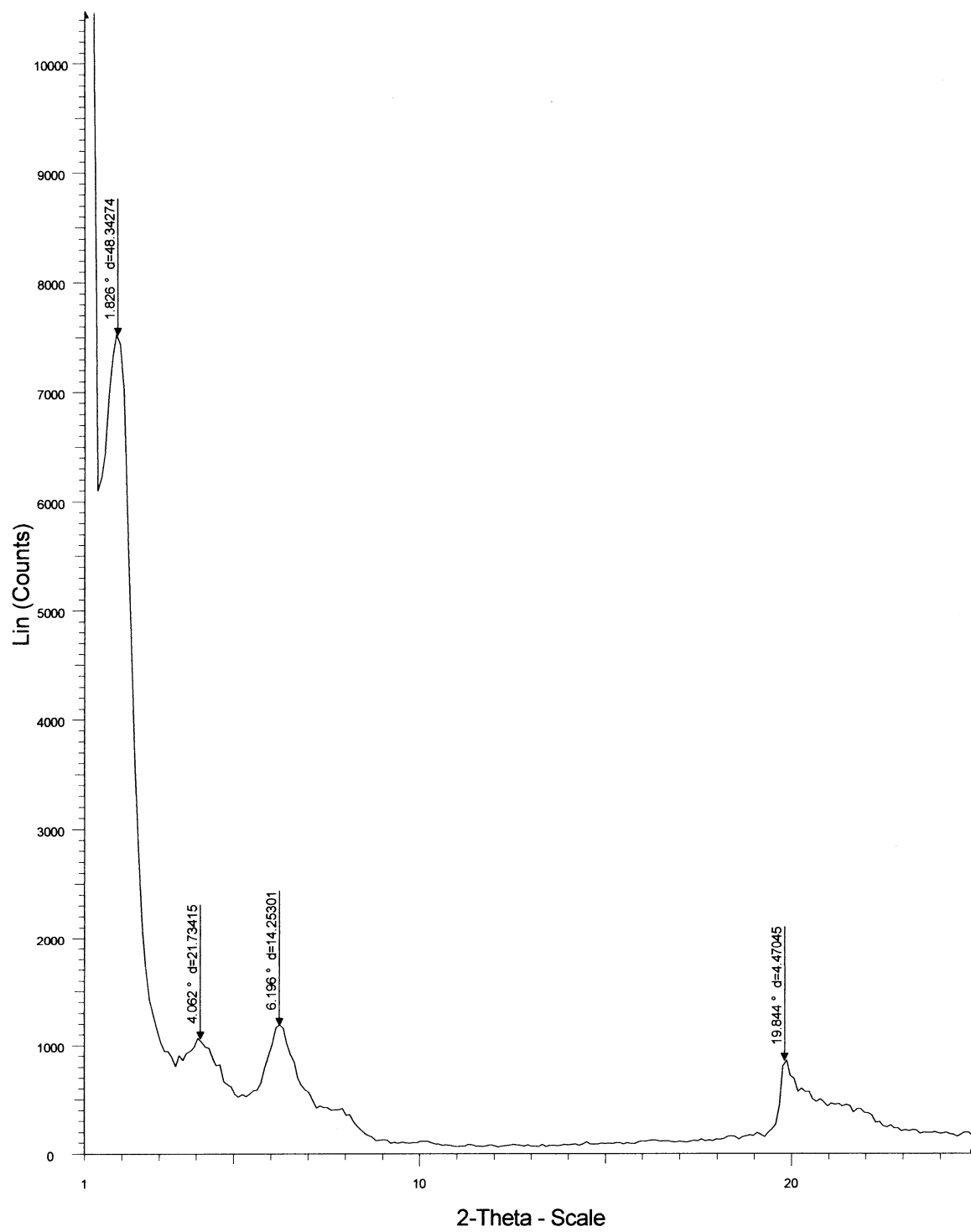


Appendix B4-b: WAXD of Aged Decyl Alcohol 2:1 Organoclay

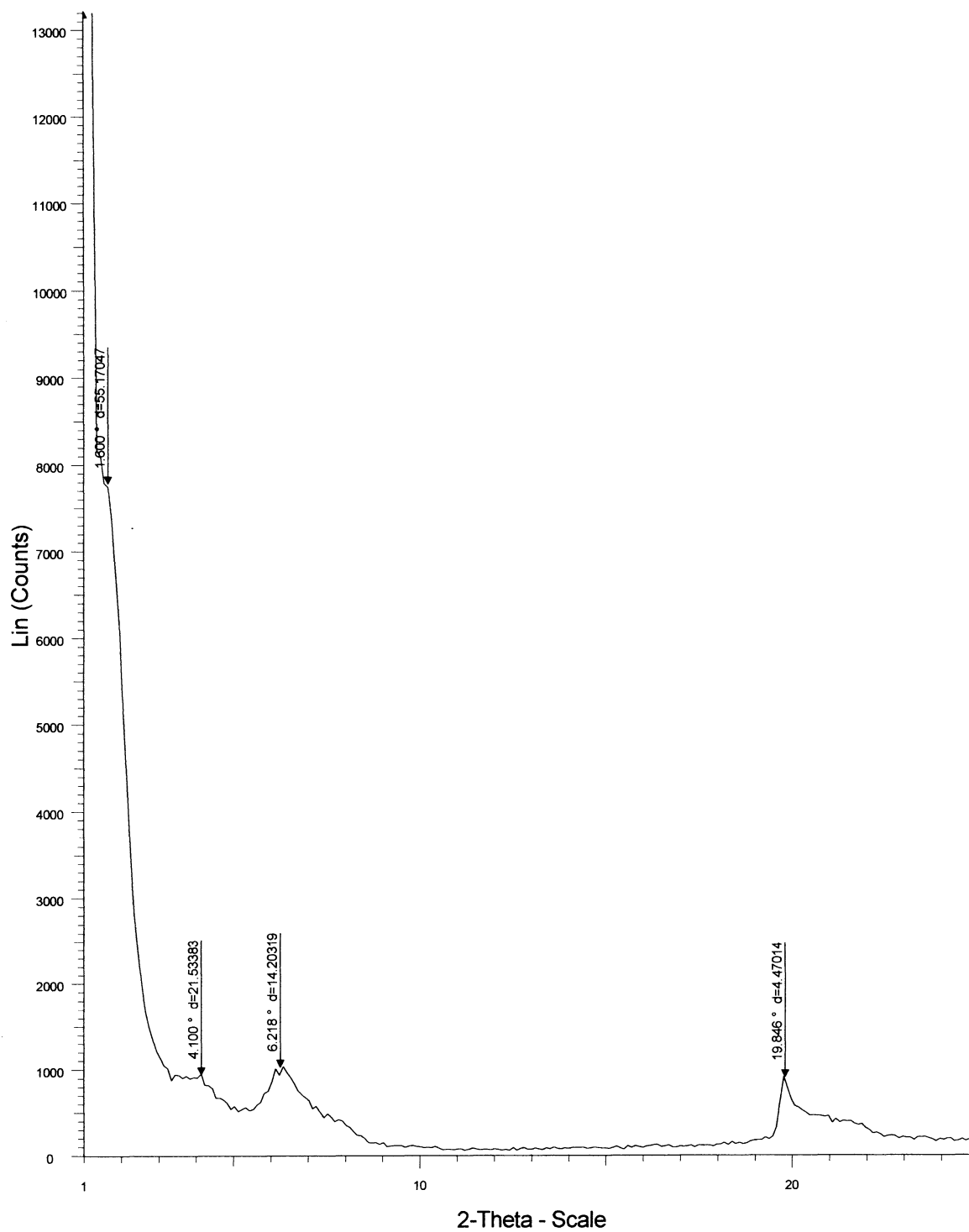
Appendix B4-c: WAXD of Aged Decyl Alcohol 3:1 Organoclay



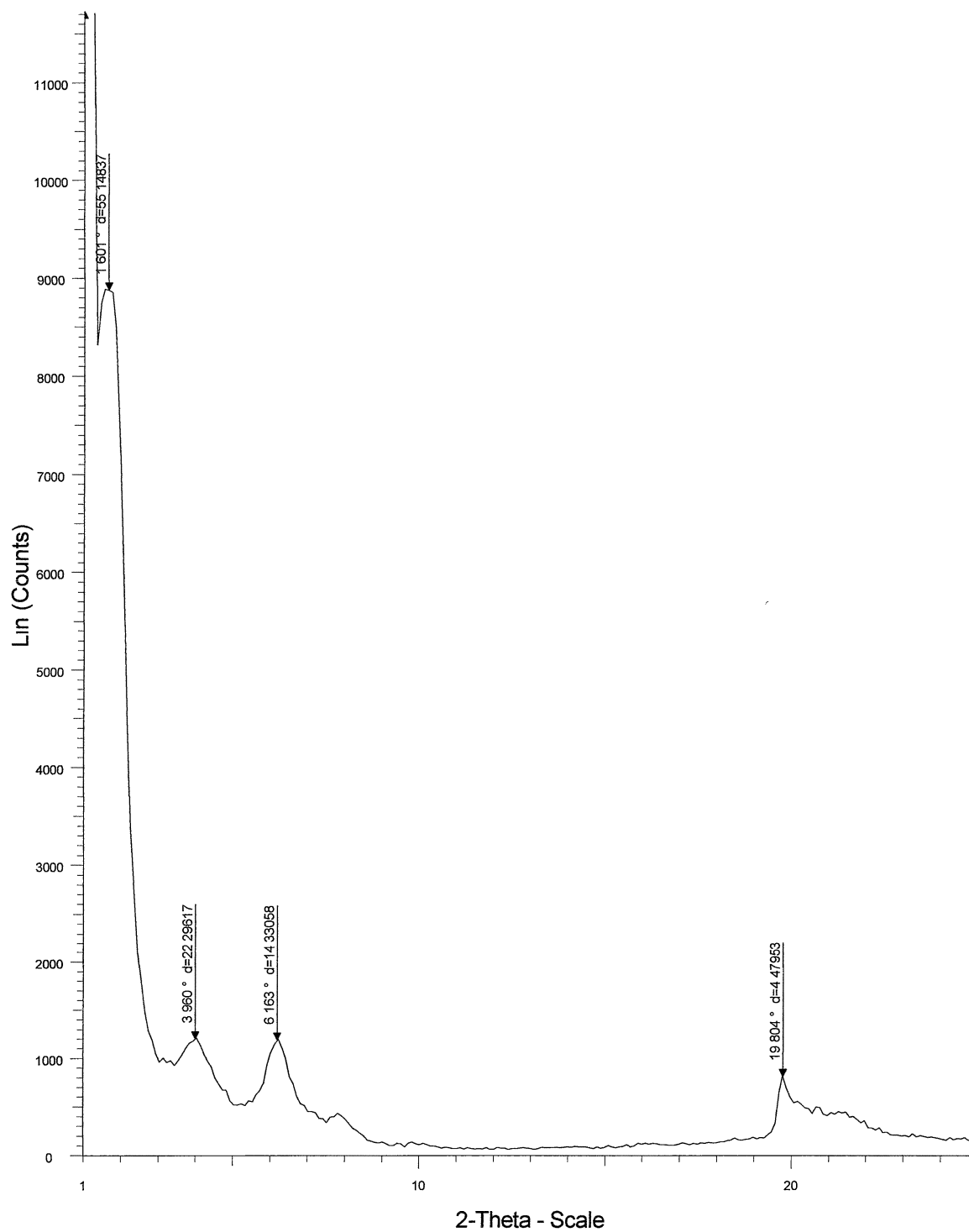
Appendix B5-a: WAXD of Aged Dodecyl Alcohol 1:1 Organoclay



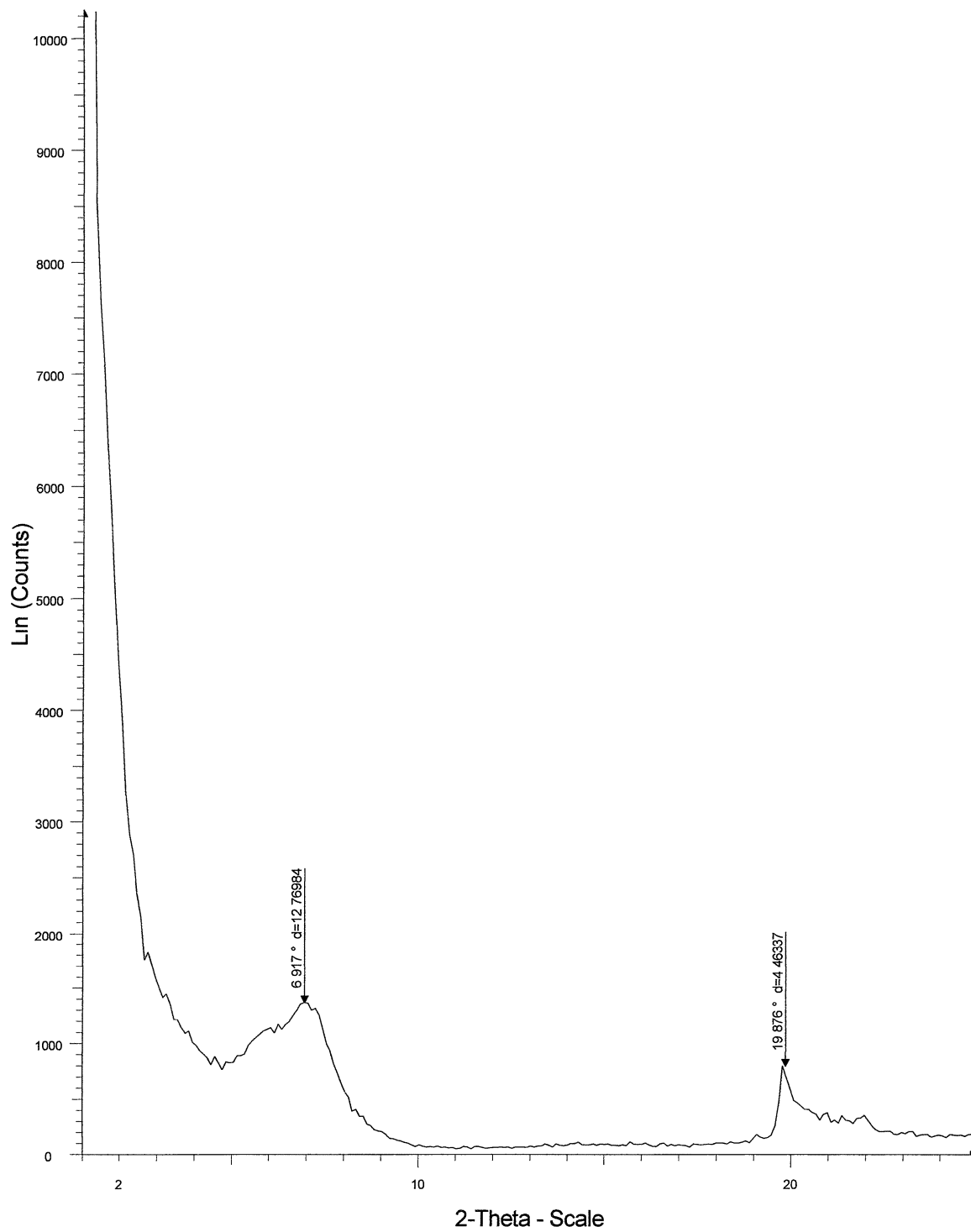
Appendix B5-b: WAXD of Aged Dodecyl Alcohol 2:1 Organoclay



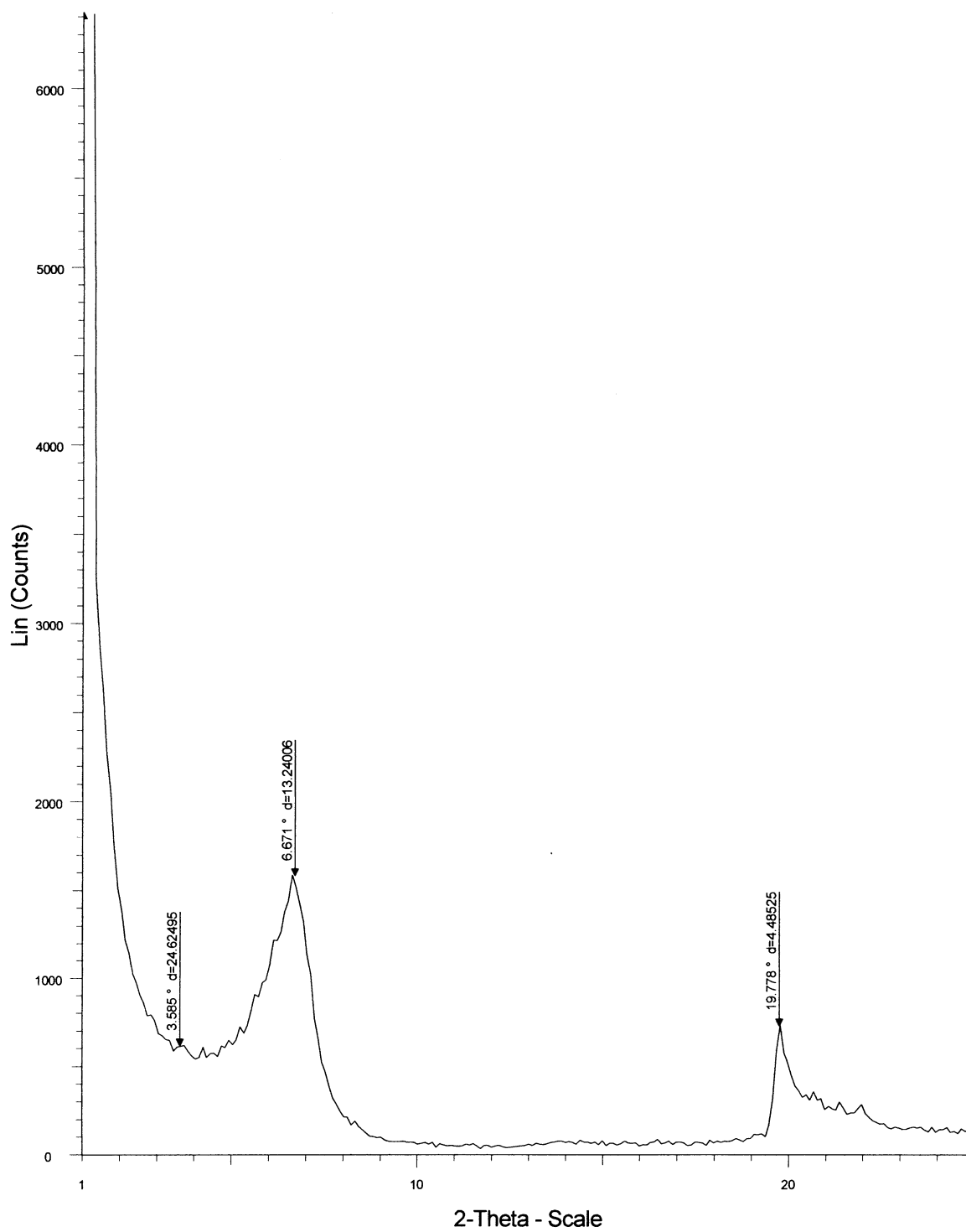
Appendix B5-c: WAXD of Aged Dodecyl Alcohol 3:1 Organoclay



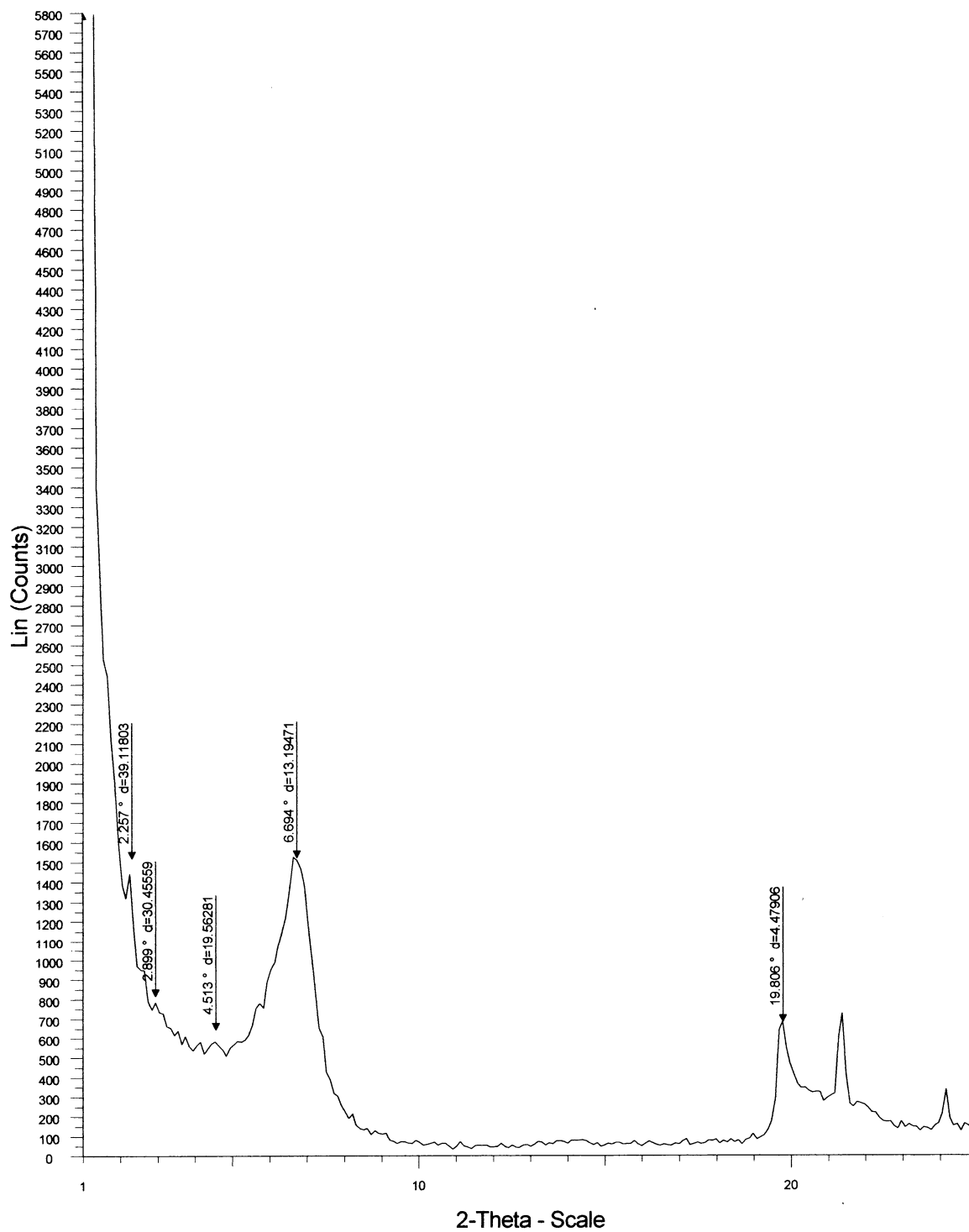
Appendix B6-a: WAXD of Aged Tetradecyl Alcohol 1:1 Organoclay



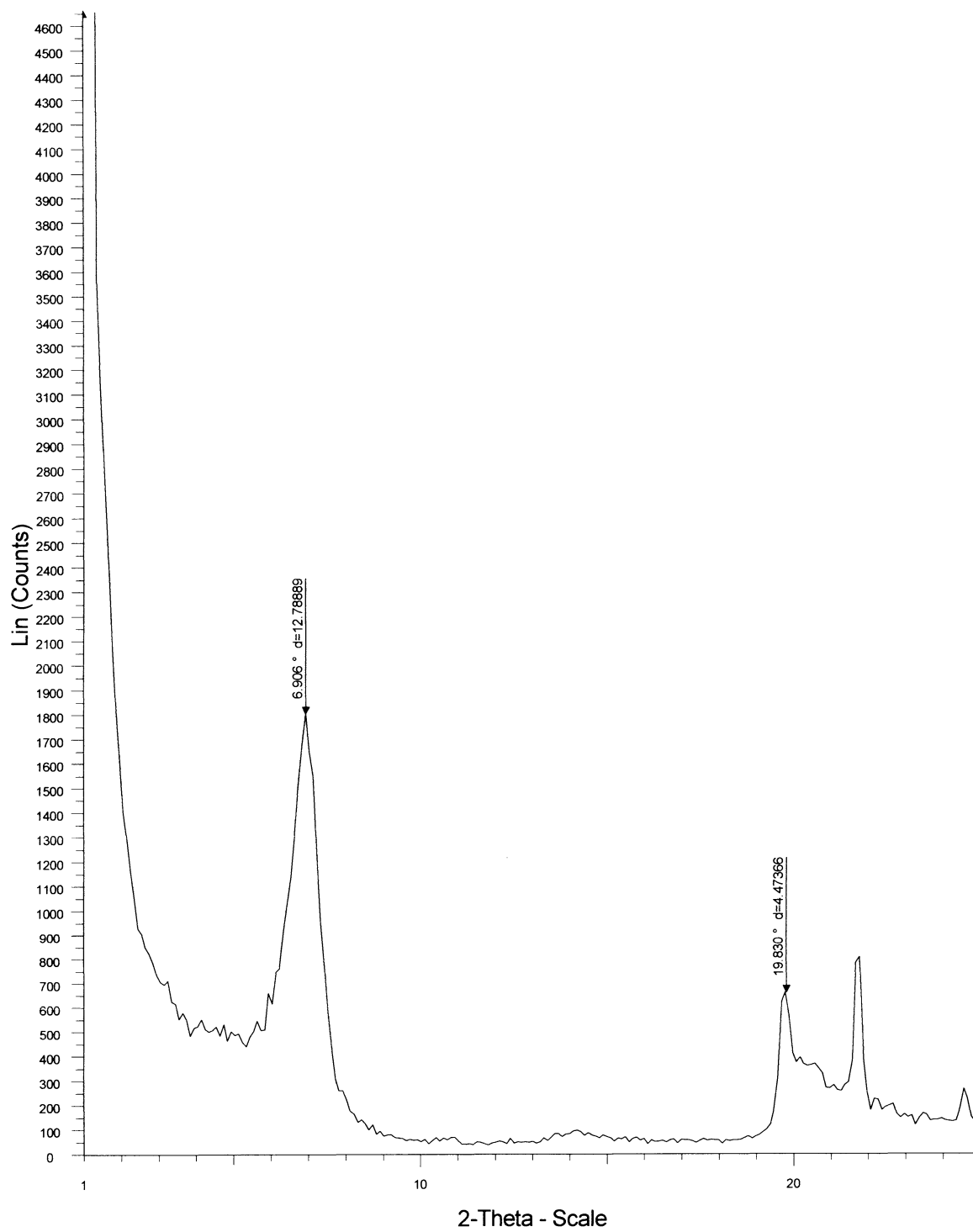
Appendix B6-b: WAXD of Aged Tetradecyl Alcohol 2:1 Organoclay



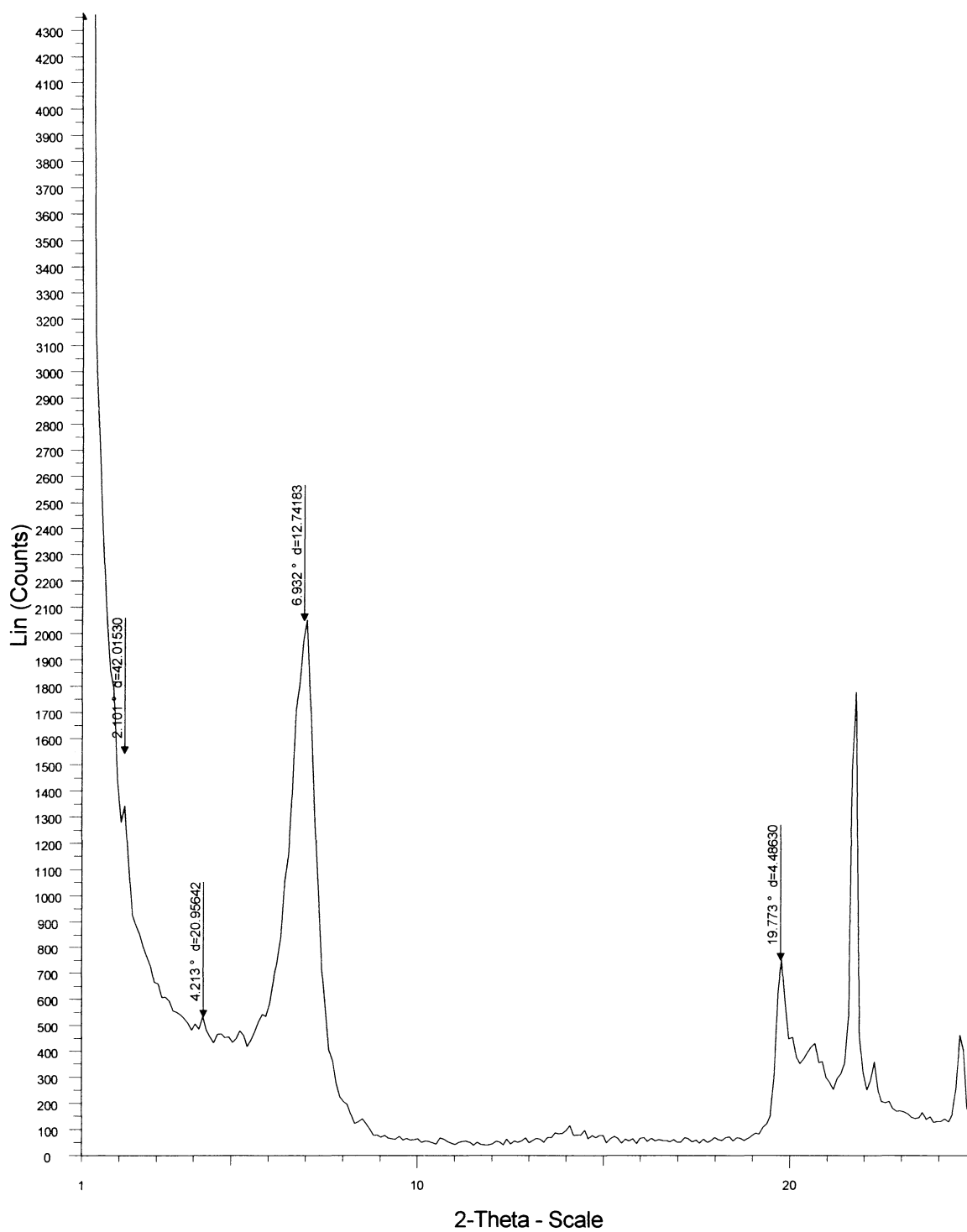
Appendix B6-c: WAXD of Aged Tetradecyl Alcohol 3:1 Organoclay

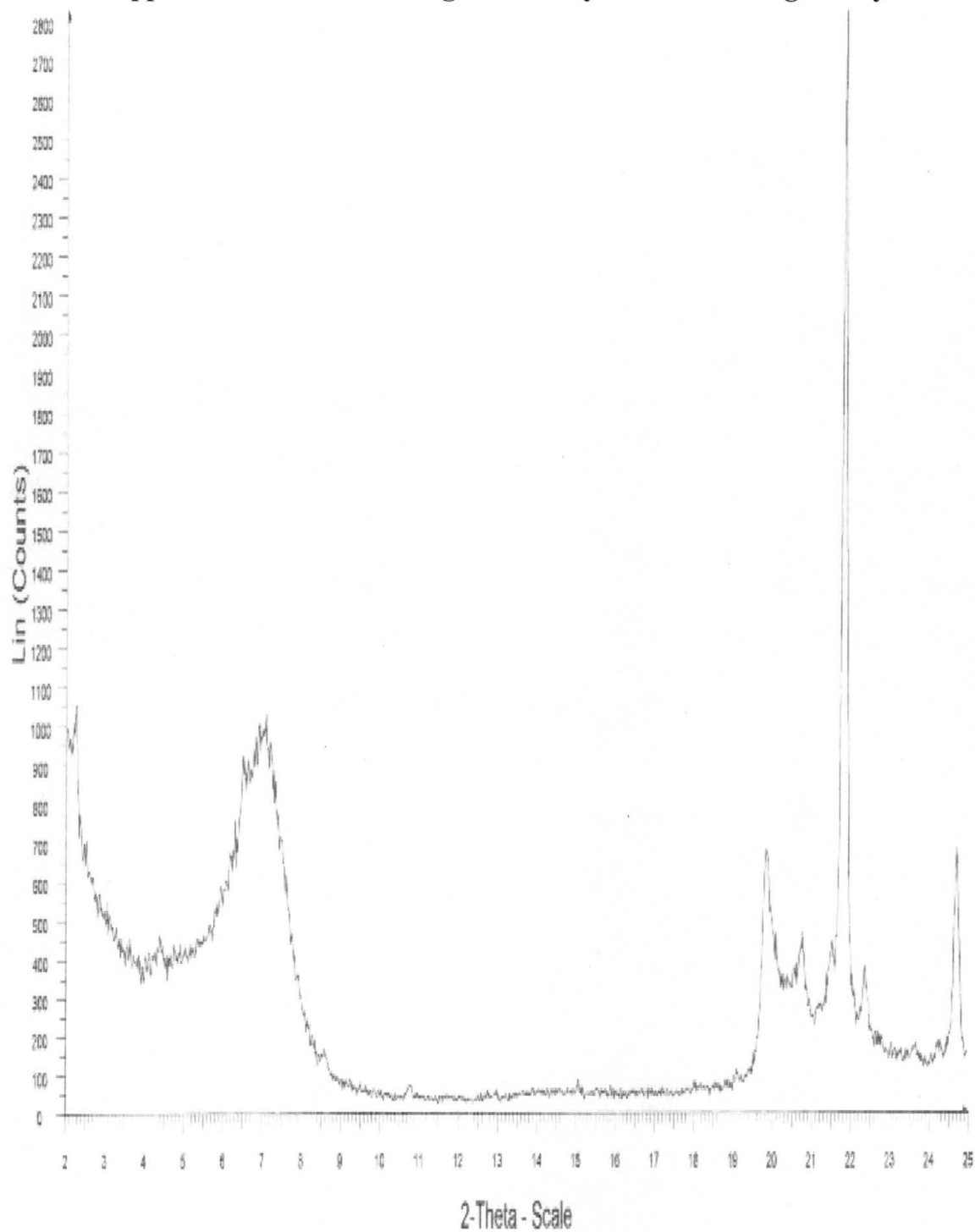


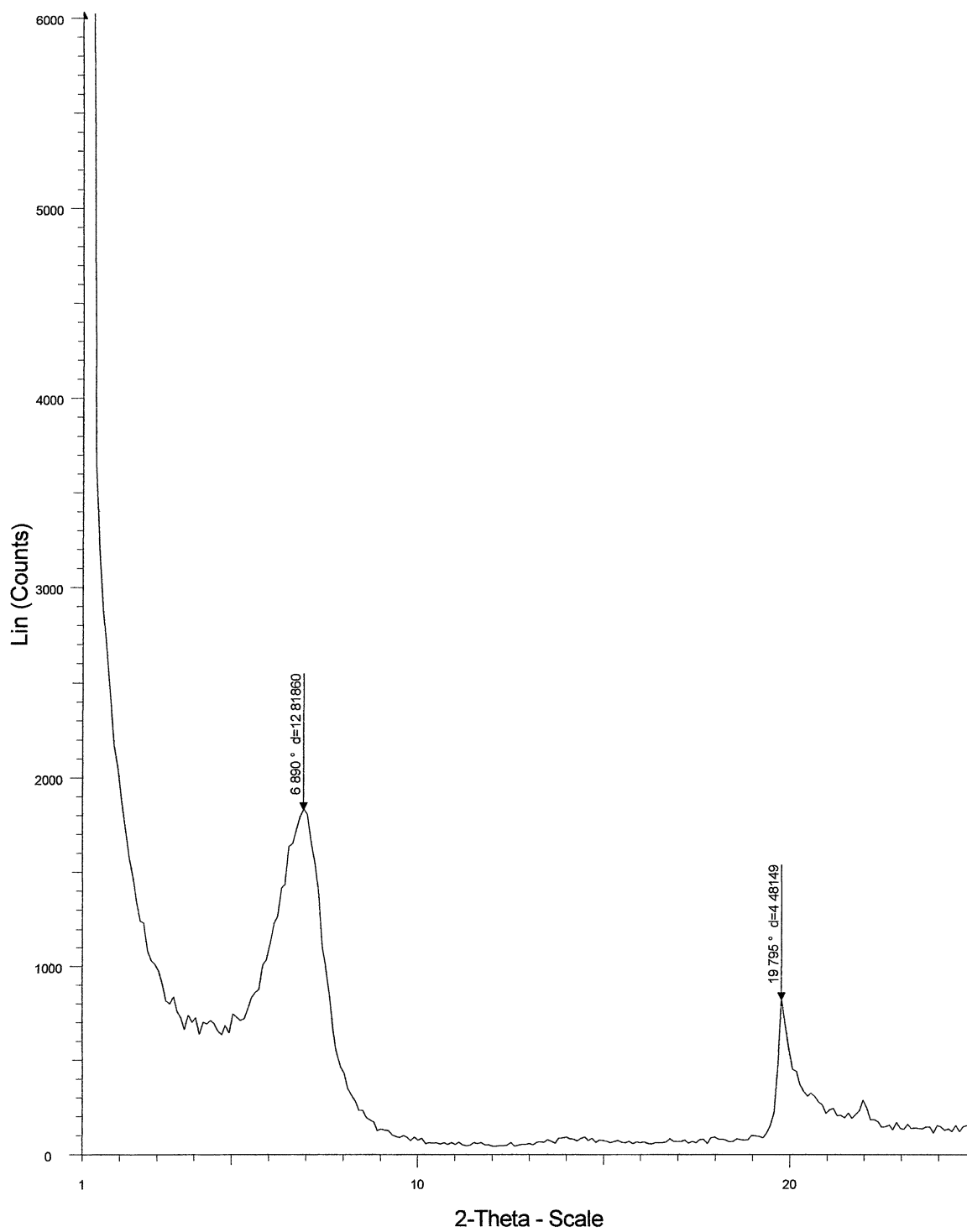
Appendix B7-a: WAXD of Aged Octadecyl Alcohol 1:1 Organoclay

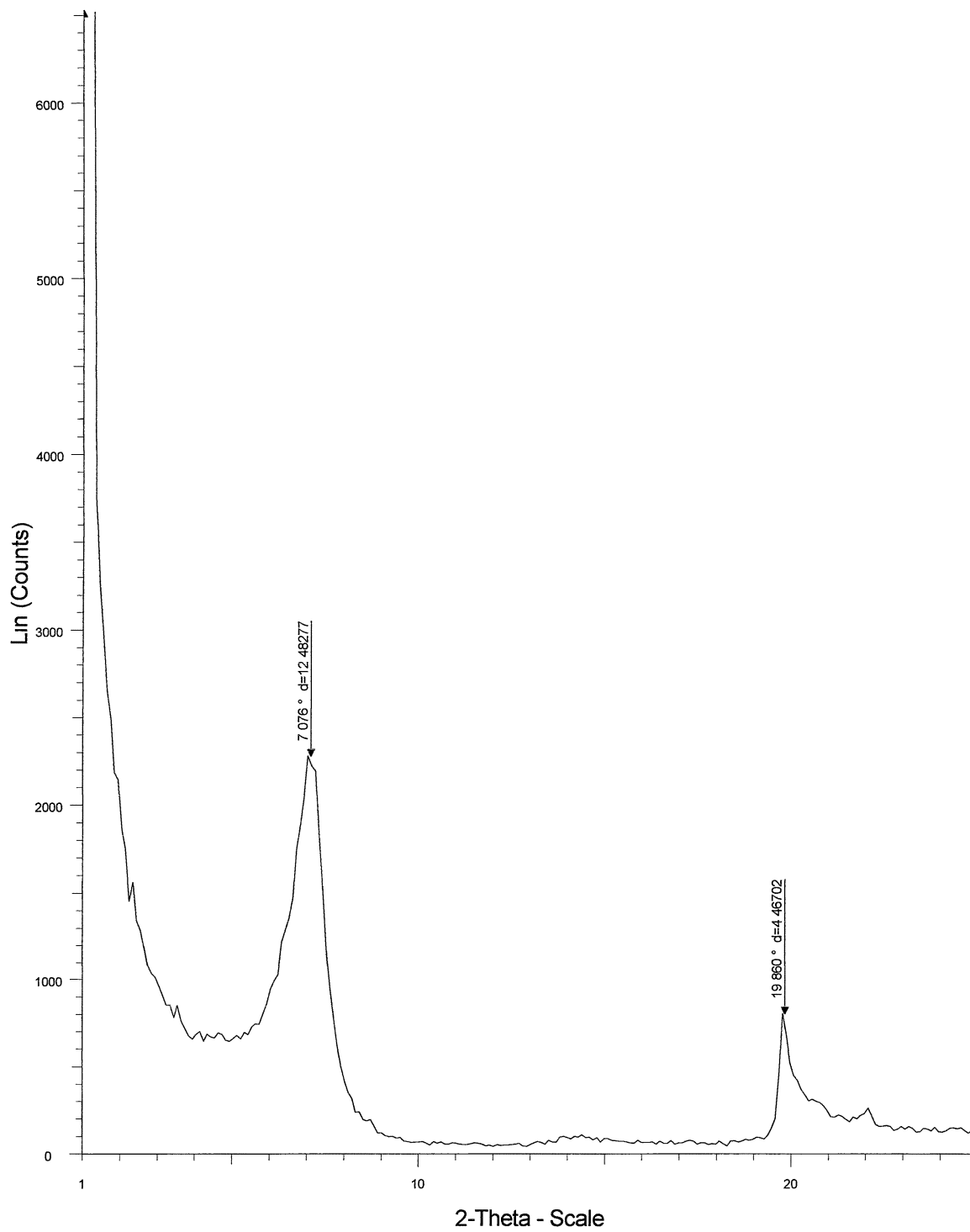


Appendix B7-b: WAXD of Aged Octadecyl Alcohol 2:1 Organoclay

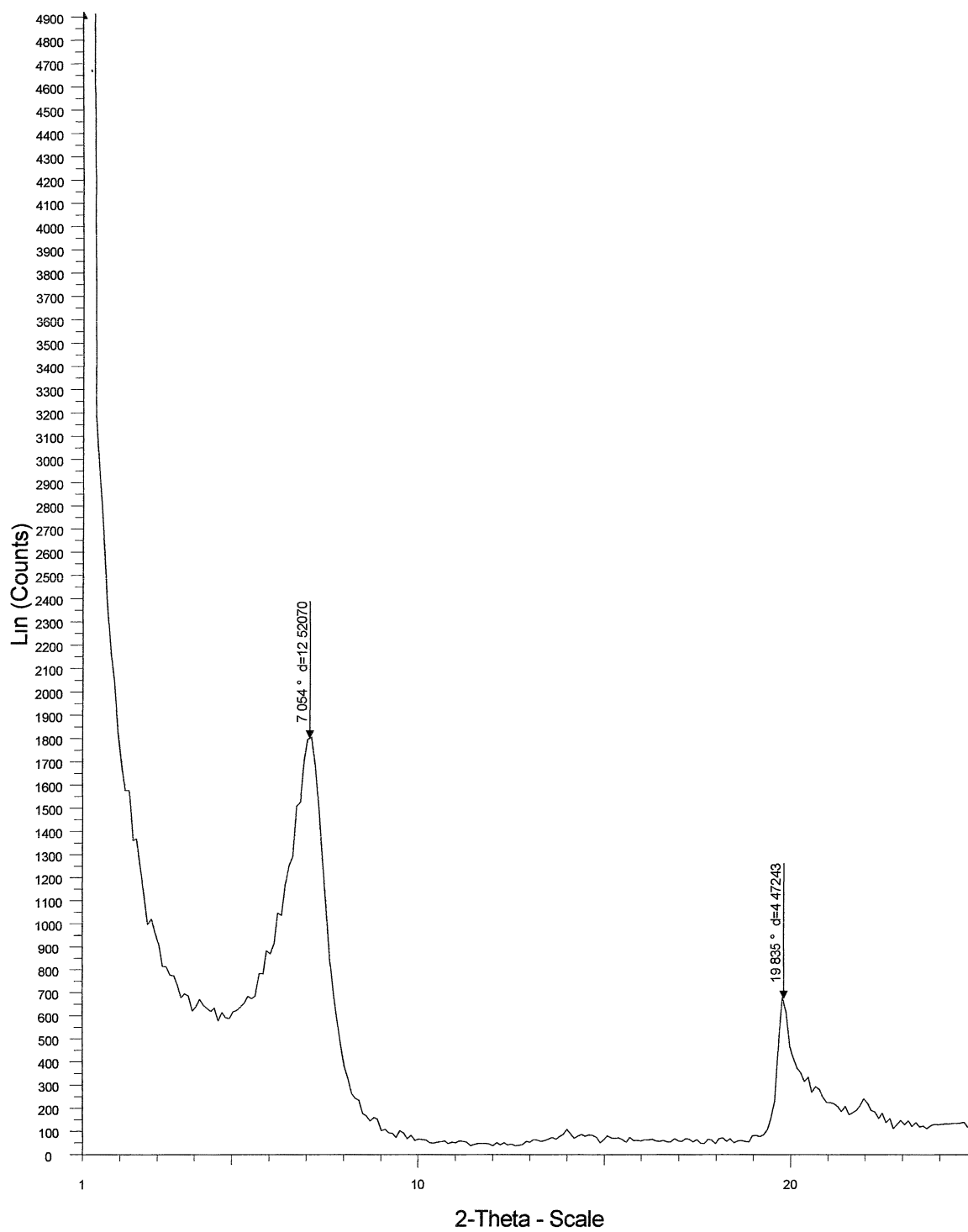


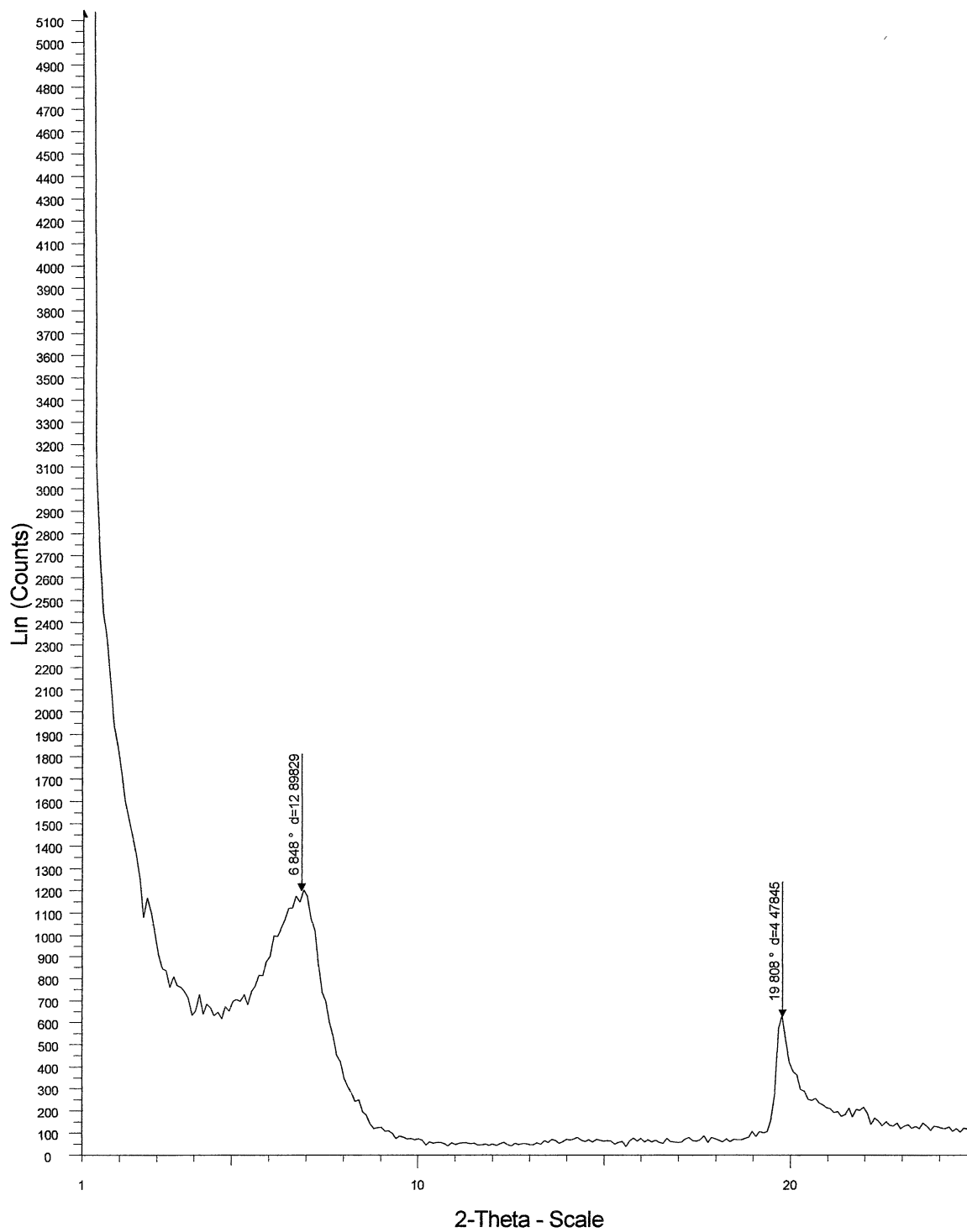
Appendix B7-c: WAXD of Aged Octadecyl Alcohol 3:1 Organoclay

Appendix B8-a: WAXD of Aged Butyl Aldehyde 1:1 Organoclay

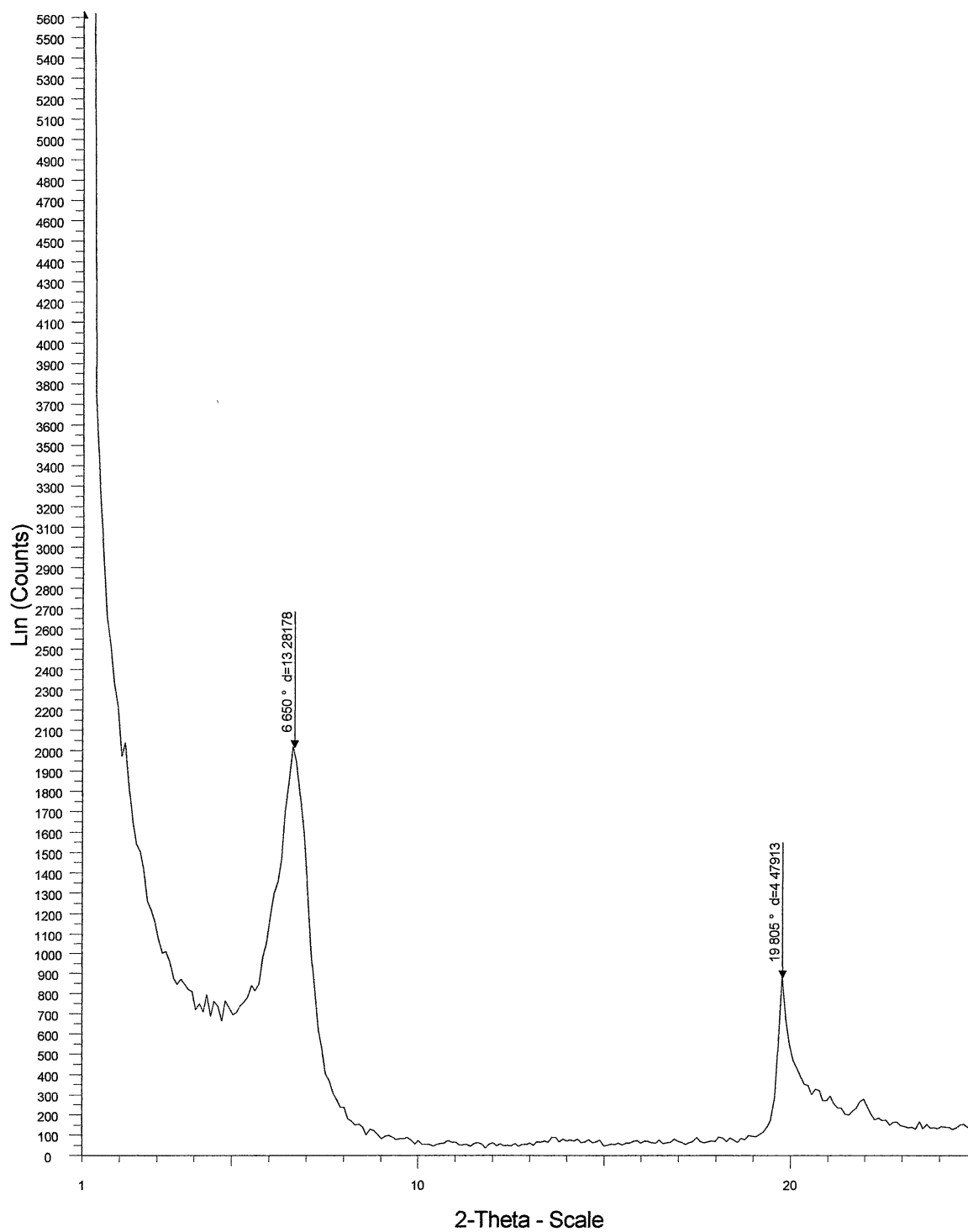
Appendix B8-b: WAXD of Aged Butyl Aldehyde 2:1 Organoclay

Appendix B8-c: WAXD of Aged Butyl Aldehyde 3:1 Organoclay

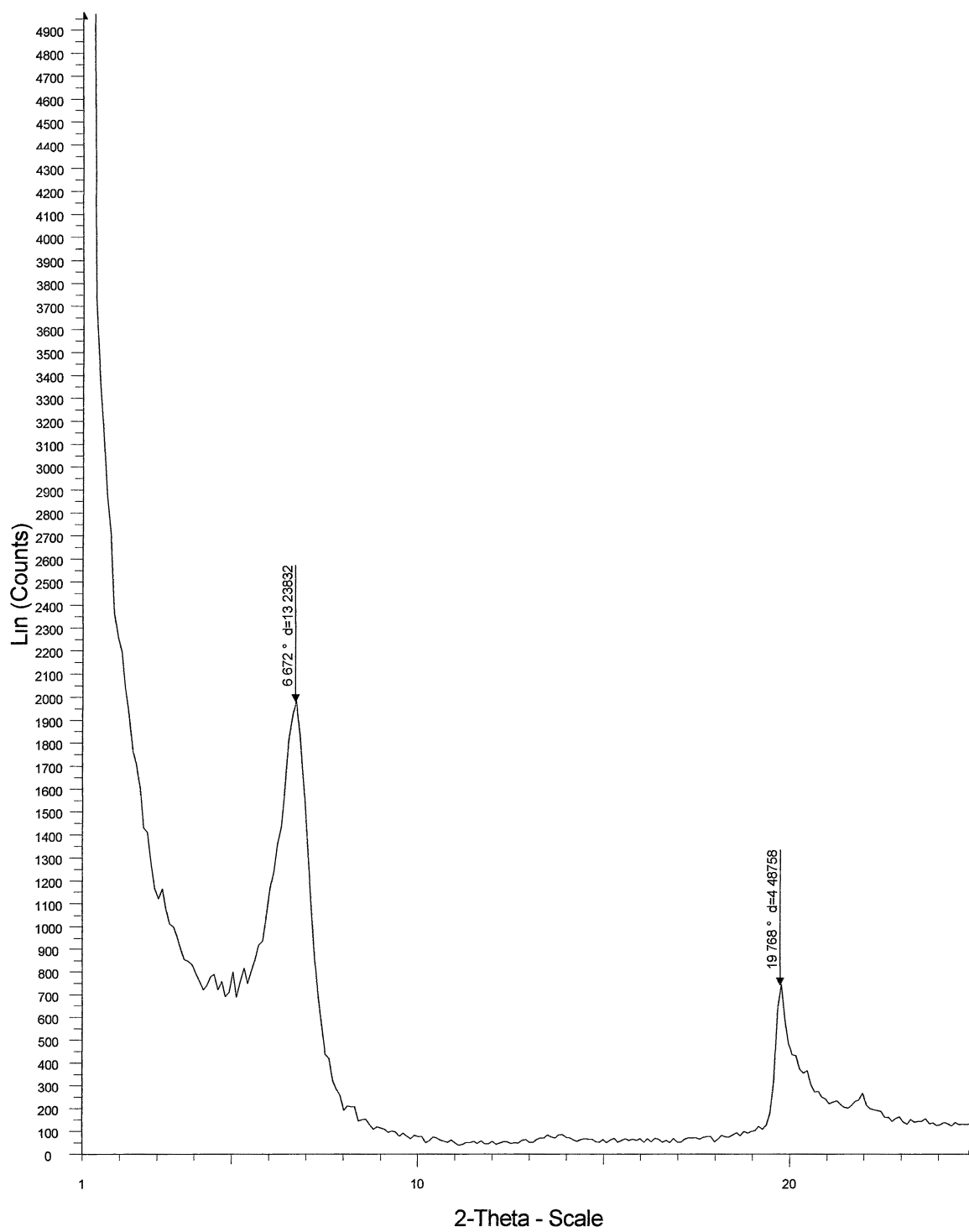


Appendix B9-a: WAXD of Aged Hexyl Aldehyde 1:1 Organoclay

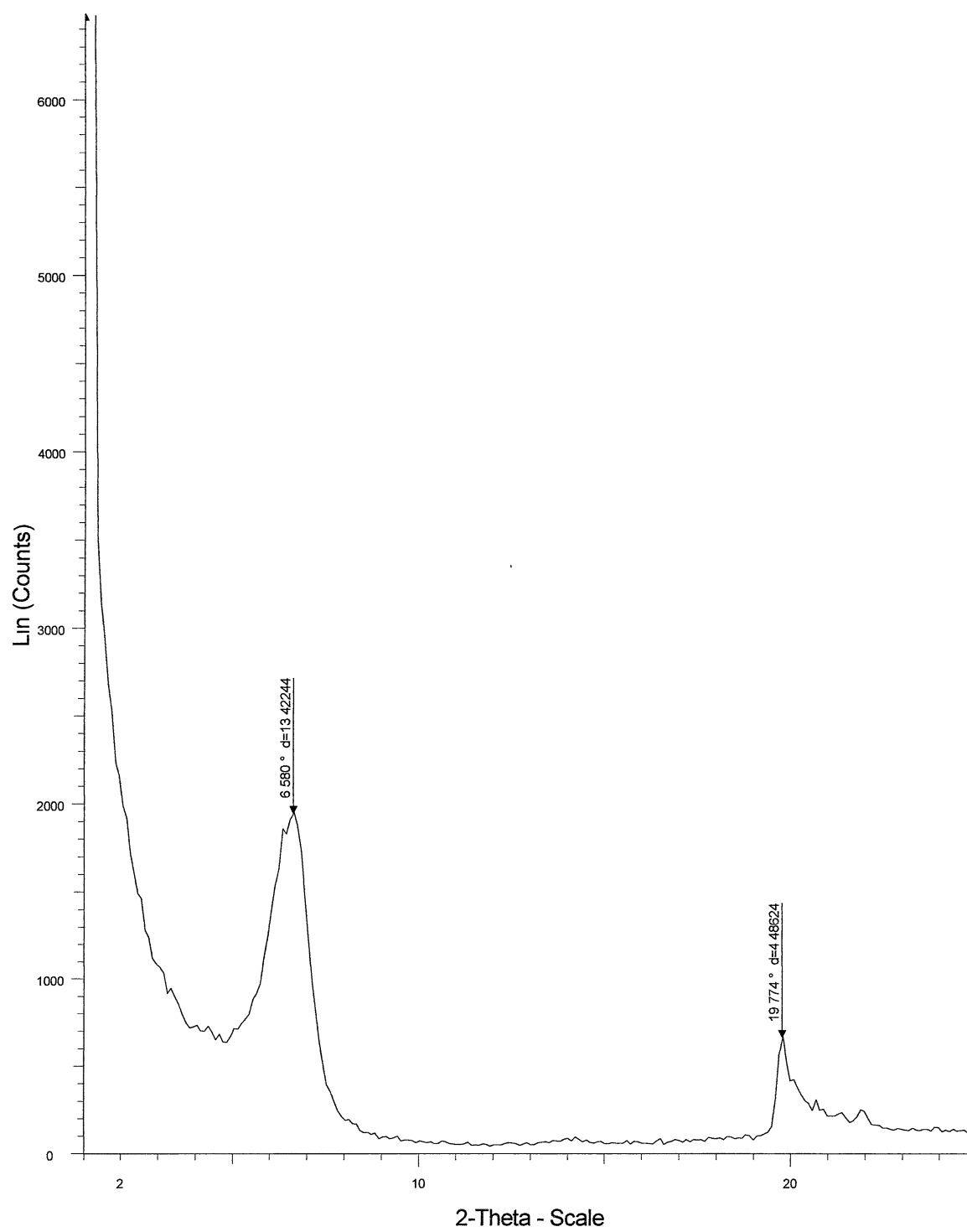
Appendix B9-b: WAXD of Aged Hexyl Aldehyde 2:1 Organoclay

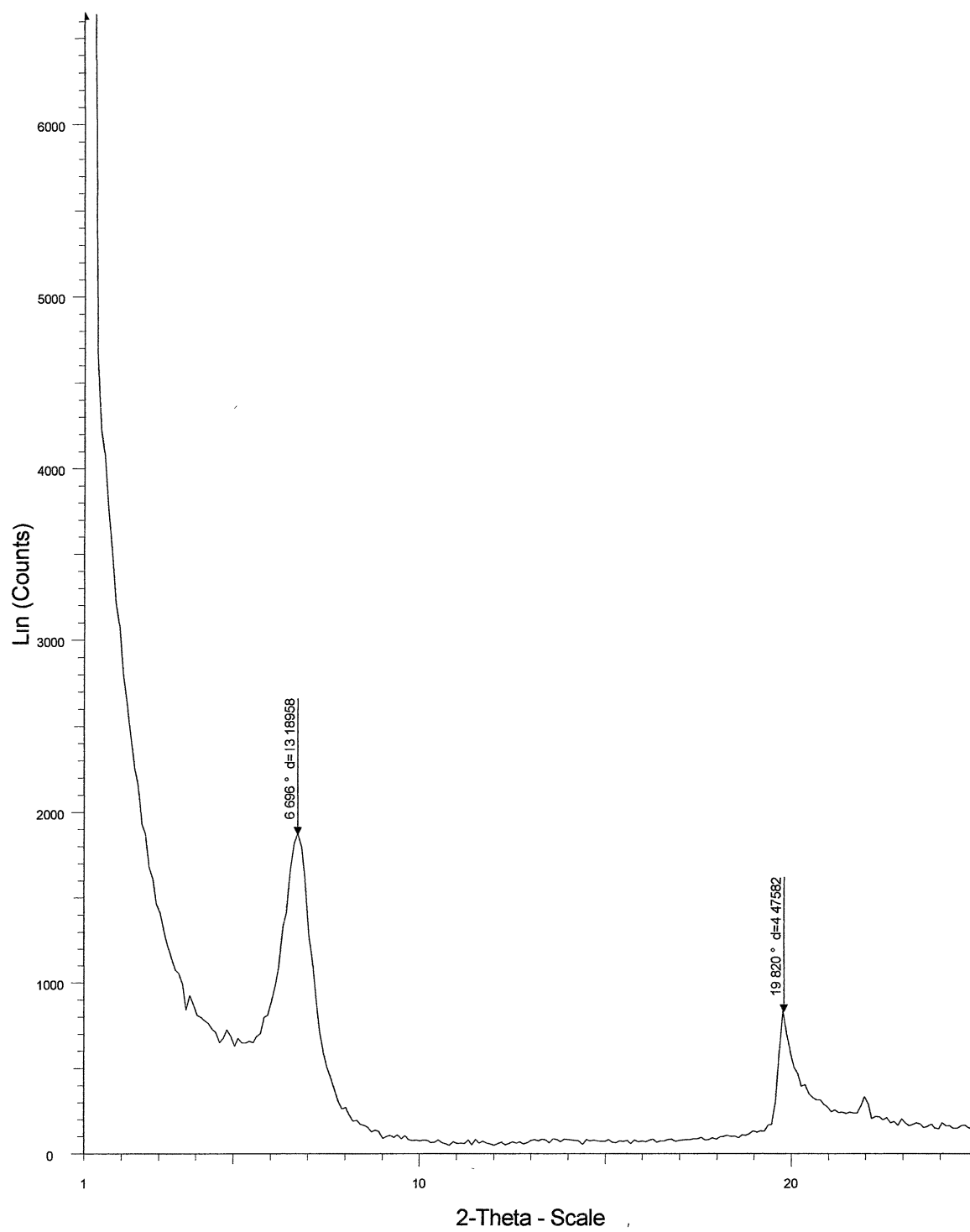


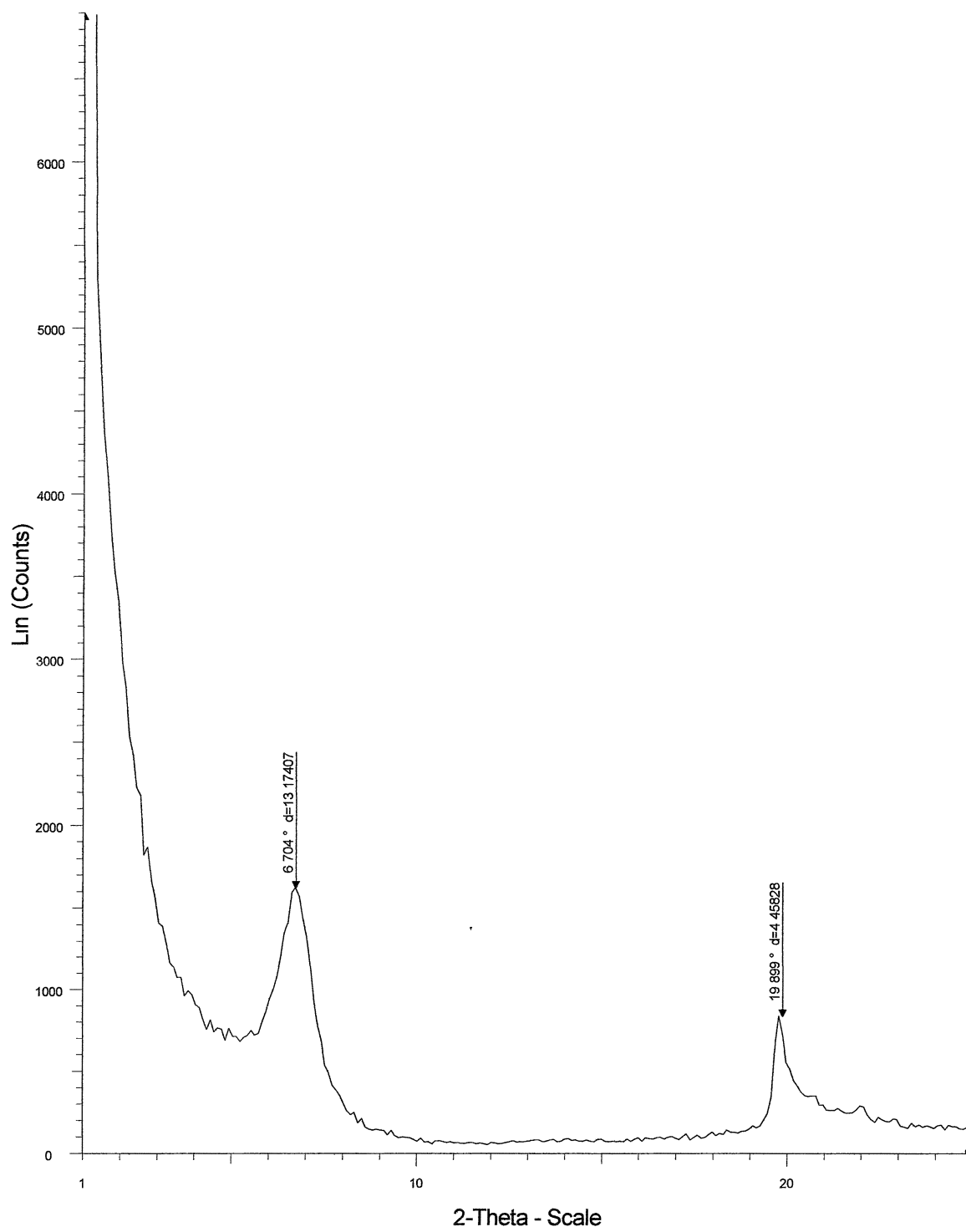
Appendix B9-c: WAXD of Aged Hexyl Aldehyde 3:1 Organoclay



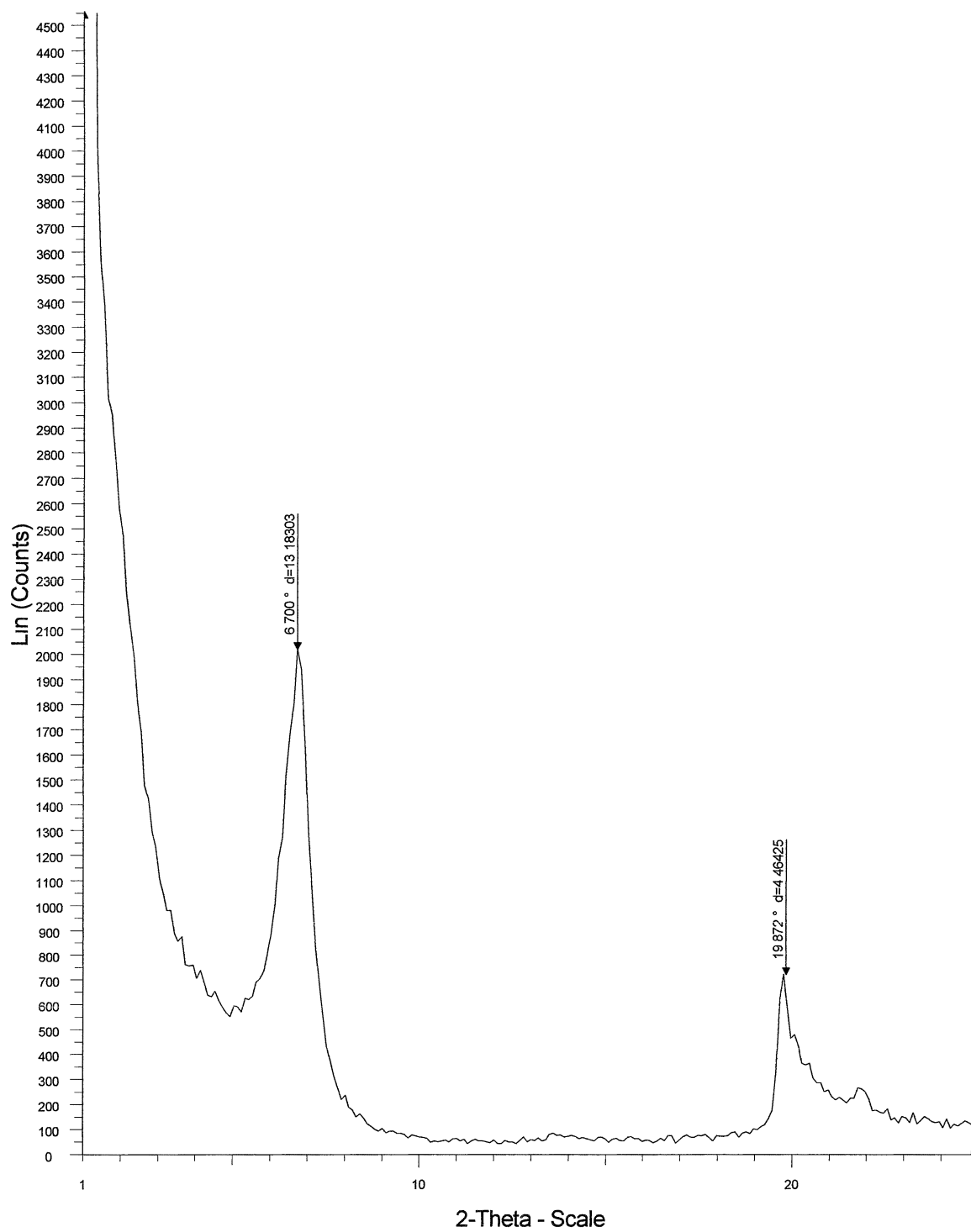
Appendix B10-a: WAXD of Aged Octyl Aldehyde 1:1 Organoclay



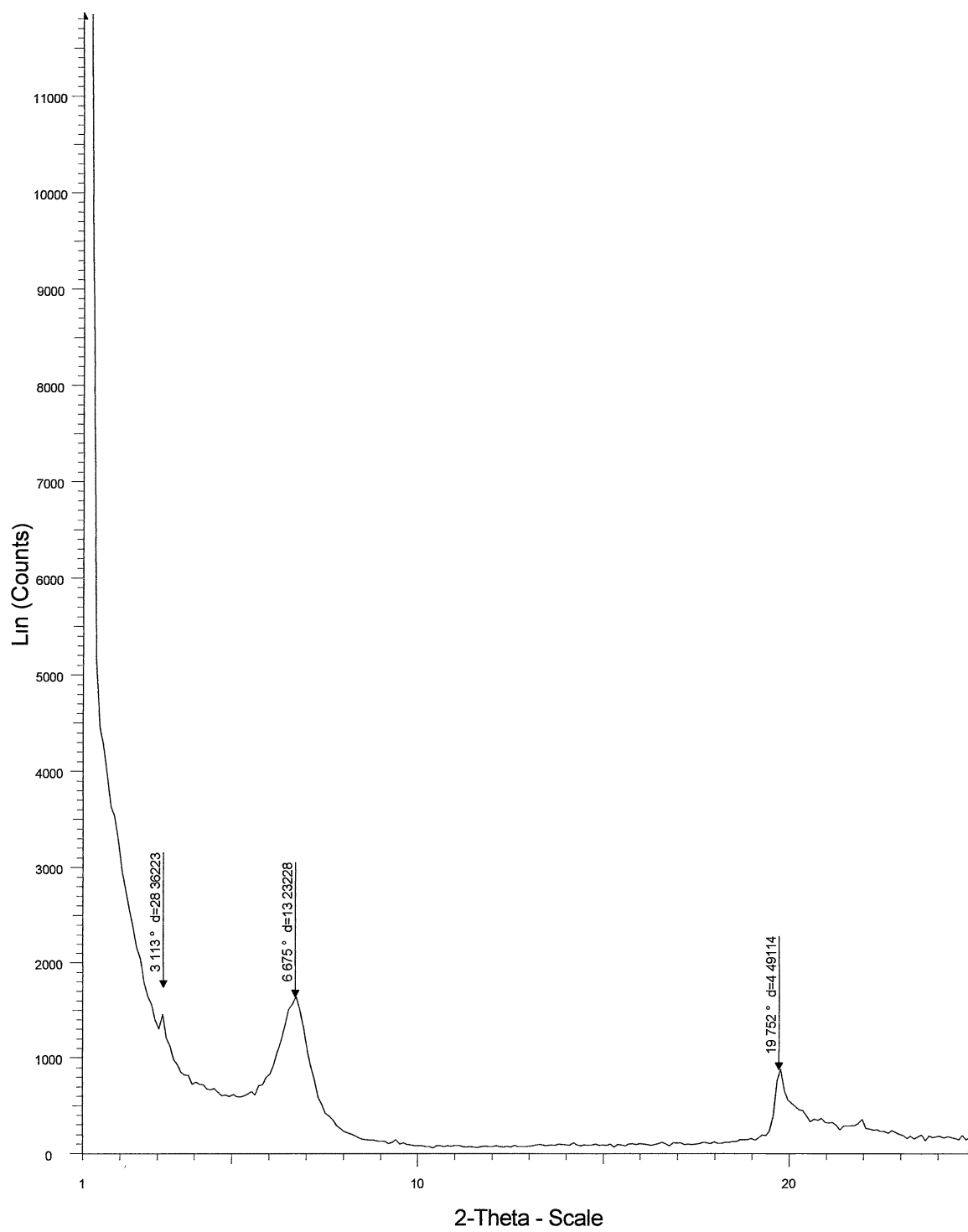
Appendix B10-b: WAXD of Aged Octyl Aldehyde 2:1 Organoclay

Appendix B10-c: WAXD of Aged Octyl Aldehyde 3:1 Organoclay:

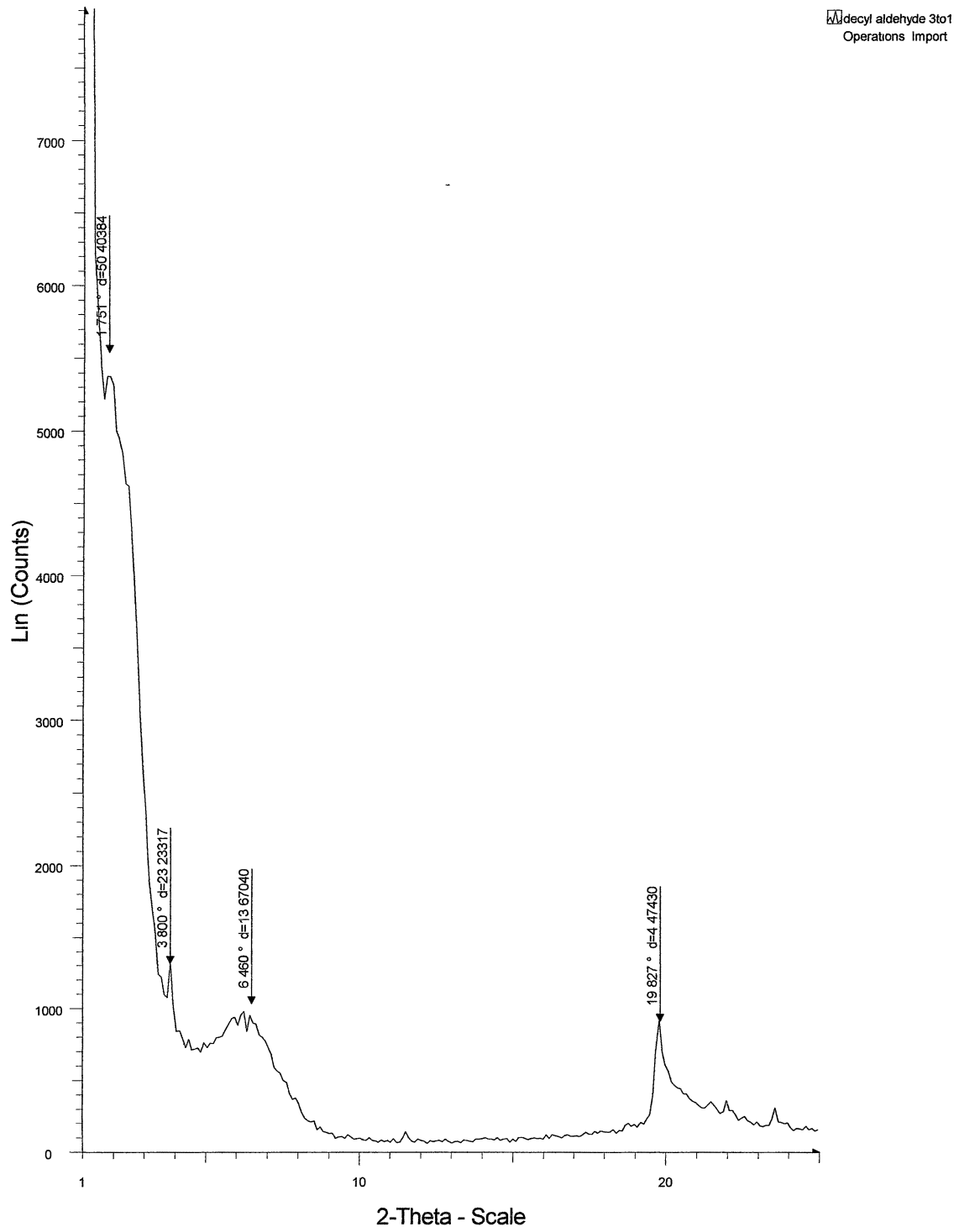
Appendix B11-a: WAXD of Aged Decyl Aldehyde 1:1 Organoclay

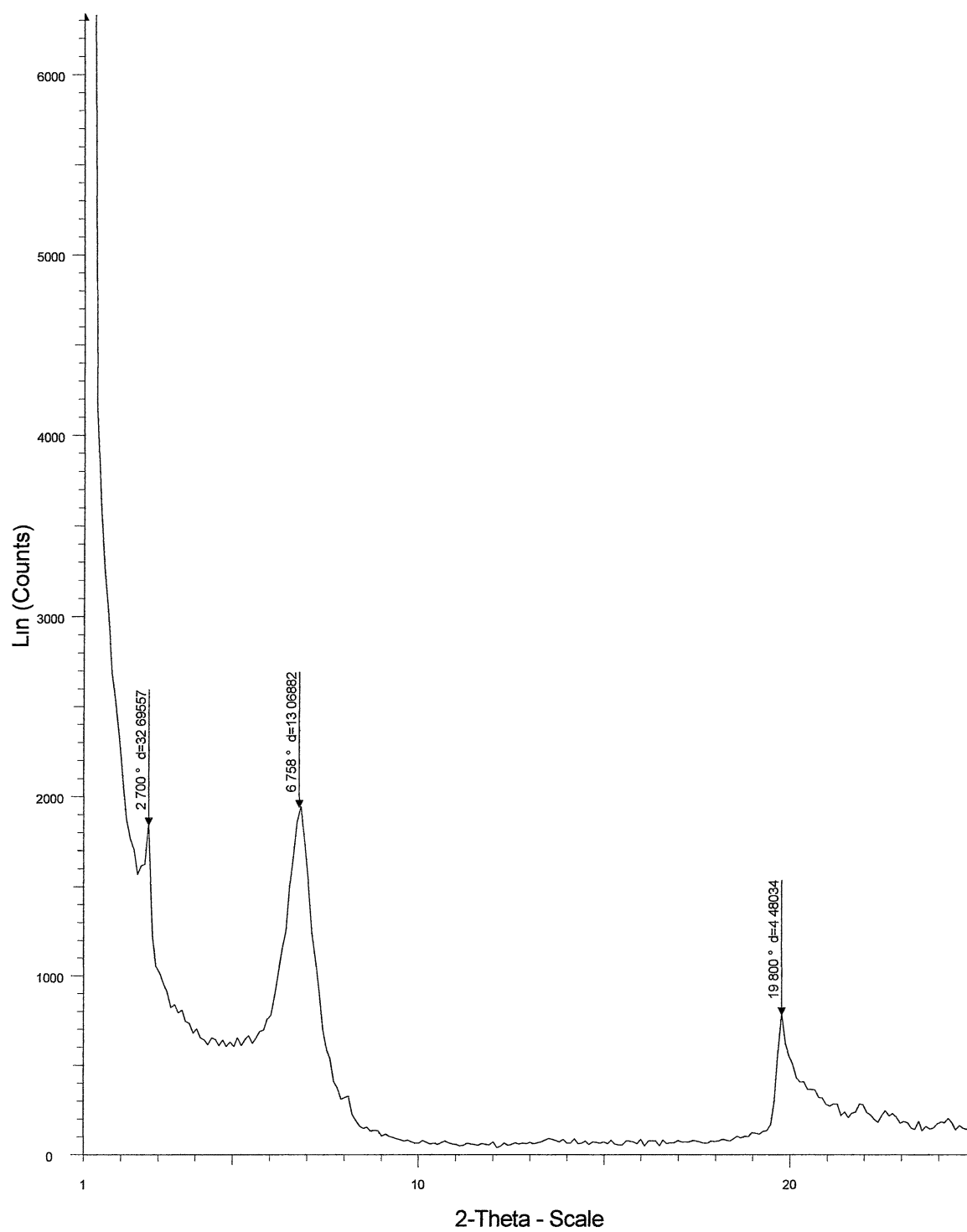


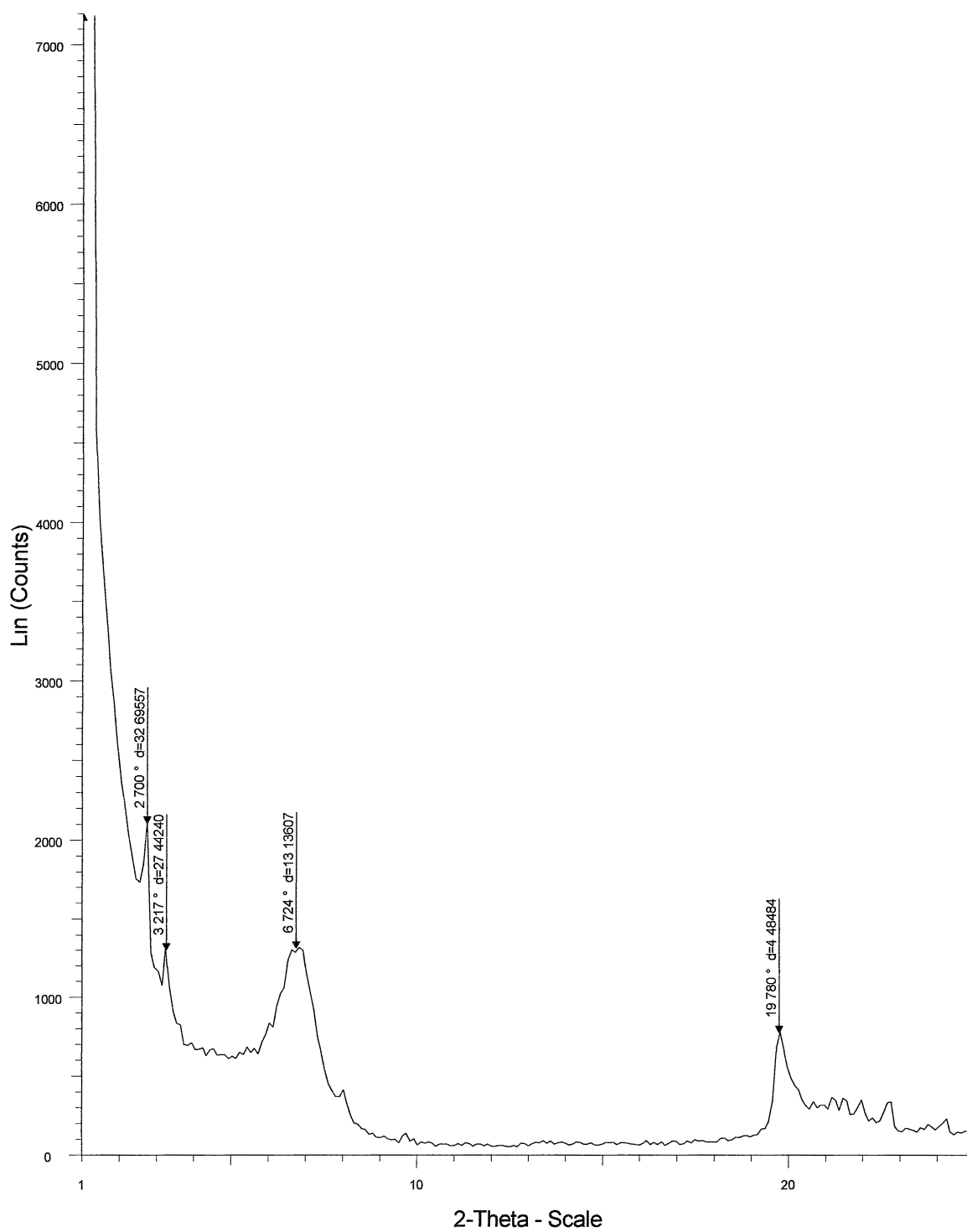
Appendix B11-b: WAXD of Aged Decyl Aldehyde 2:1 Organoclay

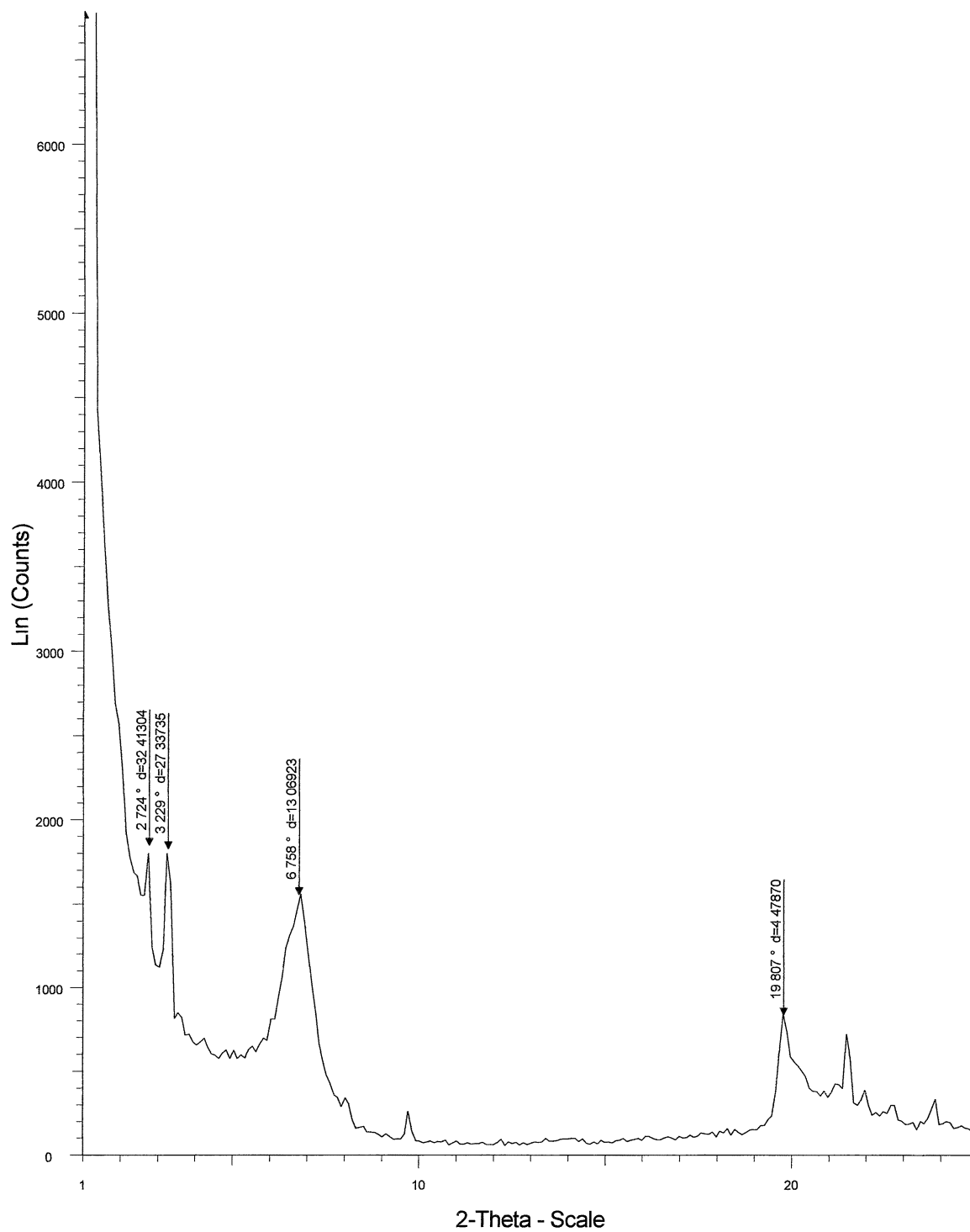


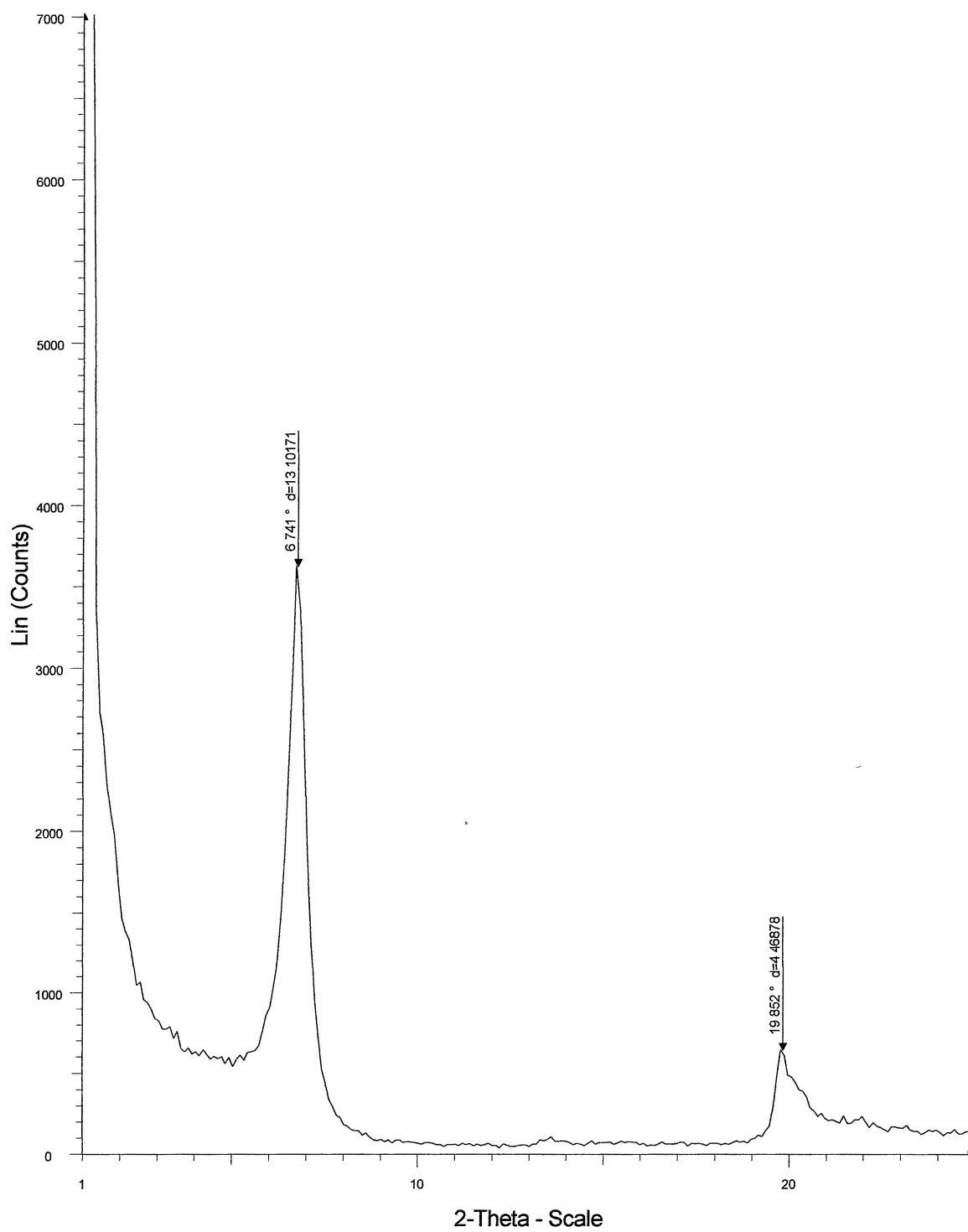
Appendix B11-c: WAXD of Aged Decyl Aldehyde 3:1 Organoclay

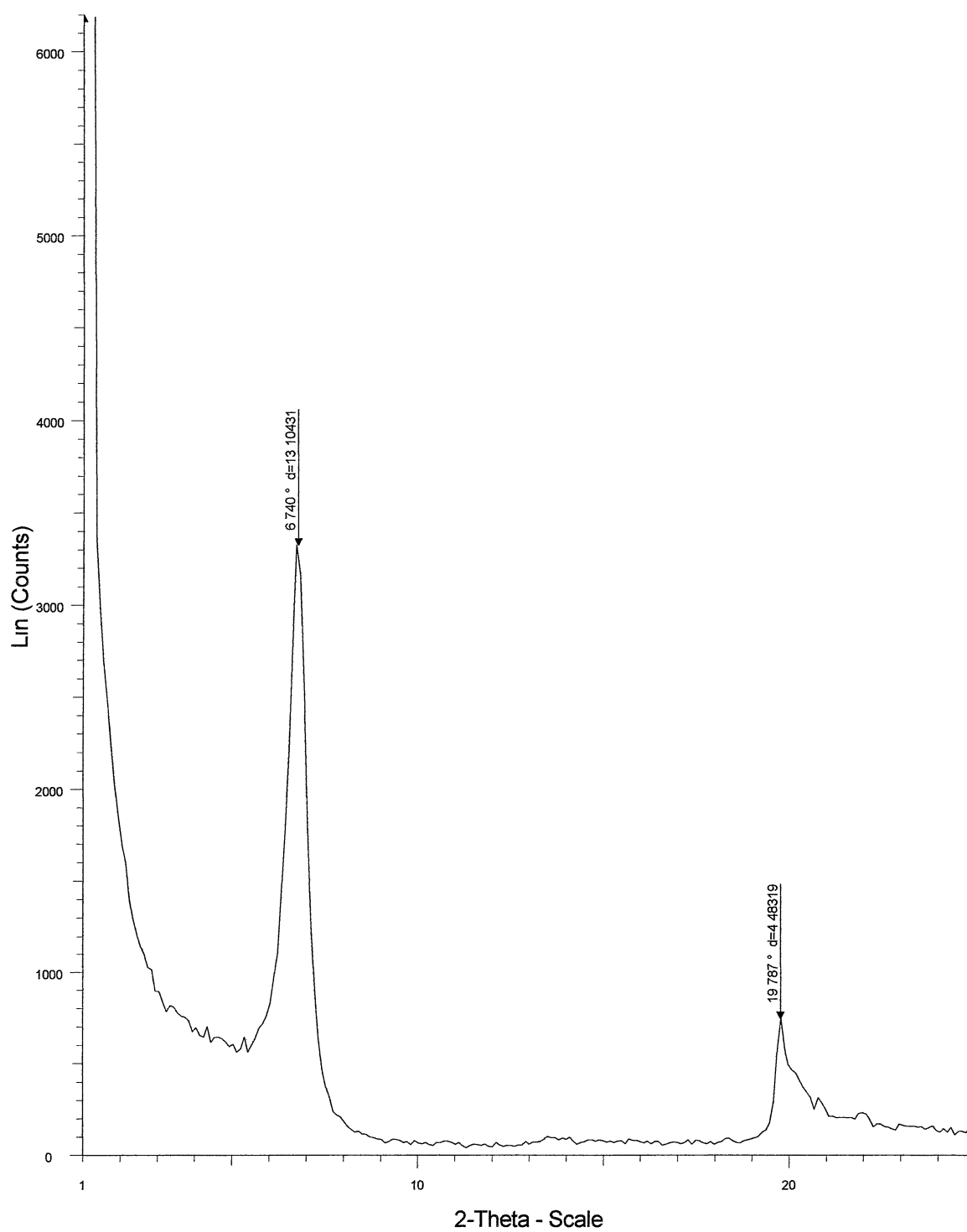


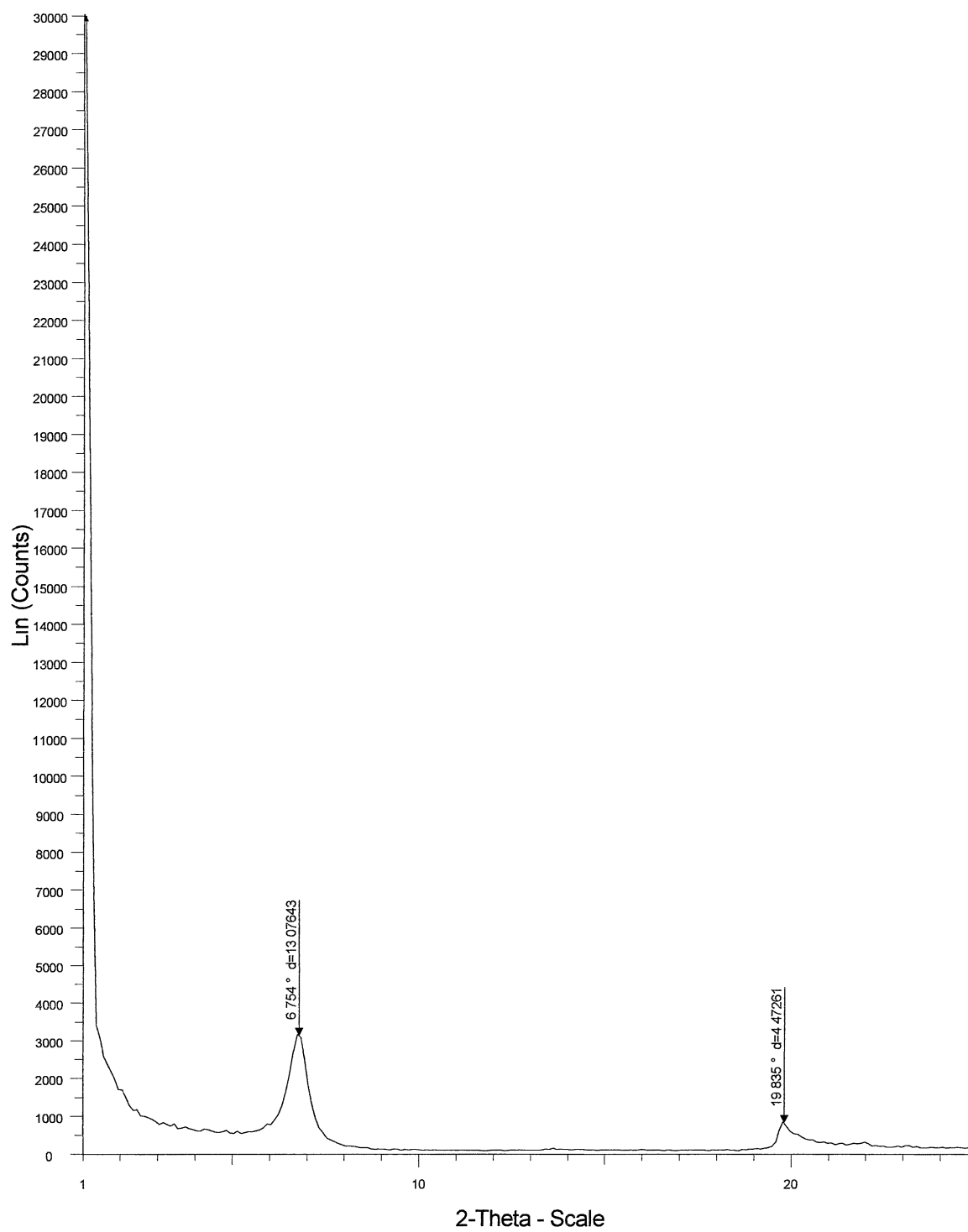
Appendix B12-a: WAXD of Aged Dodecyl Aldehyde 1:1 Organoclay

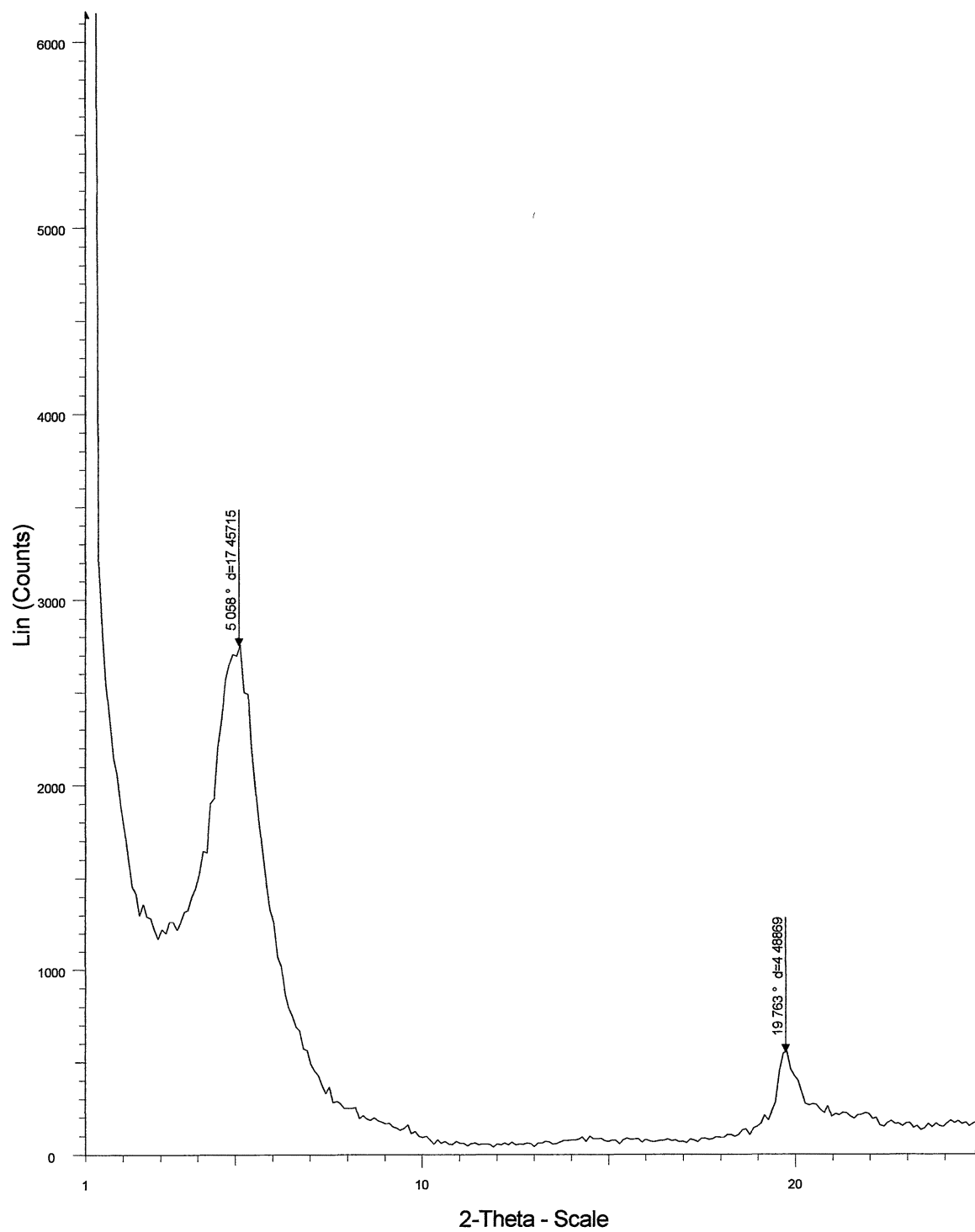
Appendix B12-b: WAXD of Aged Dodecyl Aldehyde 2:1 Organoclay

Appendix B12-c: WAXD of Aged Dodecyl Aldehyde 3:1 Organoclay

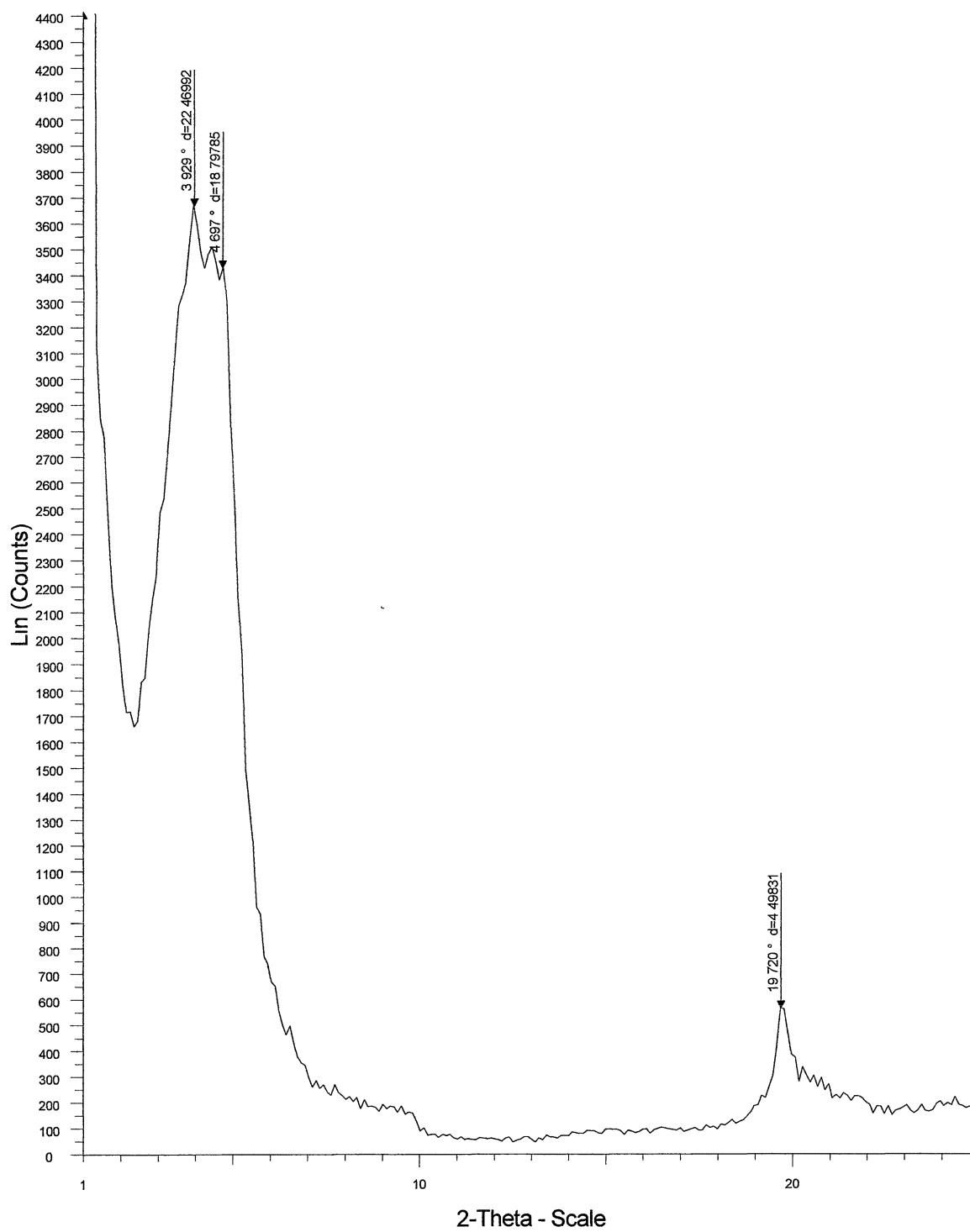
Appendix B13-a: WAXD of Aged N-Methyl Pyrrolidone 1:1 Organoclay

Appendix B13-b: WAXD of Aged N-Methyl Pyrrolidone 2:1 Organoclay

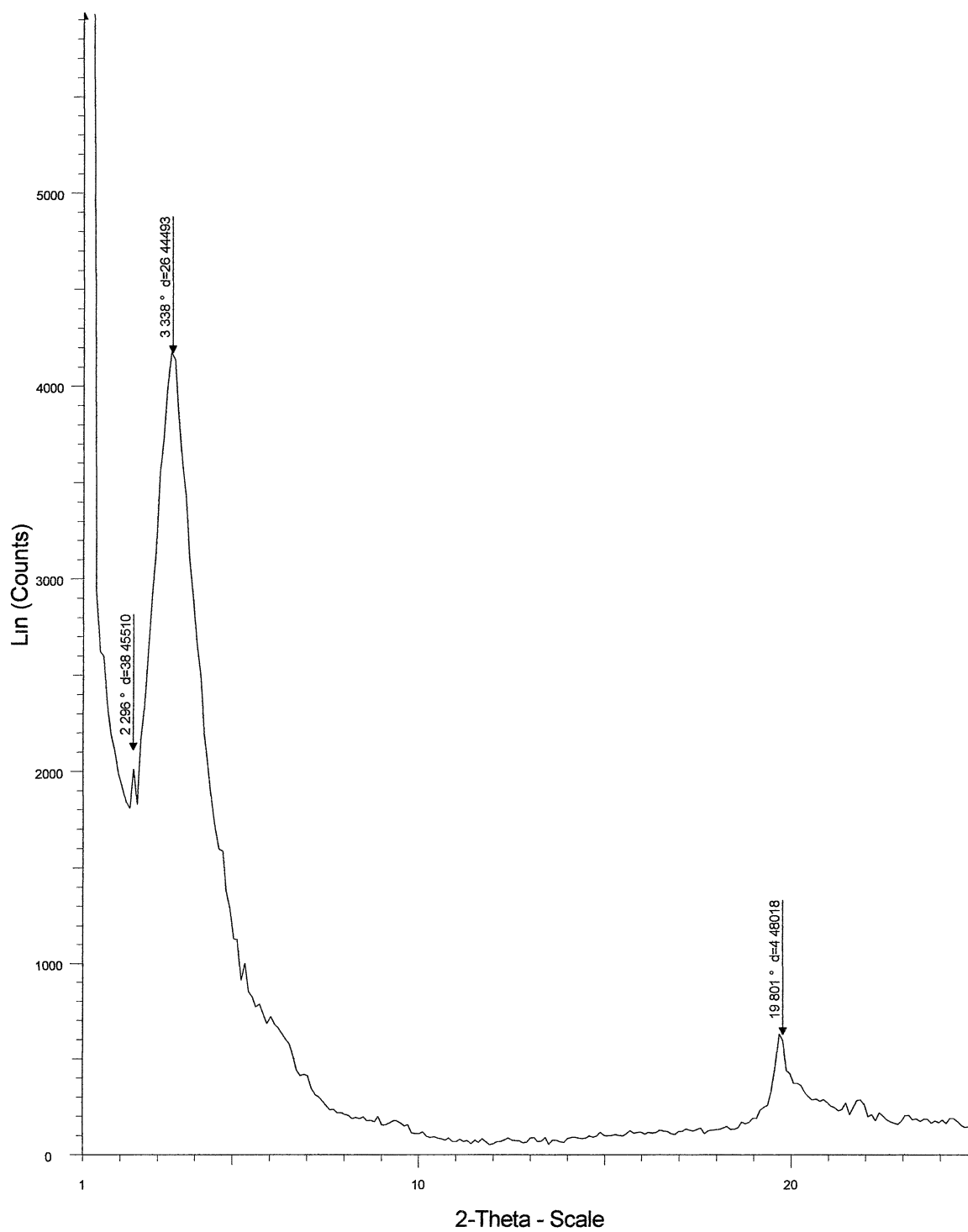
Appendix B13-c: WAXD of Aged N-Methyl Pyrrolidone 3:1 Organoclay

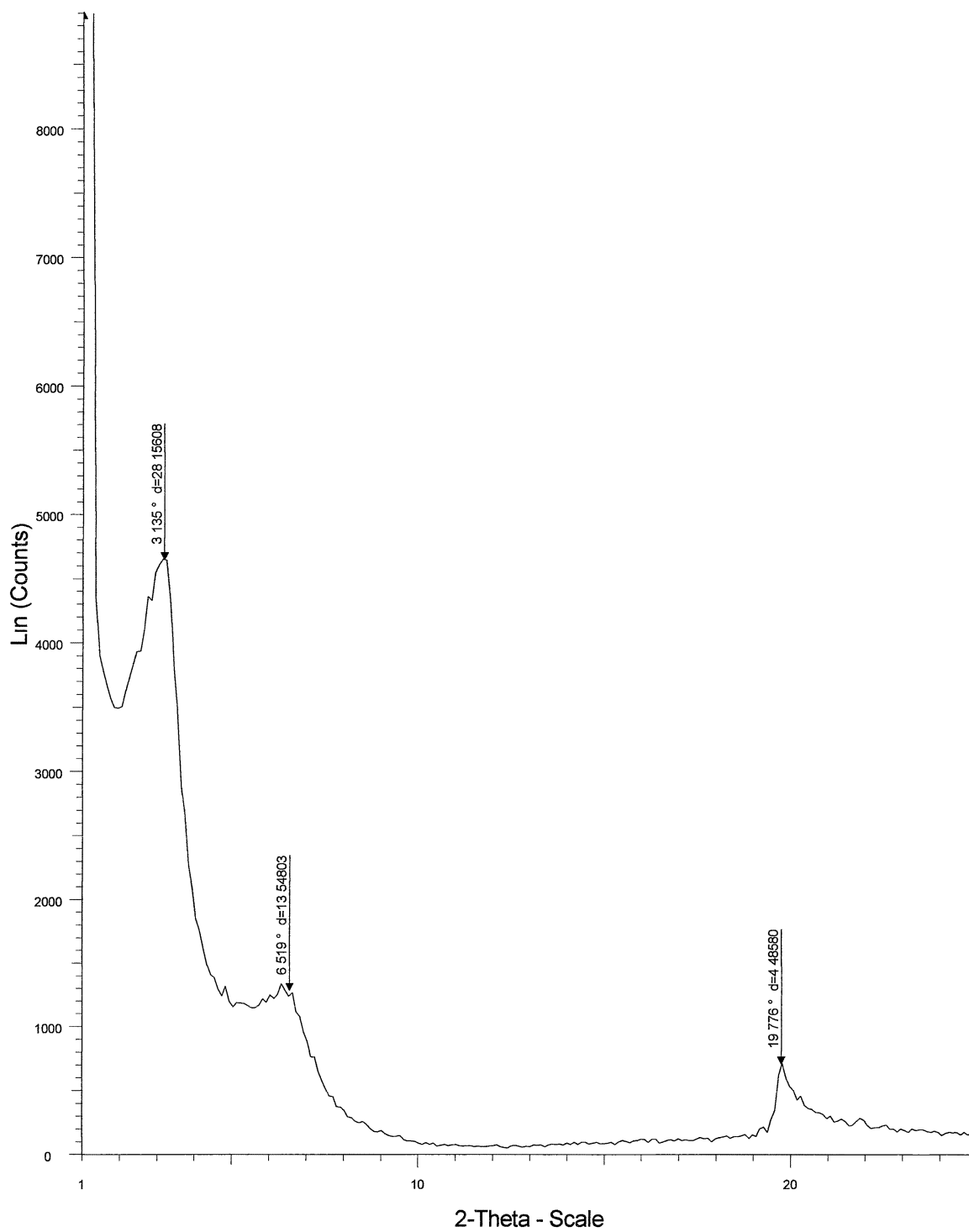
Appendix B14-a: WAXD of Aged N-Octyl Pyrrolidone 1:1 Organoclay

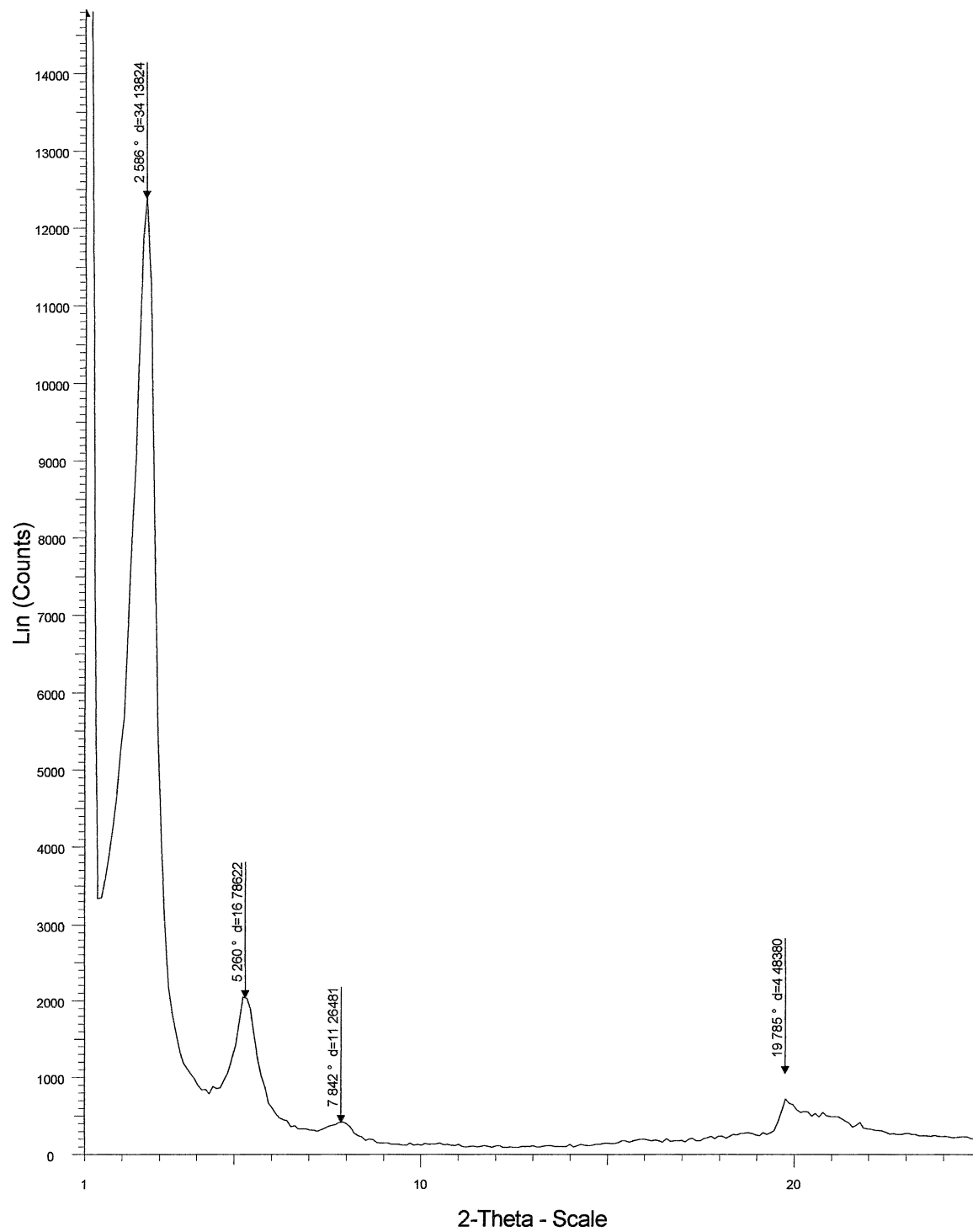
Appendix B14-b: WAXD of Aged N-Octyl Pyrrolidone 2:1 Organoclay

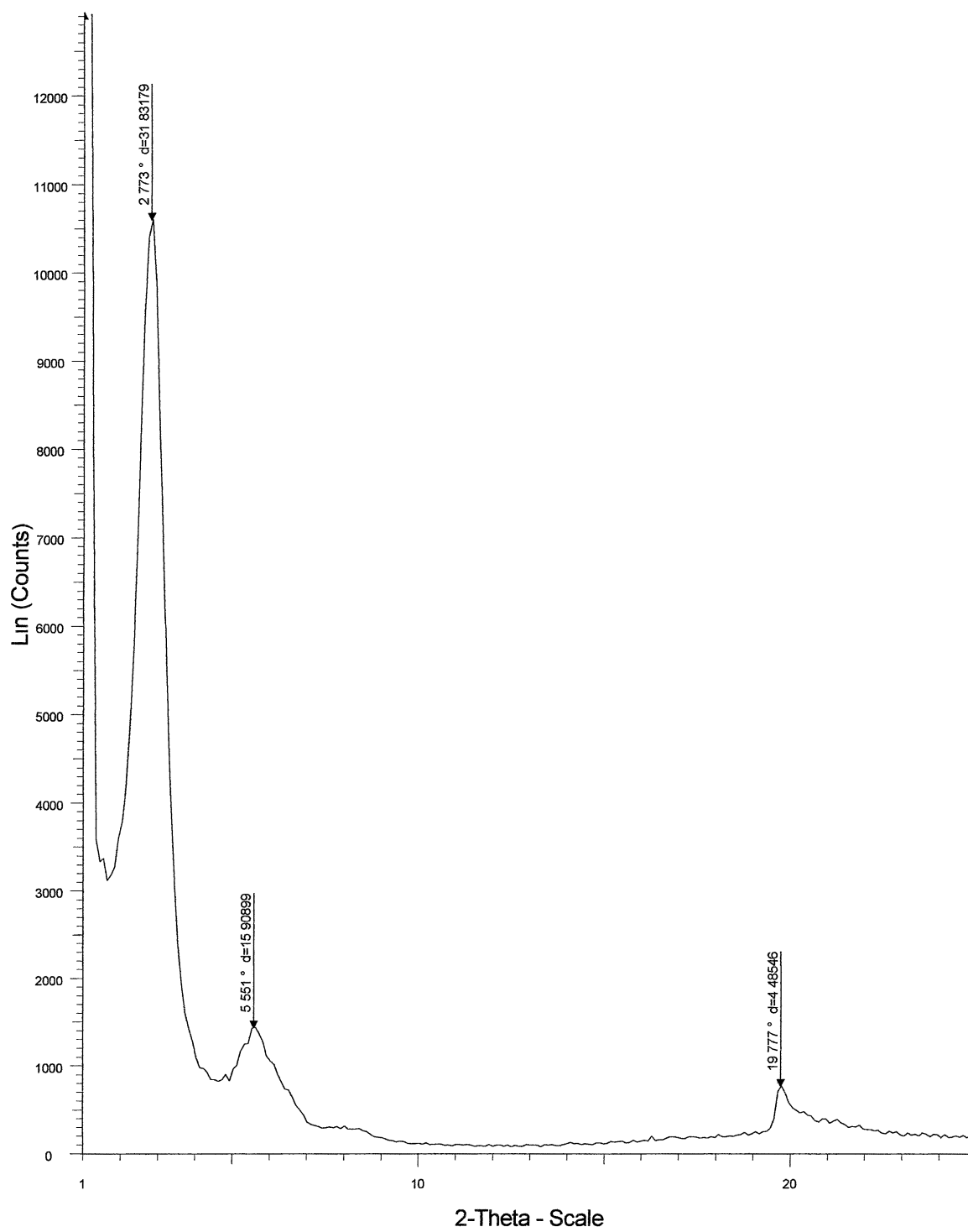


Appendix B14-c: WAXD of Aged N-Octyl Pyrrolidone 3:1 Organoclay

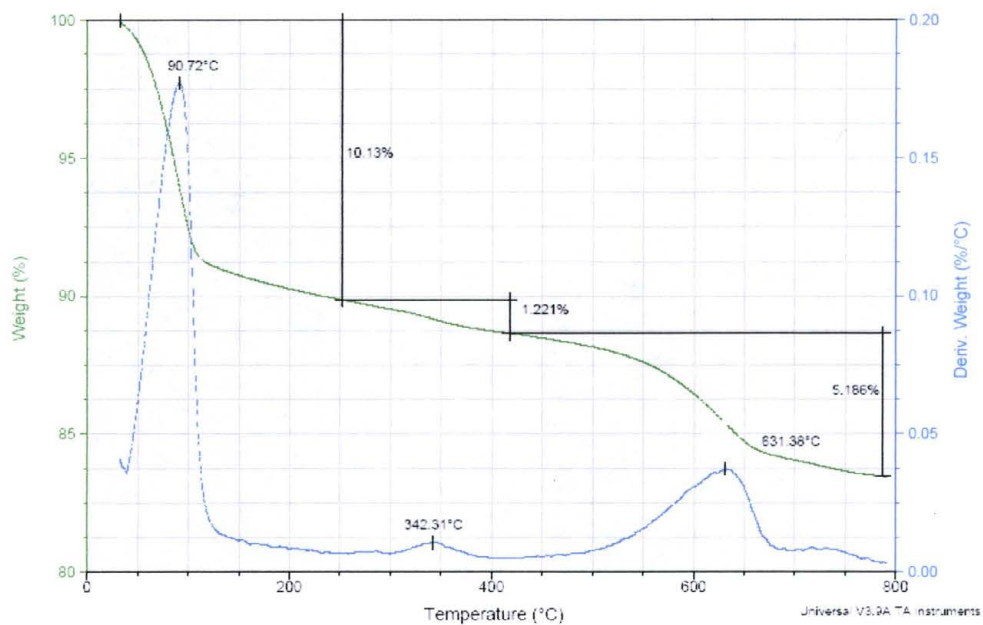
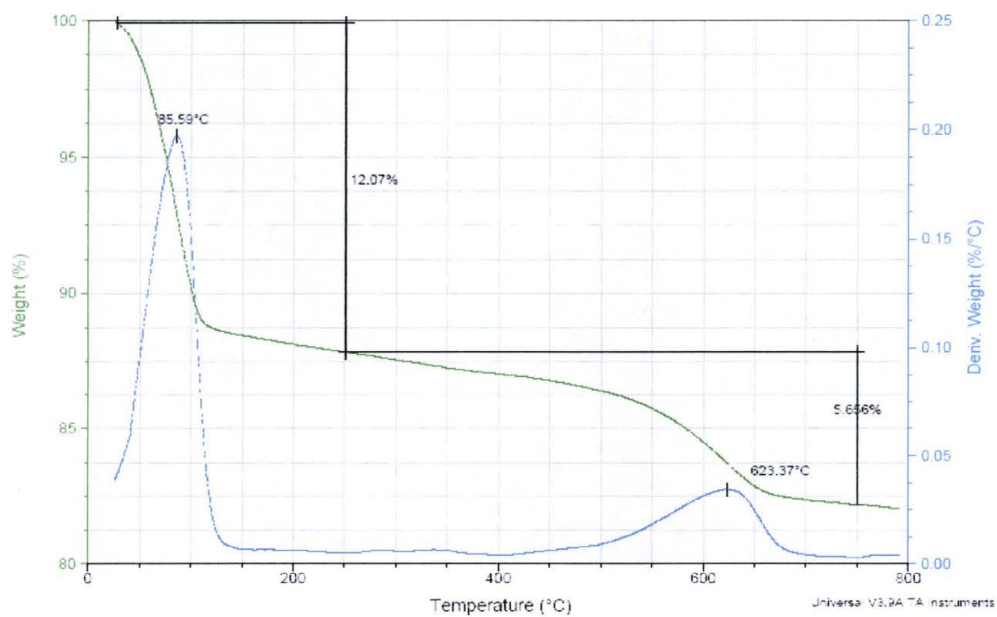


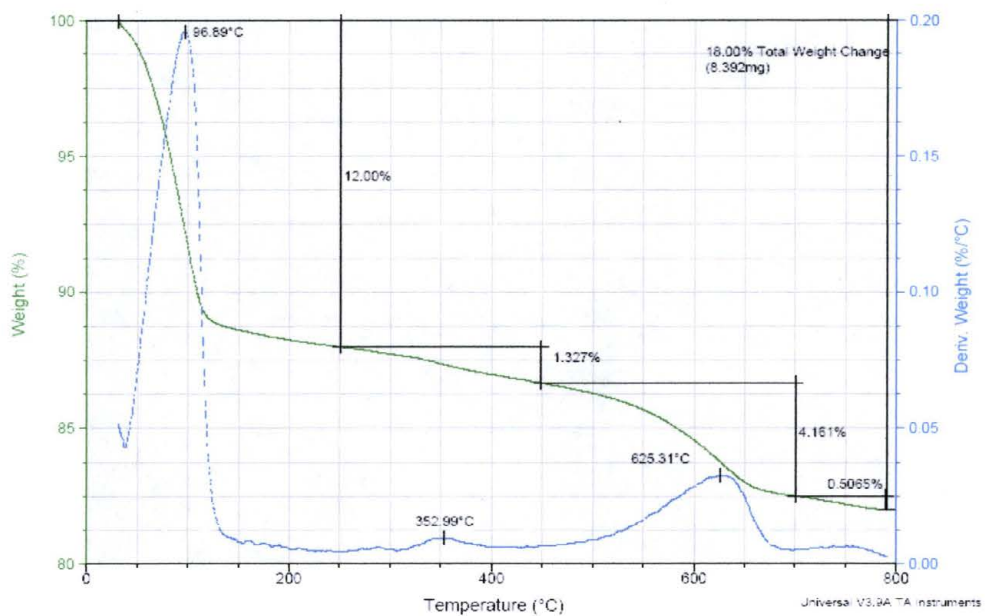
Appendix B15-a: WAXD of Aged N-Dodecyl Pyrrolidone 1:1 Organoclay

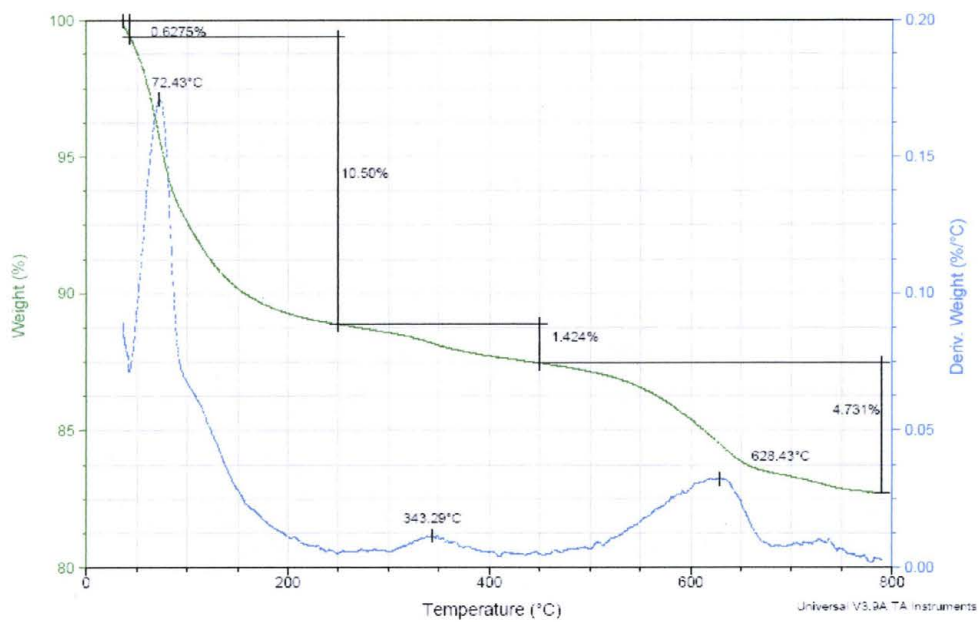
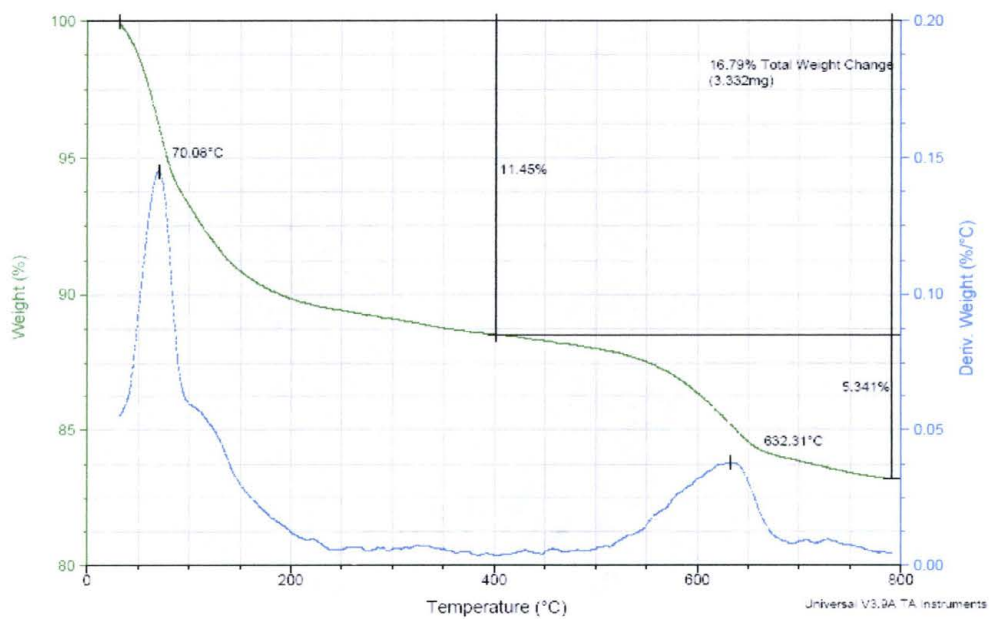
Appendix B15-b: WAXD of Aged N-Dodecyl Pyrrolidone 2:1 Organoclay

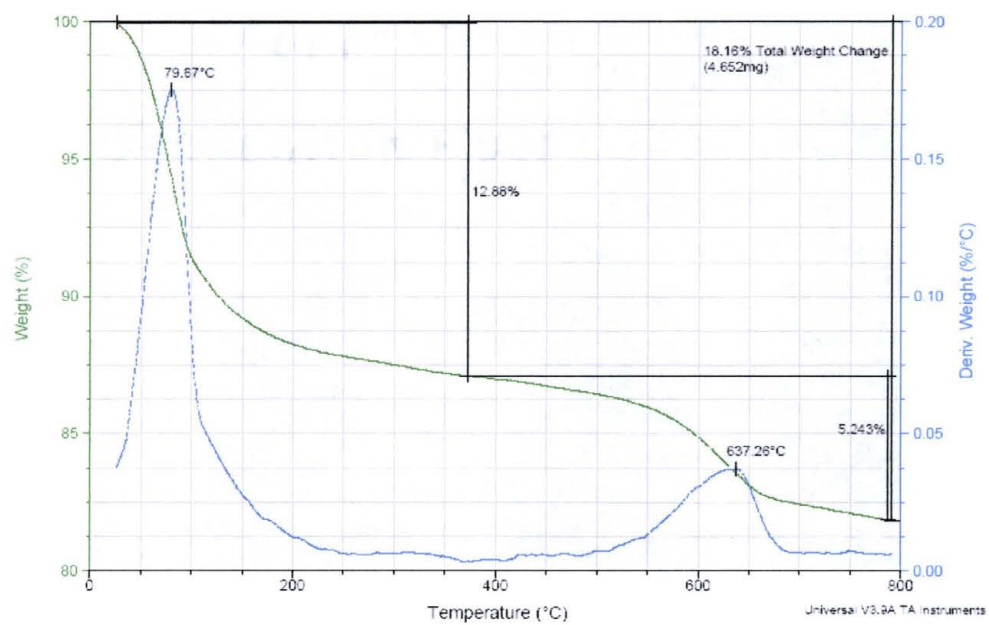
Appendix B15-c: WAXD of Aged N-Dodecyl Pyrrolidone 3:1 Organoclay

Appendix C: Thermal Gravimetric Analysis Data

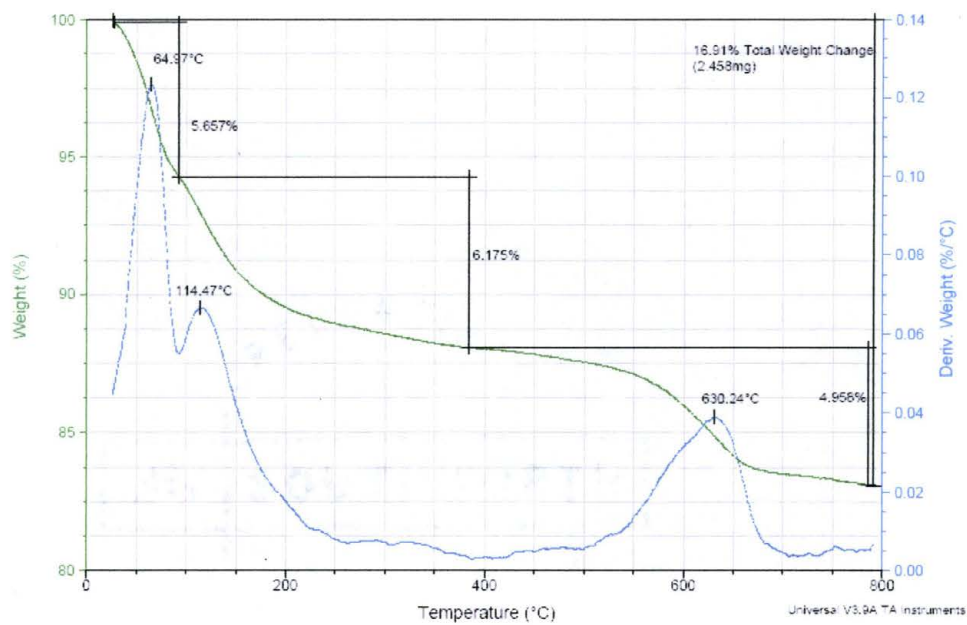
Appendix C1-a: TGA of Butyl Alcohol 1:1 Organoclay**Appendix C1-b: TGA of Butyl Alcohol 2:1 Organoclay**

Appendix C1-c: TGA of Butyl Alcohol 3:1 Organoclay

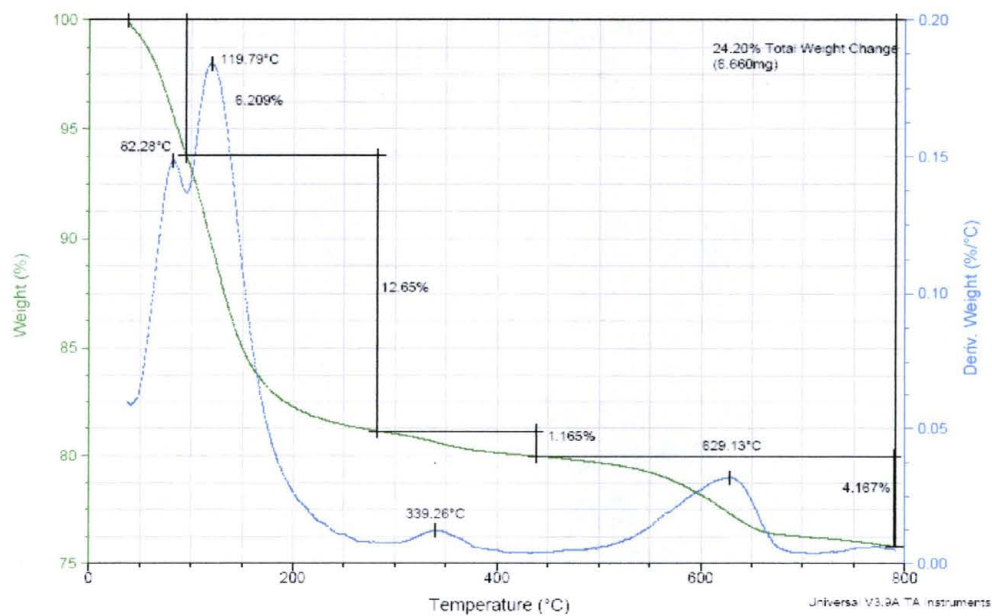
Appendix C2-a: TGA of Hexyl Alcohol 1:1 Organoclay**Appendix C2-b: TGA of Hexyl Alcohol 2:1 Organoclay**

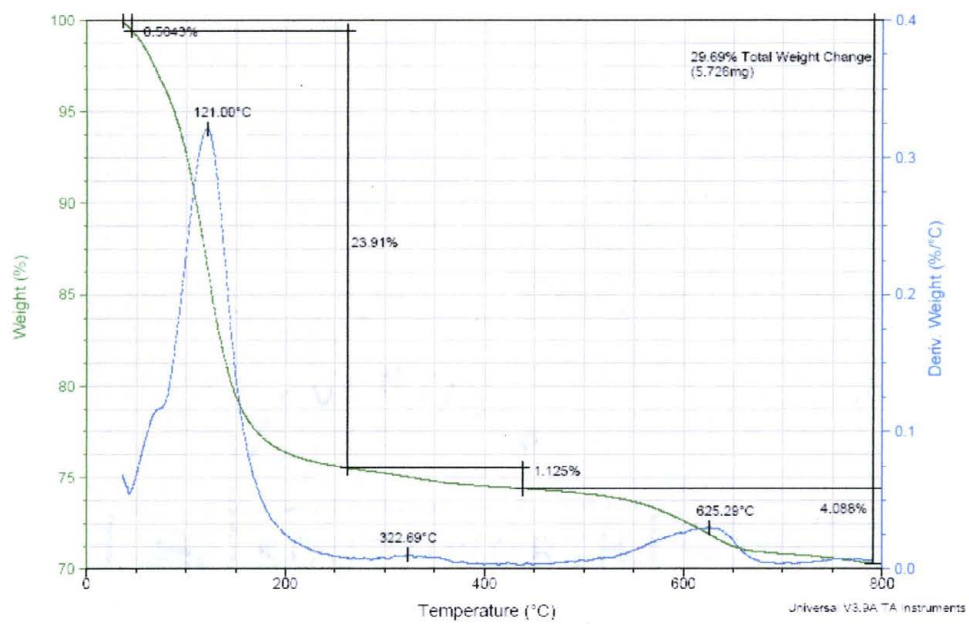
Appendix C2-c: TGA of Hexyl Alcohol 3:1 Organoclay

Appendix C3-a: TGA of Octyl Alcohol 1:1 Organoclay

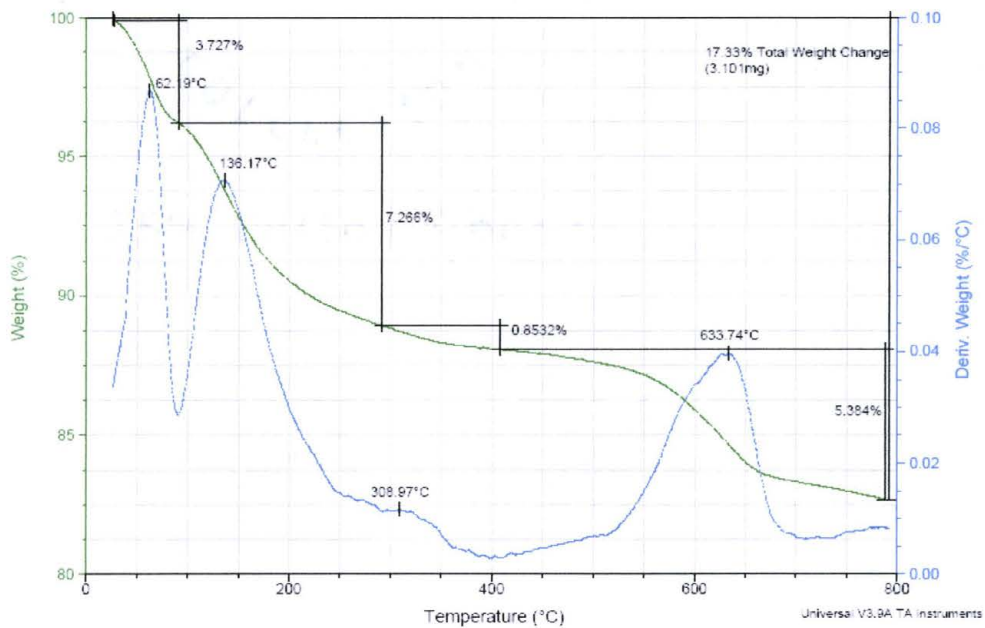


Appendix C3-b: TGA of Octyl Alcohol 2:1 Organoclay

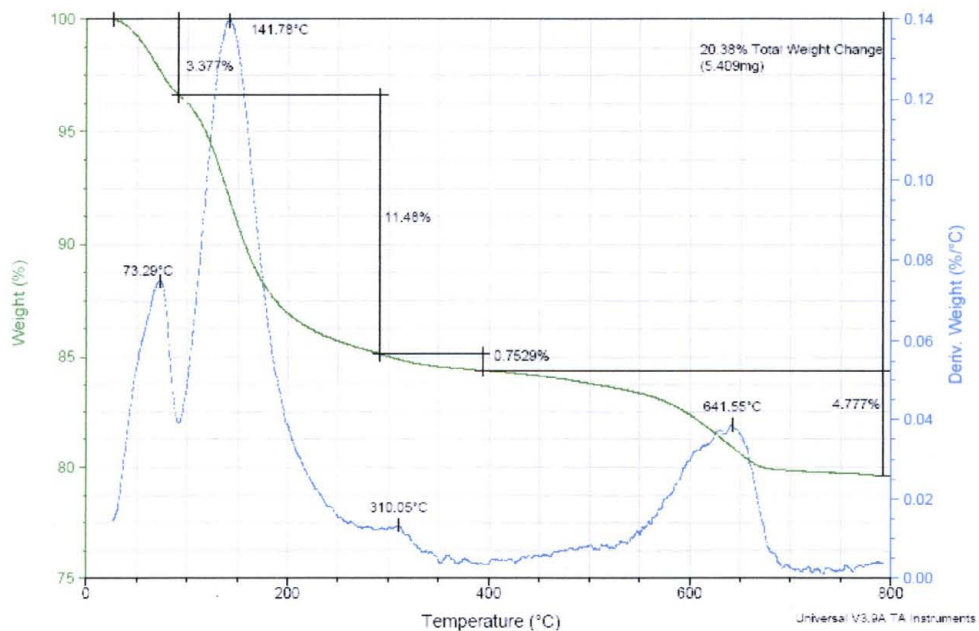


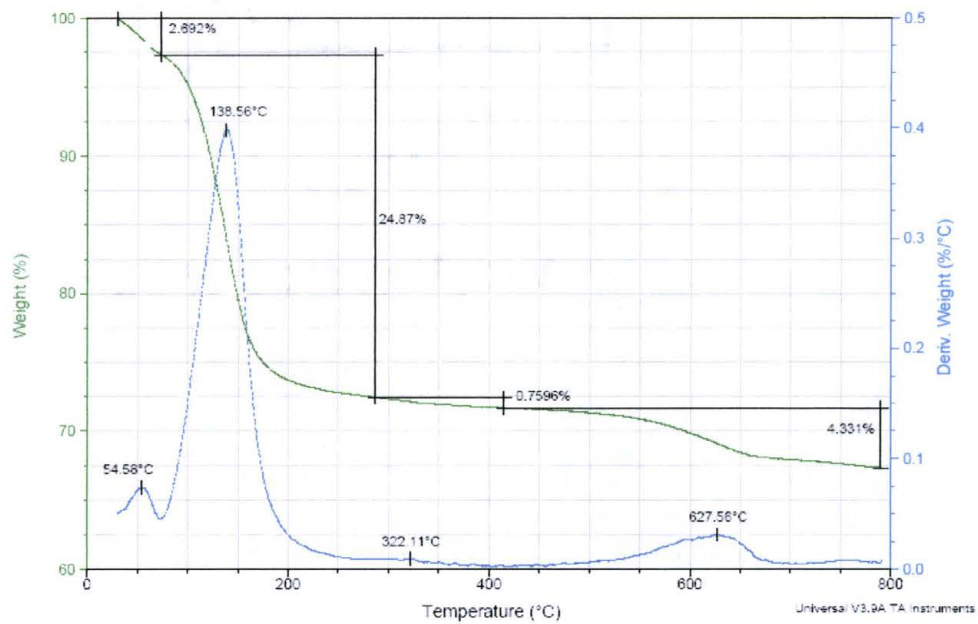
Appendix C3-c: TGA of Octyl Alcohol 3:1 Organoclay

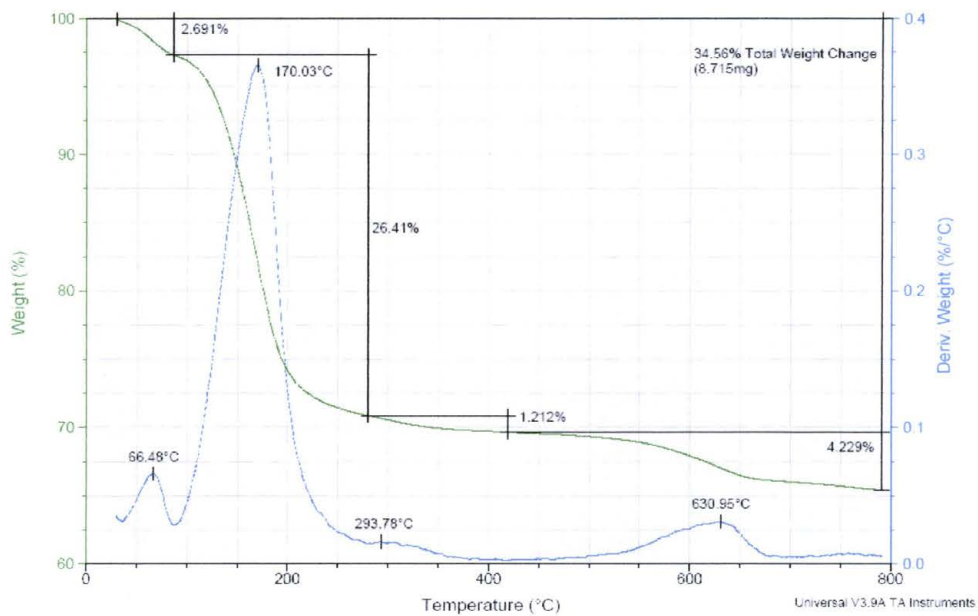
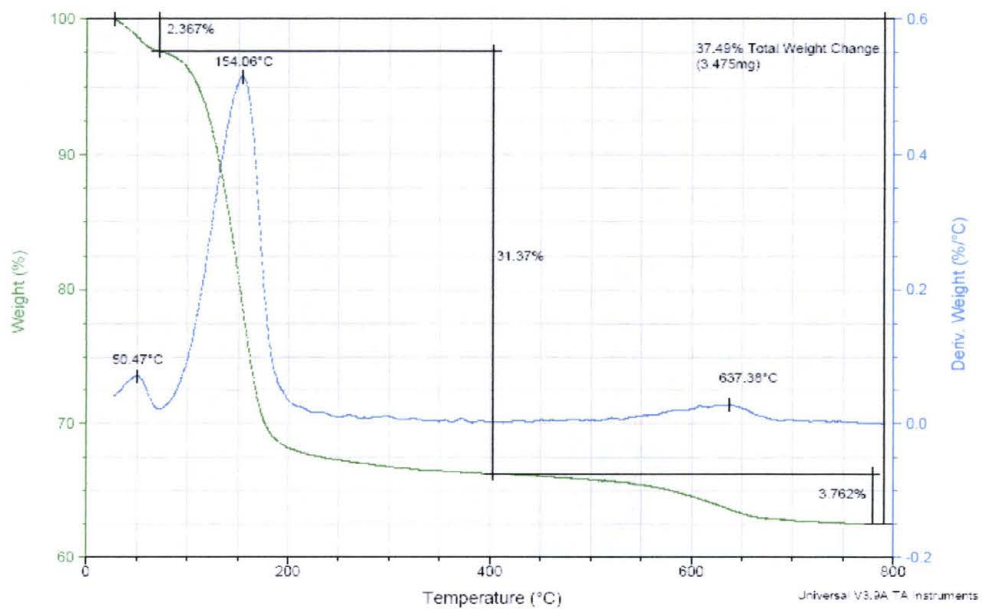
Appendix C4-a: TGA of Decyl Alcohol 1:1 Organoclay

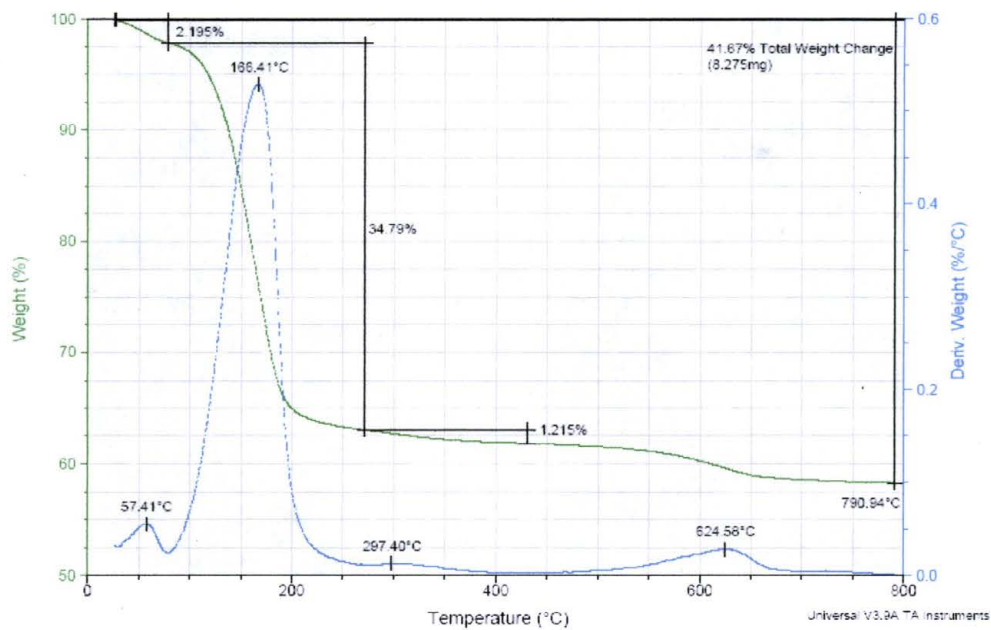


Appendix C4-b: TGA of Decyl Alcohol 2:1 Organoclay

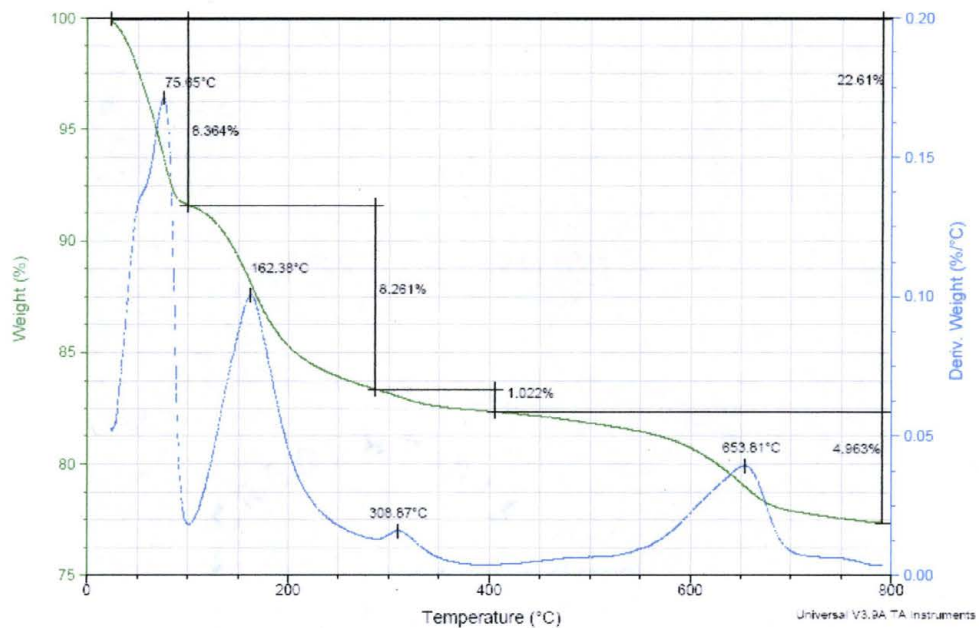


Appendix C4-c: TGA of Decyl Alcohol 3:1 Organoclay

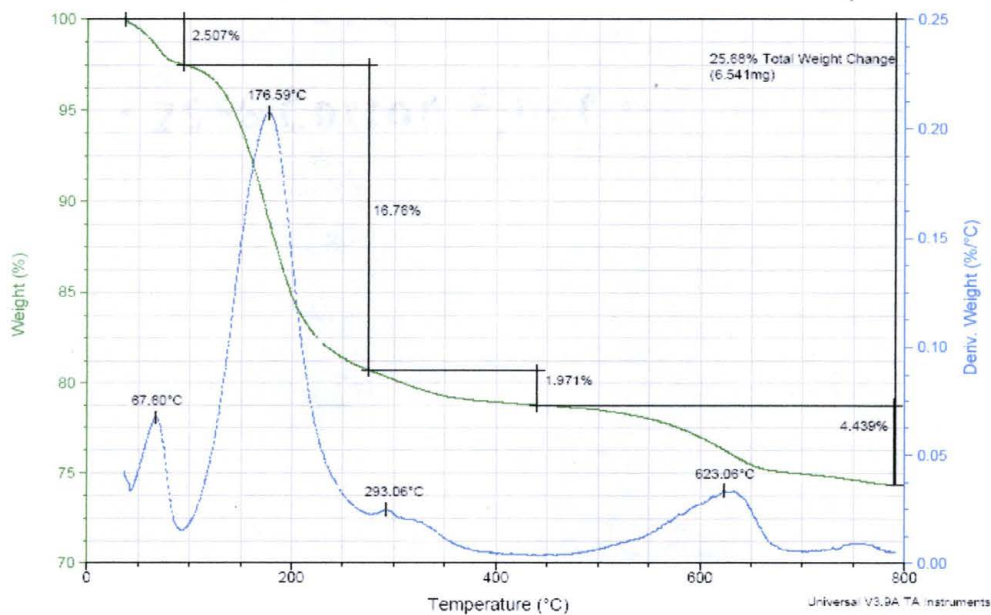
Appendix C5-a: TGA of Dodecyl Alcohol 1:1 Organoclay**Appendix C5-b: TGA of Dodecyl Alcohol 2:1 Organoclay**

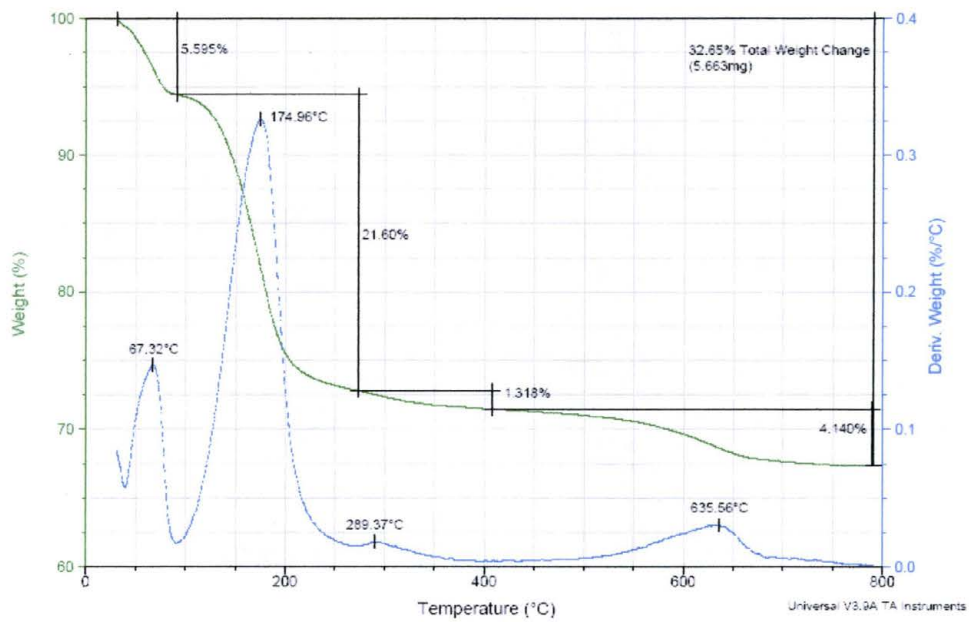
Appendix C5-c: TGA of Dodecyl Alcohol 3:1 Organoclay

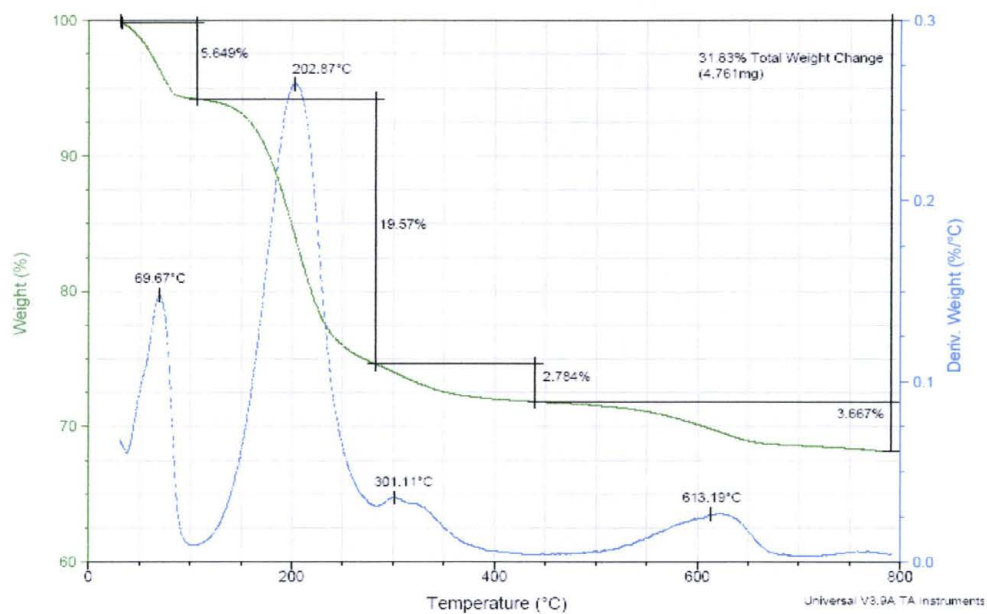
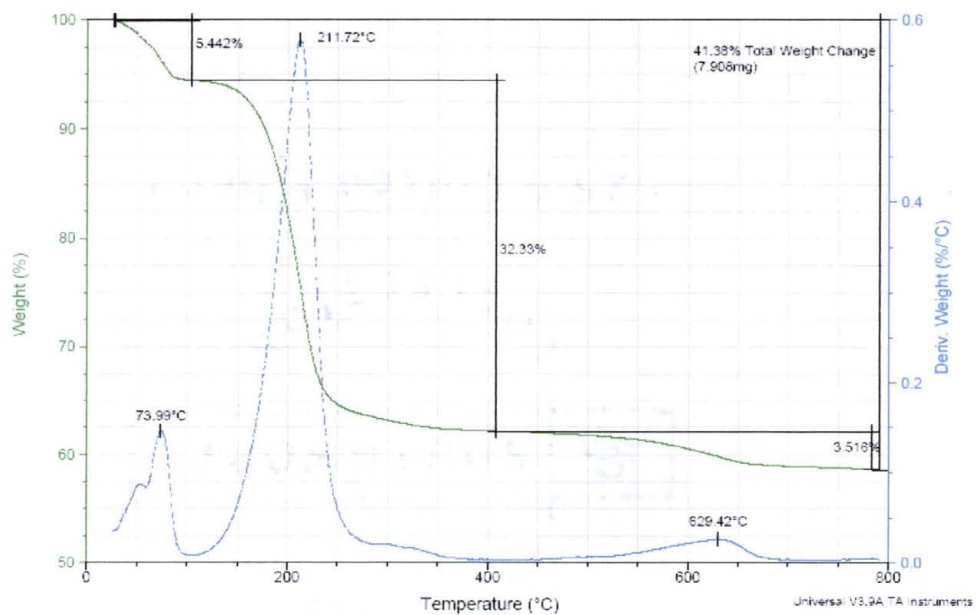
Appendix C6-a: TGA of Tetradecyl Alcohol 1:1 Organoclay

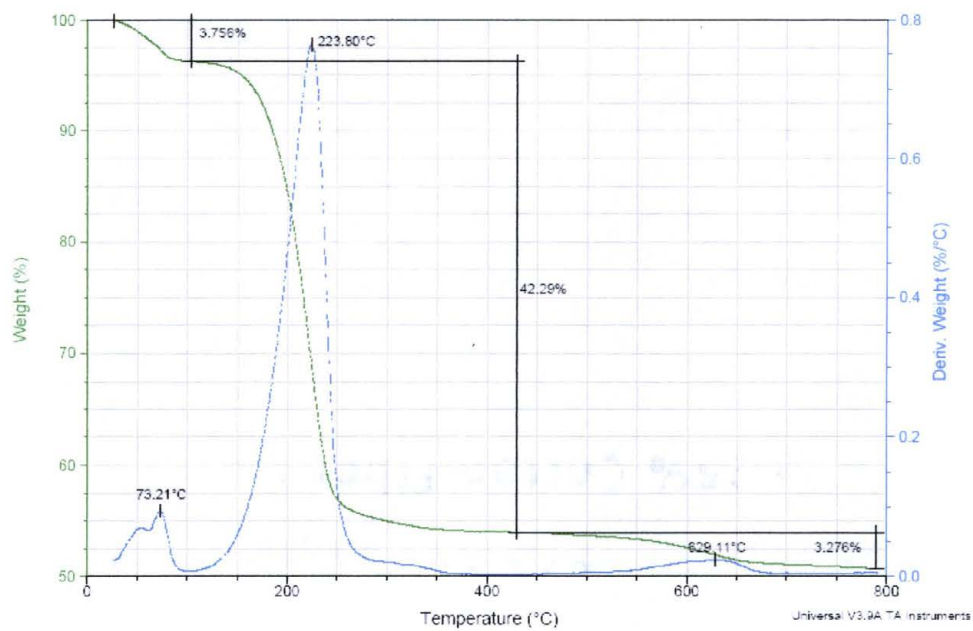


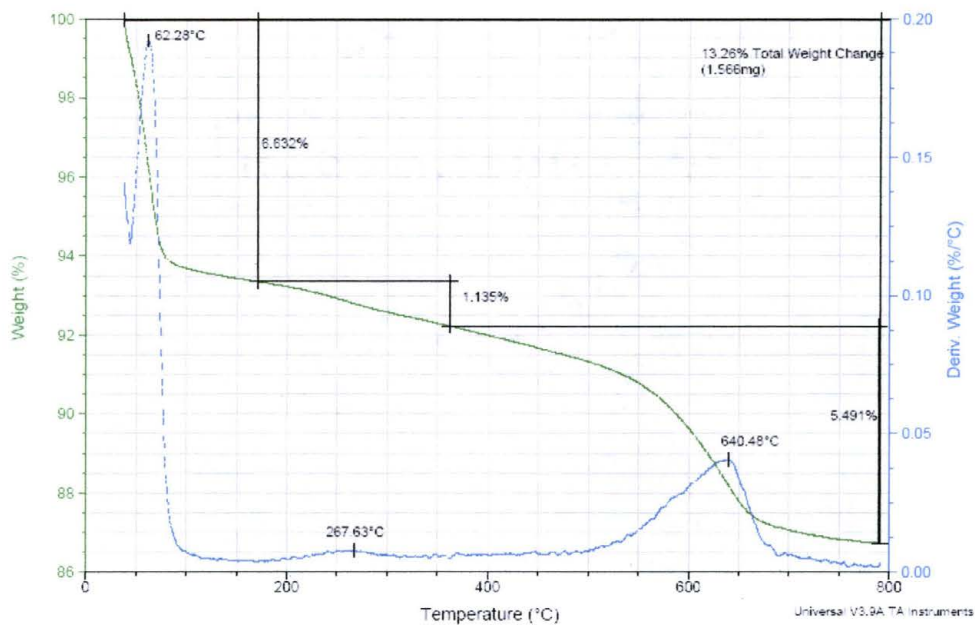
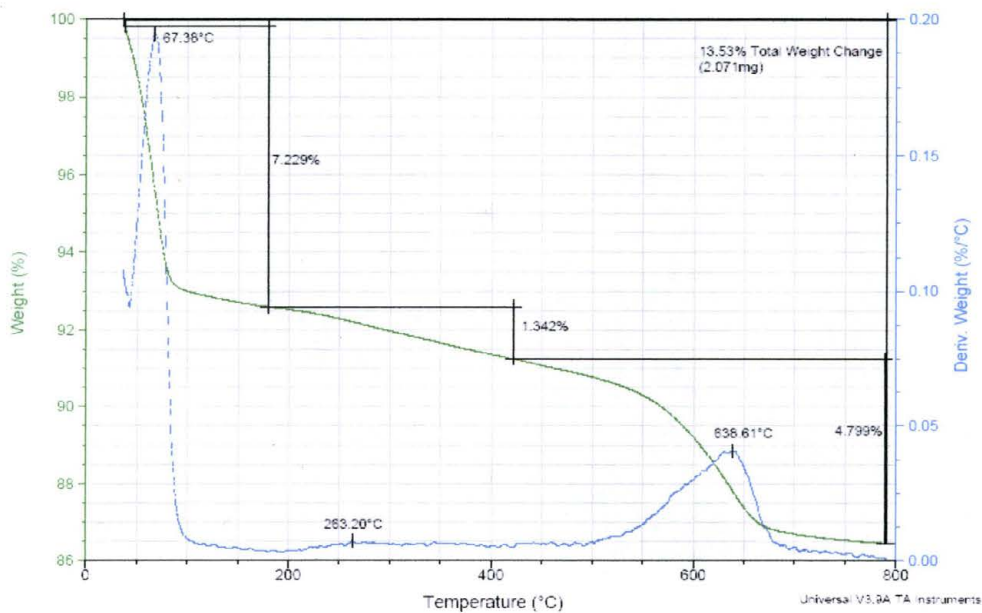
Appendix C6-b: TGA of Tetradecyl Alcohol 2:1 Organoclay

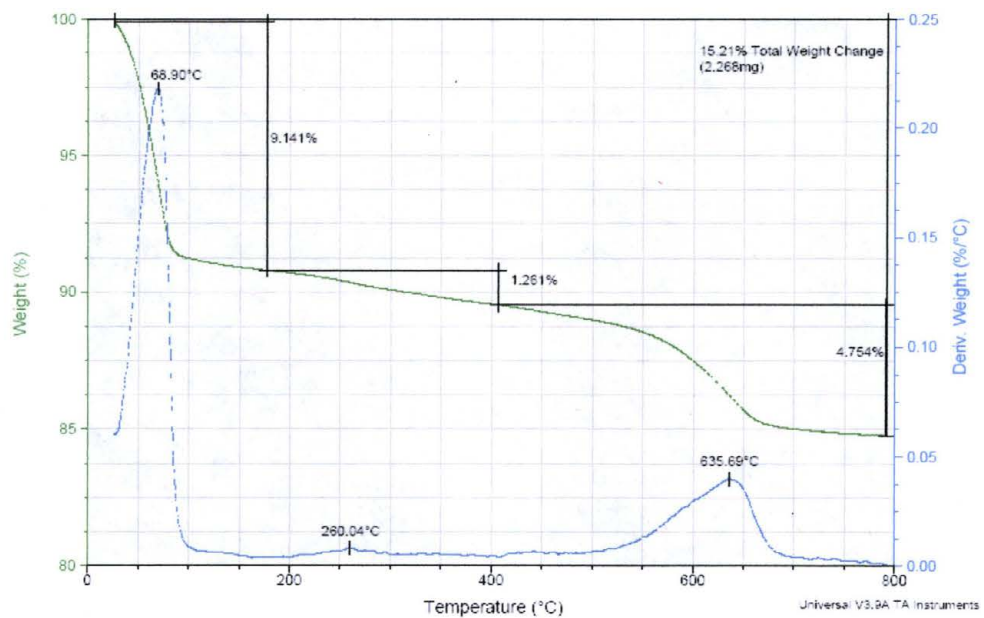


Appendix C6-c: TGA of Tetradecyl Alcohol 3:1 Organoclay

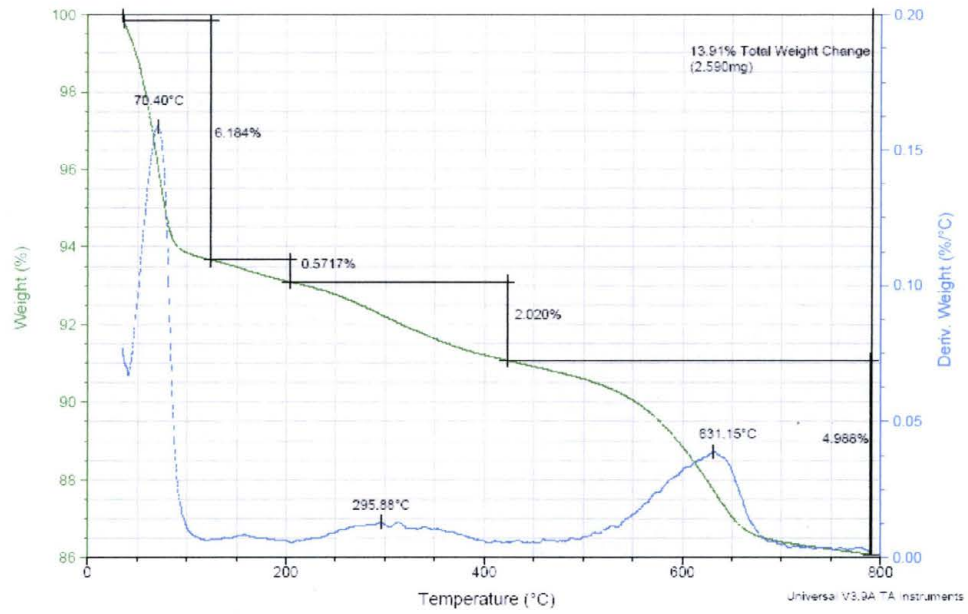
Appendix C7-a: TGA of Octadecyl Alcohol 1:1 Organoclay**Appendix C7-b: TGA of Octadecyl Alcohol 2:1 Organoclay**

Appendix C7-c: TGA of Octadecyl Alcohol 3:1 Organoclay

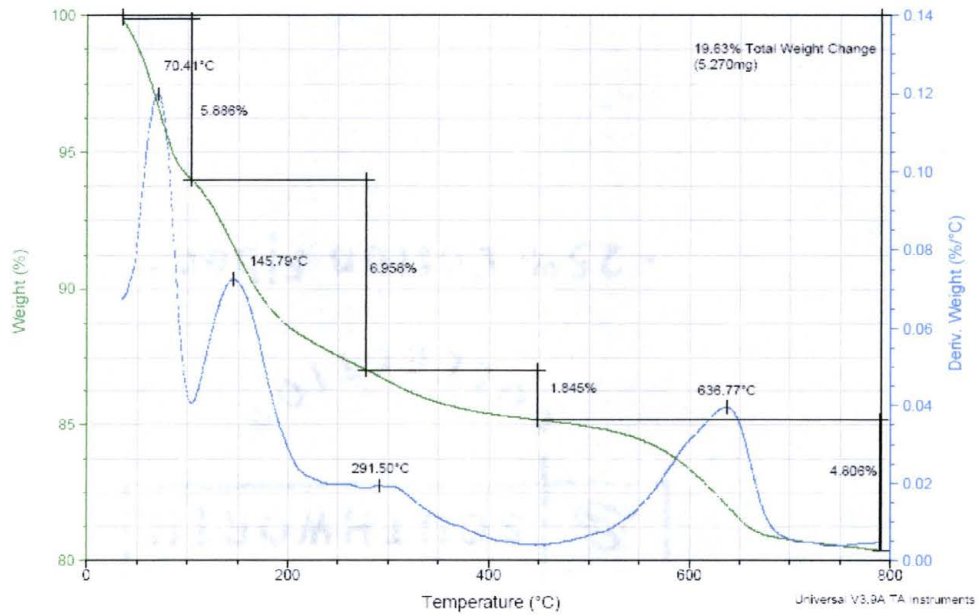
Appendix C8-a: TGA of Butyl Aldehyde 1:1 Organoclay**Appendix C8-b: TGA of Butyl Aldehyde 2:1 Organoclay**

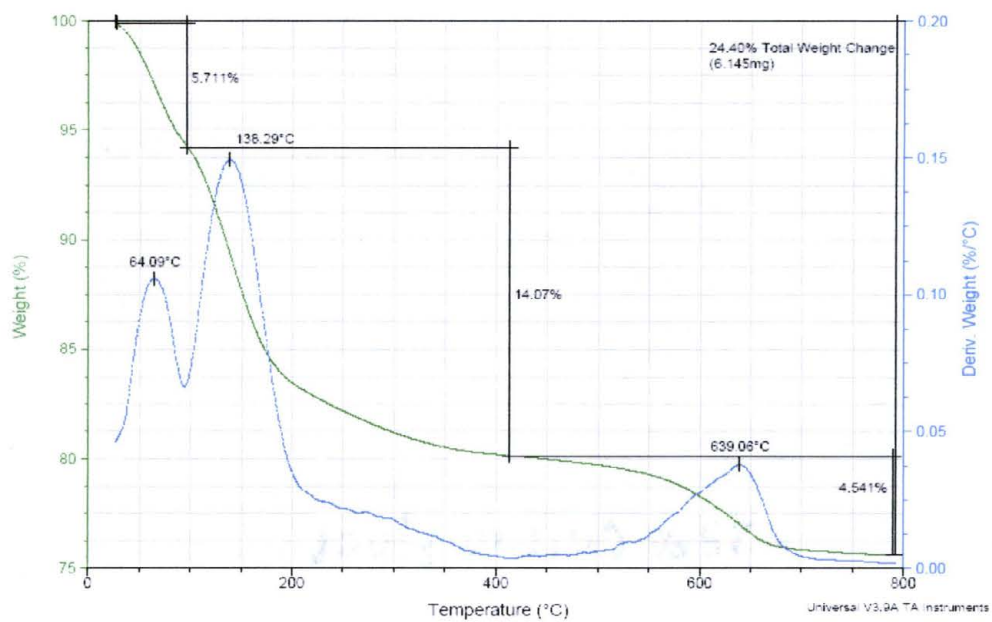
Appendix C8-c: TGA of Butyl Aldehyde 3:1 Organoclay

Appendix C9-a: TGA of Hexyl Aldehyde 1:1 Organoclay

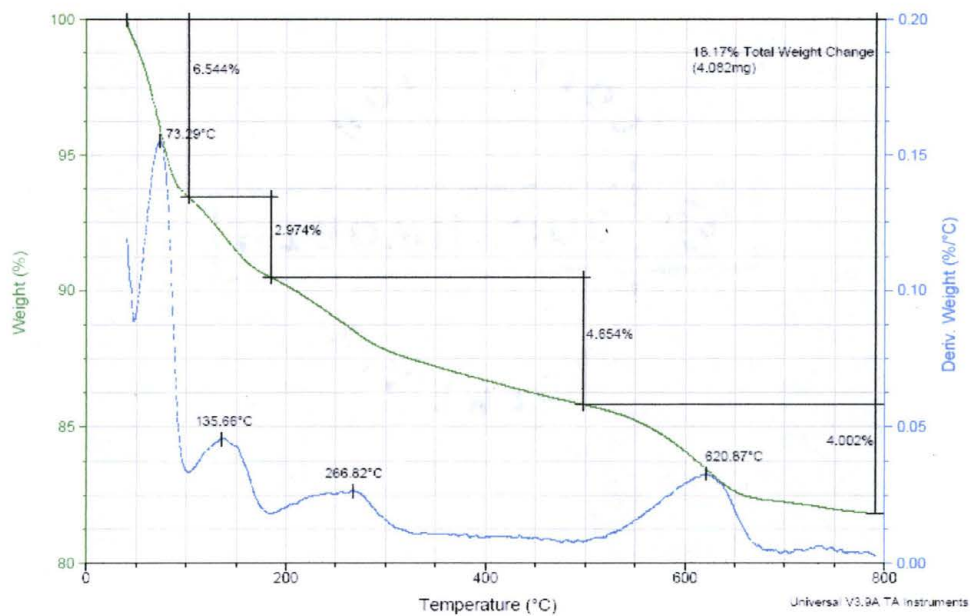


Appendix C9-b: TGA of Hexyl Aldehyde 2:1 Organoclay

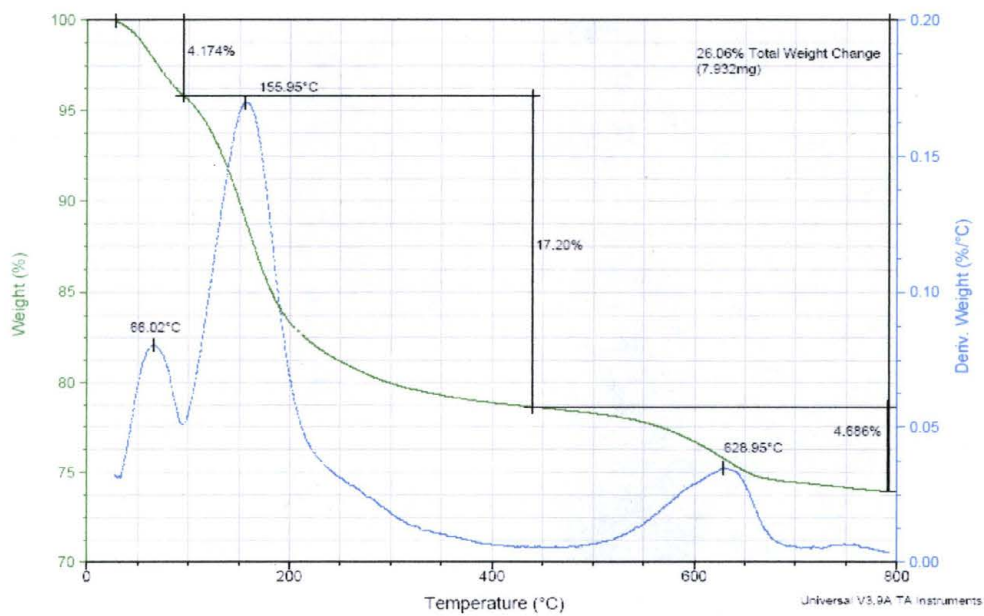


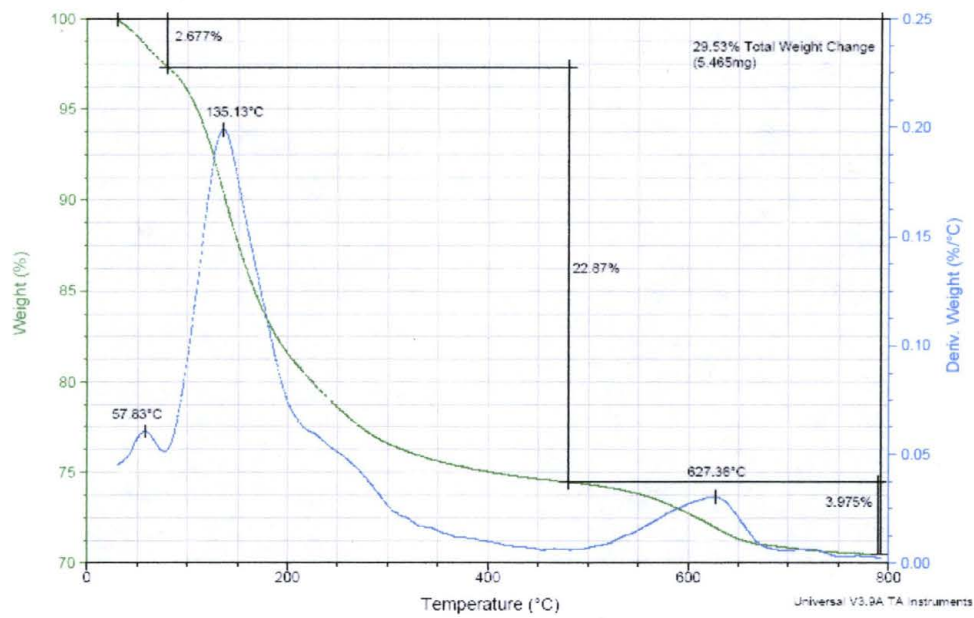
Appendix C9-c: TGA of Hexyl Aldehyde 3:1 Organoclay

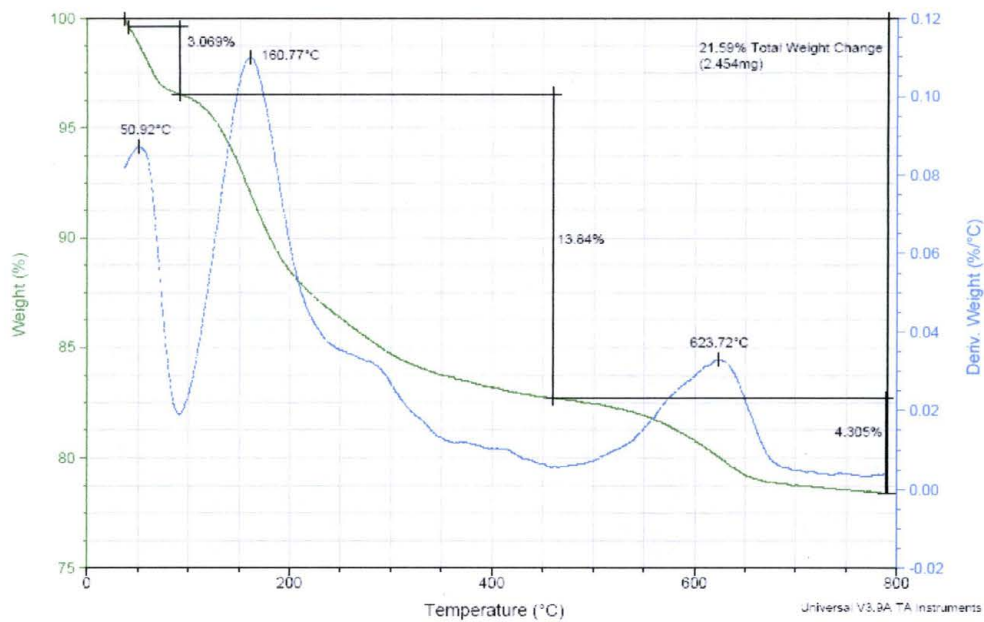
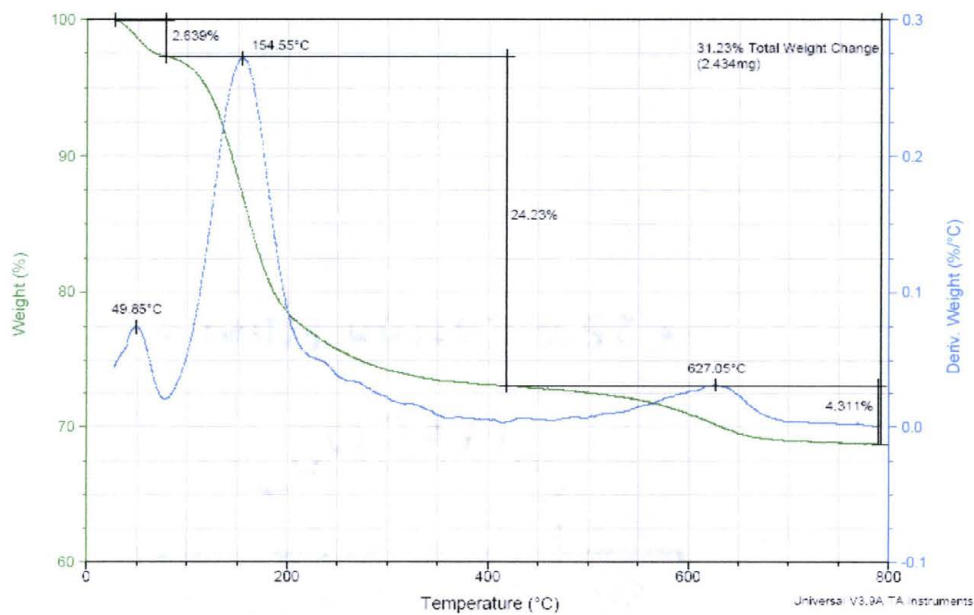
Appendix C10-a: TGA of Octyl Aldehyde 1:1 Organoclay

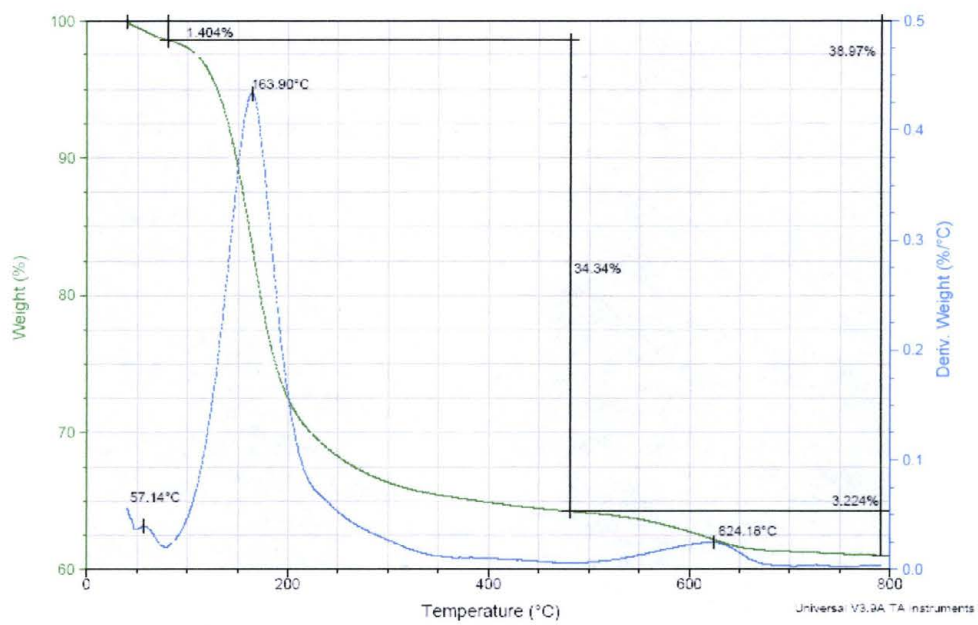


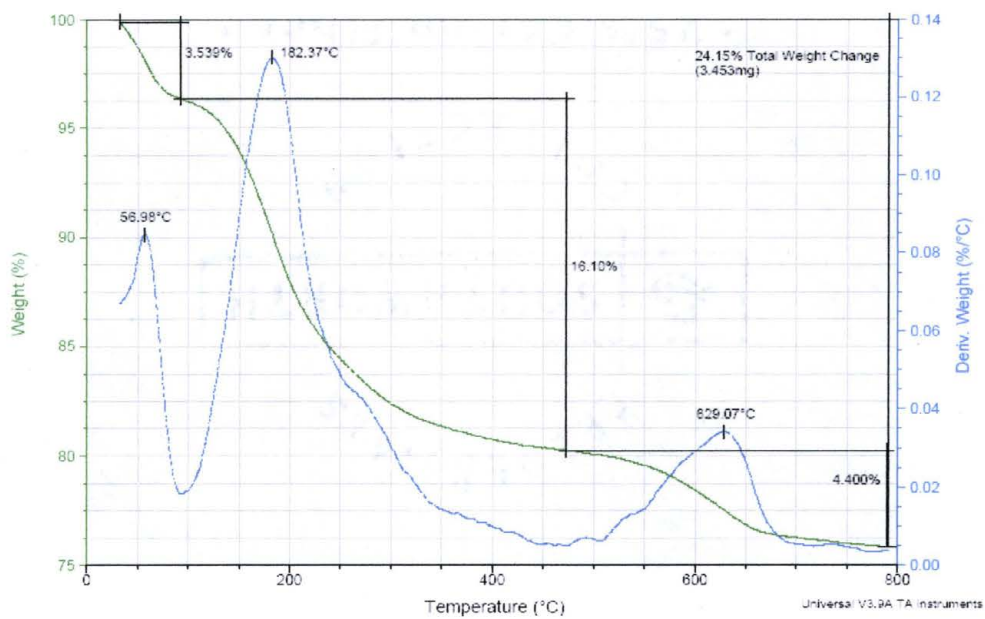
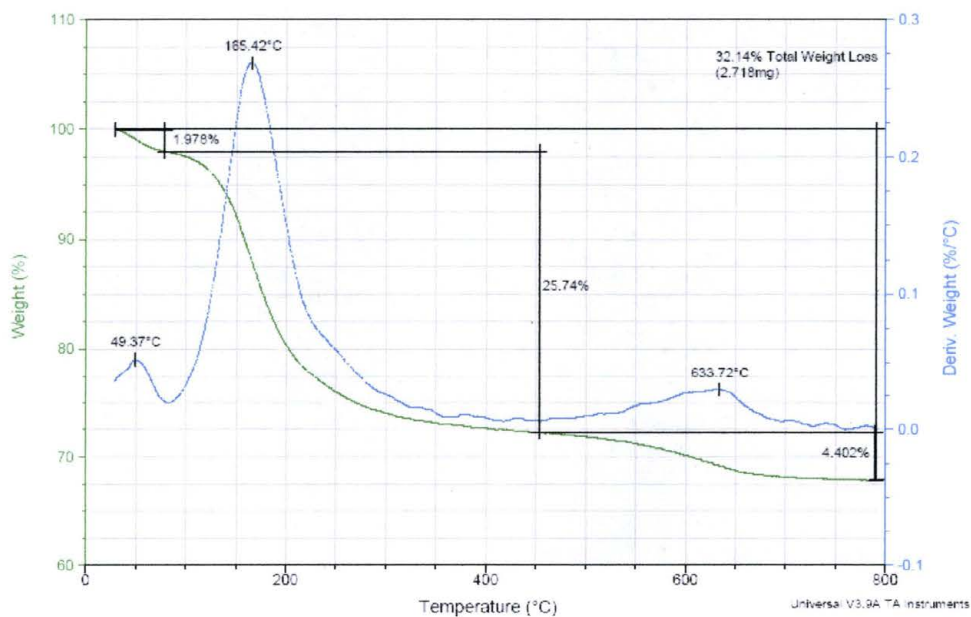
Appendix C10-b: TGA of Octyl Aldehyde 2:1 Organoclay

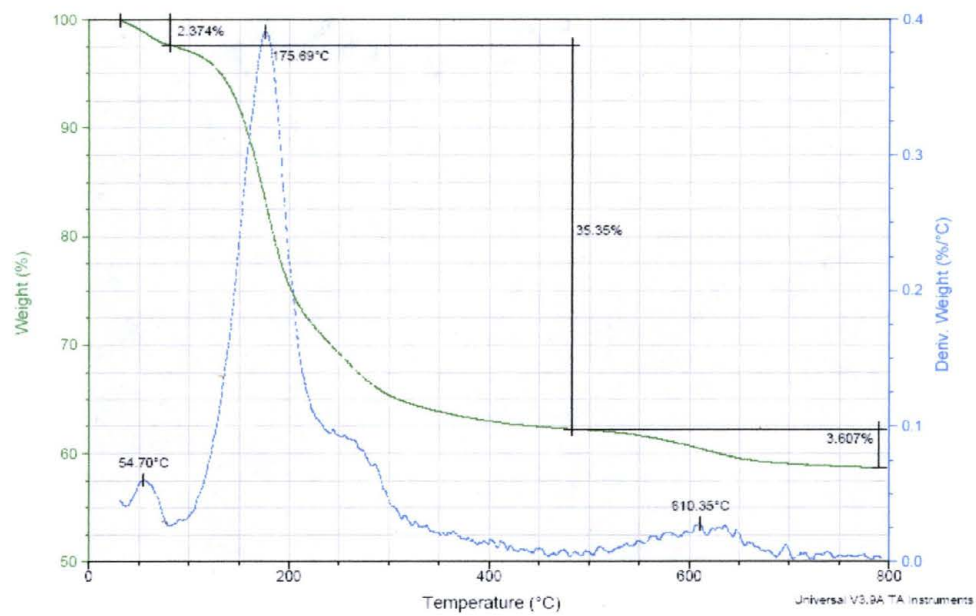


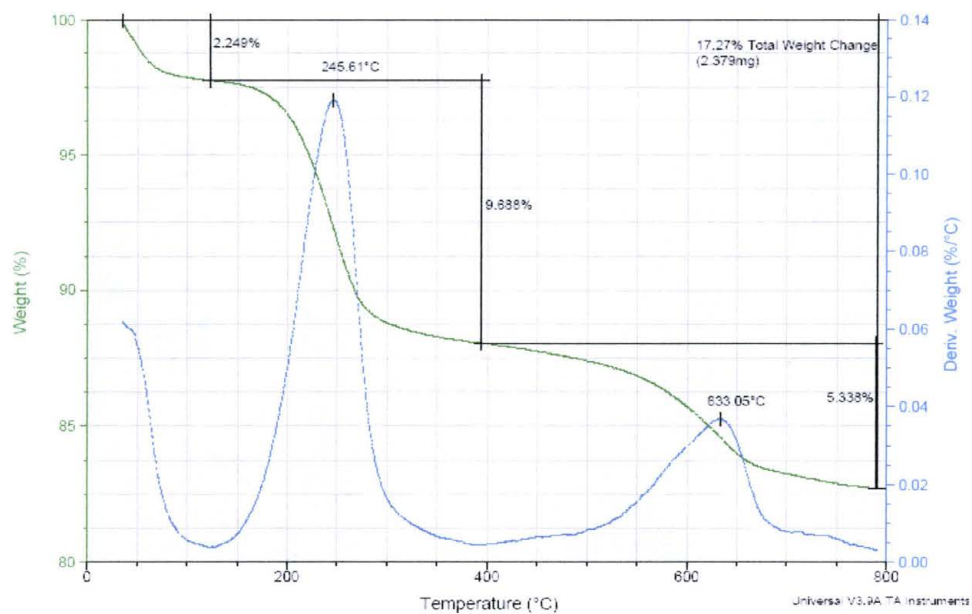
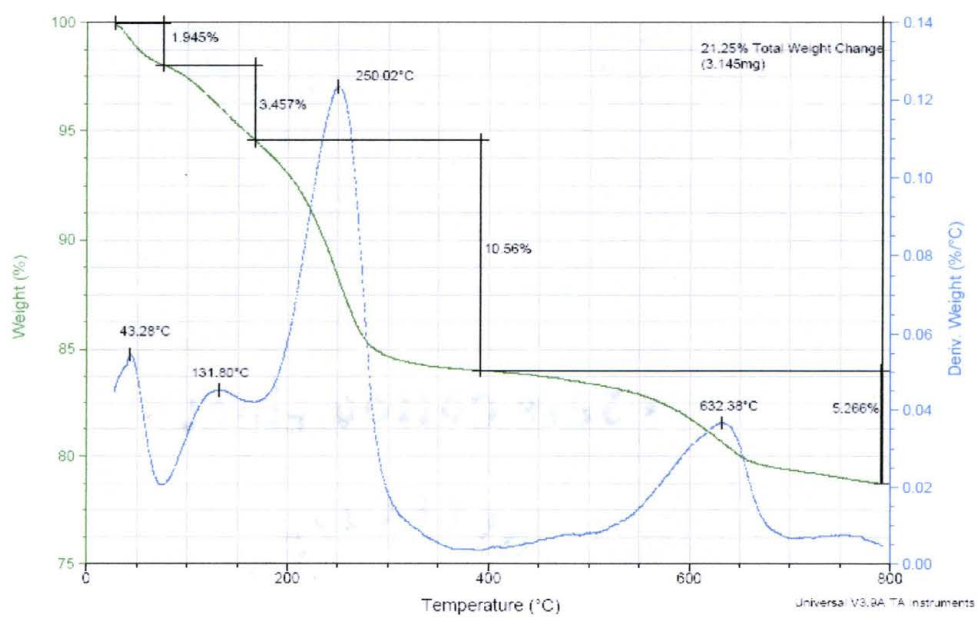
Appendix C10-c: TGA of Octyl Aldehyde 3:1 Organoclay

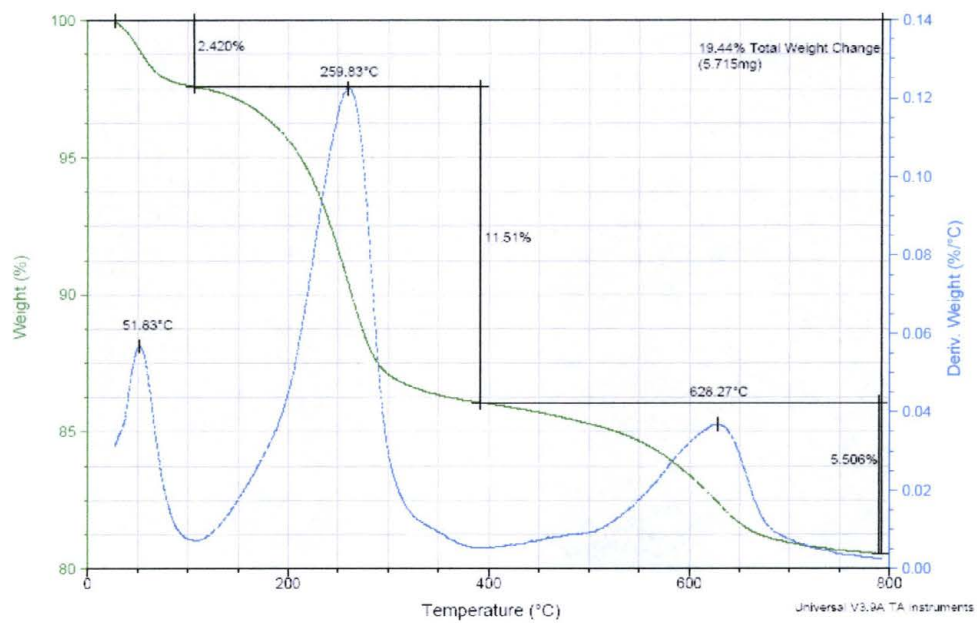
Appendix C11-a: TGA of Decyl Aldehyde 1:1 Organoclay**Appendix C11-b: TGA of Decyl Aldehyde 2:1 Organoclay**

Appendix C11-c: TGA of Decyl Aldehyde 3:1 Organoclay

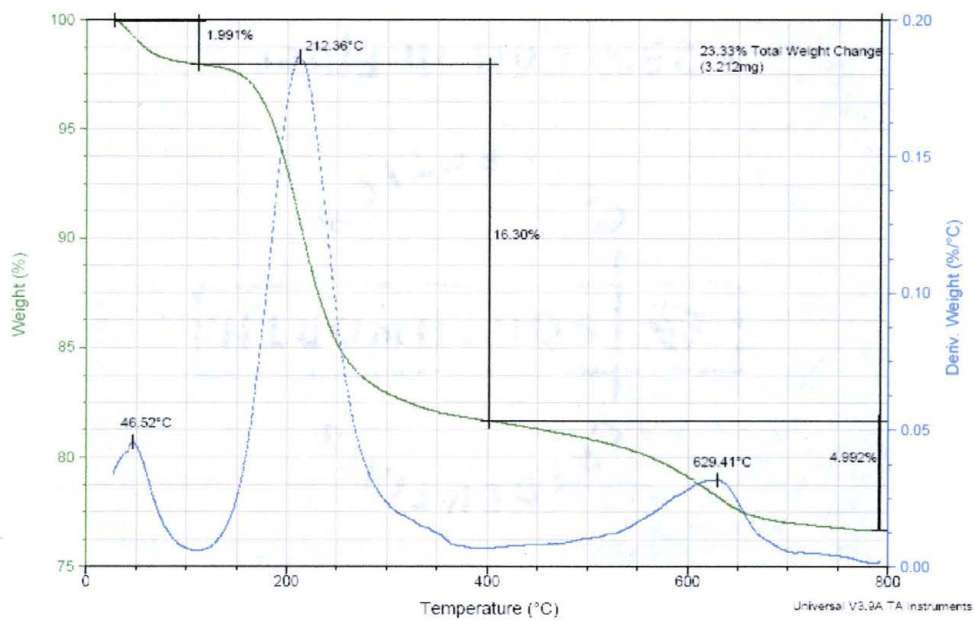
Appendix C12-a: TGA of Dodecyl Aldehyde 1:1 Organoclay**Appendix C12-b: TGA of Dodecyl Aldehyde 2:1 Organoclay**

Appendix C12-c: TGA of Dodecyl Aldehyde 3:1 Organoclay

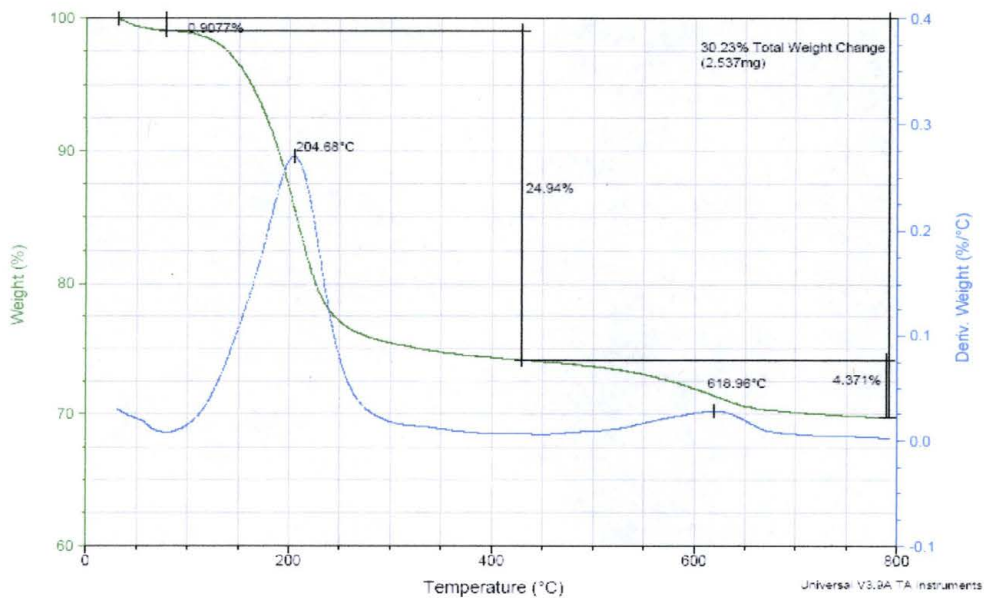
Appendix C13-a: TGA of N-Methyl Pyrrolidone 1:1 Organoclay**Appendix C13-b: TGA of N-Methyl Pyrrolidone 2:1 Organoclay**

Appendix C13-c: TGA of N-Methyl Pyrrolidone 3:1 Organoclay

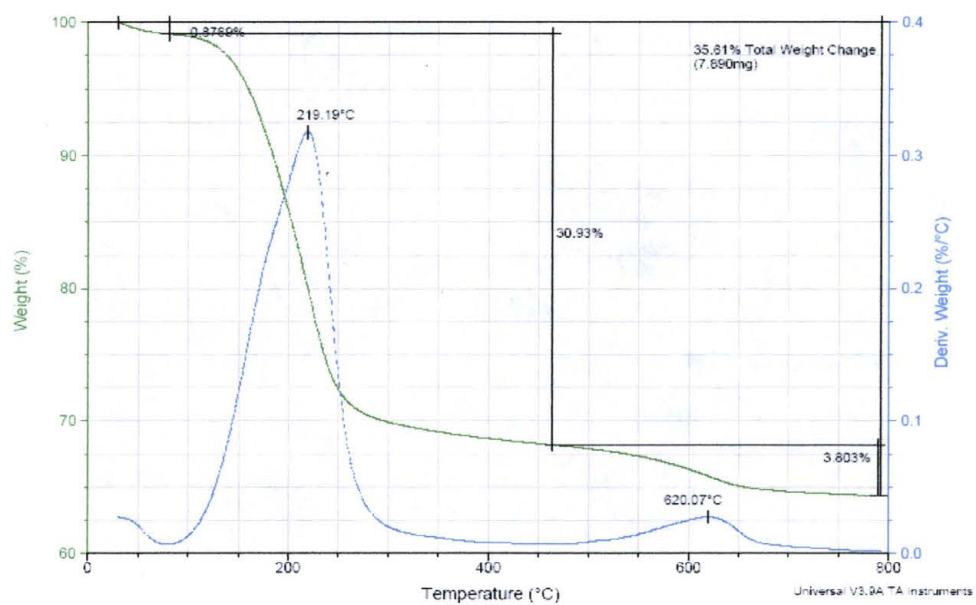
Appendix C14-a: TGA of N-Octyl Pyrrolidone 1:1 Organoclay



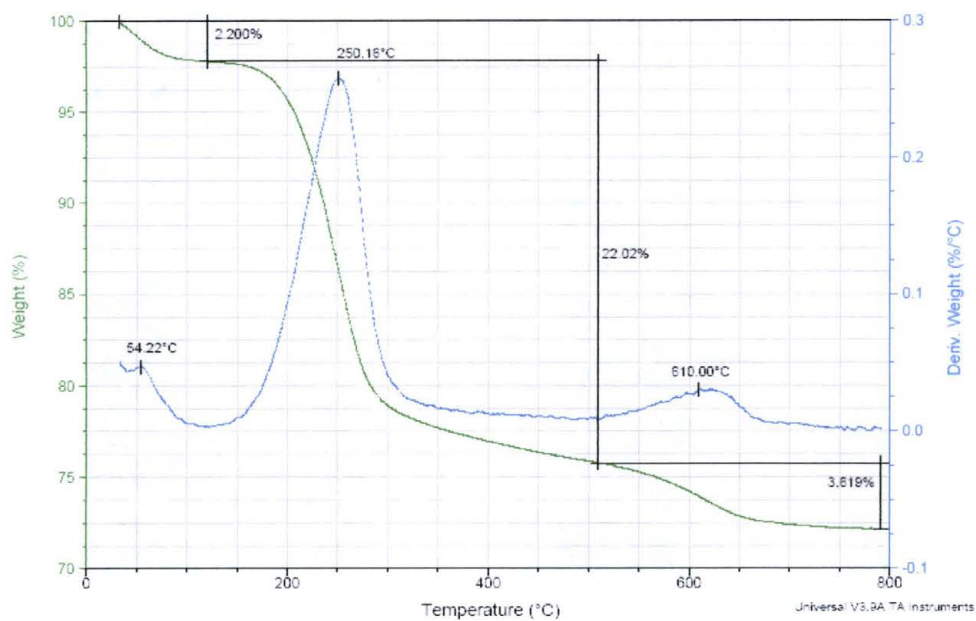
Appendix C14-b; TGA of N-Octyl Pyrrolidone 2:1 Organoclay



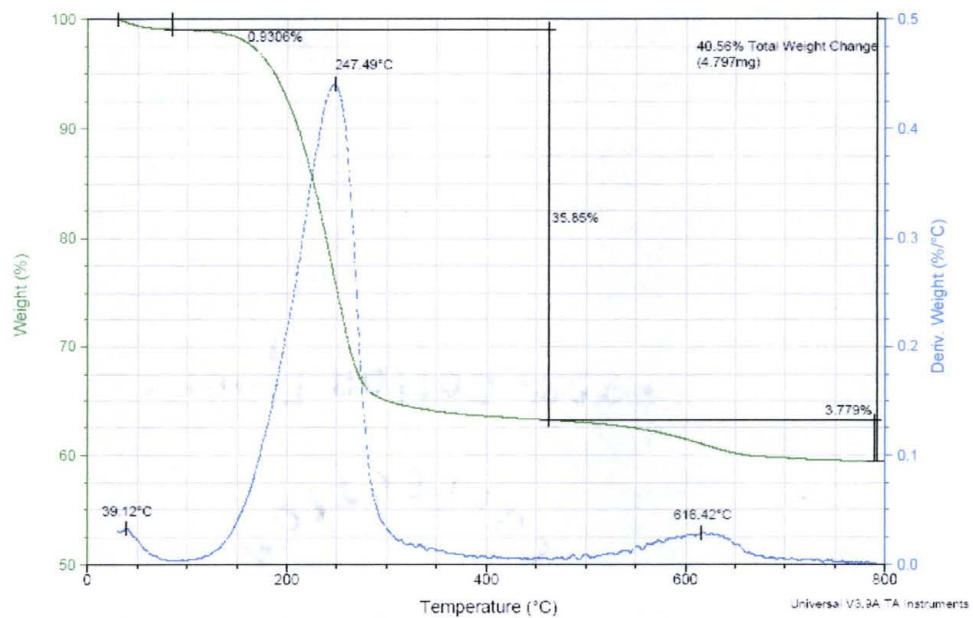
Appendix C14-c: TGA of N-Octyl Pyrrolidone 3:1 Organoclay



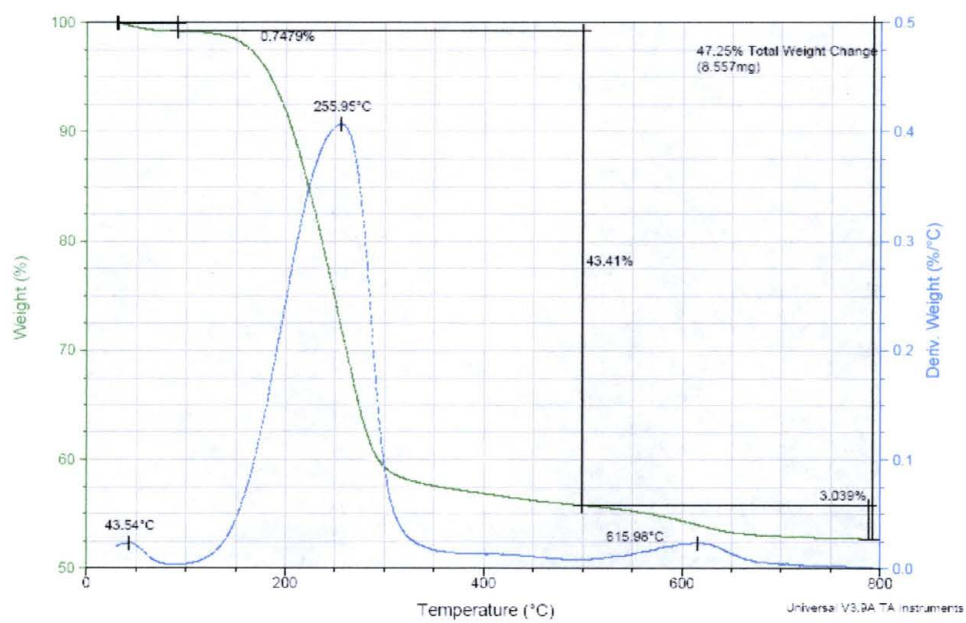
Appendix C15-a: TGA of N-Dodecyl Pyrrolidone 1:1 Organoclay



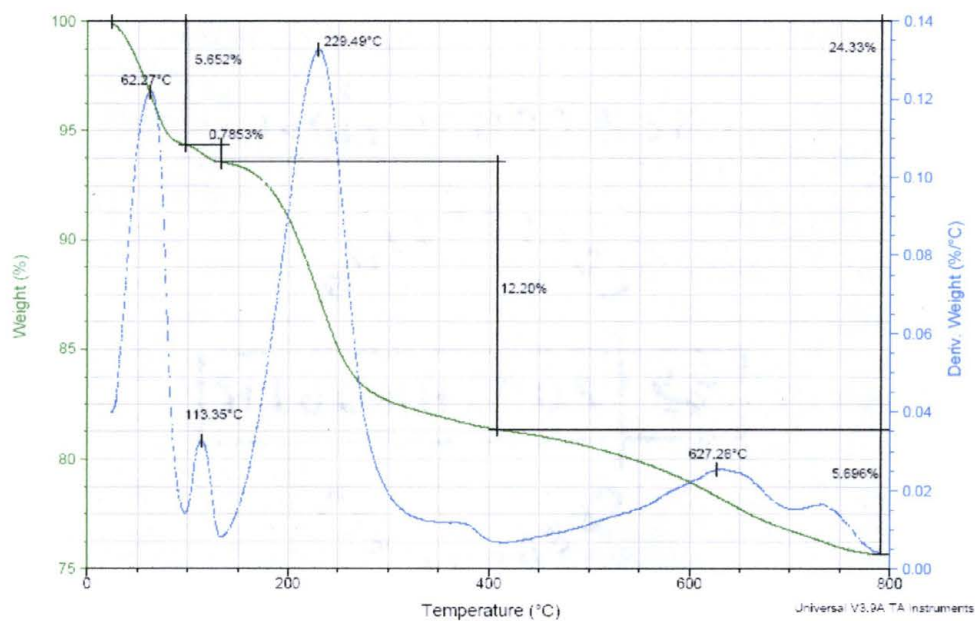
Appendix C15-b: TGA of N-Dodecyl Pyrrolidone 2:1 Organoclay



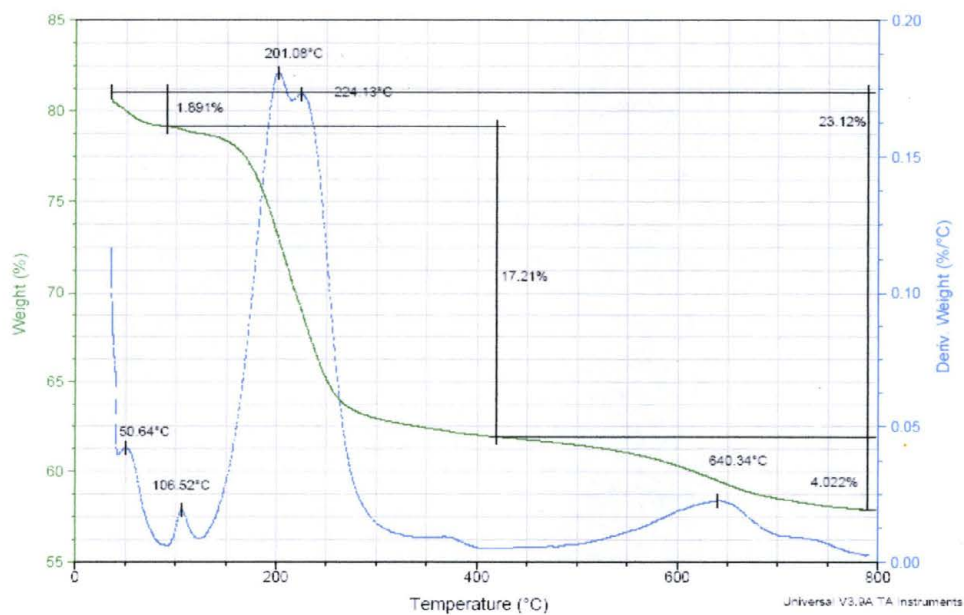
Appendix C15-c: TGA of N-Dodecyl Pyrrolidone 3:1 Organoclay



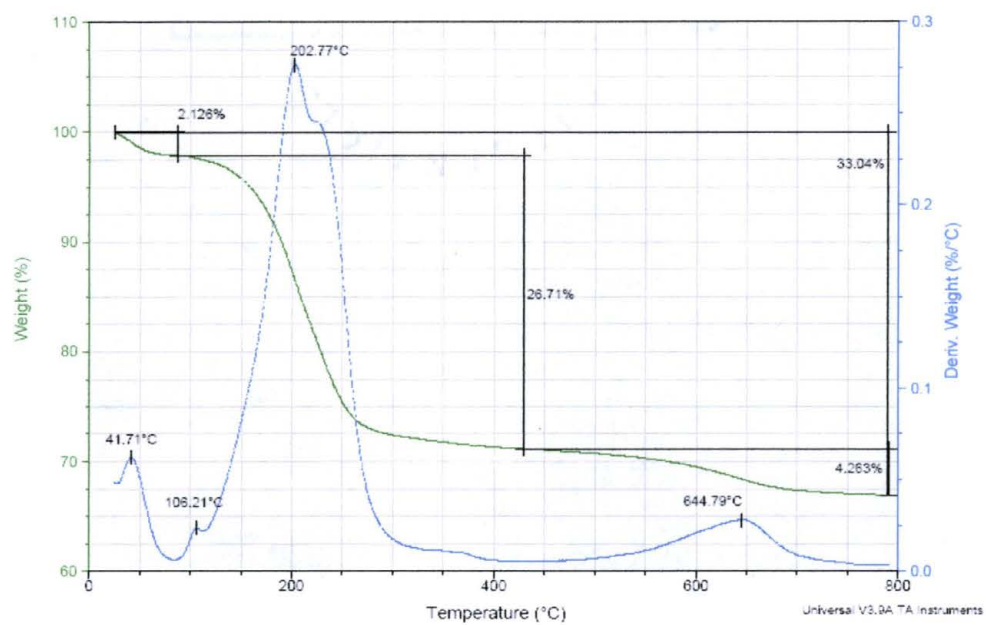
Appendix C16-a: TGA of N-Cyclohexyl Pyrrolidone 1:1 Organoclay



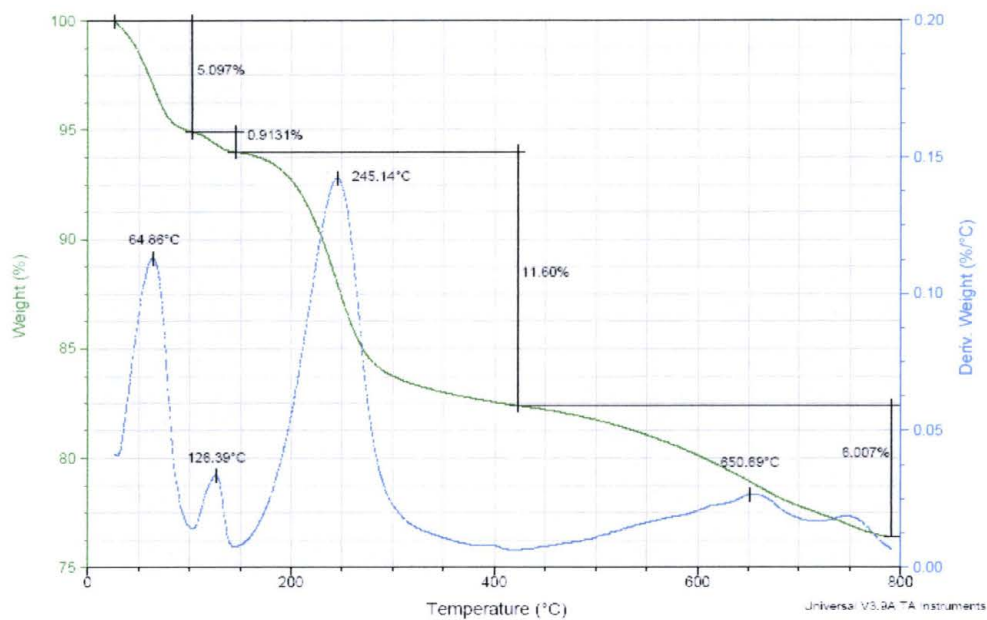
Appendix C16-b: TGA of N-Cyclohexyl Pyrrolidone 2:1 Organoclay



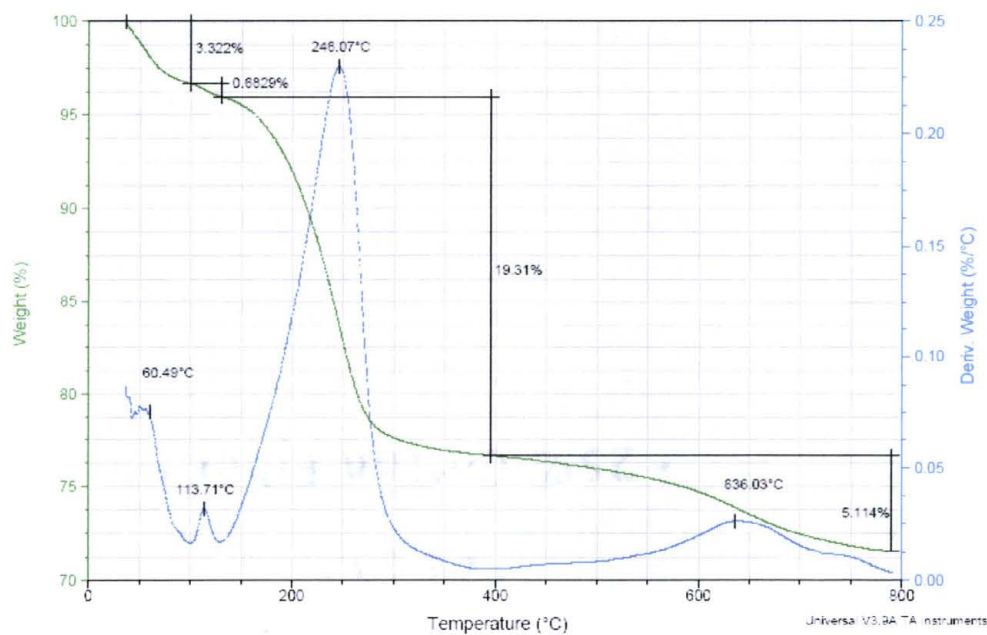
Appendix C16-c: TGA of N-Cyclohexyl Pyrrolidone 3:1 Organoclay



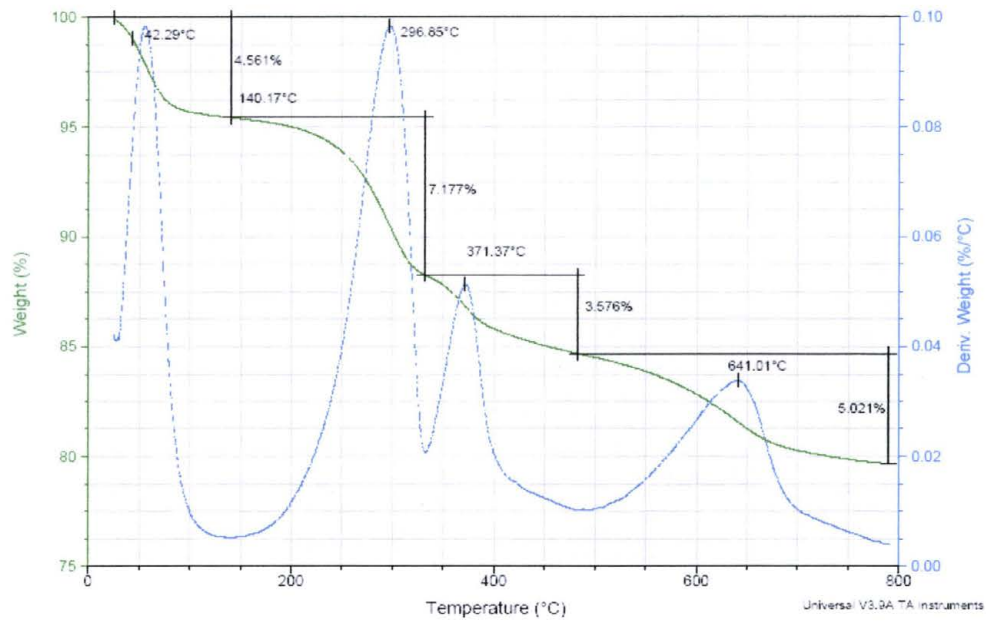
Appendix C17-a: TGA of N-Phenyl Pyrrolidone 1:1 Organoclay



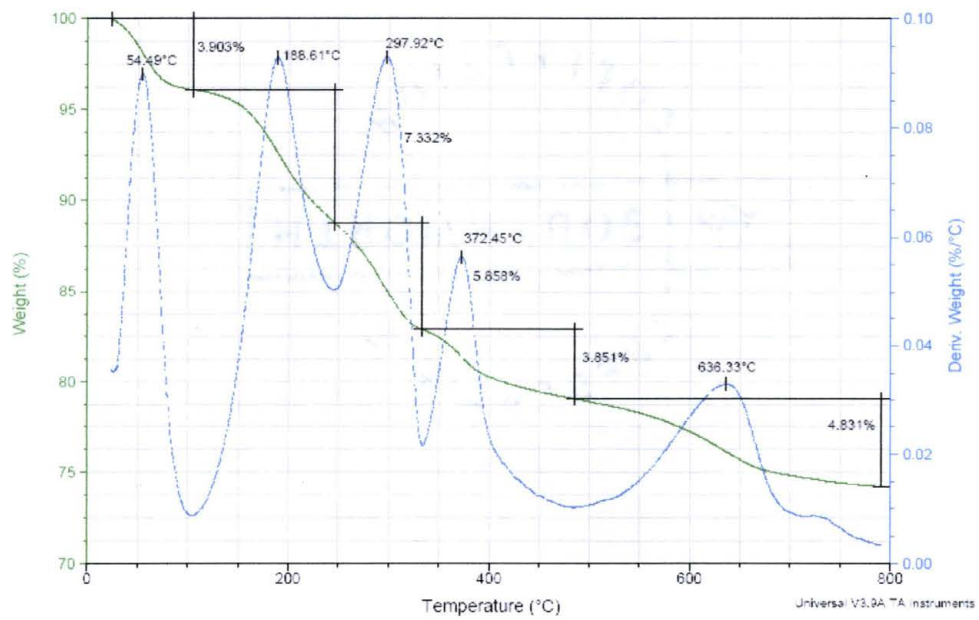
Appendix C17-b: TGA of N-Phenyl Pyrrolidone 2:1 Organoclay



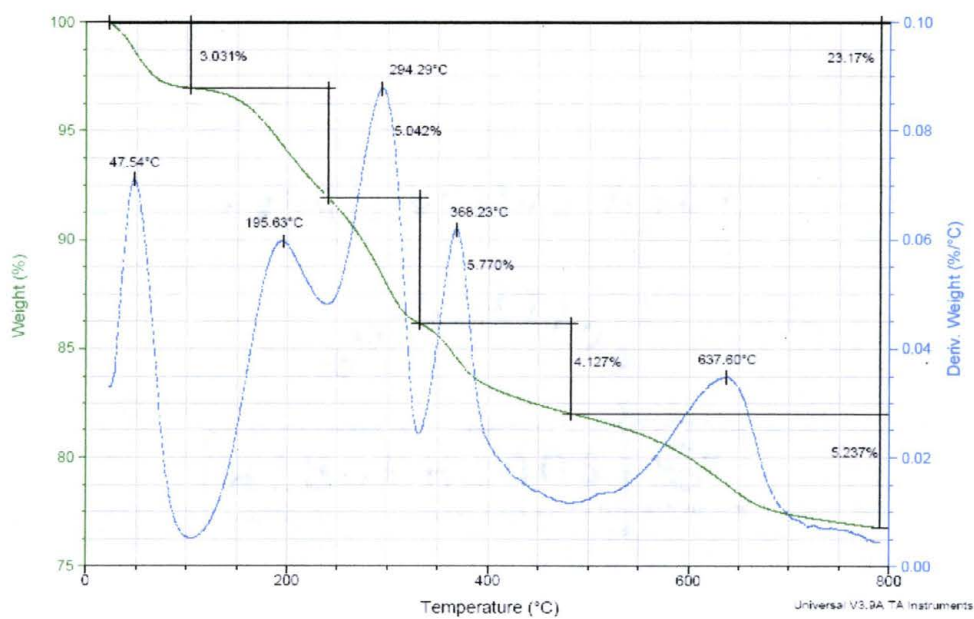
Appendix C18-a: TGA of Hydroxy Ethyl Pyrrolidone 1:1 Organoclay

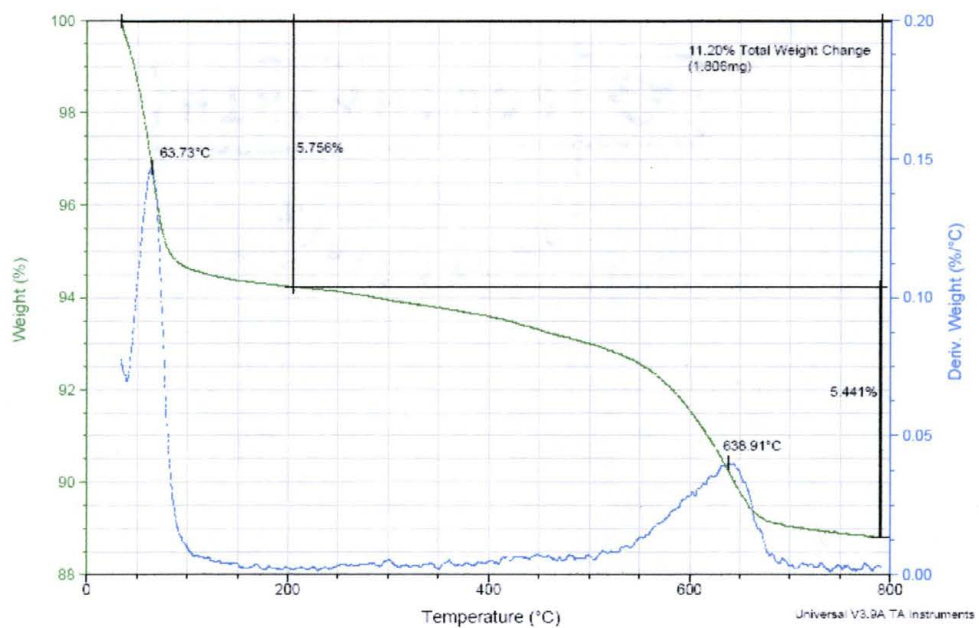


Appendix C18-b: TGA of Hydroxy Ethyl Pyrrolidone 2:1 Organoclay

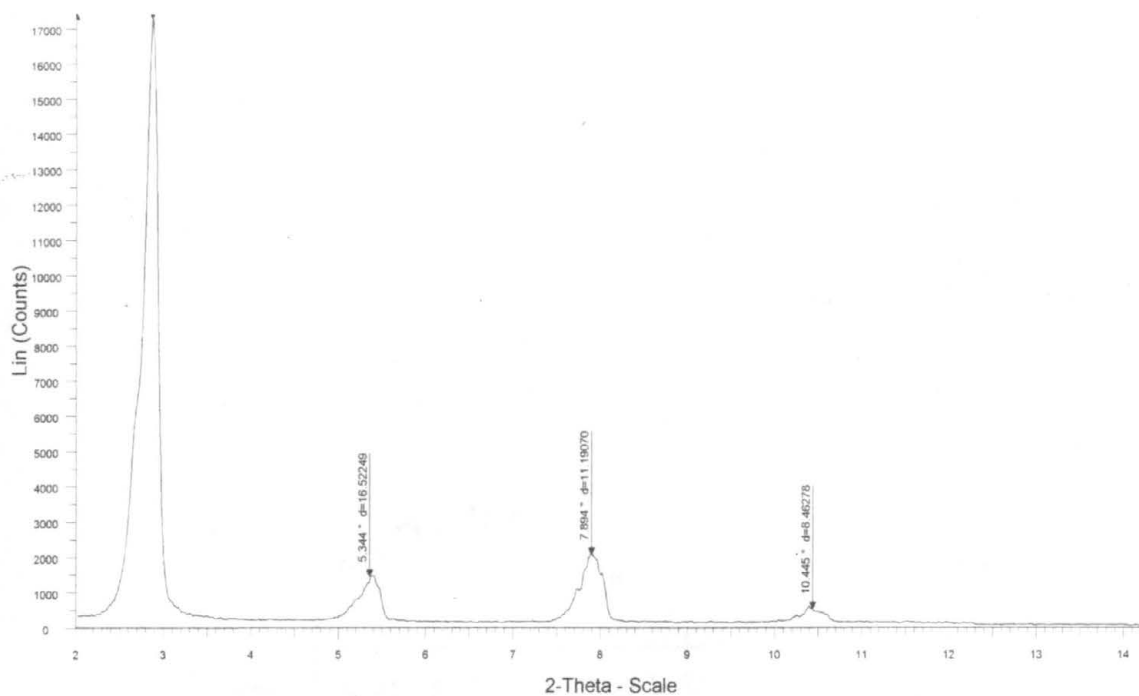
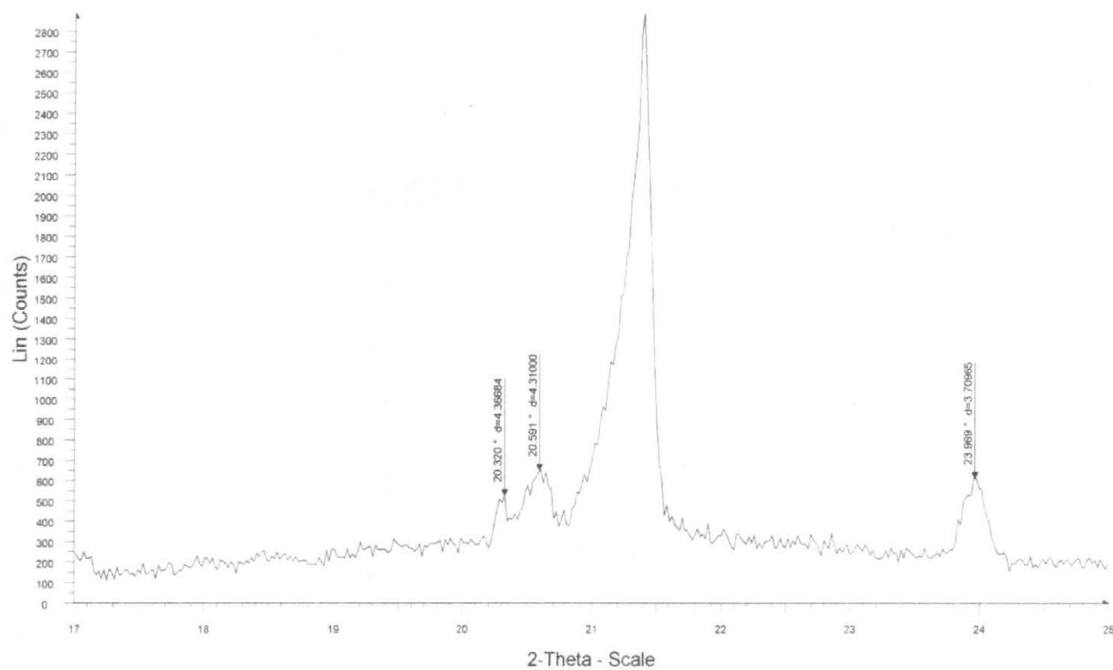


Appendix C18-c: TGA of Hydroxy Ethyl Pyrrolidone 3:1 Organoclay

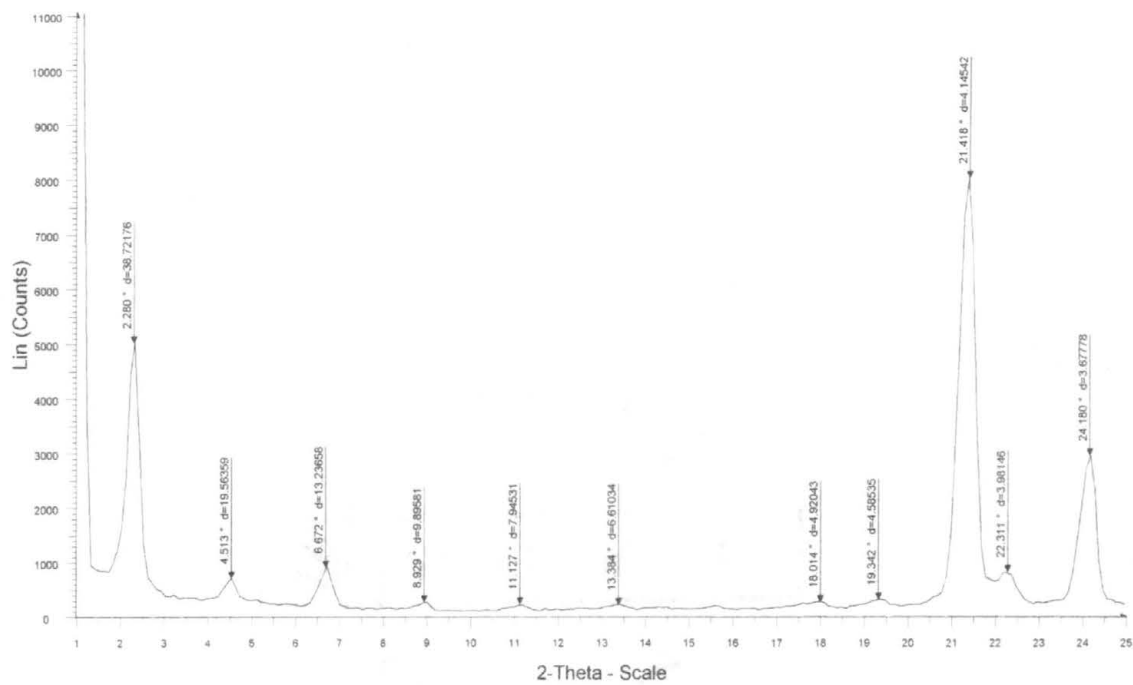


Appendix C19: Hydrated Sodium Cloisite (95 meq /100 g)

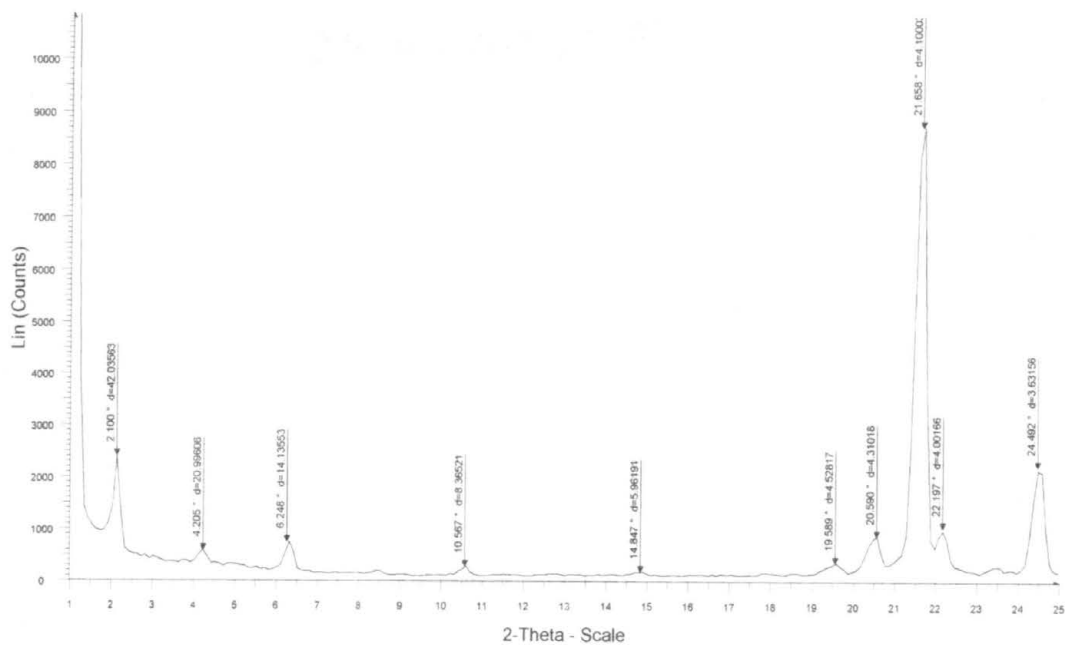
Appendix D: Wide Angle X-ray Diffractions of Pure Alcohols

Appendix D1: WAXD of Pure Alcohols**Pure dodecyl alcohol ($2\theta = 2$ to 14)****Pure dodecyl alcohol ($2\theta = 17$ to 25)**

Appendix D2: WAXD of Pure Alcohols



Pure tetradecyl alcohol



Pure octadecyl alcohol

REFERENCES

1. Hogg, T. Robust Self-Assembly Using Highly Designable Structures.
<http://www.foresight.org/Conferences/MNT6/Papers/Hogg/>. (accessed 3/2003).
2. Zhirnov, V. V.; Herr, J. C. *Computer* **2001**, 34, 34-43.
3. Stan, M. R.; Ziegler, M. M. *Proc. of the IEEE* **2003**, 91, 1941-1944.
4. Tour, J.M. *Molecular Electronics: Commercial Insights, Chemistry, Devices, Architecture and Programming*; World Scientific: New Jersey, 2003.
5. Flatt, A. K.; Dirk, S. M.; Henderson, J. C.; Shen, D. C.; Su, J.; Reed, M. A.; Tour, J. M. *Tetrahedron* **2003**, 59, 8555-8570.
6. Price, D. W.; Tour, J. M. *Tetrahedron* **2003**, 59, 3131-3156.
7. Price, D. W.; Dirk, S. M.; Maya, F.; Tour, J.M. *Tetrahedron* **2003**, 59, 2497-2518.
8. Tour, J.M.; Cheng, L.; Nackashi, D. P.; Yao, Y.; Flatt, A. K.; St. Angelo, S. K.; Mallouk, T. E.; Franzon, P. D. *J. Am. Chem. Soc.* **2003**, 125, 13279-13283.
9. *Chemistry and Technology of Polymer Additives*; Al-Malaika, S.; Golovoy, A.; Wilkie, C. A.; Blackwell Science Ltd.: Massachusetts, 1999.
10. Grims, R. E.; *Clay Mineralogy*; 2nd ed; McGraw-Hill: New York, 1968.
11. Kornmann, X.; Ph.D. thesis' Lulea University of Technology, Lulea, Sweden, 2000.
12. Maes, N.; Heylen, I.; Cool, P.; Vansant, E. F. *Applied Clay Science* **1997**, 12, 43-60.
13. Krishnamoorti, R.; Vaia, R. A.; Giannelis, E. P. *Chem. Mater.* **1996**, 8, 1728-1734

14. Beall, G. W. *Applied Clay Science* **2003**, 24, 11-20.
15. Ishida, H.; Campbell, S.; Blackwell, J. *Chem. Mater.* **2000**, 12, 1260-1267.
16. Zhao, C.; Feng, M.; Gong, F.; Qin, H.; Yang, M. *J. Appl. Polym. Sci.* **2004**, 93, 676-680.
17. Dennis, H. R.; Hunter, D. L.; Chang, D.; Kim, S.; White, J. L.; Cho, J. W.; Paul, D. R. *Polymer* **2001**, 42, 9513-9522.
18. Jordan, J. W. *J. Phys. Colloid Chem.* **1949**, 53, 294-306.
19. *Polymer-Clay Nanocomposites, Wiley Series in Polymer Science*; Beall, G. W.; Pinnavaia, T. J.; John Wiley & Sons, Ltd.: New York, 2000.
20. Briell, R. Nanoclays - Counting on Consistency. <http://www.nanoclay.com>. (accessed 7/2005).
21. Ray, S. S.; Okamoto, M. *Prog. Polym. Sci.* **2003**, 28, 1539-1641.
22. Sposito, G. Residual manganese (II) speciation in montmorillonite. http://www-esd.lbl.gov/sposito/Na_montmorillonite.html. (accessed 5/2005).
23. Beall, G. W.; Goss, M. *Applied Clay Science* **2004**, 27, 179-186.
24. Bradley, W. F. *J. Am. Chem. Soc.* **1945**, 67, 975-981.
25. Brindley, G. W.; Ray, S. *Amer. Mineralogist* **1964**, 49, 106-115.
26. Lagaly, G. *Clays and Clay Minerals, Proceedings of the Conference 1* **1975**, 23, 45-54.
27. Zanetti, M.; Lomakin, S.; Camino, G. *Macromolecular Mater. And Eng.* **2000**, 279, 1-9.
28. Moore, D. M.; Reynolds Jr., R. C. *X-Ray Diffraction and the Identification and Analysis of Clay Minerals*; Oxford University Press: New York, 1989.
29. Thomas, R. K. Simple Solids and Diffraction. <http://physchem.ox.ac.uk/~rkt/lectures/liqsolns/solids/solids.html>. (accessed 5/2005).
30. Schroeder, P. A. Lecture Notes for Clay Mineralogy. <http://www.gly.uga.edu/schroeder/geol6550/CM04.html>. (accessed 7/2005).
31. Baron, M.; Stepto, R. F. *Pure Appl. Chem.* **2002**, 74, 493-509.

32. Iskander, G. M.; Ovenell, T. R.; Davis, T. P. *Macromol. Chem. Phys.* **1996**, 197, 3123-3133.
33. Melville, R.; Sahyun, V.; Cram, D. J. *Organic Syntheses, Coll. Vol. 5* **1962**, 41, 91.
34. Zienty, F. B.; Steahly, G. W. *J. Am. Chem. Soc.* **1947**, 69, 715.
35. Sutton, R.; Sposito, G. *J. Coll. Inter. Sci.* **2001**, 237, 174-184.
36. Donald, A. M.; Windle, A. H. *Liquid Crystalline Polymers*; Cambridge University Press: Cambridge, 1994.
37. Ventolà, L.; Ramirez, M.; Calvet, T.; Solans, X.; Cuevas-Diarte, M. A. *Chem. Mater.* **2002**, 14, 508-517.

VITA

Marcus Jonathan Goss was born in Austin, Texas on May 17, 1971. After completing his work at San Marcos High School in 1989, he enrolled at Texas State University - San Marcos but withdrew and entered service in the United States Air Force in 1991. After military service, Marcus was employed in the communication and manufacturing industries in San Marcos. He received the degree of Bachelor of Science from Texas State University - San Marcos in May 2003. Marcus continued his education by entering the Graduate College of Texas State University - San Marcos. His research in clay nanocomposite surface treatments has lead to a publication in the professional journal *Applied Clay Science*. He is expected to receive the degree of Master of Science in Chemistry in December 2005.

Permanent Address: 1410 Brown Street

San Marcos, Texas 78666

This thesis was typed by Marcus J. Goss.